NUCLEAR CONNECTIVITY IN MESENCHYMAL STEM CELL DIFFERENTIATION AND ITS ROLE IN MECHANOTRANSDUCTION

Tristan P. Driscoll

A DISSERTATION
in
Bioengineering

Presented to the Faculties of the University of Pennsylvania
in Partial Fulfillment of the Requirements for the Degree of
Doctor of Philosophy
2015

Supervisor of Dissertation

_____
Dr. Robert L. Mauck
Associate Professor of Orthopaedic Surgery and Bioengineering
University of Pennsylvania

Graduate Group Chairperson

_____
Dr. Jason A. Burdick, PhD
Professor of Bioengineering, University of Pennsylvania

Dissertation Committee

Dr. Rebecca G. Wells, Associate Professor of Medicine and Bioengineering
University of Pennsylvania

Dr. Christopher S. Chen, Professor of Biomedical Engineering
Boston University

Dr. Dawn M. Elliott, Professor of Bioengineering
University of Delaware

Dr. Farshid Guilak, Professor of Orthopaedic Surgery and Bioengineering
Duke University

ACKNOWLEDGEMENTS

I would like to first and foremost acknowledge my advisor, Rob, who has been enormously influential in my development as a student of science. His excitement and energy have been critical drivers of my motivation throughout my time in his lab. I am truly grateful for the sacrifices he has made and the opportunities he has allowed me. He has worked very hard to establish a healthy and productive lab work environment. I have certainly benefited from his constant effort to provide this lab with the most advanced and efficient technologies.

I would also like to thank the other members of my thesis committee, Dr. Dawn Elliott, Dr. Chris Chen, Dr. Farshid Guilak, and Dr. Rebecca Wells, who have each contributed critical components to my work and my scientific thought process. Dr. Dawn Elliott was critical in my initial decision to come to Penn. She has taught me a great deal about mechanics, which has influenced my understanding of tissue structure and function. I had the fortunate opportunity to take Dr. Chris Chen's course during his time at Penn, which was by far the most enjoyable course of my academic career. He has taught me much about cellular mechanoregulation, and this has contributed greatly to the focus of this thesis. Dr. Rebecca Wells has given me valuable input, motivating me to focus on specific molecular signaling pathways. I am also thankful for the input of Dr. Farshid Guilak, who was a pioneer in the field of nuclear mechanics and musculoskeletal tissue engineering. His positive attitude and viewpoints on academia have been motivational and will influence my decisions going forward.

I would also like to acknowledge the many great faculty and staff of the McKay orthopaedic research laboratories. Louis Soslowlsky has done an amazing job establishing McKay as a premier orthopaedic research lab and I am very thankful for the resources that he and other faculty have worked very hard to obtain. The McKay administrative staff does a great job to ensure that the research in McKay proceeds without interruption. Arlene Adair, Gina DeRitis, Susan Dinella, Kelly McGinnis, Mia Powell and Barbara Gibson have all been extremely helpful to me during my time in McKay. A number of other faculty members here in McKay have also been very supportive. George Dodge has always been willing to provide equipment, resources and advice. He has also been a great resource for meeting new people in the field of orthopaedic research. Eileen Shore and Lachlan Smith have also provided input and insights into my work through the collaborative meetings we have here in McKay.

I have been very fortunate to work with a number of very excellent undergraduates. Ryan Nakasone and Zach Shurden were tremendously helpfully during their time in the lab. Not only were they quick to learn new things but they also taught me many things along the way. I am also very thankful for the many Mauck lab members that have directly helped me with my research. When I joined the lab Nandan Nerurkar, Brendon Baker, Alice Huang, Isaac Erickson, and Megan Farrell were all extremely helpful. Since then, many new people have joined and all have impacted my experience in some way. Claire McLeod and Sylvia Qu were both critical for collecting the AFM data in this thesis. I am also very thankful for the hard work and dedication of Liz Henning. She

does an amazing job keeping chaotic aspects of the Mauck lab at bay. Without her I know that many of my experiments would not have gone as smoothly as they did. Brian Cosgrove has established protocols for traction force microscopy in our lab and was very helpful for collecting the TFM data in this thesis. Brian has also become, and will continue to be, a great friend of mine. I have really enjoyed my time in lab with Brian and I will always value my friendship with him. Sujin Heo has also been tremendously helpful and a great friend. His initial observations of lamin a/c changes with loading are what really sparked my interest in the majority of what is contained in this thesis. Many other McKay lab members have been very supportive both inside and outside the lab: John Martin, Bhavana Mojanraj, Joseph Chiaro, Minwook Kim, DonHwa Kim, Claire McLeod, Sylvia Qu, Greg Meloni, Matt Fisher, Mike Hast, Sun Peck, Woojin Han and Spencer Szczesny have all had an extremely positive impact on my graduate experience as a whole.

This work would not have been possible without the support of my family, who has been extremely supportive of my interest in science since a young age. I am very thankful for all they have done for me. Lastly, I would like to acknowledge my wife Jillian and our dog Lola. Knowing I was going home to the two of them at the end of the day has made the most difficult and frustrating aspects of my PhD more bearable, and has motivated me throughout my time here at Penn.

ABSTRACT

NUCLEAR CONNECTIVITY IN MESENCHYMAL STEM CELL DIFFERENTIATION AND ITS ROLE IN MECHANOTRANSDUCTION

Tristan P. Driscoll

Robert L. Mauck (Advisor)

Mechanical forces transmitted through the cellular microenvironment are critically important for tissue development, homeostasis, and degeneration, particularly for tissues in the musculoskeletal system that play primary load bearing roles. When these tissues degenerate, their limited healing capacity has lead many to propose tissue engineering strategies in order to provide functional replacements. While native tissue structural and mechanical benchmarks are commonly used to quantify and validate outcomes for tissue engineering and to refine experimental approaches, these same benchmarks have not yet been extended to the cellular and sub-cellular level. This is true despite the fact that it is at this length scale where tissue specific mechanotransduction occurs. With this motivation, and building on an established biomaterial framework for engineering fibrocartilagenous tissues, this thesis further refines macro-scale functional benchmarks and defines new micro-scale benchmarks that are operative at the cellular and sub-cellular level. In doing so, we identify a number of structural attributes of the cellular cytoskeleton and its attachments to the nucleus that are important for mechanotransduction. In normal functioning tissues, maintenance of phenotype in

mechanically active microenvironments requires appropriately tuned mechanotransduction machinery. Understanding how these sub-cellular mechanoactive species (including the cytoskeleton, the nucleus, and nuclear connectivity) change with differentiation and development, as well as their role in mechanical signaling, will be of primary importance for the success of tissue engineering strategies.

TABLE OF CONTENTS

LIST OF FIGURES

CHAPTER 1: INTRODUCTION

Fiber reinforced soft tissues function to transmit forces in the musculoskeletal system, allowing for joint movement, stabilization, and congruent load transfer. The composition and organization of these tissues is critical for their function, and is regulated by the cells within. These cells are inherently mechanosensitive, responding to loads transmitted through the tissue. Thus, normal mechanical loading is critical for the development and homeostasis of fiber reinforced tissues, while aberrant mechanical loading can induce a cascade of degenerative changes that eventually results in tissue dysfunction. The limited healing capacity in these tissues has lead to the development of numerous stem cell based tissue engineering approaches, which aim to replicate bulk tissue mechanical properties based on native tissue benchmarks. While this is important for the mechanical function of these tissues, replication of cellular attributes will be crucial for the long-term maintenance of these tissues. Specifically, cellular attributes that regulate mechanotransduction are of primary importance. Mechanical loads are transmitted from the structural network of proteins outside of the cell (the extracellular matrix), through cell adhesions, to the structural network of proteins within the cell (the cytoskeleton), eventually reaching the nucleus (via transmission through the LINC complex). Mechanotransduction occurs at each of these levels, often through forced unfolding of proteins within these networks. Therefore, appropriate mechanotransduction in engineered tissues and cells, will likely require replication of the protein networks that facilitate this multi-scale strain transfer.

Thus, the overarching goal of this thesis is to quantify both bulk (tissue level) and micro-scale (cell level) strain transfer in engineered fibrous microenvironments, and to determine the extent to which this strain transfer regulates mechanotransduction in mesenchymal stem cells (MSCs) and the native tissue cells they are to replace. At the bulk scale, transfer of tensile, shear and multiaxial loads are of importance for appropriate tissue mechanical function, particularly in fibrocartilagenous tissues that are exposed to these types of loads during activities of daily living. This includes tissues such as the annulus fibrosus of the intervertebral disc and the meniscus of the knee. At the micro-scale, the structural attributes of the matrix that cells interact with can regulate strain transfer to the cell, while within the cell, a number of cytoskeletal and nucleoskeletal proteins regulate strain transfer through the cell. Using a variety of mechanical testing modalities at each of these scales, this work investigates mechanical aspects of both mesenchymal stem cells and the engineered microenvironments that regulate their behavior.

Chapter 2 of this thesis provides an outline of the extracellular matrix molecules and molecular mechanism that regulate strain transfer and mechanotransduction in cells and tissues. The extent to which tissue composition, structure, and mechanics regulate strain transmission is described. Providing motivation for this work, the specific mechanisms by which cells sense mechanical force and the importance of these mechanisms in development, homeostasis, and disease are discussed. Finally, an overview of current repair and tissue engineering strategies for damaged or degenerate fibrocartilage are

described, as well as the extent to which these approaches will likely require an understanding of the mechanotransduction mechanisms at play.

To assess the bulk and micro-scale strain transfer in engineered environments, a number of methods were developed or adapted. In chapter 3, these methods are outlined and their validation and function is described. These methods allow for quantification of bulk and micro-scale mechanical attributes of engineered matrices and the cells within.

In chapters 4 and 5, the extent to which engineered fibrocartilage is able to recapitulate native tissue shear and multi-directional mechanical properties is investigated. In this work, a previously described structural mechanism of inter-lamellar shearing in uniaxial tension, which acts to stiffen engineered laminates, is validated as functional in biaxial tension. With time in culture, laminates engineered to have opposing lamellar orientation (mimicking native annulus fibrosus) displayed increased biaxial mechanical properties compared to constructs with parallel lamellar orientation. Shear mechanical properties were found to exceed native tissue values and biaxial mechanical properties approached those of native tissue. However mechanical non-linearity, a principal functional feature in native tissues, was found to be lacking in the engineered constructs.

To address the issue of non-linearity in nanofibrous scaffolds, Chapter 6 describes an approach for patterning crimped structure into aligned scaffolds. This method is able to significantly increase scaffold mechanical non-linearity, also impacting micro-scale Lagrangian strains, nuclear orientation and the level of nuclear elongation with stretch.

Further, these crimped scaffolds increase the ERK1/2 mechanotransduction response in mesenchymal stem cells with applied stretch.

One of the key regulators of mechanotransduction and transfer of strain to the nucleus is the actin cytoskeleton and the tension within it. In Chapter 7, the importance of cytoskeletal tension in regulating strain transfer to the nucleus is assessed. Additionally, the role that this cytoskeletal strain transfer plays in the mechanical activation of the YAP/TAZ pathway with tensile loading is investigated. This work shows that while some mechanoactive signaling pathways (e.g. ERK signaling) can be activated in the absence of nuclear strain transfer, cytoskeletal strain transfer to the nucleus is essential for activation of the YAP/TAZ pathway with stretch.

Based on the results from Chapter 7, which indicated nuclear strain transfer is necessary for YAP activation with stretch, Chapter 8 addresses the extent to which this strain transfer and YAP activation is facilitated by the LINC complex components nesprin 1 giant and lamin A/C. Further, this chapter identifies nesprin 1 giant as a regulator of nuclear height, cellular adhesion size, cellular traction force, and YAP signaling in response to both substrate stiffness and dynamic tensile loading in MSCs. Comparison to differentiated fetal, juvenile, and adult fibrochondrocytes indicated that both lamin A/C and nesprin 1 giant increase with age as nuclear and tissue stiffness increase, surpassing levels in MSCs. Interestingly, nesprin 1 giant also regulated the YAP response to dynamic loading in adult meniscus cells. Fibrochondrogenic differentiation of MSCs by mechanical loading resulted in changes in nesprin 1 giant. These load induced changes

were dependent on cytoskeletal contractility and did not occur with differentiation mediated by the addition of soluble TGF-β3. Changes that occurred with mechanical or soluble differentiation, increased basal YAP nuclear localization on aligned scaffolds. In the case of mechanically induced differentiation, the YAP response to loading was desensitized.

Finally, Chapter 9 summarizes the major findings of this work and describes the implications for nuclear strain transfer and mechanical signaling in fibrous environments. Additionally, the limitations of this work are discussed, followed by suggestions of future directions for this research.

CHAPTER 2: BACKGROUND

2.1 The ECM, its mechanical components and their organization (structure function)

The natural extracellular matrix (ECM) provides structure to tissues within the body and is composed of a dense network of structural proteins and hydrated glycosaminoglycans that are intricately organized to provide a 3D tissue specific scaffolding. This allows for cell attachment and proliferation, and guides cellular morphology and differentiation. The mechanical properties of the ECM are defined by this underlying structure and composition, which is continuously remodeled by resident cells in response to the local loading environment. Thus, ECM mechanics can direct cellular processes, which in turn can regulate ECM mechanics, providing a mechanical feedback mechanism that is vitally important for both development and homeostasis of tissues within the body. When this careful balance of remodeling is altered, degeneration and/or disease processes may ensue, with the same ECM, constructed aberrantly, driving unwanted degradative or differentiation processes. In the following sections, we identify and describe the primary constituents of the ECM, describe how these constituents imbue the tissue with mechanical properties that enable transfer of physiologic loads, illustrate how these physical forces are transmitted to and through the cell to regulate biologic action, and finally, how these mechanical signals regulate ECM remodeling and refinement during development, homeostatic function, and disease.

2.1.1 ECM mechanical molecules that provide structure

There are numerous ECM molecules that provide structure to tissues and binding sites for the cells within. These molecules are synthesized, modified, and organized into tissue-specific hierarchical structures by the resident cells. Each of the numerous ECM molecules has a specific function, and often this function is to provide resistance to tensile or compressive forces. The following section will describe the major ECM molecules, how they are organized, and the mechanical function that they provide to a tissue.

Collagens:

The most abundant type of molecule in most extracellular spaces is collagen, which comprises approximately 25% of the dry weight of most tissues. Collagen is primarily organized into fibrillar structures that are important for resisting tensile loads. Multiple chemically distinct forms of collagen have been identified, though each is predicated on the same basic functional unit, a three peptide alpha helical chain stabilized by hydrogen bonds. These peptide chains have a distinct repeating pattern of Gly-Pro-X or Gly-X-Hyp where X can be various other amino acids and Hyp is a post-translationally modified version of proline called hydroxyproline (Bhattacharjee and Bansal 2005). The large abundance and repeating pattern of the small amino acid glycine is important for the formation of the very tightly bound alpha helix that is formed. These alpha helices, known as procollagen, are processed outside the cell to form ropelike fibrils, which assemble and pack together to form larger cablelike fibers (**Figure 2-1A and 2-1B**) in the case of fibrillar collagens (e.g. collagens I-III) (Bornstein and Sage 1980). In other non-

fibrillar collagens (like collagen IV) these molecules are combined to form a sheet like meshwork. In general, collagens form very robust structures that resist tensile forces. In addition to their major mechanical role, collagens also work both alone and in conjunction with other ECM molecules to direct cell alignment and facilitate transfer of strain from tissue to cell.

Glycosaminoglycans and Proteoglycans:

Glycosaminoglycans or GAGs form another class of ECM molecules that are important for tissue mechanical function. These molecules are composed of repeating disaccharide units, one of which is always an amino sugar, and form unbranched polysaccharide chains (**Figure 2-1C and 2-1D**). Often the amino sugar is sulfated, contributing to the highly negative charge of the GAG molecules. These molecules form stiff non-flexible chains that are strongly hydrophilic and tend to adopt elongated conformations (Raman, Sasisekharan et al. 2005). All GAGs except for one (hyaluronan) are covalently attached to a protein core, forming a proteoglycan. The high density of negative charges in GAGs attracts cations, such as sodium, and produces a large osmotic swelling pressure in GAG rich tissues (Buschmann and Grodzinsky 1995). This swelling pressure in combination with the high density of negative charges, which repel each other, makes GAGs well suited to resist compressive loads. Thus, tissues that must resist compression (such as cartilage) are rich in large proteoglycans. Often these molecules work in combination with collagens, which act in tension to resist the outward swelling pressure in GAG rich tissues.

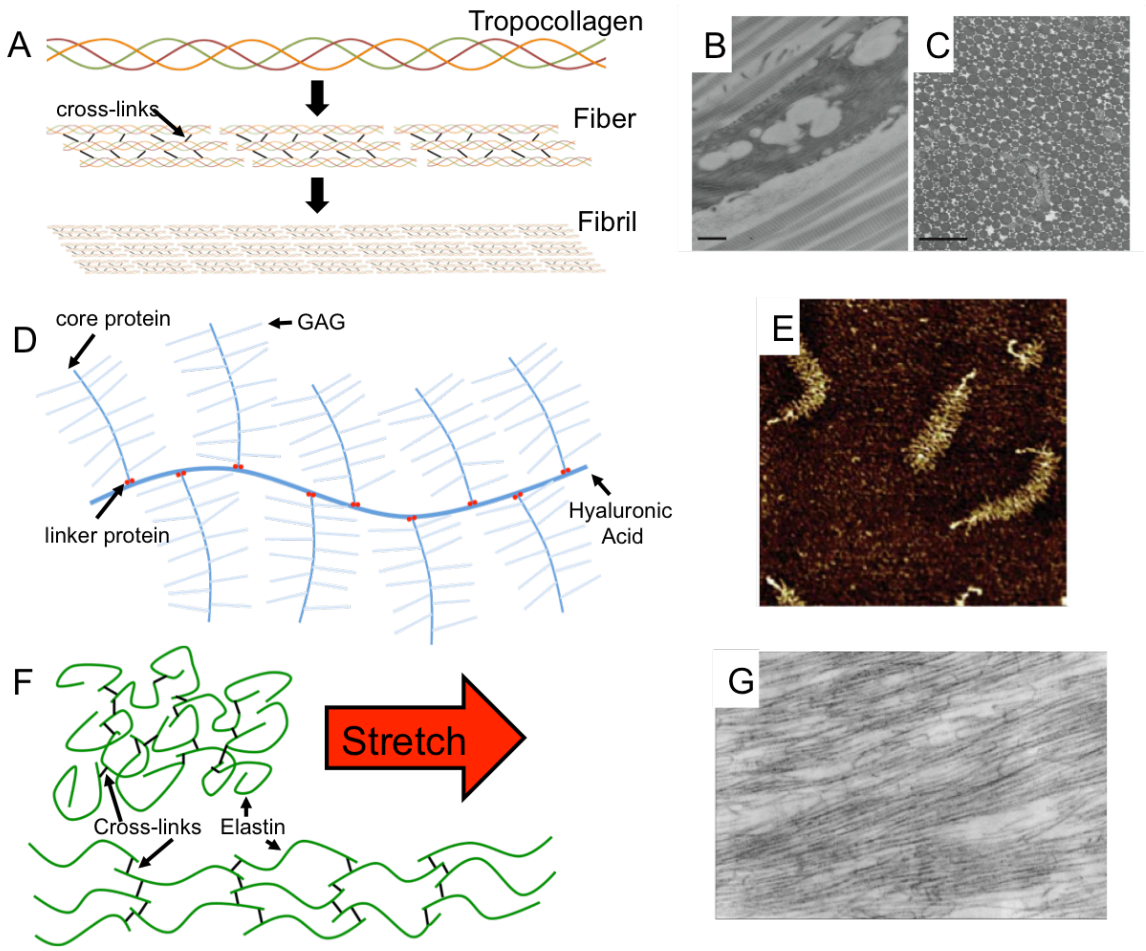

Figure 2-1: Major mechanical ECM components and their structure. Collagen is formed initially within the cell as alpha helical tropocollagen, which is then deposited into the extracellular space and further processed by cross-linking into collagen fibers (A). These fibers combine to form higher order fibrils, which can be seen by transmission electron microscopy both perpendicular to (B) and in the direction of fiber alignment (C) (images adapted from (Starborg, Kalson et al. 2013)). These cable like structures are important for resisting tensile loading. Proteoglycans are composed of sulfated glycosaminoglycans attached to a core protein that is linked to hyaluronic acid chain (D) forming a brush like structure that can be observed by atomic force microscopy (E) (image adapted from (Lee, Han et al. 2013)). The high density of fixed charges in these molecules helps them resist compressive loading. Elastic fibers contain a central core amorphous of heavily cross-linked elastin monomers (F), which straighten when stretched. Elastic fibrils form with an outer microfibrillar shell and can be viewed by transmission electron microscopy (G) (image adapted from (Kielty, Sherratt et al. 2002))

Elastin:

While collagens and GAGs provide resistance to tension and compression, a third molecule, elastin, is important for enabling large and recoverable elastic deformations, such as those that occur in skin and blood vessels. This protein is very hydrophobic, due to the high content of hydrophobic amino acids and very few polar groups. Elastin is synthesized as a soluble precursor molecule, tropoelastin, and is then heavily modified and cross-linked. Tropoelastin is deposited onto a preformed template of fibrillin-rich microfibrils such that mature elastic fibers are composed of a core of amorphous cross-linked elastin and an outer microfibrillar shell (Kielty, Sherratt et al. 2002). In the unloaded state this amorphous elastin adopts a random coiled confirmation (**Figure 2-1F**); this allows the structure to undergo large deformations and to recoil quickly and completely when unloaded.

Cell binding ECM molecules:

Along with these principle load-bearing ECM molecules there exist numerous smaller molecules that facilitate the interactions between ECM structural units, as well as between cells and their ECM. These molecules form a close relationship with the cells and provide feedback communication through which cells are regulated and which cells can remodel. A sequence common to most of these cell binding molecules is the peptide sequence Arginine-Glycine-Aspartic acid (RGD). This peptide sequence allows cell binding through integrins, a family of cell surface transmembrane receptors that facilitate cell-ECM connections. Some RGD containing ECM molecules include Fibronectin, Fibrinogen, Laminin, Tenascin, Vitronectin, Thrombospondin and Entacin (Buck and

Horwitz 1987, Bourdon and Ruoslahti 1989). Each has specific functions and increased prevalence in certain tissues, but all are capable of binding other ECM molecules and contain the cell binding RGD domain. Often, these cell-adhesive ECM molecules also contain binding sites for growth factors or other signaling molecules, which can be released or activated with applied mechanical force (Wipff, Rifkin et al. 2007), providing a matrix level mechanotransduction mechanism that will be discussed further in the latter sections of this chapter.

In addition to binding RGD containing ECM molecules, cells can bind and interact with other sites within ECM molecules. There are two main families of receptors that cells use to bind to ECM molecules, integrins and syndecans (Morgan, Humphries et al. 2007). Integrins are transmembrane proteins that bind to ECM molecules as sets of heterodimers, with an alpha and a beta subunit, and can cluster with the help of other proteins to form large focal adhesions. While 8 of the 24 integrins can bind to the common RGD sequence found in many ECM molecules, others are able to bind to other ECM motifs (Humphries, Byron et al. 2006). LDV-binding integrins are able to interact with an acidic motif that is functionally related to RGD, allowing for additional interactions with fibronectin, fibrinogen and tenascin. Another set of integrins, known as A-domain β1 integrins, can directly interact with collagen and laminin. These integrins bind to collagen using a critical glutamate-containing motif (GFOGER) (Emsley, Knight et al. 2000). Syndecans are a family of membrane proteoglycans that act as receptors for ECM molecules and growth factors. These molecules allow cells to snare and interact

with a wide variety of ECM molecules and can play a critical role in integrin based focal adhesion formation (Bernfield, Gotte et al. 1999).

2.1.2 Hierarchical structural organization of the ECM

The building blocks of the ECM are organized into an hierarchical structure to provide distinct mechanical function in tissues. In the case of collagens, procollagen molecules are extracellularly cleaved and then assembled into larger structures. In the case of tissues like tendon and ligament, which are subjected to large tensile loads in one preferential direction, collagen molecules are organized into a highly aligned and interconnected network to resist these loads. However, in the case of cartilage, which is subjected to large compressive loads, the collagen molecules resist a GAG induced swelling pressure in all directions, necessitating a network of fibrillar collagen without a single preferential alignment. Thus, ECM hierarchy is highly dependent on both tissue type and the particular mechanical function of the tissue.

2.1.3 ECM mechanical function

Understanding and describing native tissue mechanical properties is important in determining how physiologic forces are transmitted through the multi-scale ECM to the level of the cell to regulate function. These same properties can serve as benchmarks in the development and validation of novel biomaterials or engineered replacement tissues, especially in the case of load bearing tissues. Important properties to understand in this context are the elastic modulus, anisotropy, non-linearity and viscoelasticity of a given

tissue. These mechanical properties of the ECM can be quantified and described using solid mechanics (Gurtin 1981).

Elastic Deformations:

When force is applied to a tissue, it elongates in the direction of force application. In some cases, this deformation is instantaneous and increases linearly as the load is increased, following Hooke's law, which can be used to describe many elastic materials:

$$\frac{F}{A} = \sigma = E\varepsilon = E\left(\frac{l + \Delta l}{l}\right)$$

Where σ is the stress (force over area) and ε is the strain (normalized elongation) in the material. This relationship can be used to determine the material property E, known as the Young's modulus of the material (**Figure 2-2A**). In elastic materials, the applied deformation can be fully reversed when the load is removed. Under normal physiologic loading, some tissues act as elastic materials, and recover completely from the applied deformation when the load is removed. Often, these tissues also display deformation in the unloaded directions. That is, when a tensile load is applied in one direction, there is a contraction in the directions perpendicular to that, resulting in a decrease in the cross-sectional area of the tissue. This behavior is known as the Poisson effect and the relative magnitude of these perpendicular strains is referred to as the Poisson's ratio (ν_{xy}) (**Figure 2-2D**), another material property that is likely important not only for tissue function but for facilitating the cellular response within a tissue. Tissues that are required to withstand very large loads in one direction, such as tendons and ligaments, tend to display a very large Poisson's ratio because of the highly aligned and crimped ECM structure that is

required to withstand this intense uniaxial loading (Reese, Maas et al. 2010). This itself is yet another important mechanical characteristic of tissues and is referred to as anisotropy.

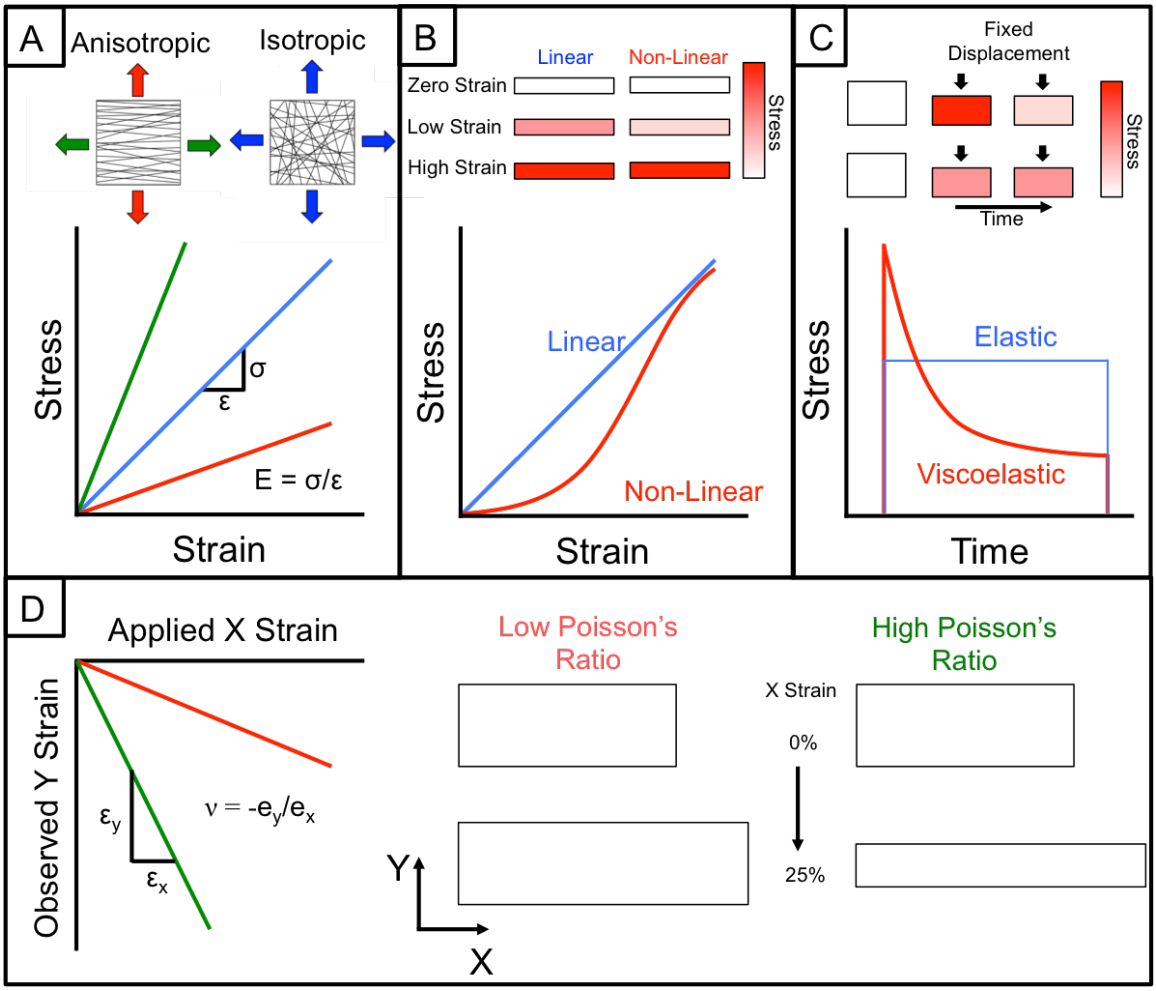

Figure 2-2: Mechanical attributes important for tissue function. Tissues that are loaded heavily in a single direction, often display anisotropy (A), or preferential alignment of ECM molecules in one direction. This results in mechanical properties that are significantly higher in one direction such that the ratio of stress to strain (modulus, E) is higher in that direction. Fibrous tissues also often display non-linearity (B) such that the ratio of stress to strain is not constant. Viscoelasticity is a common characteristic of hydrated tissues that are exposed to large compressive loads (C) and results in a time dependent stress-strain response. Another mechanical parameter that is regulated by tissue structure is the Poisson's ratio (D).

This is defined as the ratio of strains in the perpendicular vs. applied strain direction. Some tissues stretch while showing very little compression in the transverse direction. Other tissues, that possess a high degree of anisotropy, can display very large lateral compressive strains that surpass the applied strain.

Isotropy vs. Anisotropy:

Tissues with a very high degree of alignment in one direction are referred to as mechanically anisotropic, meaning that they have direction dependent mechanical properties (**Figure 2-2A**). In the case of a single fiber direction, these tissues are referred to as transversely isotropic, meaning they have equal mechanical properties in any plane transverse to the fiber direction but display different mechanical properties in the fiber direction. Higher orders of anisotropy also exist in some tissues, with some displaying multiple levels of transverse isotropy and others displaying distinct mechanical properties in each direction. Other tissues, which display equal properties in all directions, are referred to as isotropic. This isotropy or anisotropy is governed by the organization of the ECM molecules within the tissue and can range from very anisotropic to almost perfectly isotropic. This organization is important for the mechanical function of a tissue and can influence the mechanical cues seen by cells. Often this organization can be altered with increased tissue deformation resulting in strain dependent mechanical properties, referred to as non-linearity.

Non-Linearity:

Highly aligned tissues often display a crimped or wavy structure in their unloaded configuration, where the collagen fibers undulate with a defined periodicity. During early phases of deformation of such tissues, these crimped fibers straighten, followed by

a phase in which the straightened fibers elongate. This gives rise to a stress versus strain curve that has two distinct regions (**Figure 2-2B**). The first region is referred to as the 'toe' region that has a lower elastic modulus while the second 'linear' region has a higher elastic modulus. This crimp structure, along with the associated non-linear stress-strain response is an essential mechanical characteristic that enables tissue to undergo low force deformations (so that energy expenditures can be minimized) while at the same time providing for a higher modulus at greater strains (protecting the tissue from undue deformations).

Viscoelasticity:

Another structural feature of tissues that can regulate the stress-strain response is the viscoelasticity. Biologic tissues are highly hydrated and often contain fixed negative charges that are covalently bound to the ECM, especially in the case of proteoglycan rich tissues such as cartilage. Solids are capable of displaying perfectly elastic material properties, in that load immediately induces a strain and that this strain is recovered immediately following the release of load. Tissues however, especially those rich in water and fixed charges, display time-dependent strain in response to a step load, due to their viscous water component (Figure 2-2C). Thus, most tissues are referred to as viscoelastic, displaying properties of both an elastic material and a viscous fluid. The combination of water and fixed charge in biologic tissues also induces a hydrostatic pressure within the tissue that can play a critical mechanical role, but also regulates the cellular deformations within a tissue in a time dependent manner (Screen, Toorani et al. 2013).

2.2 Multi-scale strain transfer and its regulation of cellular behavior

While the primary purpose for the organization and composition of a tissue is to provide structure and mechanical function, tissue structure also regulates the manner in which mechanical signals are transduced to and experienced by cells within. Both the mode and magnitude of the mechanical load are important for regulating cell behavior, and it is the transfer of these macro-scale deformations to the micro-scale, where cells reside, which regulates the cellular response. Additionally, intracellular structures can play a role in transmission of strain through the cell, affecting the extent to which mechanosensitive proteins within the cell are activated, and regulating the cellular interpretation of specific mechanical signals.

2.2.1 Macro scale mechanical signals and their modes/magnitudes

Loading Modes:

The types of mechanical loads that tissues are subjected to can range from relatively simple unidirectional loading, like those seen in tendon, to more complex multidirectional loads like those seen in the intervertebral disc (O'Connell, Johannessen et al. 2007) or the aortic arch (Draney, Herfkens et al. 2002). Common modes of tissue loading include tension, compression, and shear. The structure and composition of a tissue are matched to withstand a specific loading environment and the resident cells respond favorably to 'normal' loading of that tissue and unfavorably to 'abnormal' loading. Changes in tissue loading boundary conditions and strain mode often lead to

tissue adaptation. For example, in tendon that is surgically wrapped around bone such that increased compressive loading occurs, there is tissue adaptation resulting in the formation of a fibrocartilaginous metaplasia (Wren, Beaupre et al. 2000). Additionally, in the case of athletes that train to perform repetitive overhead throwing, adaptations to the shoulder joint and its tendons can occur.

Loading Magnitudes:

The magnitudes of stress and strain a tissue is subjected to are also highly variable, as are the cellular responses to these signals. In the case of tissues such as tendon and cartilage, strains on the order of ~50% result in detrimental cellular responses (Legerlotz, Jones et al. 2013). However, in tissues such as lung, these strains are perfectly normal and necessary for homeostasis of the tissue (Napadow, Mai et al. 2001, Gutierrez, Suzara et al. 2003). Often, tissues will remodel to reduce excessive strains (Eberth, Cardamone et al. 2011) when possible, or will otherwise deteriorate due to failure events (Fung, Wang et al. 2010) that occur when exposed to excessive strains.

There are numerous examples of tissues that adapt to changes in loading magnitude. Muscle and bone are two of the most obvious examples, both exhibiting an increase in tissue mass with increased usage/loading and a decrease when under-loaded. In bone, this was first described in 1892 by the German anatomist and surgeon Julius Wolf (Frost 1994). These types of changes are often apparent in athletes, such as tennis players that use a dominant arm, leading to increases in bone and muscle mass in that arm (Kontulainen, Sievanen et al. 2003). Loading related changes are also obvious in other

musculoskeletal soft tissues such as tendon and cartilage. For example, in the case of overloaded tendon, fatigue damage can accumulate with time, leading to decreased mechanical properties and inducing a cellular remodeling response (Fung, Wang et al. 2010).

The cardiovascular system is also highly regulated by mechanical loading, adapting by growing or shrinking based on the magnitude of the mechanical signals observed. Major mechanical signals experienced in the cardiovascular system are the fluid (blood) hydrostatic pressure as well as the fluid shear stress imposed on cells lining the blood vessel walls (Chen, Li et al. 1999). It has been shown that with exercise, shear stress can regulate conduit artery wall thickness (Thijssen, Dawson et al. 2011). Similarly, these types of changes can occur in disease. In the case of extended hypertension, the increases in fluid shear are thought to result in fibrotic changes in both cardiac (Heagerty, Aalkjaer et al. 1993) and renal tissues (Grabias and Konstantopoulos 2014). These changes then perpetuate the disease state by increasing both vascular resistance and shear stress. Additionally, increases in loading magnitude in the cardiovascular system can induce remodeling. For example, when hypertension is induced in a mouse model via aortic banding, both thickening and stiffening of the aortic wall occurs as an adaptation to the increased hemodynamic pressures (Eberth, Cardamone et al. 2011).

2.2.2 Transfer from tissue to cell

In addition to the mode and magnitude of strain regulating the cellular response, the extent to which strain is magnified or attenuated as it is transferred from tissue scale to cell scale can impact the cellular response (Bruehlmann, Hulme et al. 2004, Screen, Lee

et al. 2004, Upton, Gilchrist et al. 2008, Han, Heo et al. 2013). Strain transfer is dependent on both the structure and composition of the ECM. For instance, collagen fiber sliding can lead to both attenuation and magnification of strains at the cellular level (Bruehlmann, Matyas et al. 2004). Additionally, concentrated pockets of ECM molecules, such as those observed in the knee meniscus, can attenuate strain transfer to the cells within (Han, Heo et al. 2013). In addition to these structural features regulating strain transfer to the cells, the specific molecules that cells bind to can play an important role in regulating how a cell responds to a specific tissue stiffness or specific mechanical perturbation.

The adhesions that the cell makes to the ECM are crucial in regulating both transmission of strain through the cell (Maniotis, Chen et al. 1997) and the activation of mechanosensitive molecules at the cell surface (Chen, Li et al. 1999). Cells interact with ECM molecules using both integrins and syndecans. Integrins interact with numerous cytoskeletal elements, allowing for transfer of strain across the cell membrane and into the structural network of the cell. Different integrins bind to specific ECM proteins that a cell is in contact with, and can regulate the manner in which a cell interprets a specific mechanical signal (Seong, Tajik et al. 2013).

2.2.3 Transfer from cell to nucleus/signal output

Once a mechanical signal reaches the cell, it can activate stretch sensitive signaling molecules at the cell surface or be transmitted deep within the cell through the network of structural cytoskeletal proteins. There are numerous mechanotransduction pathways that

mediate the transfer of mechanical signals into changes in biochemical reaction kinetics and gene expression. Mechanical force applied to the extracellular matrix results in deformations of the cell adhesions and the cellular membrane, and these deformations can activate a number of mechanosensitive membrane proteins (Orr, Helmke et al. 2006). Forces are also transmitted via the cytoskeleton to the nuclear membrane (Maniotis, Chen et al. 1997) and can result in rapid mechanical activation at sites distant from the cell membrane (Na, Collin et al. 2008) and within the nucleus (Guilluy, Osborne et al. 2014). Thus, it has been proposed that changes in nuclear morphology and strain of nuclear membrane proteins may provide a more direct mechanotransduction pathway centered at the nucleus (Wang, Butler et al. 1993). Indeed, modulation of nuclear shape results in significant correlative changes in gene expression (Thomas, Collier et al. 2002). The nucleus is also considerably stiffer (2-4 fold) than the rest of the cell (Guilak, Tedrow et al. 2000), and this stiffness can increase as a function of differentiation (Pajerowski, Dahl et al. 2007). Thus, mechanotransduction in the natural ECM is dependent on a network of tissue specific strain transfer machinery that regulates transmission of organ level strains, over multiple length scales, to protein level strains within the resident cells. Inherent within this system are a number of highly controlled feedback mechanisms through which cells and matrix inform and direct each other. The first level of activation occurs at the cell membrane, and can involve opening of stretch sensitive ion channels (Folgering, Sharif-Naeini et al. 2008), release of signaling molecules (Burnstock 2009), activation of cell surface receptors (Pan, Ma et al. 2012), or activation of cellular adhesion sites (Tzima, Irani-Tehrani et al. 2005, Geiger, Spatz et al. 2009). These signals

are then amplified and propagated through biochemical signaling cascades (Kolch 2005) that ultimately result in changes in gene expression.

Many mechanosensory elements are located near or within the cell membrane and can be activated by numerous types of external as well as cell generated forces. These mechanosensory events are dependent on both the type and organization of the ECM molecules through which forces are transmitted and can initiate soluble signaling cascades within the cytoplasm that eventually result in changes in cellular behavior, activity, and transcription.

Stretch Sensitive ECM Proteins

There are a number of ECM proteins located near the cell membrane which themselves have been shown to be stretch sensitive. These proteins can signal through exposure of cryptic binding domains or through release of bound growth factors with mechanical deformation. As mentioned, cells bind to different ECM molecules using different integrins. In the case of binding to fibronectin, the α5 integrin binding site within fibronectin is hidden in the absence of tension (Seong, Tajik et al. 2013). However, as tension builds (with increasing substrate rigidity, for example), this integrin-binding site is exposed, allowing for activation of focal adhesion kinase (FAK). Interestingly, this is not the case for the α2 integrin binding site within collagen I. For collagen, integrin binding and FAK activation occurs independently of collagen tension, and can even occur when soluble collagen is added to non-adherent cells (Seong, Tajik et al. 2013).

In addition to mechanosensitive ECM molecules at the cell surface, there are also pockets of growth factors stored within the ECM near the cell membrane that can be made available upon cell and/or tissue deformation. These pockets can be activated and released when cell generated tractions are applied to the ECM, resulting in downstream activation of cellular surface receptors for these growth factors. One example of this is the growth factor TGF-β1, which has been shown to form extracellular pockets in cultured lung myofibroblasts (Wipff, Rifkin et al. 2007). Growth factors can also be released from the cell itself in response to loading, initiating what is referred to as autocrine signaling (acting on self) and paracrine signaling (acting on nearby cells). Pressure applied to vascular endothelial cells causes rapid activation of endothelial growth factor receptor (EGFR) and ERK 1/2 via release of EGF, which acts in an autocrine manner to activate cells (Tschumperlin, Dai et al. 2004). In cardiac myocytes, BMP-2 acts as an autocrine/paracrine factor that activates the transcription factor GATA-4 (Tokola, Rysa et al. 2014). Cartilage has also been shown to use autocrine/paracrine signaling. With pressure induced strain, chondrocytes display increased membrane potentials that are dependent on the presence of the cytokine interleukin 4 (Millward-Sadler, Wright et al. 1999). Often, autocrine and paracrine signaling can induce opening of ion channels. One of the most studied examples of this is the purinergic signaling pathway, which involves the release of ATP.

Stretch Sensitive Ion Channels

There are a number of ion channels within the cell membrane that are stretch sensitive, opening when force is applied. For example, in endothelial cells it has been observed that

in response to membrane stretch, applied by a patch electrode, the opening frequency of calcium channels in the membrane increases (Lansman, Hallam et al. 1987). Calcium signaling cascades can also be activated through purinergic signaling, under which stimulated cells release ATP through hemi-channels or vesicular exocytosis. This ATP can then activate P2 receptors on the cell surface, leading to rapid opening of voltage activated calcium channels (Burnstock and Ralevic 2014). These calcium signals can then lead to downstream transcriptional changes via calcium binding proteins such as calmodulin (Berridge, Bootman et al. 2003).

Piezo channels are a type of ion channel that is mechanosensitive. These are stretch sensitive non-selective cation channels that open when force is applied to the cell membrane. Piezo channels are very large transmembrane proteins, predicted to span the membrane between 30 and 40 times (Volkers, Mechioukhi et al. 2014). In many cells, these proteins are important for sensing gentle touch stimuli and in others, can provide sensing of noxious mechanical stimuli (Volkers, Mechioukhi et al. 2014). These channels have been shown to be constitutively active in liposomes, indicating that cytoskeletal proteins are not necessary for their function (Gottlieb and Sachs 2012) but may be required in order to maintain their mechanosensitivity. Many other stretch sensitive ion channels, such as ENaC, TRPM4, TRPM7, TREK1, TREK2, and TRAAK channels are known to be sensitive to membrane tension, and in many cases dependent on cytoskeletal elements to activate appropriately (Martinac 2014). Other channels however, are mechanosensitive even in artificial bilayers that lack cytoskeletal

components (Brohawn, Su et al. 2014), increasing their opening probability in proportion to the level of tension applied the membrane.

Membrane proteins can also be sensitive to osmotic changes that cause activation with mechanical loading. In tissues like cartilage that are rich in proteoglycan and contain a high density of fixed charges, tissue loading can induce large changes in osmotic stress. Cells within these types of tissues often express high levels of the transient receptor potential vanilloid 4 (TRPV4) calcium channel (Phan, Leddy et al. 2009). This particular channel is highly sensitive to changes in osmolarity, allowing for sensation of mechanical signals via the changes in osmolarity that they produce (Mow, Wang et al. 1999). In tissues such as cartilage, this has been shown to be one of the main mechanisms by which cells sense mechanical signals (O'Conor, Leddy et al. 2014), and signaling through these channels is indispensible for appropriate tissue homeostasis (O'Conor, Griffin et al. 2013). Additionally, it has been shown that pharmacologic agonists directed at this channel can stimulate engineered cartilage to produce increased levels of ECM molecules and improve mechanical properties without the addition of mechanical loading (O'Conor, Leddy et al. 2014).

Stretch Sensitive Adhesion Complexes

There are also a number of force sensitive molecules that localize to cell-ECM adhesion complexes (Geiger, Bershadsky et al. 2001). Over the last decade, the specific roles each of these proteins play has started to come into focus, due in large part to the use of new techniques such as super resolution microscopy (Kanchanawong, Shtengel et al. 2010),

atomic force microscopy (AFM) (del Rio, Perez-Jimenez et al. 2009) and FRET based molecular force sensors (Grashoff, Hoffman et al. 2010).

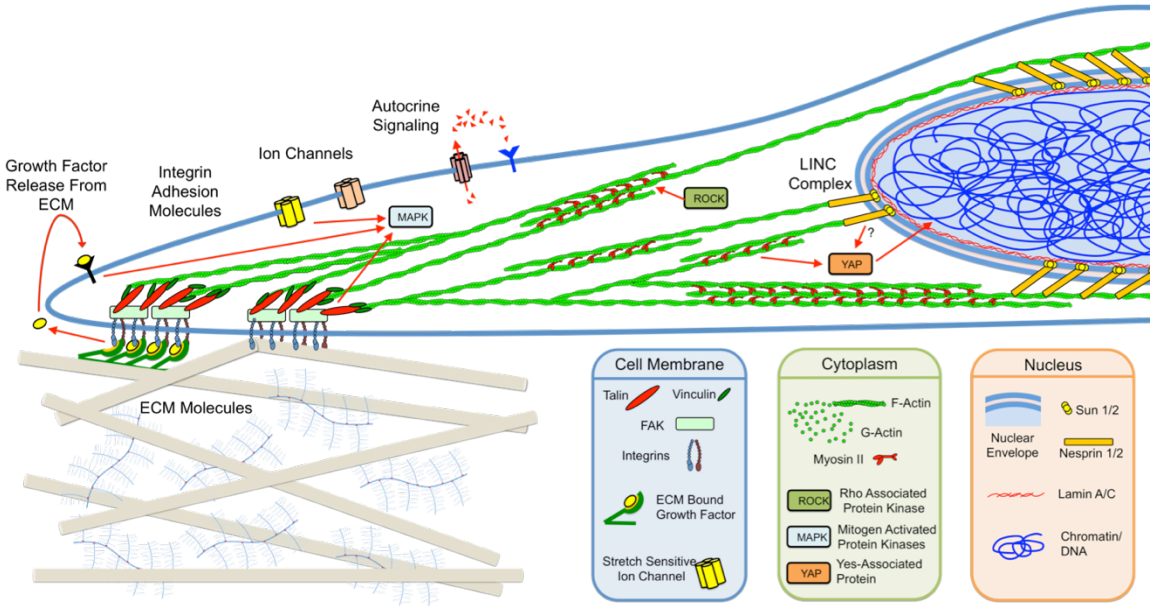

Figure 2.3: Cells sense mechanical signals through numerous mechanosensitive pathways. They probe the mechanics of their ECM environment, using their contractile actin cytoskeleton to pull on integrin connections to the ECM. At the cell membrane many proteins can sense mechanical force, including stretch sensitive ion channels and stretch sensitive adhesion molecules. The contractile cytoskeleton is also connected to intracellular structures like the nucleus, allowing for transmission of forces into the cell.

One of the first force sensitive adhesion molecules discovered was focal adhesion kinase (FAK). FAK is an adhesion scaffolding protein that can also act as a kinase when phosphorylated by Src family kinases. FAK has many cellular functions and plays a role in numerous cellular activities. It is located at the base of adhesions, close to the cell membrane (Kanchanawong, Shtengel et al. 2010), due to its direct interactions with integrins. FAK can play an important role in the initiation of adhesion formation, but is not required for adhesions to form (Calderwood, Campbell et al. 2013). Because of FAK's close associations with integrins, part of its force sensing ability comes from the

force dependent unfolding of the fibronectin within the ECM that integrins are bound to. FAK is also able to bind a number of other adhesion molecules, including Talin, Paxillin, Grb2, Ezrin, Src and p130Cas (Grigera, Jeffery et al. 2005). Additionally, FAK activation can lead to activation of a number of other downstream soluble signaling pathway, such as the ERK 1/2 MAPK signaling pathway (Franchini 2012).

Another force sensitive adhesion molecule with the ability to bind integrins and regulate adhesion size and stability is Talin. Talin is composed of a head domain, which binds phosphoinositide membranes and beta integrins, and a tail domain, which binds to actin and other adhesion molecules. The talin molecule itself has been shown to be mechanosensitive, undergoing conformational changes with applied force that regulate binding to other adhesion molecules. Specifically, it has been shown in single molecule AFM experiments that force applied to talin results in at least three independent vinculin binding events (del Rio, Perez-Jimenez et al. 2009), indicating that talin senses force and can recruit vinculin when force is applied.

Vinculin is another adhesion complex molecule that can undergo force dependent folding and unfolding, leading to destabilization or stabilization of adhesions. Using an engineered FRET tension sensor that was incorporated into the vinculin molecule, it has been shown that high tension on vinculin leads to assembly of adhesions and that low tension on vinculin leads to their disassembly (Grashoff, Hoffman et al. 2010). While vinculin is not necessary for focal adhesion growth, it is important for coupling of adhesions to retrograde actin flow and for generation of traction forces on substrates

(Thievessen, Thompson et al. 2013). Additionally, mutations in the vinculin tail domain result in much slower disassembly of adhesions when traction force is removed, via the inhibition of rho kinase. Moreover, loss of this actin binding tail region of vinculin perturbs the cells ability to repolarize in response to cyclic stretching (Carisey, Tsang et al. 2013). This indicates that a major role for vinculin is to stabilize adhesions and to sense when adhesions should be disassembled. It has also been shown that vinculin recruitment to adhesions is regulated by FAK mediated phosphorylation of another adhesion protein paxillin (Pasapera, Schneider et al. 2010). Thus, mechanosensing at adhesions is dependent on a complex interplay between multiple adhesion molecules.

Integrin based adhesion molecules are crucial for cell-matrix adhesions and the mechanical signaling that occurs through these adhesions. However, another class of adhesive molecules, known as cadherins, can play a critical role in cell-cell adhesions and regulate mechanotransduction events that occur between cells that are directly touching. These cell-to-cell connections are very important in mechanical signaling that regulates development of tissues (Gumbiner 2005, Harris and Tepass 2010) as well as in the normal homeostasis of tissues with high cell content. The specificity, strength, and signaling that occurs through these cell-cell adhesions allows for the formation of complex 3-dimentional tissue structures through the processes of polarization, invagination, intercalation, sorting, convergence and extension (Gumbiner 2005). At the sites of these cadherin cell-cell junctions there are cytoskeletally-connected adhesions that form and are composed of multiple adhesion molecules. These adhesion molecules also display sensitivity to mechanical force. For example, in vascular endothelial cells it

has been shown that a cadherin based complex composed of PECAM-1, VE-cadherin, and VEGF receptor 2 is essential for the fluid shear stress induced reorientation of cells, and that this complex plays a role in aortic inflammatory NF-κB signaling in vivo (Tzima, Irani-Tehrani et al. 2005). Interestingly, some molecules which are traditionally thought to be mostly important for integrin based mechanosensing, such as vinculin, also localize in a force dependent manner to cell-cell cadherin based connections, and can play a role in strengthening these adhesions (Miyake, Inoue et al. 2006, Thomas, Boscher et al. 2013). It has also been shown that twisting of magnetic beads coated with cadherins triggers actin, alpha-catenin and E-cadherin dependent cell stiffening (le Duc, Shi et al. 2010, Barry, Tabdili et al. 2014). In summary, both cell-cell adhesions and cell-ECM adhesions can play a critical role in the formation of organized tissues and the mechanosensing that occurs within tissues. Both types of adhesions are also known to transmit forces intracellularly, allowing for activation of additional force sensitive molecules within the cell.

Cytoskeletal mechanotransduction

Once force has been transmitted through the cell membrane via cytoskeletally associated adhesion molecules, it can be transferred to the cytoskeleton, and on to subcellular organelles. Force applied to integrin molecules at the cell surface, via RGD coated magnetic beads, is resisted by the presence of an intact actin cytoskeleton (Wang, Butler et al. 1993). When actin polymerization is inhibited using cytochalasin D, larger cell strains are observed for the same level of force (Wang, Butler et al. 1993). Thus, extracellular forces can be transmitted across the cell surface to the cytoskeleton. Within

the cytoskeleton there exists another set of mechanosensitive molecules, which can be activated with stretch. The activation of these molecules is heavily dependent on the tension within the pre-stressed cytoskeletal network. One such molecule is the tyrosine-protein kinase Src. Using a similar surface bound magnetic bead system, in combination with a florescent Src activity reporter, it has been shown that force applied to the cell surface can induce rapid activation of Src at sites deep within the cytoskeleton that co-localize with sites of large microtubule displacements (Na, Collin et al. 2008). This activation is dependent on the presence of actin filaments as well as tension within those filaments (Wang, Butler et al. 1993).

Another cytoskeletally dependent mechanosensor is the YAP (Yes-associated protein) / TAZ (transcriptional coactivator with PDZ-binding motif) complex, which has been shown to be important for sensing of both substrate stiffness (Dupont, Morsut et al. 2011) and stretch within a 3D network (Bertrand, Ziaei et al. 2014). These two transcription factors are activated and translocate to the nucleus on stiff (40kPa) substrates but are not activated on soft (0.7kPa) substrates. This activation is dependent on the ability of the cell to spread and exert tension on its microenvironment using the contractile actin cytoskeleton (Dupont, Morsut et al. 2011). Further, these proteins have been shown to play a critical role in substrate stiffness dependent stem cell fate decisions. Knockdown of YAP and TAZ or inhibition of cell contractility prevents osteogenesis induced by stiff substrates and instead induces adipogenesis (Dupont, Morsut et al. 2011).

Nuclear mechanotransduction

Numerous mechanosensitive proteins are dependent on the cytoskeleton for activation, and once force has been transmitted through adhesions and the cytoskeleton, it may converge at the nuclear envelope to instigate additional signaling processes (**Figure 2-3**). While the nucleus is traditionally thought to function solely as the container of for the cells genome that regulates transcriptional processes, recent findings have shown additional non-genomic functions that impact the entire cell, including cytoskeletal organization and function. The nuclear envelope contains a number of cytoskeletal binding proteins that have been shown to display force sensitivity. Indeed, the transmission of this force to the nuclear envelope is dependent on both a patent cytoskeleton and connections it makes with the cytoskeleton. Physical cytoskeletal to nuclear interactions were first shown via micromanipulation of subcellular deformations (Maniotis, Chen et al. 1997). In that work, actin and intermediate filaments were shown to be necessary for stabilization of the nucleus whereas inhibition of microtubule assembly decreased nuclear movement when a needle was pulled through the cytoplasm (Maniotis, Chen et al. 1997). More recently, it has been shown that a class of spectrin repeat containing structural proteins, known as nesprins, make connections with actin (Padmakumar, Abraham et al. 2004, Crisp, Liu et al. 2006), intermediate filaments (Wilhelmsen, Litjens et al. 2005), and microtubules (Roux, Crisp et al. 2009) that are important for the transmission of strain to the nuclear envelope (Lombardi, Jaalouk et al. 2011).

These nesprin connections to the nuclear envelope make up a complex that is referred to as the linker of the nucleoskeleton and cytoskeleton (LINC complex) and is composed of

membrane bound structural proteins that interact with cytoskeletal and chromatin elements. These proteins include nesprins 1-4, SUN 1-2, lamin A/C, and emerin as well as a number of others. Nesprins are located in the outer nuclear membrane and make connections between cytoskeletal elements and SUN proteins. Nesprins 1 and 2 contain an actin binding calponin homology domain at their N-terminus, enabling connections to F-actin structures (Zhang, Skepper et al. 2001, Padmakumar, Abraham et al. 2004). SUN proteins are embedded in the inner nuclear membrane and connect nesprins to the nuclear lamina (Crisp, Liu et al. 2006). This nuclear lamina is made up of a number of intermediate filament proteins including A and B type lamins and emerin (Simon and Wilson 2011). A number of these LINC complex proteins are force sensitive. Lamin A/C, for instance, scales with both tissue and nuclear stiffness across multiple orders of magnitude (Swift, Ivanovska et al. 2013), from the softest tissues, like brain and fat, to the stiffest tissues, like bone. Furthermore, increases in substrate stiffness change both the phosphorylation and turnover of lamin A/C (Buxboim, Swift et al. 2014). Another LINC complex protein, emerin, is phosphorylated in response to force applied through nesprin 1 to isolated nuclei, and this phosphorylation recruits lamin A/C to the nuclear envelope, stiffening the nucleus (Guilluy, Osborne et al. 2014). Lamin A/C and emerin have also been shown to play a role in the previously mentioned YAP/TAZ (Guilluy, Osborne et al. 2014) and MRTF (Ho, Jaalouk et al. 2013) pathways, indicating that changes in the LINC complex may provide feedback through cytoskeletal changes that affect mechanotransduction.

Because of the fact that the LINC complex forms direct connections to the chromatin within the nucleus, it has been postulated that forces applied to the nucleus through the LINC complex may act to directly regulate chromatin structure, resulting in epigenetic changes in chromatin that regulate gene expression and cell phenotype (Wang, Tytell et al. 2009, Martins, Finan et al. 2012). Despite the fact that almost every human cell has two copies of the genome with all the information that gives rise to an organism, histone proteins organize the DNA within the genome such that specific cellular phenotypes are produced. Histone proteins can undergo multiple types of modification, which regulate their structure and function, and include methylation, acetylation, phosphorylation, ubiquitination, and SUMOylation of lysine residues (Martins, Finan et al. 2012). This combination of DNA and modified histone proteins can exist in either a lightly compacted euchromatin state or a more highly compacted heterochromatin state. Euchromatin is thought to be more permissive to transcription and correlates with regions of DNA that are actively being transcribed, whereas the dense nature of heterochromatin makes it less permissive to transcription and correlates with silenced genes. Interestingly, chromatin structure can be regulated by mechanical cues. The organization of the substrate which cells are adherent to regulates both histone deacetylase (HDAC) activity and histone H3 acetylation state (Li, Chu et al. 2011), with aligned microgroove substrates inducing more H3 acetylation. Imposing geometric constraints on cell spreading area also regulates HDACs, with larger spread areas resulting in lower nuclear HDAC3 and higher H3K9 acetylation levels (Jain, Iyer et al. 2013). Osmotic mechanical signals can also alter chromatin density. Within seconds following hyperosmotic challenge, chromatin structure is dramatically altered in chondrocytes (Irianto, Swift et al.

2013). Similarly, force applied to cells using a magnetic bead system induces rapid and reversible changes in chromatin structure that is dependent on the presence of actin filaments (Iyer, Pulford et al. 2012). Combined, these results indicate that the nucleus itself is mechanosensitive, responding to forces transmitted through the actin cytoskeleton and the LINC complex.

Mechanotransduction in the native tissue environment occurs at multiple scales, requiring transmission of strain from the tissue level, through ECM molecules to the cells within. Once mechanical signals reach the cell, mechanosensing events can occur at the cell membrane or at sites within the cell, as force is transmitted through the cytoskeleton and to the nucleus. This multi-scale strain transfer is heavily dependent on the composition and organization of the ECM as well as the boundary conditions of the mechanical loads that are applied. The mechanosensing that occurs within this multi-scale structure is important not only for normal tissue homeostasis, but can also play a role in both development and degeneration of a tissue.

2.3 Mechanical Loading in ECM Development, Homeostasis, and Degeneration

Mechanical loading plays a crucial role both the formation and development of numerous tissues within the body. Force regulates the formation of strained tissues of the cardiovascular, pulmonary and musculoskeletal systems such as blood vessel, heart, kidney, lung, muscle, tendon, cartilage, bone and fibrocartilage (Mammoto and Ingber 2010, Shwartz, Blitz et al. 2013). Additionally, mechanical forces generated by cells play

an important role in the formation of tissues that see fairly little mechanical loading, such as brain (Franze 2013), lymphatics (Schwartz and Simons 2012), and mammary glands (Zhu and Nelson 2013). Mechanical forces are also important for the normal maintenance of the ECM within tissues, stimulating cells to degrade, produce, and replace old or deteriorating matrix molecules. Thus, when loading is removed, many tissues undergo atrophy and deterioration. Overloading can also have detrimental affects, resulting in structural changes and failure events that lead to degeneration. Additionally, mechanical factors can play a role in genetic diseases, causing cells to misinterpret mechanical forces, produce inappropriate mechanical forces, or deposit inappropriately stiff matrix. Several case examples of loading in development, homeostasis, and disease processes are provided below.

2.3.1 Development

Temporal control

The developmental process as a whole relies on exquisitely controlled timing of signaling events, many of which involve the timing at which muscular or cellular mechanical forces are present. In the case of the lymphatic and cardiovascular systems, for example, pumping of the heart and movement of fluid is required prior to valve formation, and in the absence of a beating heart, many valves and vessels will not form (Lucitti, Jones et al. 2007). In the case of the knee meniscus, joint forces applied through the musculature are required for its formation in the embryo. When these forces are absent, the knee meniscus fails to form (Mikic, Johnson et al. 2000) (**Figure 2-4A**). Additionally, these muscle forces are important for joint formation. The loss of muscle forces acting on the

joint results in joint loss at the elbow, shoulder, wrist, metacarpals and hip (Kahn, Shwartz et al. 2009). This is because muscle forces are required for maintenance of progenitor cell fate and for disruption of the cell-cell cohesion that occurs at the joint surface. These forces are also responsible for altering the synthesis and degradation of ECM components. One such component is hyaluronic acid, which becomes apparent at the joint line when cavitation is initiated (Craig, Bayliss et al. 1990). High levels of HA at the joint line are though to promote cell separation by saturating HA binding proteins on the cell surface, leading to decreased ECM mechanical properties. While these tissue level forces applied through the musculature are crucial for the formation of complex tissue structures, there are also cellular forces that are necessary for very early tissue formation.

Spatial control

Very early in the developing embryo, mechanical connections between cells play a critical role in the sorting of progenitor cells into the three different germ layers. This sorting is driven by tissue surface tension, which acts at intercellular membrane adhesions. Based on different adhesion strengths, cells can separate into groups, similar to the manner in which liquid drops with different surface energies separate (Steinberg 1963). This cell sorting is dependent on the cadherin connections between cells, with the surface expression level of cadherin correlating linearly with the tissue surface tension (Foty and Steinberg 2005). In fact, mixing of two cell populations expressing different levels of the same cadherin molecule can result in separation of the cells into a core shell structure, with central region cells expressing high levels of cadherin and outer regions

cells expressing lower cadherin. Traction forces induced by gradients in growth factor release can also drive cell sorting. In zebra fish, the different germ layers display differential actomyosin based cell-cortex tension that is regulated by TGF-β signaling and is a key factor in progenitor cell sorting (Krieg, Arboleda-Estudillo et al. 2008). Indeed, many developmental processes require cellular traction forces (Mammoto and Ingber 2010).

Once cells have been sorted, many tissue structures are formed by folding and dorsal closure events that occur within a sheet of cells. Folding events are initiated by cells that constrict their apical membrane while expanding their basal membrane. This involves local myosin enrichment at the apical membrane and is dependent on cytoskeletal force generation (Sawyer, Harrell et al. 2010). Many soluble factors can play a role in this process, by regulating actomyosin based cellular contractility. This includes transcription factors such as Snail and Twist, which can induce collective cell contractions that are important for invagination (Martin, Kaschube et al. 2009). This can also include growth factors, like bone morphogenetic protein 2 (BMP2), which is important for appropriate ventral folding morphogenesis. Loss of BMP2 expression prevents foregut invagination and results in aberrant heart positioning (Gavrilov and Lacy 2013). Following invagination many tube like structures are formed through dorsal closure events. These are cytoskeletally driven changes in tissue shape, which cause cells within a sheet to come within close proximity of each other. Cells are then able to reach out towards each other with filipodial protrusions, closing the gap and fusing the tissue (Jacinto, Wood et al. 2000).

Cellular mechanical forces continue to be important as organs begin to form in the later stages of embryonic development. Bone and cartilage formation are both regulated by mechanical signals. Externally applied compressive loading of the rat ulna suppresses longitudinal growth by decreasing mineralization in the growth plate and increasing the size of the hypertrophic zone (Ohashi, Robling et al. 2002). In the developing kidney, fluid shear forces promote epithelial movements that are necessary for nephron formation in zebrafish (Vasilyev, Liu et al. 2009). These fluid forces are also important for the development of the aorta. When these forces are increased by artery ligation, chick embryos display increased type I and III collagen content that results in higher aortic mechanical properties (Lucitti, Visconti et al. 2006). In the developing mouse lung, loss of muscle contraction in the diaphragm induced by loss of the MyoD gene leads to pulmonary hypoplasia (Inanlou and Kablar 2003). This is the result of reduced lung cell proliferation and loss of the thyroid transcription factor-1 (TTF-1) gradient. Together, these results indicate that the mechanical forces experienced by cells within the developing embryo are important for organ formation, and that abnormal mechanical signals can cause severe developmental defects.

2.3.2 Homeostasis

Once a stable tissue has been developed, maintenance of this complex structure requires constant cellular input. Cells are continually breaking down and replacing molecules within the ECM, and this process is heavily dependent on mechanical input. Without appropriate mechanical input many tissues atrophy, degrading their structure and

mechanical properties, making them prone to injury. This is because, in heavily loaded tissues, cells make decisions for ECM remodeling based on these mechanical inputs. Some well-known examples of this are muscle and bone. In cases where muscle is not used for extended periods of time, due to immobility or casting of a joint, the muscles associated with that joint will degrade both their structure and force generating capabilities and the bones will often lose bone mass and density (Krasnoff and Painter 1999). This is also observed in astronauts, who display reduced bone and muscle mass after extended time in space (Carmeliet, Vico et al. 2001, Lang, LeBlanc et al. 2004). Tendon is also sensitive to loss of loading. Muscle inhibition has been shown to quickly decrease the expression of the tendon transcription factor scleraxis and results in decreased mechanical properties (Maeda, Sakabe et al. 2011) (**Figure 2-4B and 2-4C**). In the cardiovascular system, constant remodeling driven by mechanical factors is necessary for appropriate function. In cases where fluid flow in a vessel is blocked, vessel regression will quickly occur (Brownlee and Langille 1991, Meeson, Palmer et al. 1996, Baffert, Le et al. 2006). With extended bed rest, it has been observed that patients display reduced cardiac filling, stroke volume, and cardiac output (Krasnoff and Painter 1999). As is true with many tissues, when inappropriate mechanical loading (due to over or under loading) or inappropriate mechanosensing (due to genetic mutations) occurs, degenerative processes often ensue.

2.3.3 Degeneration

Many degenerative processes can be induced or perpetuated by mechanical loading. This can include degenerative changes caused by a single or multiple overloading events, but

can also be the result of inappropriate mechanical sensing by cells. Overloading events can induce immediate degradative and inflammatory cellular responses, but can also cause a slow progression of degenerative changes over a period of years, whereby cells exposed to super-physiologic loading respond by gradually remodeling the surrounding matrix. In the case of some diseases, where genetic mutations are involved, cells may deposit matrix that is inappropriately organized or composed, resulting in abnormal mechanical properties. In other cases, where cellular mechanosensory proteins are mutated, mechanical loading results in an inappropriate cellular response to load.

Overloading

Overloading can occur as the result of quick hyperphysiologic loads which induce large strains and lead to rupture of both ECM molecules and the cells embedded within, causing cell death and matrix degradation through release of matrix degrading enzymes. In the case of cartilage, rapidly applied stresses that reach 20-50 MPa cause rupture of matrix and extensive cell death in the superficial layer of cartilage (Lewis, Deloria et al. 2003). Isolated chondrocytes are able to withstand ~75% compressive strain before membranes rupture (Nguyen, Wang et al. 2009). However, the isolated chondrocyte membrane alone only has an elastic range of 3-4%, beyond which rupture occurs (Moo, Amrein et al. 2013). This discrepancy is due to the fact that chondrocytes are able to protect themselves from strains using a membrane reservoir, which extends when strain is applied, but is limited and dependent on the strain rate (Moo, Amrein et al. 2013). In the case of ligaments, cells respond to higher than normal strains (12-14%) by increasing matrix metalloproteinase activity. Specifically, the amount and activity of MMP-2 is

increased when these strains are applied to cells isolated from human anterior cruciate ligaments (Zhou, Lee et al. 2005). Less extreme hyperphysiologic loading over extended periods of time can also cause degenerative changes. In the case of tendon, overuse injuries are common in athletes. In particular, runners are prone to overuse injuries of the Achilles (Lorimer and Hume 2014) and overhead throwers are prone to overuse injuries in the rotator cuff tendons (Rizio and Uribe 2001). Normal loading is important for stimulating tendon cells to maintain the surrounding ECM. However, fatigue loading of tendons leads to fiber kinking and widening of the interfiber spaces (Fung, Wang et al. 2010) and can also cause tendon cells to express inflammatory cytokines, such as interleukin-6 (Legerlotz, Jones et al. 2013).

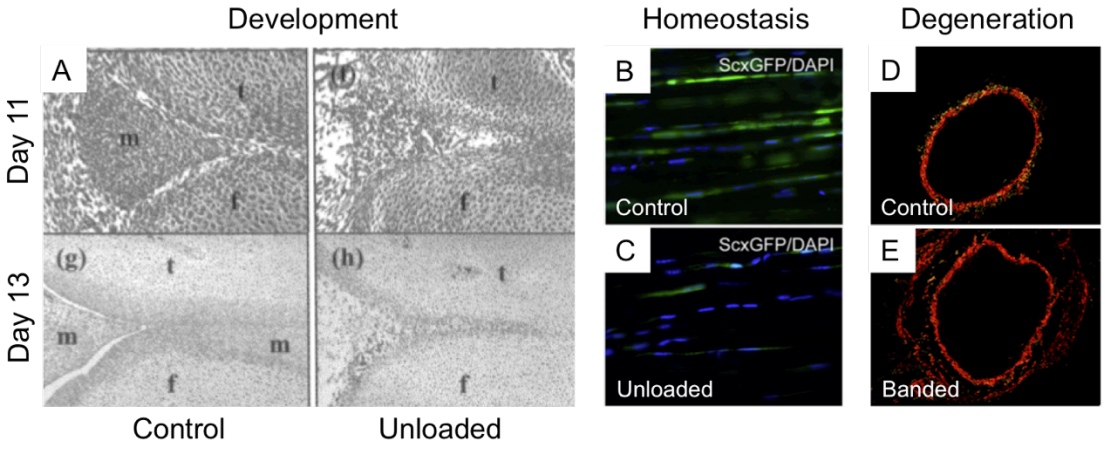

Figure 2-4: Mechanical loading regulates the development, homeostasis and degeneration of tissue extracellular matrix composition and function. In the developing meniscus, loading forces through the musculature are necessary for the formation of the tissue (A) (image adapted from (Mikic, Johnson et al. 2000)). Without this loading the meniscus does not form. In mouse tendon, muscle loading is necessary for maintenance of expression of the tendon transcription factor scleraxis (B,C) (adapted from (Maeda, Sakabe et al. 2011)). Without these muscle forces scleraxis expression is lost and the tendon ECM is not appropriately maintained, losing mechanical structure and function. Mechanical loading can also induce degenerative changes. In a mouse muscle model of hypertrophy, banding of the aorta results in fibrotic changes and an increases in aortic size due to alterations in mechanical forces sensed by endothelial cells (D,E) (adapted from (Eberth,

Cardamone et al. 2011)). This results in an increase in collagen I deposition and altered biaxial mechanical properties.

The cardiovascular system is also prone to chronic overloading induced changes in the ECM, brought about by resident cells. Cells within the cardiovascular system respond to both fluid shear stress and circumferential stretching induced by the pressure within the system. Blood pressure is regulated mainly by the diameter of smaller resistance arteries, which lead in to the capillary beds. When blood pressure is elevated, the cells within these resistance arteries contract so that blood flow is kept constant in the downstream capillaries. However, in a disease state, where blood pressure remains elevated for extended periods of time, these cells will remodel arterial walls, thickening the wall so that the increased tension can be resisted (Folkow 1993). This can eventually lead to changes in the compliance of the wall and compromises vessel elasticity (Intengan, Deng et al. 1999), preventing the system from responding to quick changes in pressure. This is likely due to the accumulation of collagen, since the collagen content is increased in arteries of hypertensive patients (Intengan, Deng et al. 1999) and in animal models of hypertension (Intengan, Thibault et al. 1999, Eberth, Cardamone et al. 2011) (**Figure 2-4D and 2-4E**). These changes in structure can also induce changes in flow pattern, often exacerbating the flow irregularities that occur at vessel bifurcations (Malek, Alper et al. 1999) and leading to increased expression of inflammatory mediators (Li, Haga et al. 2005). These sites also show an increased likelihood of developing atherosclerotic lesions, composed of lipids and necrotic cores with cholesterol crystals and calcification (Li, Haga et al. 2005). In addition to overloading causing disease related changes in

ECM structure and composition, many genetic diseases manifest in a similar manner, due to the inappropriate mechanosensing that these mutations can induce.

Diseases

Many diseases are the result of disruption in the multi-scale force transmission between the ECM, the cytoskeleton and the interior of the nucleus (Jaalouk and Lammerding 2009). Defects in mechanotransduction caused by inherited or acquired mutations often elicit changes in ECM composition and structure, resulting in disease. Additionally, mutations that directly perturb the ECM can alter mechanical forces acting on cells, often resulting in pathologies.

In the cardiac system, there are over 400 different mutations that have been identified, which cause cardiomyopathy (Barry, Davidson et al. 2008). Most of these mutations occur in genes that code for structural proteins within the cardiac cell, causing inappropriate mechanosensing and reduced force generation (Barry, Davidson et al. 2008). This leads to compensation through hypertrophy. In the kidney, mutations in polycystins 1 and 2 result in loss of primary cilium mediated calcium signaling (Nauli, Alenghat et al. 2003). This leads to the formation of fluid filled cyst within the kidneys and loss of kidney function in what is referred to as polycystic kidney disease.

In the musculoskeletal system, muscular dystrophies occur when forces generated by the sarcomeres are inappropriately transferred to the ECM because of mutations in the dystrophin-associated protein complex at the plasma membrane (Heydemann and

McNally 2007), which normally works to shield the cell membrane from excessive stress. These mutations make cells prone to membrane damage and causes excessive ERK1/2 MAP kinase activation with stretch (Kumar, Khandelwal et al. 2004). Eventually, these diseases lead to the progressive degeneration of muscle. Mutations in cytoskeletal proteins such as desmin, titin and myosin can also result in muscular dysfunction, likely due to the impact they have on cellular mechanics and mechanosensing (Hoshijima 2006). Interestingly, muscular dystrophies can also be caused by mutations in proteins of the nuclear envelope. Specifically, mutations in lamin A/C, emerin and nesprins can disturb intracellular structure and force transmission, inducing muscular degeneration. With lamin A/C mutations that are known to cause Emery-Dreifuss muscular dystrophy, cells exhibit fragile nuclei, decreased nuclear mechanics, and reduced activation of mechanosensitive genes with stretch (Lammerding, Schulze et al. 2004). Loss of another nuclear envelope protein, emerin, has been shown to result in increased strain-induced apoptosis and reduced mechanosensitivity despite their normal nuclear mechanical properties (Lammerding, Hsiao et al. 2005). Additionally, mutations in the family of nuclear envelope proteins that connect the nucleus to the cytoskeleton (nesprins) can induce a variety of diseases, including two types of Emery Dreifuss muscular dystrophy (EDMD-4 and EDMD-5) (Zhang, Bethmann et al. 2007) as well as dilated cardiomyopathy (Puckelwartz, Kessler et al. 2010). These diseases often manifest in tissues that are highly mechanically active, resulting in defects in muscles, joints, and bones (Attali, Warwar et al. 2009).

Alterations in cell and ECM mechanics have also been observed to play a critical role in the development and progression of cancer (Jaalouk and Lammerding 2009). Cytoskeletal reorganization is one of the key changes in tumor cells that develop invasive phenotypes (Huang and Ingber 2005). The Rho family of GTPases often drives these changes through regulation of cytoskeletal tension (Sahai and Marshall 2002). The tumor environment itself can also induce cytoskeletal changes, since it is often remodeled to have higher ECM stiffness than the surrounding tissue. In mammary tumor cells, stiff matrices allow clustering of integrins and elevated Rho-ROCK-dependent cytoskeletal tension (Paszek, Zahir et al. 2005). This disrupts cell-cell junctions and enhances ERK and FAK signaling, allowing for increased cell proliferation. Inhibition of ROCK or ERK signaling can prevent this malignant phenotype. Thus, ECM stiffness is an important regulator of tumor growth that is sensed through ROCK and ERK mechanotransduction pathways.

2.4 Tissue Engineering of Fiber Reinforced Soft Tissues

2.4.1 Injury and Degeneration of Fiber Reinforced Soft Tissues

Of the many tissues that are governed by mechanical loading and degenerate with age, fiber reinforced tissues of the musculoskeletal system are particularly problematic due to their low vascularity and limited healing capacity. In particular, fibrocartilages like the meniscus of the knee and the annulus fibrosus of the intervertebral disc often become injured or degenerate with age, requiring surgical intervention. Current meniscal treatment strategies most commonly involve removal of damaged tissue via partial or total meniscectomy. While this approach can alleviate symptoms, the long-term affects

are detrimental to knee joint function, often accelerating induction of osteoarthritis of the knee (Andersson-Molina, Karlsson et al. 2002). This is due, in large part, to alterations in contact area and contact stresses that occur in the joint when meniscus tissue is removed (Baratz, Fu et al. 1986). Because of this, a number of surgical techniques have been adopted in an effort to repair the meniscus and restore joint mechanics. These include: suturing and stabilizing the tears (Rodeo 2000), biodegradable fixation devices (Kesto, Esquivel et al. 2013), or total meniscal allograft (Rath, Richmond et al. 2001). Unfortunately, these treatment strategies usually result in only partial restoration of joint mechanics, and are often susceptible to mechanical failure (Rath, Richmond et al. 2001, Kesto, Esquivel et al. 2013). In the intervertebral disc of the spine, degeneration also commonly occurs, leading to alterations in tissue structure and mechanics that are often symptomatic (Bogduk 1991). Similarly, treatment commonly involves removal of damaged tissue (discectomy). This is often followed by fusion of the adjacent vertebral segments (Deyo, Gray et al. 2005). While this strategy does alleviate symptoms, normal spine mechanics are not restored, and increased loading in adjacent discs can lead to further degeneration (Levin, Hale et al. 2007).

2.4.2 Tissue Engineered Fibrocartilage Replacements

Because of the issues with current treatment strategies for degenerate fibrocartilage tissues, there is a clinical demand for regenerative therapies. Many recent approaches have focused on engineering replacements. These types of strategies aim to enable permanent restoration of biomechanical function, avoiding the issues with artificial replacement (e.g. wear debris and limited lifespan). As is true for regeneration of any

load bearing tissue, a primary goal in these studies is to replicate the structure and mechanical function of the tissue (Nerurkar, Elliott et al. 2010). Given that both the disc and the meniscus are exposed to complex multi-directional loading, this mechanical function will likely require validation of construct properties under multi-directional and shear loading. Despite this, the majority of tissue engineering studies to date have focused on validation of engineered constructs based simply on biochemical content and unidirectional (compressive and tensile) mechanical properties (Bowles, Williams et al. 2009, Nerurkar, Baker et al. 2009, Bowles, Gebhard et al. 2011, Baker, Shah et al. 2012). There is a need to recapitulate not only uniaxial modulus, but also shear and biaxial mechanical attributes. Additionally, many fiber reinforced tissues show highly non-linear mechanical behavior and this non-linearity is important for their mechanical function. In the Chapters 4, 5 and 6 of this thesis are focused on quantifying and attaining these more complex mechanical attributes.

A wide variety of scaffolding materials have been developed for fiber-reinforced tissue engineering applications (Sommerlath and Gillquist 1993, Klompmaker, Veth et al. 1996, Sato, Asazuma et al. 2003, Shao and Hunter 2007, Ballyns, Wright et al. 2010, Bowles, Gebhard et al. 2011). Commonly, these materials possess a fibrous structure, which provides anisotropic mechanical properties (Baker and Mauck 2007). These scaffolds can be composed of woven or non-woven meshes of synthetic or biologic fibers. Fiber directionality is commonly instilled in order to facilitate the directed matrix deposition necessary for recapitulation of anisotropic tissue structure and mechanical function. One scaffold fabrication technique that is particularly promising is the polymer processing

technique referred to as electrospinning. Electrospinning has been applied to both synthetic and natural polymers, allowing for fibers to be formed with diameters ranging from 50 nm up to several microns in diameter. In this process a polymer solution is extruded from a spinneret charged to very high voltage at a constant flow rate. The application of high voltage results in charge buildup, which causes the polymer molecules in the expelled solution to repel each other to the point that they overcome the surface tension of the solution. This results in emission of the polymer in the form of a fine jet, which can be collected on a grounded surface. Modification of this technique allows for fiber alignment to be instilled, by collection of polymer fibers on a rotating mandrel (**Figure 2-5A and 2-5B**). This alignment is able to direct the alignment of adherent cells (**Figure 2-5C**). Further, this alignment has been shown to direct the alignment of cell deposited matrix molecules, providing a promising method for fabrication of engineered fibrocartilagenous tissues with near native mechanical properties (Baker and Mauck 2007, Nerurkar, Baker et al. 2009).

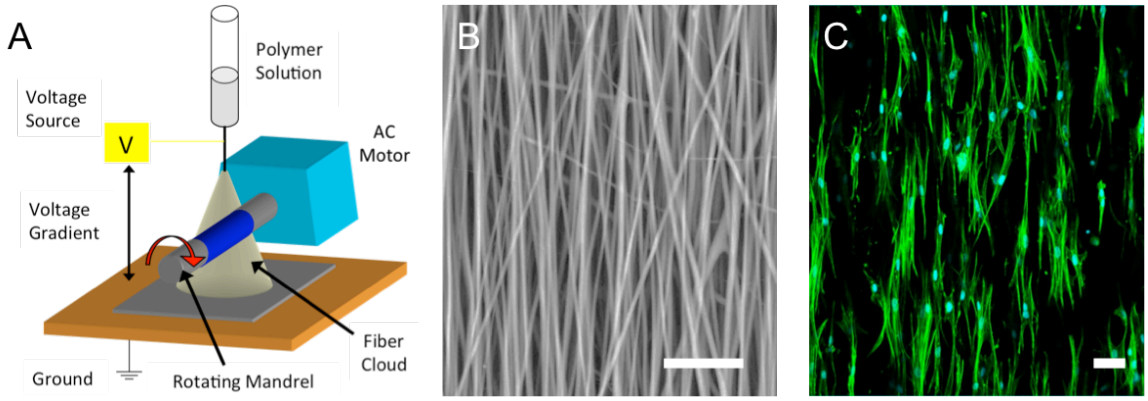

Figure 2-5: Schematic of electrospinning setup used for fabrication of aligned nanofibrous scaffolds (A). Scaffolds display highly aligned fibrous structure when viewed by scanning electron microscopy (B, scale = 20um) and are able to direct the alignment of adherent cells (C). Image depicts staining of F-actin (phalloidin, green) and nuclei (DAPI, blue) in mesenchymal stem cells (scale bar = 50um).

2.4.3 Mechanical Regulation of Fiber Reinforced Soft Tissues

While a number of novel tissues engineering strategies show great promise for engineering fibrocartilagenous replacements, a complete understanding of the cellular mechanotransduction machinery within these constructs will be crucial for their success in dynamically loaded environments. As described above, multi-scale strain transfer, and the cellular response to this strain, is critically important for development (Mikic, Johnson et al. 2000) and homeostasis (Maeda, Sakabe et al. 2011) in these tissues. Additionally, inappropriate mechanical signaling often results in degeneration and disease. One important regulator of mechanotransduction is the structural network of proteins within the cell. These elements transmit force through the cell and activate stretch sensitive molecules within. Cells that exist in native fibrocartilage have mechanotransduction machinery that is exquisitely adapted and tuned for normal function. However, in tissue engineering applications, sources for native tissue cells are often limited, requiring other cell sources for construct fabrication. Mesenchymal stem cells are one such cell source that has shown promise, particularly for engineering of musculoskeletal tissues (Singh, Onimowo et al. 2014). Mesenchymal stem cells display multi-lineage differentiation potential, and this differentiation is heavily regulated by mechanical factors (McBeath, Pirone et al. 2004, Engler, Sen et al. 2006, Baker, Shah et al. 2011). Despite this, the majority of tissue engineering studies have not focused on the mechanical signaling in the cell types that are used, which will be important for their long-term stability in dynamically loaded environments. In chapters 7 and 8 of this

thesis, a number of structural and mechanical aspects of the cell, which are important for mechanotransduction in these microenvironments, are investigated.

CHAPTER 3: DEVICE AND METHODS DEVELOPMENT

3.1 Intro

To investigate the Aims outlined in this thesis, a number of methods and devices were developed or adapted. In this chapter, these approaches will be outlined and their validation and application demonstrated. This includes methods used for mechanical testing of tissue-engineered constructs at the macro-scale, visualize of strain transmission to the micro-scale, and additional methods for quantifying and perturbing cell mechanical attributes at the micro-scale. The overarching goal in developing these methods was to allow for quantitative mechanical comparisons between native and engineered cells/tissues at both the macro (bulk ECM) and micro (cytoskeletal and nuclear) scales. The bulk ECM analysis allows for mechanical comparisons to native tissue benchmarks, while the micro-scale analysis provides insights into the necessary structural and mechanical features of the cells within and helps to establish new benchmarks at this level. In engineering replacement tissues, particularly those that are heavily loaded, replicating mechanical attributes at both of these scales will likely be necessary.

3.2 Biaxial and Shear testing of Engineered Constructs

Previously, our lab developed methods for engineering fiber-reinforced tissues including both the meniscus of the knee and the annulus fibrosus of the intervertebral disc (Baker

and Mauck 2007, Nerurkar, Baker et al. 2009, Baker, Shah et al. 2012). Both of these tissues are important for appropriate joint load transfer and function, requiring them to undergo multi-directional loading as the joint bends or twists. Despite this mechanical requirement, the majority of fibrocartilage tissue-engineering studies (including our own) have focused on the replication of biochemical content and uni-directional tensile or compressive properties (Bowles, Williams et al. 2009). Since both shear and biaxial mechanical properties are important for the function of these tissues (Nerurkar, Elliott et al. 2010) quantification of these properties in engineered constructs provides a means for assessment of function in these varied loading modalities.

Shear mechanical testing was performed using a setup developed in the Elliott lab and attached to an Instron 5848 (Jacobs, Smith et al. 2011). This setup allows for application of simple shear to a sample while simultaneously acquiring images of the speckle coated surface for analysis for optical strain analysis. Samples are gripped using custom aluminum fixtures, which are submerged in a PBS bath (**Figure 3-1A**). Testing protocols were adapted from Jacobs et al 2011, and two different sample aspect ratios were tested for each sample orientation to determine the efficiency of shear transfer. Samples were speckle coated with black enamel paint to allow for texture correlation and then loaded into the bath. The micrometer driven stage allowed for application of a 1% tensile pre-strain on the sample, which was held for 5 min. Samples were then preconditioned in shear to +/-10° for 20 cycles at 0.05 Hz and then ramped at a rate of 3° per minute to γ=10° (**Figure 3-1B**). Images of the sample were acquired every 5 seconds throughout the ramp and used for calculation of average Lagrangian shear strains in the sample using

Vic2D (Correlated Solutions, Columbia, SC). Strain measurements were also taken at 10% intervals across the sample in order to evaluate strain homogeneity for each aspect ratio. This method was used for the assessment of shear properties of engineered scaffolds in Chapter 4.

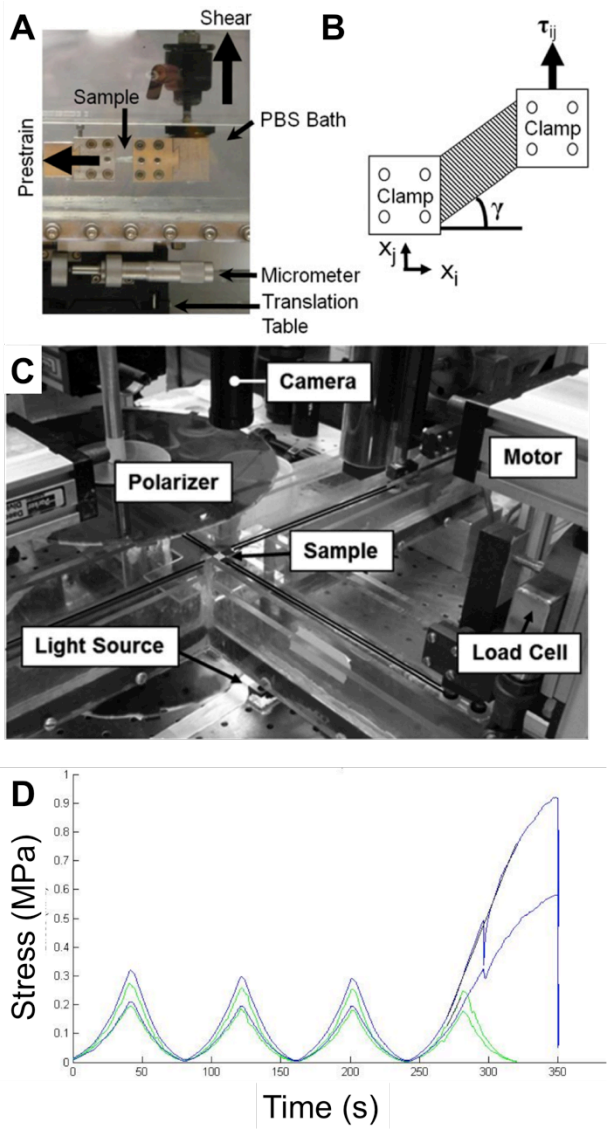

Figure 3-1: Mechanical Testing Setups. Image of the shear mechanical testing setup (A) developed by Jacobs et al with schematic of strain angle (γ) applied (B) (setup image adapted from (Jacobs, Smith et al. 2011)). Image of the biaxial mechanical testing device (C) depicting the sample attached via hooks and silk sutures to pulleys mounted on motor driven load cells (setup image adapted from (Szczesny, Peloquin et al. 2012)). Preliminary biaxial mechanical testing results for the 1:1 test in the X1 and X2 direction of an opposing bilayer grown for 6 weeks. Plotted is the stress

(MPa) vs. time (s) for a test running in optical strain control. The first set of 4 cycles is shown in green and the second set of cycles (after a 1 hour rest) is shown in blue with a ramp to failure in the 4th cycle to ensure linear region modulus calculation.

Biaxial mechanical testing was performed using a custom biaxial mechanical testing machine built in the Elliott lab (O'Connell, Sen et al. 2012, Szczesny, Peloquin et al. 2012) (**Figure 3-1C**). This device allows for samples to be strained in biaxial tension within a PBS bath using optically measured strains to control displacements. Real-time feedback of surface displacements allows for application of specific strains in both sample directions. However, this requires some optimization of the feedback parameters based on the specific sample mechanical properties. Strains were applied using four hooks attached to each edge of the sample and secured to pulleys on the biaxial device via 2-0 braided silk sutures. Four strain markers were attached in the middle 50% of the sample with cyanoacrylate and used for real-time Lagrangian strain control. Preliminary experiments were performed on aligned electrospun scaffolds oriented with the primary fiber direction at 30° from the first principal axis of loading. This allowed for optimization of both strain regime to be tested and feedback parameters for optical strain application. The ability to load in two directions simultaneously allows for multiple loading ratios, which span the physiologic range, to be tested. As such, testing was performed to sub-yield strains so that multiple tests with different strain ratios could be performed on the same sample. In preliminary experiments, samples were pre-strained to 1% at 0.01% strain/sec and then cyclically strained at to 3, 4, or 5% strain 4 times with a 1:1 strain ratio at 0.075% strain/sec. The sample was allowed to rest for 1 hour and this same test was repeated to determine if yield had occurred and to determine if multiple tests could be performed on the same sample. In this second test, the fourth ramp was

run to failure in order to determine if the linear region of the stress-strain curve was being reached. These tests showed that 4% strain allowed for repeatable testing to be performed that reached the lower end of the linear region without inducing yield (**Figure 3-1D**). Thus, this testing protocol was validated and chosen for testing of tissue engineered annulus fibrosus laminates in Chapter 5.

3.3 Micro-tensile Device for Tracking and Quantification of Nuclear Deformation

In order to track and analyze nuclear deformation in live cells, a microscope mounted tensile device was developed. This device allows for cell seeded electrospun scaffolds to be quickly loaded into a pre-warmed, optically transparent, media bath containing phenol-free DMEM with HEPES. A raised platform allows for quick gripping of samples with a set gauge length of 50mm (**Figure 3-2 A-C**). Samples that have been stained with Hoechst (10ug/ml for 10 min) are gripped in the device and imaged as strain is applied. Dual-stepper motors allow for application of equal displacement to each end of the sample so that cells in the center of the sample can be imaged and tracked at 20X magnification. Cells are stretched in 3% increments (1% / second) to 15% strain with images acquired at each strain level. Post-processing (described in the next section) is performed in MATLAB and allows for calculation of normalized nuclear deformations and inter-nuclear Lagrangian strains.

Device validation was performed using both bulk Lagrangian surface strains using Vic2D analysis of speckle coated scaffolds and inter-nuclear Lagrangian strains of cell seeded scaffolds. Additionally, a second set of grips was built that allows for fixation of the

lateral edges of the scaffold **(Figure 3-3A)**. Fixation of the lateral edges allows for reduction of lateral scaffold contraction that occurs due to the large (1.2-1.4) Poisson's ratio of these highly aligned and highly porous materials. Both surface strain analysis (**Figure 3-3B**) and inter-nuclear strain analysis (**Figure 3-3D**) showed that strains in the stretch direction reached close to the applied strain and that very large compressive strains occurred in the perpendicular (X_2) direction.

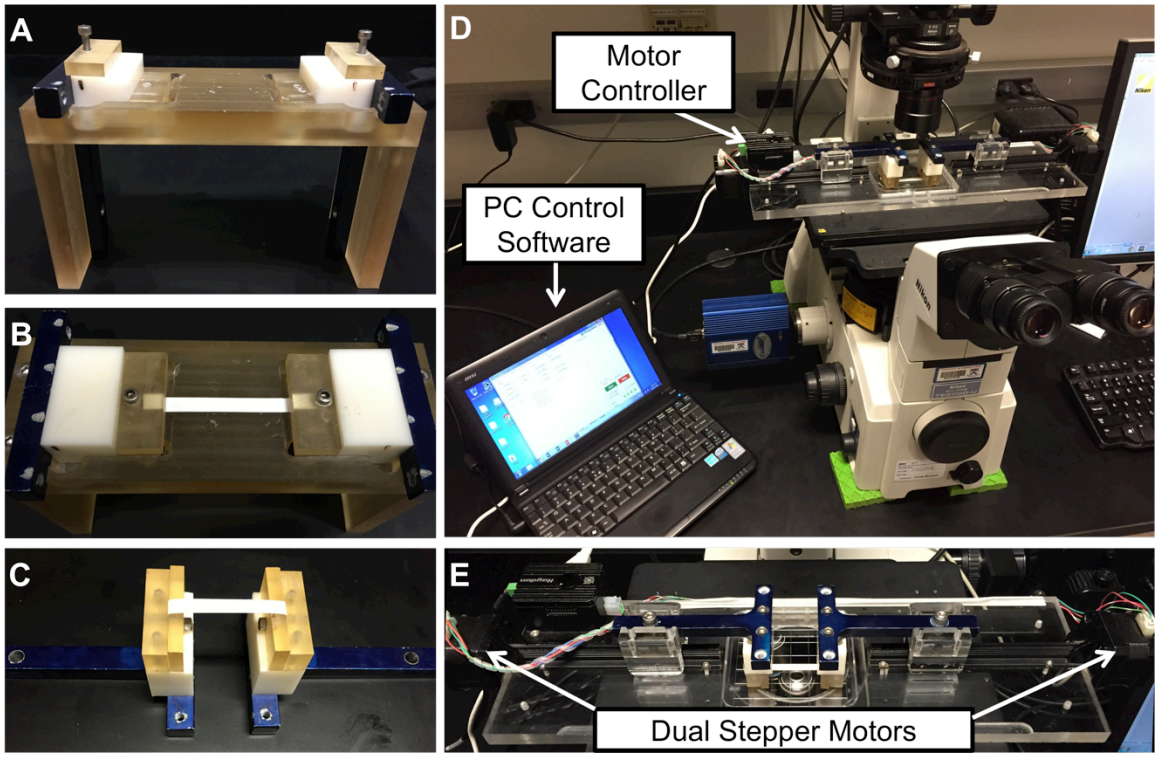

Figure 3-2: Micro-tensile Device. Micro-tensile device setup for quantification of nuclear deformation. A raised setup platform (A) allows for quick loading of scaffolds into grips (B) using a single screw on each side. Sample is then flipped (C) into a media bath and secured into the tensile device on an inverted microscope (D). Dual stepper motors driven by a USB controller allow for tracking of single cells with strain (E).

Fixation of the lateral edges significantly reduced these compressive strains (**Figure 3-3B,D Fixed**). Nuclear deformation was observed to gradually increase as the applied

strain increased (**Figure 3-3C**). Interestingly, this fixation also significantly reduced the nuclear deformation (**Figure 3-3C**). These results indicated that this device can be used to apply accurate scaffold strains and that these strains induce nuclear deformation that can be tracked at high resolution in single cells. Additionally, this data indicates that the Poisson's ratio of the scaffold plays a significant role in nuclear deformation, and that restriction of scaffold lateral contraction can reduce the nuclear deformations observed.

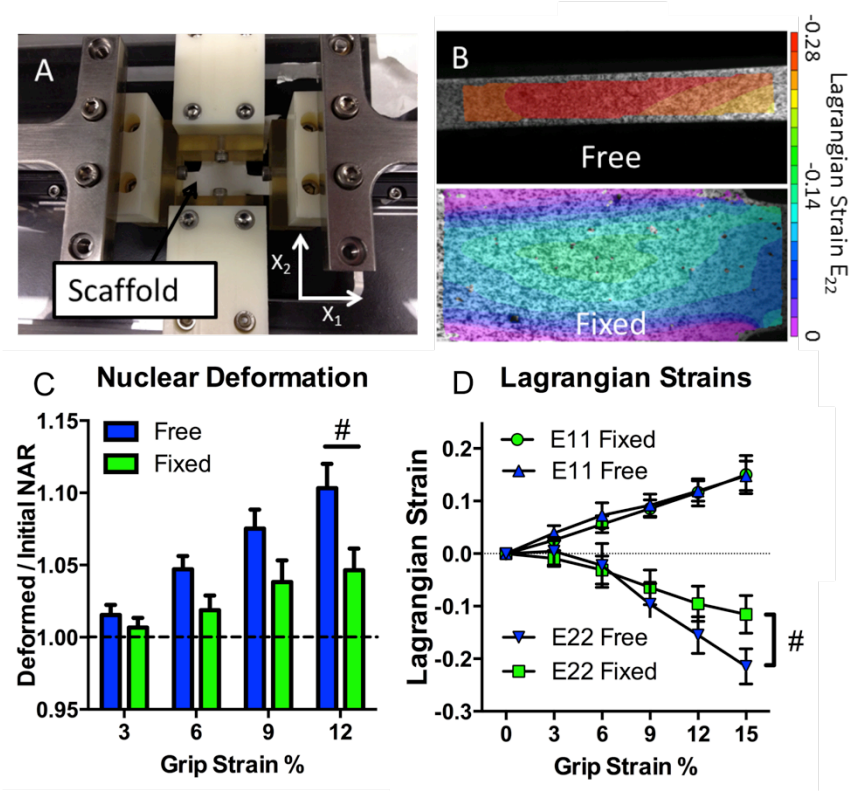

Figure 3-3: Lateral grips allow for restriction of lateral compression (A). Surface strain analysis of speckle coated scaffolds (Vic2D) (B). Quantification of nuclear deformation based on changes in nuclear aspect ration (NAR) for free vs. fixed boundary conditions (C, n= 17-39 cells/group). Quantificaiton of Lagrangian strains for triads of nuclei on scaffolds (D). E11 indicates strain in the stretch direction and E22 indicates shear perpendicular to this direction (# $p<0.05$).

3.4 Analysis Software for Deformation and F-Actin

Nuclear deformations and inter-nuclear Lagrangian strains are quantified using MATLAB. For nuclear deformations, Hoechst images are sequentially loaded (in strain order) and nuclei are detected using the canny edge detection algorithm, which identifies edges based on gradients in signal intensity. These edges are then dilated, filled, and grouped into objects for each image. The point selection tool is then used to match nuclei in sequential images, so that normalized deformations and Lagrangian strains can be calculated. Each object (grouping of pixels for each nucleus) is subjected to principal component analysis, similar to the method developed by Baker et al (Nathan, Baker et al. 2011, Baker, Shah et al. 2012). This gives the first and second eigenvectors, the first of which indicates the orientation and magnitude (length) of the first principal axis of the nucleus and the second of which gives the orientation and magnitude of the second principal axis. The ratio of these two nuclear lengths (long axis / short axis) is calculated as the nuclear aspect ratio (NAR) similar to that used by Stella et al (Stella, Liao et al. 2008). These nuclear aspect ratios can then be normalized to the initial nuclear aspect ratio for that specific cell. Thus, this measurement gives quantification of nuclear deformation, and is a combination of deformation observed in both directions (elongation in stretch direction and compression in the lateral direction). When different treatments are applied to the cell, a nuclear deformation index (**NDI**) can then calculated for each experimental group by normalizing nuclear deformation at each strain level to the mean deformation observed for the control group at that same strain level. To calculate this index, the average nuclear deformation (**nNAR**, nuclear aspect ratio normalized to undeformed state) is calculated at each strain level. These averages are then used to

normalize the nuclear deformation at each of the 5 strain levels (**i=1-5**) to the associated deformation in the control group at that strain level using the following formula:

$$\boldsymbol{NDI} = \frac{(\boldsymbol{nNAR_{Ti}} - \mathbf{1}) - (\boldsymbol{nNAR_{CiAve}} - \mathbf{1})}{(\boldsymbol{nNAR_{C15\%Ave}} - \mathbf{1})} * \mathbf{100}$$

Where **i** indicates the applied strain level (3, 6, 9, 12, 15%), **T** indicates treatment group, **C** indicates control group, and **Ave** indicates average at that strain level.

Local Lagrangian strains can also be calculated using triads of nuclei as fiducial markers at each strain level to ensure consistent local deformations across scaffolds and experimental conditions. First, the displacements for each point are calculated based on a reference image. These displacements are then used to calculate the deformation gradient tensor **F**:

$$\boldsymbol{F_{ij} = dx_i / dX_j}$$

Where x indicates the deformed point locations, X indicates the undeformed locations, and i and j indicate the principal directions. This tensor can then be used to calculated the Lagrangian strain tensor **E**:

$$\boldsymbol{E_{ij} = \frac{1}{2}\,(F^T F - I)}$$

Components of this tensor give the two-dimensional strains in the two principal directions as well as the shear strain.

Another metric used, which is useful for determining changes in F-actin near or interacting with the nucleus, is quantification of F-actin in the projected area of the nucleus. This analysis uses similar methods to edge detect nuclei in epi-fluorescent images (**Figure 3-4B**). These outlines are then used as a mask to crop the associated actin images. The total F-actin signal in this area is then summed and normalized to the nuclear area to give average actin intensity in the projected area of the nucleus (**Figure 3-4 B**).

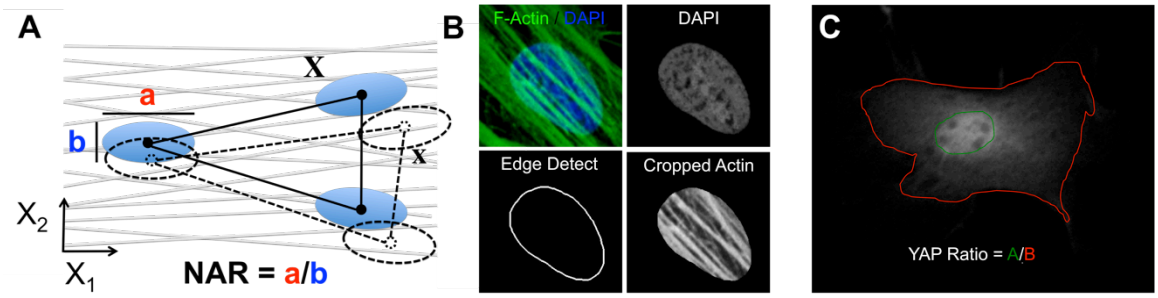

Figure 3-4: Image analysis methods. (A) Nuclear deformation and micro-scale Lagrangian strains can be calculated from triads of nuclei in a deformed (x) and undeformed configuration (X). Nuclear deformation is calculated based on changes in the nuclear aspect ratio (NAR). (B) F-actin intensity in the area of the nucleus is calculated by edge detection of the DAPI. This outline can then be used to crop the actin signal in the region of the nucleus. (C) YAP staining quantification is performed by calculating a ratio of the YAP signal in the region of the nucleus (green region) divided by the YAP signal in the cytoplasm (red region). These outlines are determined from staining of the nucleus (DAPI) and the actin cytoskeleton (Phalloidin).

The nuclear outline is also used for quantification of the nuclear and cytoplasmic levels of YAP/TAZ. Images of cells stained for YAP/TAZ, F-Actin (phalloidin) and nuclei (DAPI) are quantified (**Figure 3-4 D**) by taking the average YAP signal intensity in the

area of the nucleus (using the DAPI outline) divided by the average signal intensity in the area of the cytoplasm (F-Actin outline). This ratio provides a quantitative metric for YAP localization in the cell.

3.5 Multi-Well Dynamic Tensile Bioreactor

In order to assay the mechanobiologic response to short-term and long-term dynamic tensile loading, we developed a multi-well tensile loading bioreactor system based on a previously developed device designed by Brendon Baker (Baker, Shah et al. 2011). The original design allows for loading of a single group at a time. In order to load multiple groups/media conditions simultaneously, we adapted this device to a multi-well format (**Figure 3-5A**). This device uses a linear actuator (Bi-slide, Velmex MN10-0050-E01-LR) that moves two platens simultaneously in opposite directions and is driven by a large liquid cooled (Koolance, Exos-2) stepper motor (Velmex, PK296-03AA-A6-3/8). This allows it to be run in a CO_2 and temperature controlled incubator (**Figure 3-5B**) without changing the environmental conditions. Mounted to the platens are two modified T-bars, which connect to 4-sets of grips that are submerged in a 4 well tissue culture dish (Nunc). This allows for simultaneous loading of up to 4 groups of 4 scaffolds within isolated media chambers. The device is controlled using a stepper motor controller (Velmex, VXM-1) connected via USB to a laptop computer. This allows for application of sinusoidal displacements of frequencies up to 5Hz and strains up to 10%. For experiments, cell seeded scaffolds were loaded to 3% strain at 1Hz. This was chosen based on previous studies in which this loading was shown to enhance the maturation of cell seeded constructs (Baker, Shah et al. 2011). These types of loads were previously

validated in aligned scaffolds and shown to result in elastic and recoverable deformations for upwards of 200,000 cycles with only modest (~6%) decreases in stiffness (Baker, Shah et al. 2011).

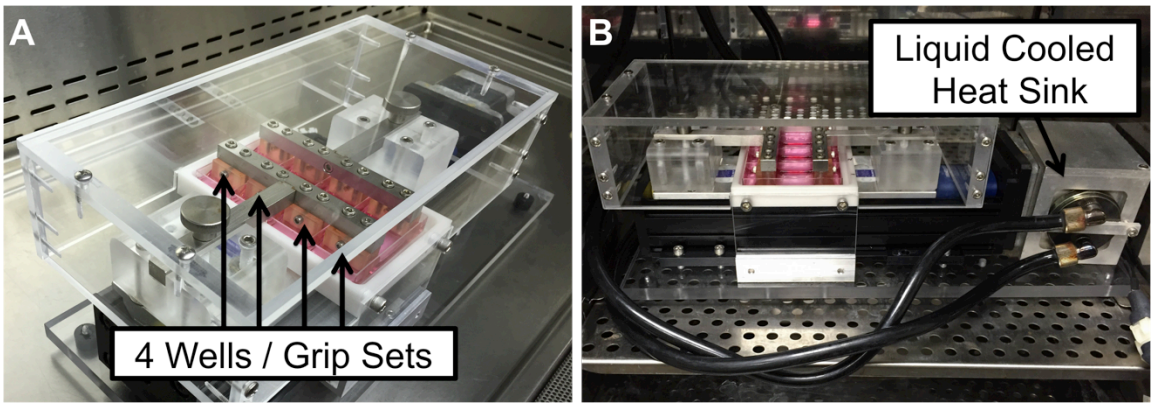

Figure 3-5: Multi-well dynamic tensile bioreactor allows for simultaneous loading of up to 4 groups isolated in separate media chambers (A). Liquid cooled heat sink allows for extended loading in a temperature and CO_2 controlled incubator.

3.6 Lentiviral Vectors for Knockdown of LINC Complex Proteins

To assess the importance of specific components of the LINC complex, lentiviral vectors were developed and verified. Knockdown of LINC complex components was performed using miR RNAi delivered using a lentiviral vector based system (Block-it Lentiviral Pol II miR RNAi Expression System with EmGFP, Invitrogen). Lamin A/C was knocked down using a BLOCK-iT Pol II miR validated miRNA control vector and a non-targeting control vector miR-neg Control was used as a control for all experiments involving knockdown. Three nesprin 1 giant vectors were designed and the miRNA sequence that resulted in the highest levels of knockdown was used (N1G sequence: TGCCGAGGACCTTCATCTTCT). Vectors were synthesized using miRNA sequence containing oligos that were annealed and ligated into pCDNA6.2-GW/ Em-GFP. miRNA containing cassettes were then transferred to pLenti6/V5-DEST via Gateway cloning

reaction and sequenced prior to viral production in HEK293FT cells. Virus (media supernatant) was tittered by infection of MSCs and selection for blasticidin resistance (at 14 days) or analysis of %GFP positive cells (at 4 days) using a flow cytometer (FACSCaliber, Beckson Dickson, with CellQuest Pro software). For all experiments, cells were infected with virus overnight. Four days post infection cells were trypsinized and re-seeded on glass, polyacrylamide gels, tissue culture plastic, or aligned electrospun scaffolds for assays. Knockdown was verified by dot blot for nesprin 1 following 1MDa size filtration (**Figure 3-6A**) or by western blot and immunostaining for lamin A/C (**Figure 3-6B and 3-6C**).

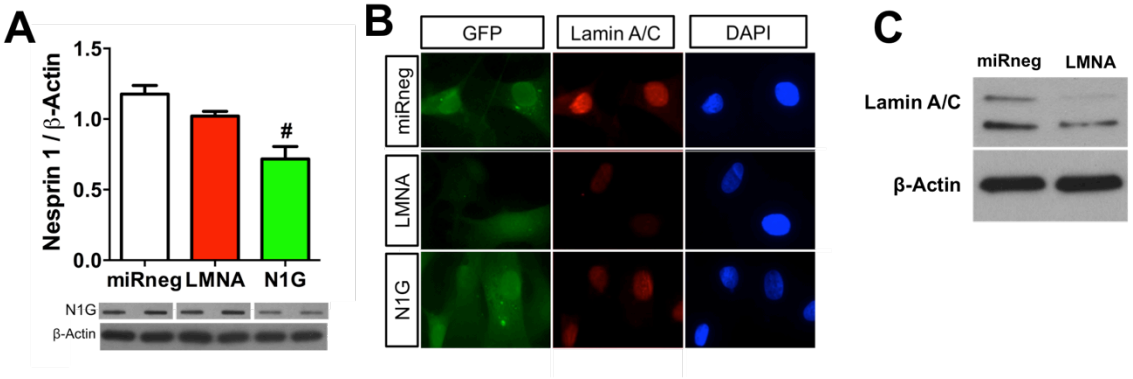

Figure 3-6: Verification of nesprin 1 giant knockdown by dot blot for nesprin 1 following 1MDa size filtration of whole cell lysate (A) (mean +/-SD n=3/group). Verification of lamin A/C knockdown by immunostaining of lamin A/C (B) and western blot for lamin A/C (C).

CHAPTER 4: FIBER ANGLE AND ASPECT RATIO INFLUENCE THE SHEAR MECHANICS OF ORIENTED ELECTROSPUN NANOFIBROUS SCAFFOLDS

4.1 Intro

Fibrocartilages are distributed throughout the body and play critical roles in motion and load transmission across joints. These dense connective tissues are typified by an organized and hierarchically distinct collagenous structure. For example, the knee meniscus, which transmits loads from the femur to the tibia, is composed of highly organized collagen bundles that pass circumferentially through the semi-lunar tissue and provide for its mechanical anisotropy in tension (Proctor, Schmidt et al. 1989, Petersen and Tillmann 1998, Setton, Guilak et al. 1999). Likewise, the annulus fibrosus (AF) of the intervertebral disc of the spine resists tensile, compressive and shear loading as motion occurs between two adjacent vertebral bodies. The AF is composed of alternating ±30° layers of aligned collagen fibers embedded in a non-fibrillar matrix of hydrated proteoglycans (Hickey and Hukins 1980, Cassidy, Hiltner et al. 1989). Proper mechanical function of both the intervertebral disc and the meniscus is dependent upon this structure and composition (Humzah and Soames 1988, Fithian, Kelly et al. 1990), however, both are compromised in the pathologic transformations associated with tissue degeneration. Current treatments such as meniscectomy (for meniscus) and discectomy and spinal fusion (for AF) aim to relieve pain but are not ideal due to their inability to restore function and their tendency to accelerate degeneration in the joint and/or adjacent discs (Levin, Hale et al. 2007, Harrop, Youssef et al. 2008).

Tissue engineering strategies present a promising alternative that could allow for regeneration of these fibrous structures and restoration of native tissue structure and function. Indeed, many groups have explored generation of whole meniscus (Chiari, Koller et al. 2006, Kelly, Robertson et al. 2007, Ballyns, Gleghorn et al. 2008), disc analogues (Mizuno, Roy et al. 2006, Nesti, Li et al. 2008, Nerurkar, Sen et al. 2010), and disc substructures (Baer, Wang et al. 2001, Sato, Kikuchi et al. 2003, Wilda and Gough 2006, Chou, Akintoye et al. 2009, Gruber, Hoelscher et al. 2009) with a variety of materials and starting cell populations. Due to the large and multi-directional forces experienced by these tissues *in vivo*, a successful engineered construct must resist considerable load magnitudes (i.e., multiples of body weight) under tensile, shear, and compressive configurations (Vadher, Nayeb-Hashemi et al. 2006, Nerurkar, Elliott et al. 2010). For instance, circumferential tensile stresses in the AF (due to pressurization of the nucleus pulposus under axial spinal loads), are often combined with torsional motion of the spine, which generates direct shearing of the AF. The microstructural organization of the native AF is well suited to withstand this loading environment. Accordingly, a structurally motivated tissue engineering strategy may be necessary in order to generate a construct that is functionally commensurate with the native tissue when subject to the full range of loading modalities present *in vivo*.

To specifically address the structural basis of function in engineered tissues, our group and others have employed aligned nanofibrous scaffolds formed by electrospinning (Nesti, Li et al. 2008, Yang, Kandel et al. 2008, Gruber, Hoelscher et al. 2009).

Electrospinning is a scaffold fabrication process in which ultra-fine polymer strands are formed by the electrostatic drawing of a polymer towards a collecting surface (Li, Tuli et al. 2005, Mauck, Baker et al. 2009). Collection of fibers on a rotating mandrel generates aligned scaffolds (Li, Mauck et al. 2007). Furthermore, these nanofibrous scaffolds direct meniscus (Baker and Mauck 2007), AF (Nerurkar, Elliott et al. 2007) and mesenchymal stem cell (MSC) (Nerurkar, Baker et al. 2009) alignment and subsequent matrix deposition, recapitulating tissue micro-architecture (Nerurkar, Baker et al. 2006, Nerurkar, Elliott et al. 2007). With time in culture after cell seeding, single-lamellar constructs can match mechanical properties of native meniscus (Baker, Nathan et al.) and AF (Nerurkar, Mauck et al. 2008, Nerurkar, Baker et al. 2009) when evaluated in tension. These findings suggest that nanofibrous assemblies that mimic the anisotropic and hierarchical structure of the native tissues direct tissue formation and match several key mechanical benchmarks.

While these data suggest promise for this approach to fibrous tissue engineering, the shear properties of such constructs have not yet been evaluated. Thus it is not yet clear whether these nanofiber-based tissue constructs can withstand the considerable shear stresses incurred *in vivo*. Indeed, despite the importance of this loading modality in many tissues, no engineered AF or meniscus construct has been evaluated in shear, and only a small number of studies have quantified the shear properties of the native meniscus and AF (Anderson, Woo et al. 1991, Zhu, Chern et al. 1994, Iatridis, Kumar et al. 1999, Fujita, Wagner et al. 2000, Jacobs, Morelli et al. 2010). Due to the practical difficulty of applying pure shear to a sample, most AF and meniscus shear testing has been performed

on cylindrical, cuboidal, or planar samples under compressive or tensile pre-strains. Of these, simple shear of planar samples is appealing because the application of tensile pre-strains allows for combined fiber stretch and shear as it occurs *in situ*. For such a configuration, however, finite element studies of ligament have shown that sample aspect ratio is an important determinant of the strain field, which can be heterogeneous across a sample with magnitudes considerably lower than the applied strain (Gardiner and Weiss 2001). This is an important consideration for the AF and meniscus, where sample aspect ratio is limited by tissue geometry. Additionally, the effects of fiber orientation and fiber stretch on shear properties is difficult to assess in native tissue (Cassidy, Hiltner et al. 1989, Petersen and Tillmann 1998). If the shear properties of an engineered meniscus or AF construct are to be deemed adequate, comparisons need to be made to native tissue values.

Thus, the objective of the present study was to quantify the effects of fiber angle and sample aspect ratio on the shear properties of aligned electrospun scaffolds, and to determine how extracellular matrix deposition by resident MSCs modulates the measured shear response. Using experimentally measured material properties, a finite element model was constructed to determine the effect of aspect ratio and fiber orientation on the shear strain distributions within these nanofibrous assemblies. Next, scaffolds with varying fiber angle were tested in simple shear with two different aspect ratios in order to compare experimentally measured and model predicted strain distributions. Finally, samples with an aspect ratio similar to AF shear testing studies were seeded with MSCs

and assayed for functional growth (shear mechanics and biochemistry) with time in culture.

4.2 Materials and Methods

4.2.1 Scaffold Fabrication

Aligned nanofibrous poly(ε-caprolactone) (PCL) scaffolds were fabricated by electrospinning as described previously (Baker and Mauck 2007, Nerurkar, Elliott et al. 2007). Briefly, a 14.3% w/v solution of PCL (Bright China, Hong Kong, China) was prepared in a 1:1 mixture of tetrahydrofuran and N,N-dimethylformamide (Fisher Chemical, Fairlawn, NJ). This solution was ejected via syringe pump at 2.5 mL/h through a spinneret charged to +13 kV. Fibers were collected for 6 hours on a grounded rotating mandrel with a surface velocity of 10 m/s. This resulted in a scaffold sheet of ~600 μm thickness from which rectangular samples (3 x 16 mm and 8 x 14 mm) were cut with their long axes oriented at angles of 0°, 30°, 45°, 60° and 90° with respect to the prevailing fiber direction (Nerurkar, Elliott et al. 2007). Samples were stored in a desiccator until mechanical testing or cell seeding.

4.2.2 Shear Mechanical Testing

A custom simple shear testing device was used to measure the shear properties of scaffolds and engineered constructs. Details on device development and validation are provided in (Jacobs, Morelli et al. 2010). Briefly, the shear device was designed as an attachment to an Instron 5848 (Canton, MA) electromechanical testing system. Samples

were placed horizontally between two serrated grips, with one grip attached to the Instron vertical actuator and the other attached to a vertical post mounted on the base-plate of a tank filled with phosphate buffered saline. A horizontal micrometer driven stage was incorporated into the tank to allow for application of tensile pre-strains in the horizontal direction. A mounting track was employed to align and load samples into the removable grips prior to insertion into the bath. Two load cells were incorporated into the system: a 5 N load cell on the vertical axis to measure shear loads and a 9.8 N submersible load cell (model 31 submersible, Honeywell, Minneapolis, MN) on the horizontal axis to measure tensile loads generated during pre-strain and shearing.

Prior to mechanical testing, sample cross-sectional area was measured using a custom laser device (Guerin and Elliott 2007). Samples were then speckle coated with black enamel paint to allow for texture correlation strain analysis (below) (Nerurkar, Han et al.). Samples with two different X:Y aspect ratios were investigated **(Figure 4-1)**. Grip-to-grip distances for 2:1 and 1:2 aspect ratios were 6 mm and 4 mm, respectively. Samples were loaded into the device with fibers oriented oblique to the X-direction by an angle θ, as depicted in **Figure 1A**. A 1% tensile pre-strain **(Figure 4-1A)** was applied along the X-direction and held for 5 minutes. Samples were next preconditioned in shear to ±10° for 20 cycles at 0.05 Hz and then ramped at a rate of 3° per minute to 10°. Images were captured by digital camera (Basler, Exton, PA) every 5 seconds throughout the ramp and used to determine the average Lagrangian shear strain (E_{xy}) for the middle 50% of the sample **(Figure 4-1B)** using Vic2D texture correlation software (Correlated Solutions Inc., Columbia, SC). Shear stress was calculated as the measured shear force

divided by the cross-sectional area. Apparent shear modulus was calculated from the last 25% of the strain ramp for the stress-strain curve. The deformation gradient tensor was determined from surface deformations and used to calculate fiber stretch, which was defined as the ratio of deformed to undeformed length along the direction of scaffold fiber alignment. Additionally, strain measurements were taken at 10% intervals across the samples using sets of 4 points (**Figure 4-1B**) to evaluate strain homogeneity at the peak of the strain ramp.

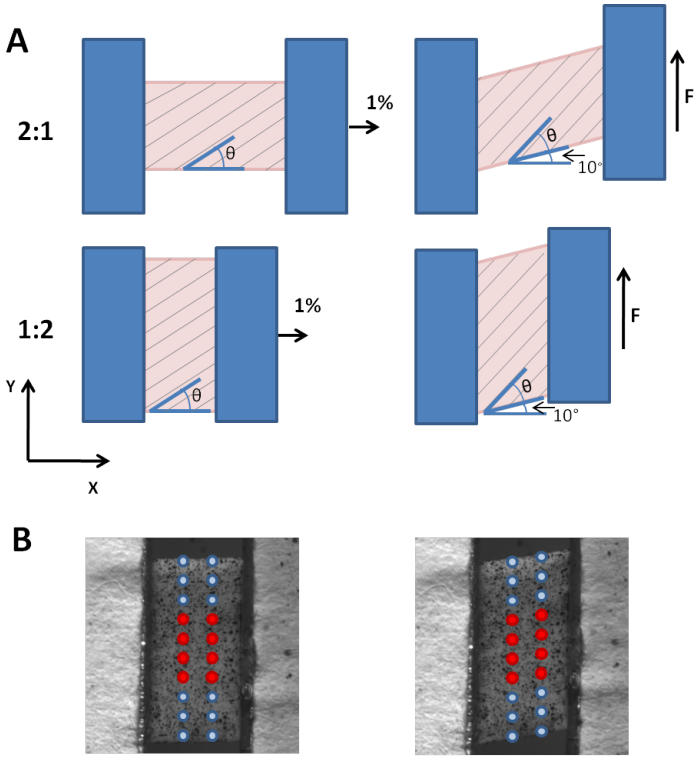

Figure 4-1: Schematic representation (A) for coordinate system, pre-strain (1%) and shear loading with force F to 10° for samples with aspect ratios of 2:1 and 1:2 and with changing fiber angle Θ. Strain marker positioning (B) shown on speckle-coated 1:2 sample for modulus calculation (red) and strain homogeneity analysis (red and blue).

4.2.3 Modeling

Finite element (FE) modeling was performed in order to predict strain distributions for samples with varying fiber orientations and aspect ratios. This was accomplished using the COMSOL3.5a structural mechanics module (COMSOL, Burlington, MA) with an assumption of plane stress. The scaffold was taken to be linearly elastic and transversely isotropic, which required five independent mechanical properties (E_x = 28 MPa, E_y = 3 MPa, v_{xy} = 0.4, v_{yz} = 0.2 and G_{xy} = 1.6 MPa). These values were determined experimentally (Heo, Nerurkar et al. 2011). The material axis was defined using a second material coordinate system that was rotated by the angle $\theta = 30°$, 60° or 90° about the z-axis so that each experimentally tested fiber orientation could be captured via the same five input parameters. Shear was applied with a prescribed displacement boundary condition in the global coordinate system. Solutions were visualized as contour plots of the shear strain (E_{xy}) and strains along the centerline were used for comparison with experimental results.

4.2.4 Cell-Seeded Construct Culture and Analysis

Cell-laden constructs were formed by seeding electrospun scaffolds with MSCs and culturing under pro-fibrochondrogenic conditions for up to 12 weeks (Baker and Mauck 2007, Baker, Nathan et al.). MSCs were isolated from the femurs and tibiae of two 3-6 month old calves within 12 hours of slaughter, as described previously (Mauck, Yuan et al. 2006, Huang, Yeger-McKeever et al. 2008). Cells were expanded on tissue culture plastic in basal medium (high glucose DMEM containing 1% penicillin, streptomycin, fungizone and 10% fetal bovine serum) to passage 2. Scaffolds with fiber orientations of 0°, 45° and 60° were sterilized and rehydrated using decreasing concentrations of ethanol

(100, 70, 50, 30%, 1 hour/step) and then washed for 1 hour in PBS. Scaffolds were then incubated in 20 μg/mL fibronectin in PBS for 16 hours and washed again with PBS prior to seeding (Nerurkar, Baker et al. 2009). Scaffolds were seeded and cultured in non-tissue culture treated six-well plates. Each scaffold received 50 μL of cell solution (1 x 10^7 cells/mL) on one side followed by a one hour incubation at 37 °C. The opposite side of each scaffold was then seeded with another 50 μL of cell solution and incubated for an additional two hours. Each well was then filled with 4 mL of basal media, which was replaced after 24 hours with 4 mL of a chemically defined media (DMEM, 0.1 mM dexamethasone, 40 μg/mL L-Proline, 100 mg/mL Sodium Pyruvate, 1% Insulin, Transferrin, Selenium/Premix, and 1% penicillin, streptomycin and fungizone supplemented with 10 ng/mL Transforming Growth Factor-β3). Chemically defined media was replaced twice weekly for the duration of the study.

At 4, 8 and 12 weeks, samples were removed from culture and subjected to simple shear testing (as above) followed by biochemical analyses (n = 5/orientation/time point). Following mechanical testing, dry weight was measured following 24 hours lyophilization, and samples digested with papain (Baker and Mauck 2007). Total glycosaminoglycan and DNA content were determined using the 1,9-dimethylmethylene blue (DMMB) dye binding assay and the PicoGreen assay, respectively, and each were normalized to the sample dry weight (Baker, Nathan et al.).

4.2.5 Statistics

The effect of fiber orientation on shear modulus was evaluated by one-way analysis of variance with Tukey's *post hoc* test, with significance set at $P < 0.05$. Comparisons of shear modulus were made between fiber orientations for a given aspect ratio. Additionally, comparisons of shear modulus for cell-seeded constructs were made between time-points. Pearson's comparison was performed for linear correlation between fiber stretch and shear modulus with goodness of fit represented as R^2 values and significance for deviation from zero set at $P < 0.05$. Samples with fiber stretch less than 1.0 (fiber compression and buckling) were not included in the linear correlations.

4.3 Results

4.3.1 Strain Homogeneity

Based on previous theoretical models and anatomic constraints on native tissue sample geometry, two different aspect ratios were evaluated, 1:2 or 2:1 with respect to the gauge length. Finite element analysis showed that samples with a 1:2 aspect ratio had a more homogeneous distribution of shear strain for each fiber orientation (**Figure 4-2**). Moreover, predicted peak shear strain values for the 1:2 condition were very close to the 0.088 applied shear strain **(Figure 4-2)**. In addition to their dependence on aspect ratio, predicted shear strain magnitudes and distributions were dependent on the fiber orientation of the scaffold. This variation was most noticeable for the 2:1 aspect ratio, where the peak strain decreased as the fiber angle increased. For the 2:1 aspect ratio, the 0° model attained strain in central regions of ~0.08 (compared to the 0.088 shear strain

applied to the boundaries), while for samples with fiber directions of 60° and 90°, central strain decreased to ~0.04 **(Figure 4-3A)**. Modeling of the 1:2 aspect ratio showed less variation in the magnitude of strain in the central region, with all orientations displaying strain magnitudes close to the 0.088 applied strain **(Figure 4-3C)**.

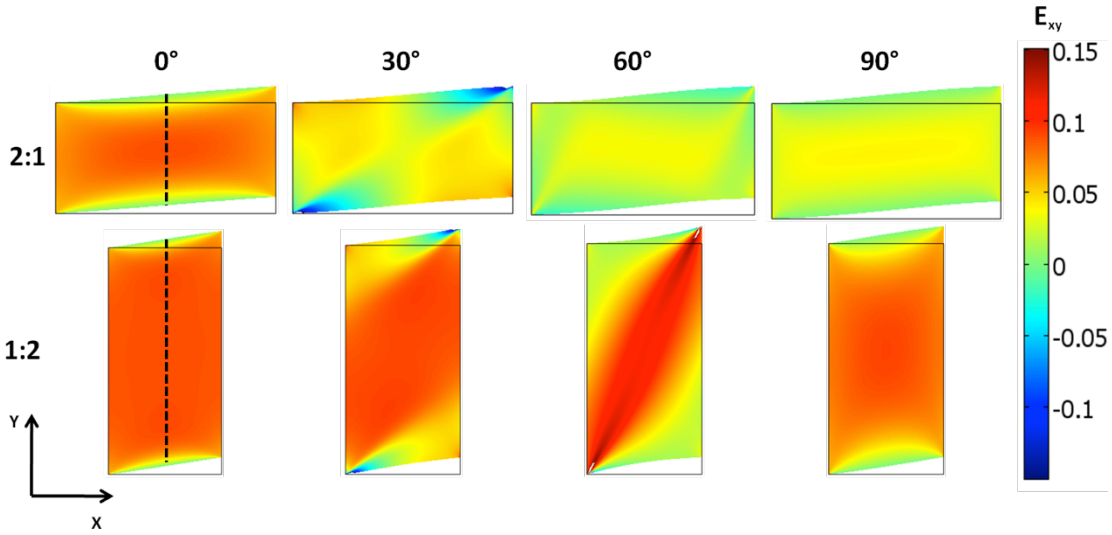

Figure 4-2: Finite element analysis of planar samples in simple shear with different aspect ratios (2:1 and 1:2) as a function of varying fiber orientation (0°, 30°, 60°, 90°). Surface plots depict Lagrangian shear strain (E_{12}).

When these two configurations were evaluated experimentally through surface analysis, measured strains were similar to those predicted by the FE model **(Figure 4-3)**. Overall, the observed strains for the 1:2 aspect ratio were larger and more homogeneous than those observed for the 2:1 aspect ratio. The experimentally measured shear strain was normalized to the applied shear strain and plotted as a function of marker location **(Figures 4-3B and 4-3D)**. For the 2:1 aspect ratio, the magnitude of the measured strains decreased considerably as the fiber angle increased, and the 60° and 90° samples had very low strains across the entire scaffold expanse **(Figure 4-3B)**. The FE model successfully predicted this inhomogeneous strain distribution as well as the changing

strain magnitudes as fiber angle increased for 2:1 samples **(Figure 4-3A)**. For the 1:2 aspect ratio, strains at the top and bottom edges of the samples were low and the strains became less homogeneous as the fiber angle increased **(Figure 4-3D)**. The magnitude and distribution of these experimentally measured strains also corresponded well with the model-predicted strains for this 1:2 aspect ratio **(Figure 4-3C)**.

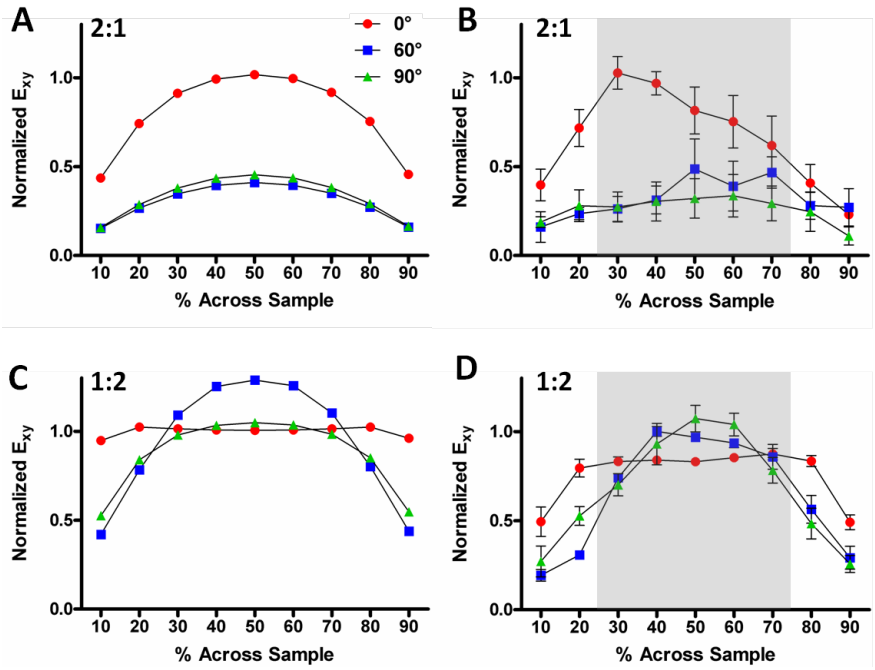

Figure 4-3: Model predicted (A,C) and experimentally measured (B,D) and strain distribution across electrospun scaffolds in the Y direction along the centerline for samples with a 2:1 (A,B) and 1:2 (C,D) aspect ratio. Grey region indicates the relatively homogeneous strain region that was used for calculation of shear modulus. Strain is normalized to the applied strain (E_{xy} = 0.088). Experimental results indicate mean ± SEM (n=5 per Θ).

4.3.2 Orientation and Aspect Ratio Dictate Measured Shear Properties

The shear modulus was next computed from mechanical tests, using the average shear strain in the middle 50% of each sample. The apparent shear modulus of scaffolds was dependent on the sample aspect ratio. For the 2:1 aspect ratio, fiber orientation had an effect on the apparent shear modulus only for the 30° samples compared to 0° and 60° (P

< 0.05; **Figure 4-4A**). In contrast, for the 1:2 aspect ratio, the apparent shear modulus of the 30°, 45° and 60° samples were all significantly higher than the other fiber orientations ($P < 0.05$; **Figure 4-4B**).

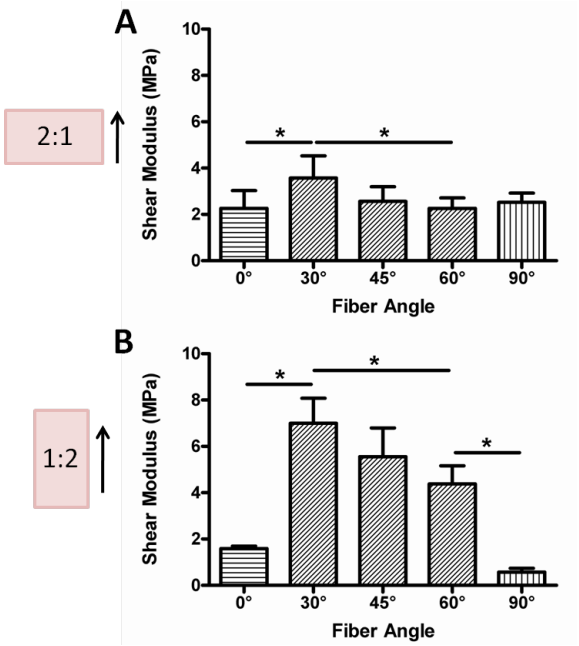

Figure 4-4: Experimentally measured apparent shear moduli samples with a 2:1 (A) or 1:2 (B) aspect ratio. * = $P < 0.05$ between indicated fiber angles. Results indicate mean ± SD (n = 5 per Θ).

Observed fiber stretch corresponded well with the apparent shear modulus. The 2:1 samples had a significantly higher fiber stretch ($P < 0.05$) for the 30° orientation, and likewise had a higher apparent shear modulus (**Figure 4-5A**). However, because little fiber stretch was observed in all other fiber orientations for this aspect ratio, the correlation of fiber stretch with the apparent shear modulus was not significant and the slope was not different from zero ($R^2 = 0.22$, slope = 30.3 ± 15.1, $P = 0.064$, **Figure 4-5B**). Conversely, the 1:2 aspect ratio samples had higher fiber stretch ratios, which were dependent on fiber orientation (**Figure 4-5C**). Moreover, there was a strong correlation

between fiber stretch and apparent shear modulus (R^2 = 0.51, **Figure 4-5D**), with a slope that deviated significantly from zero (slope = 83.6 ± 19.9, P < 0.001).

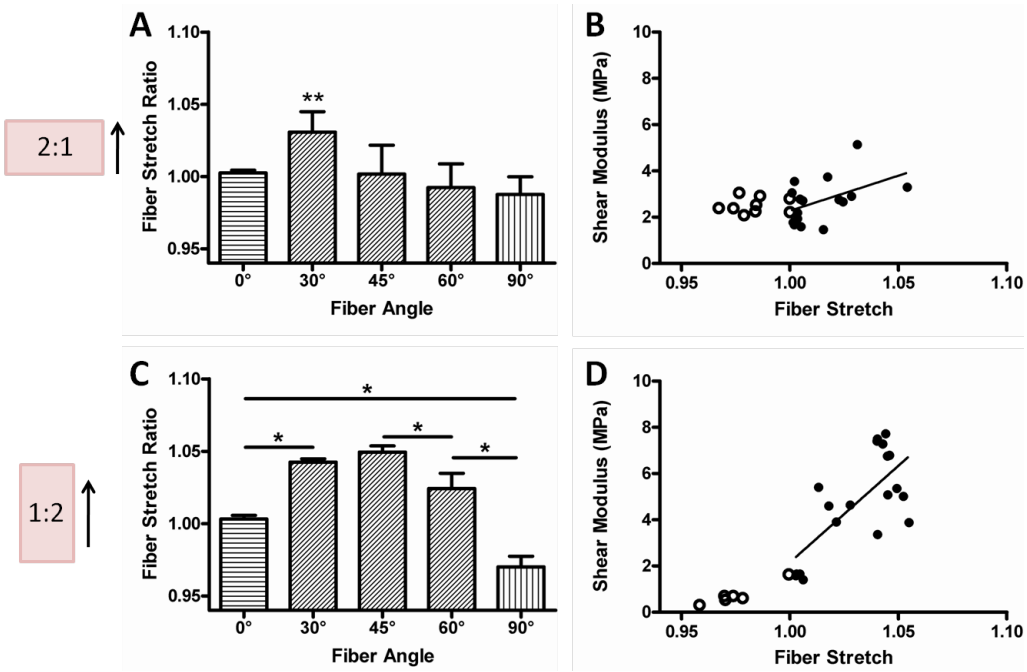

Figure 4-5: Experimentally measured fiber stretch ratios (A,C) for samples with a 2:1 (A-B) or 1:2 (C-D) aspect ratio with correlation plots of shear modulus vs. fiber stretch (B,D). Open circles indicate samples with fiber stretch less than 1 which were not included in the regression analysis. * = P < 0.05 between indicated fiber angles, ** = P < 0.05 compared to 0°, 60° and 90°. Results indicate mean ± SD (n = 5 per Θ).

4.3.3 Shear Properties of MSC Seeded Constructs

The 2:1 aspect ratio was chosen for cell seeded experiments so that comparisons could be made with native AF and meniscus tissues, where sample size is limited by anatomical shape. Samples with θ = 0°, 45° and 60° fiber orientations were chosen due to their relevance to the physiologic shearing of the meniscus and intervertebral disc that occurs with load bearing. From 0 to 12 weeks, the apparent shear modulus for θ = 45° samples increased by ~30% (P < 0.05; **Figure 4-6A**). Increases for θ = 0° and 60° constructs trended upwards (P < 0.12). DNA content and s-GAG content did not significantly vary

between fiber orientations, and so data was pooled for 0°, 45° and 60° samples. DNA content per dry weight decreased significantly from week 4 to weeks 8 and 12 ($P < 0.05$, **Figure 4-6B**), while s-GAG content increased significantly over this same time course ($P < 0.05$, **Figure 4-6C**).

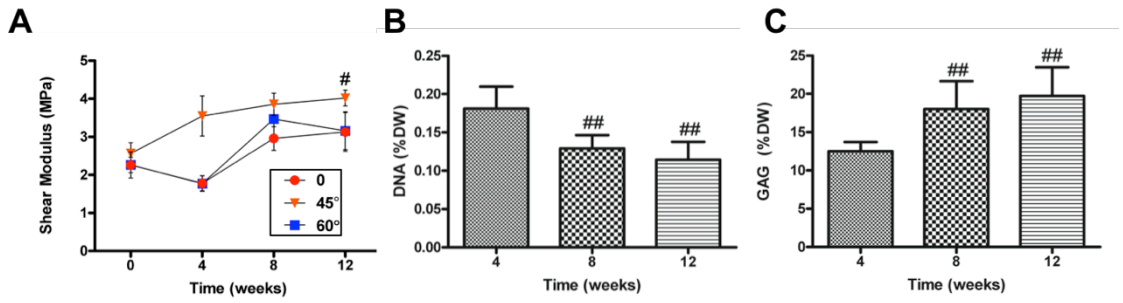

Figure 4-6: Functional growth of MSC-laden constructs with fiber angles of 0°, 45° and 60°. Experimentally measured apparent shear moduli (A), DNA content per dry weight (DW) (B) and s-GAG per dry weight (C). # = $P < 0.05$ compared to unseeded scaffold (0 weeks), ## = $P < 0.05$ compared to 4 weeks. Results indicate mean ± SD (n = 5 per Θ per time point).

4.4 Discussion

Dense fibrocartilaginous tissues such as the knee meniscus and the AF of the intervertebral disc present considerable challenges for tissue engineering and regenerative medicine. The low cellularity and vascularity of these tissues in the adult limits intrinsic repair, while the ordered structure defines precise mechanical functionalities that are difficult to reproduce in synthetic implants. Oriented electrospun nanofibrous scaffolds prescribe cell, and subsequently, matrix directionality. These biomaterials recreate several key attributes of fiber-reinforced tissues, including mechanical anisotropy in tension. When seeded with cells, these constructs mature *in vitro* and match key mechanical benchmarks, including a near-native uniaxial tensile modulus (Mauck, Baker et al. 2009). However, fibrocartilages are exposed to dynamic and multi-directional loads

(including compression and shear) *in vivo*, and successful implementation of an engineered replacement tissue will likely also require mechanical functionality in this context. To address this, the present study evaluated the properties of aligned nanofibrous electrospun scaffolds with varying aspect ratios and fiber orientations in simple shear. Fiber orientation was analyzed given its physiologic relevance and direct correlation with tensile properties (Nerurkar, Elliott et al. 2007), while aspect ratios were considered given past findings of shear strain inhomogeneity in oriented tissues such as tendon and ligament (Gardiner and Weiss 2001). Alterations in shear properties were also evaluated as a function of matrix deposition for mesenchymal stem cell seeded constructs. Fiber orientation and sample aspect ratio significantly influenced the response of scaffolds in shear and, with time in culture, the shear modulus of MSC laden constructs increased.

In addition to their potential for directing tissue formation for replacement of degenerate disc and meniscus, nanofibrous scaffolds also serve as useful analogs for understanding structure-function relationships in fiber-reinforced materials, and in constructs as they change with matrix deposition (Nerurkar, Sen et al. 2010) or with or material degradation (Baker, Nerurkar et al. 2009). Within both acellular and cell-seeded scaffolds, one can readily alter a number of structural parameters, including the degree of fiber dispersion (Li, Mauck et al. 2007), the connectivity between fibers (Kidoaki, Kwon et al. 2005), and fiber orientation with respect to testing direction (Nerurkar, Elliott et al. 2007). These parameters are difficult or impossible to precisely control using native tissue samples, given constraints of samples size, matrix organization, and composition. In addition to

control of structural parameters, relatively simple linear and transversely isotropic finite element models can be used to describe deformation of these nanofibrous scaffolds under varying boundary conditions and sample sizes with good fidelity. For example, in this study, measured and predicted shear strain distributions in oriented scaffolds corresponded very well with one another. This is further confirmed by the finding of a maximum shear strain in samples of ~50% of applied shear for 90^o samples, consistent with (Gardiner and Weiss 2001). These findings indicate, as shown previously for uniaxial tension (Nerurkar, Mauck et al. 2008), that shear deformations of these scaffolds can be modeled using continuum assumptions.

Having validated the shear testing methods for this study, we next determined the shear modulus of oriented scaffolds across a range of fiber angles and aspect ratios. For these studies, shear strain was captured in the inner 50% of the scaffold width (**Figure 4-1B**), where strains were most homogenous, regardless of aspect ratio. Results demonstrated that both aspect ratio and fiber orientation influence the apparent shear modulus. For samples with a 2:1 aspect ratio, only one orientation (30^o) resulted in an increased apparent shear modulus relative to other orientations. Conversely, for the 1:2 aspect ratio, apparent shear modulus of samples with orientations of 30^o, 45^o, and 60^o were higher than 0^o or 90^o. Computation of fiber stretch from surface strain measurements helps to explain these findings: i.e., when minimal fiber stretch occurs, little direction-dependence is observed in the apparent shear modulus, while when fiber stretch is maximized, apparent shear modulus increases. For example, the 2:1 samples showed increased fiber stretch only for the 30^o samples, which had a higher apparent shear

modulus. In the 1:2 aspect ratio samples, where fiber stretch was high for all off-axis orientations, correspondingly higher apparent shear moduli were measured.

Given the translational potential of these scaffolds for meniscus and AF repair, it is also useful to compare their measured properties to those reported for native tissue. Native annulus fibrosus has a shear modulus of 200 – 500 kPa (Fujita, Wagner et al. 2000, Jacobs, Morelli et al. 2010). These values are for AF samples with multiple lamellae oriented at ±30° with respect to the shearing direction. This would correspond to 60° samples tested in this study, which had an apparent shear modulus of ~2,500 kPa as acellular scaffolds, and increased to ~4,000 kPa with time in culture as single-layer MSC-seeded constructs. The addition of a second layer with -60° fiber orientation would most likely decrease the apparent shear modulus as it would increase the cross sectional area but provide a layer undergoing no fiber stretch. Like the AF, the meniscus shear modulus ranges from 100 – 400 kPa (Anderson, Woo et al. 1991, Zhu, Chern et al. 1994). Shearing in the meniscus would correspond to the 0° samples tested in this study, whose shear moduli were ~2,500 kPa, both as acellular scaffolds and with time in culture. Reported values for both AF and meniscus shear properties from the literature are for testing configurations in which minimal fiber stretch occurs, and so primarily represent the extrafibrillar 'matrix' shear properties (Yin and Elliott 2005).

Even in the absence of fiber stretch, the measured shear modulus of electrospun scaffolds was quite high (~2MPa). This apparent shear modulus can be thought of as an extrafibrillar 'matrix' shear modulus, which, in the case of acellular scaffolds, reflects the

connectivity of fibers to one another as well as the frictional interactions that resist reorientation with shear deformation. When fiber stretch does occur, the apparent shear modulus is additive of this baseline matrix shear modulus and contributions from fiber stretch. This 'matrix' shear modulus for the nanofibrous constructs in this study is up to one order of magnitude higher than native values, even for unseeded scaffolds. A defining challenge of fibrocartilage tissue engineering arises from the natural design of these tissues, which enables resistance to very large stresses in tension while permitting large deformations under shear stresses. From a design/tissue engineering perspective, this is a significant challenge that must be addressed through scaffold modifications and directed tissue deposition. For example, the cell generated extracellular matrix is likely more deformable in shear than the PCL scaffold, and so a more rapidly degrading polymer, such as poly(lactic-co-glycolic acid) (Baker, Nerurkar et al. 2009), may bring shear properties closer to native values as it degrades and is replaced by cell generated extracellular matrix.

There are a number of additional considerations that these findings motivate. First, this study only addressed the quasi-static response of scaffolds and constructs in shear, whereas physiologic loading is generally dynamic. Additionally, the use of structures reinforced by a single fiber population makes comparisons to native tissue difficult: both the AF (+/- 30°) and the meniscus (0°/90°) are multi-lamellar structures. Future studies will thus investigate shear properties of nanofibrous laminates for a range of ply angles, under both quasi-static and dynamic testing modalities. This will not only improve comparisons to native tissues, but will allow for analysis of inter-lamellar connections in

shear, which contribute to uniaxial tensile properties through an inter-lamellar shearing mechanism (Nerurkar, Baker et al. 2009). These assemblies may also allow for better interpretation of native tissue shear testing results, where tested samples are less controlled, more heterogeneous, and have more variable fiber orientation and lamellar proportions. Future studies will also investigate the use of scaffolds with multiple polymer components. These fibrous composite scaffolds allow for manipulation of scaffold mechanical and structural parameters (Baker, Gee et al. 2008, Baker, Nerurkar et al. 2009). For instance, by including a population of sacrificial poly(ethylene oxide) fibers, scaffold pore sizes can be increased to promote cellular infiltration (Baker, Gee et al. 2008). Likewise, manipulation of solvent volatility can be used to modulate fiber-fiber connectivity (Kidoaki, Kwon et al. 2005) and its role in establishing the 'matrix' shear modulus in these constructs can be assessed. Indeed, these two last features may be used to 'design down' the shear properties of scaffolds to better match native tissue levels and so avoid aberrantly high shear stresses immediately upon implantation.

4.5 Conclusions

If engineered fibrocartilage constructs are to be successful, they must function adequately in the multidirectional loading environment they will be subjected to when implanted *in vivo*. This will require that they resist tensile, compressive and shear loading. Proper analysis of these constructs in shear requires a thorough understanding of the testing method, which, in the case of simple shear testing, is dependent upon the fiber orientation and aspect ratio of the sample. For aligned electrospun scaffolds, a 2:1 aspect ratio results in low fiber stretch and minimal dependence on fiber orientation, while a 1:2

aspect ratio increases fiber stretch so that mechanical anisotropy in shear is observed. Additionally, MSC generated matrix enhances the properties of these constructs in shear. While the shear properties of these constructs appear to be more than adequate, it is likely that additional processing techniques will be necessary to obtain shear properties closer to native values.

CHAPTER 5: BIAXIAL MECHANICS AND INTER-LAMELLAR SHEARING OF STEM-CELL SEEDED ELECTROSPUN ANGLE-PLY LAMINATES FOR ANNULUS FIBROSUS TISSUE ENGINEERING

5.1 Intro

The annulus fibrosus (AF) of the intervertebral disc is a dense fibrocartilage that plays an essential role in motion and load transmission in the spine. The multi-directional loads to which the AF is subjected are resisted by collagen fibers arranged in a distinct angle-ply lamellar structure that alternates between (+/-) 30° with respect to the transverse axis of the spine (Cassidy, Hiltner et al. 1989). This specialized organization is vital for the proper transmission of tensile, shear and compressive loads that arise with movement of the spine (Humzah and Soames 1988). With degeneration, structural organization and mechanical properties of the AF decrease, resulting in abnormal function (O'Connell, Guerin et al. 2009, O'Connell, Sen et al. 2012). Current treatments options, including discectomy and spinal fusion, do not restore mechanical function to the disc, and as such, often result in degeneration of adjacent discs (Levin, Hale et al. 2007). This indicates a need for regenerative strategies that restore mechanical function for all relevant loading regimes, ideally matching native tissue benchmarks (Nerurkar, Elliott et al. 2010). Given the direct relationship between AF structure and function, it is likely that the multi-lamellar hierarchical structure of the native tissue will need to be replicated in any repair material to achieve such a goal.

A number of approaches have been taken for AF and whole disc tissue engineering, with most combining multipotent or AF cells with hydrogel or polymer scaffolds (Park, Lutolf et al. , Nesti, Li et al. 2008, Wan, Feng et al. 2008, Nerurkar, Elliott et al. 2010, Nerurkar, Sen et al. 2010, Bowles, Gebhard et al. , Lazebnik, Singh et al. 2011). However, most of these efforts focus on replication of disc biochemical content and distribution, rather than multi-lamellar microstructure and function. We have previously adopted an electrospinning-based approach to generate scaffolds for multi-lamellar AF tissue engineering (Li, Mauck et al. 2005, Nesti, Li et al. 2008, Mauck, Baker et al. 2009, Nerurkar, Baker et al. 2009). Scaffolds can be formed with a highly aligned fibrous structure that instructs alignment of cells and their subsequent matrix deposition (Baker and Mauck 2007). Seeding these scaffolds with mesenchymal stem cells (MSCs) and culture in chemically defined conditions leads to marked increase in biochemical content and mechanical properties (Baker and Mauck 2007, Nerurkar, Elliott et al. 2007). Moreover, assembly of these single layers into multi-lamellar angle-ply structures produces constructs that replicate the AF anatomic form, microstructure, and uniaxial tensile mechanical function (Nerurkar, Elliott et al. 2007, Nerurkar, Baker et al. 2009). However, while the AF does experience tensile loads, most tensile stresses are applied biaxially as the disc is subjected to multi-axial loads and is constrained by its attachment to the vertebral bodies (Shirazi-Adl, Shrivastava et al. 1984, Schmidt, Heuer et al. 2009, Hollingsworth and Wagner 2012). Our previous studies only tested these constructs under uniaxial tension or compression (Nerurkar, Baker et al. 2009, Baker, Nathan et al.

2010); biaxial mechanical analysis would allow for evaluation in a more physiologic and structurally relevant loading configuration.

In addition to their direct role in AF replacement, electrospun biologic laminates also provide a model system in which to study the development of AF structure-function relationships (Nerurkar, Han et al. 2010). Previous studies suggested that the angle-ply lamellar structure of the AF gives rise to an inter-lamellar shear stiffening effect, where the stress in one lamella can be transferred to adjacent lamellae through shearing of a sufficiently stiff inter-lamellar matrix (Michalek, Buckley et al. 2009, Nerurkar, Baker et al. 2009, Schmidt, Heuer et al. 2009). Thus, the connection between lamellae could play a crucial role in establishing and enhancing AF functional properties. Under uniaxial loading, this inter-lamellar shear stiffening effect arises from reorientation of lamellar fibers in the direction of load. Under pure biaxial strain, fiber reorientation would be minimized, and so the role of this stiffening mechanism would be expected to be less apparent. The objective of this study was to determine the dependence of biaxial mechanical properties on lamellar orientation and inter-lamellar shearing in bilayer nanofibrous scaffolds seeded with bovine MSCs.

5.2 Materials and Methods

5.2.1 Construct Fabrication and Culture:

Aligned poly(ε-caprolactone) (PCL) scaffolds were fabricated via electrospinning from a 14.3% w/v solution of PCL (BrightChina, Hong Kong, China) in a 1:1 solution of dimethylformamide and tetrahydrofuran (Fisher Chemical, Fairlawn, NJ) as in (Nerurkar,

Elliott et al. 2007). Polymer solution was extruded (2.5 ml/hour) from a 18 gauge needle charged to 13 kV and collected onto a grounded mandrel rotating at 10m/s (Nerurkar, Elliott et al. 2007). Rectangles (24 x 26 mm^2) of scaffold were removed at $\theta = 0°$ and 30° relative to the prevailing fiber direction, hydrated with decreasing concentration ethanol washes (100, 70, 50, 30, 0% EtOH, 1hr/step), and soaked in fibronectin (20 mg/ml) for 16 hours (Nerurkar, Baker et al. 2009). Juvenile bovine MSCs were isolated from the tibio-femoral bone marrow and expanded for 2 passages. Single scaffold layers were seeded on each side with $8x10^5$ MSCs and cultured in chemically defined media composed of Dulbeccos's modified Eagle's medium (Invitrogen, Grand Island, NY), 0.1 μmol/L dexamethasone (Sigma, St. Louis, MO), 40 μg/mL L-proline (Sigma, St. Louis, MO), 100 μg/mL sodium pyruvate (Sigma, St. Louis, MO), 1% insulin, transferrin, selenium premix (BD Biosciences, San Jose, CA), 1% penicillin, streptomycin, and fungizone, and 10 ng/mL transforming growth factor β-3 (R&D Systems, Minneapolis, MN) (Huang, Stein et al. 2009). After 2 weeks of pre-culture under free-swelling conditions, angle-ply laminates (APL) were constructed with (+/+) 0°, (+/-) 30°, and (+/+) 30° fiber orientations **(Figure 5-1B)**. APL constructs were assembled by placing individual scaffold layers between two pieces of porous polypropylene (Small Parts Inc, Logansport, IN) which were held in apposition for the first 10 days of culture with a sterile aluminum foil cinch (Nerurkar, Baker et al. 2009) **(Figure 5-1A)**. These fiber angle combinations were chosen to investigate the effect of inter-lamellar shearing on the biaxial tensile response. Eight weeks post-apposition, 13x13 mm^2 central region samples were removed from the larger APL construct and tested in biaxial tension, followed by analysis of biochemical content.

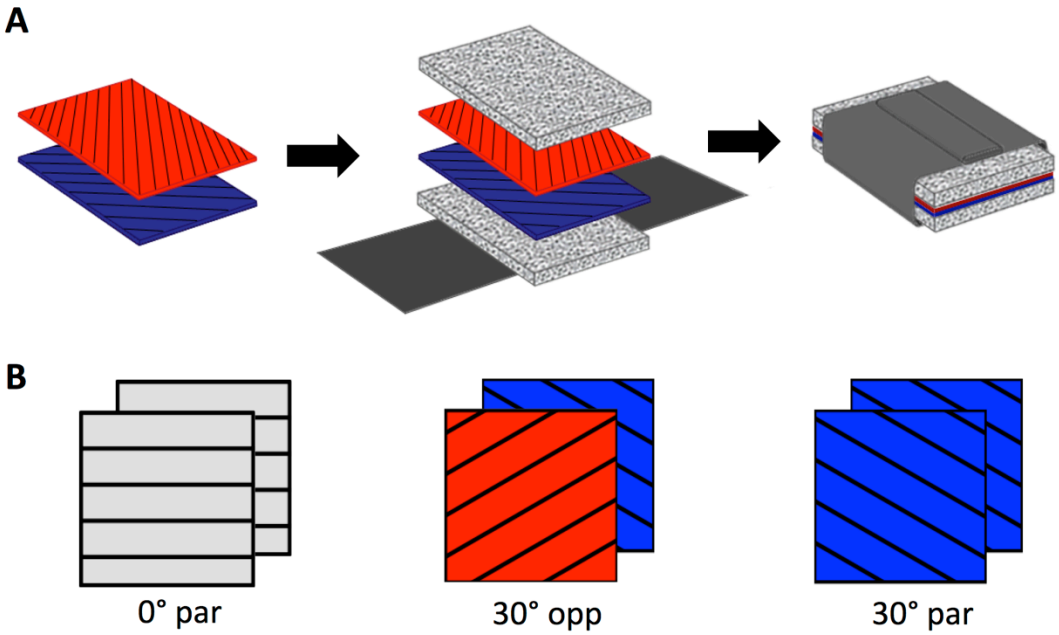

Figure 5-1: Schematic of bi-lamellar construct fabrication process (A) and of construct lamellar orientations (B). par = parallel orientation, opp = opposing orientation.

5.2.2 Histology

At 8 weeks post-apposition, samples (n=2 per group) were frozen in OCT freezing medium (Sakura Finetek USA Inc., Torrance, CA) and cryosectioned through their entire cross-section (24 x 0.6 mm^2) to 12 μm thickness. Sections were stained for collagen with Picrosirius Red or proteoglycans with Alcian blue (Sigma, St. Louis, MO), and imaged using an Eclipse 90i upright microscope with a CCD camera and the NIS-Elements software package (Nikon Instruments, Melville, NY).

5.2.3 Mechanical Testing

Samples (n=4/group) were loaded into a custom biaxial testing device (O'Connell, Sen et al. 2012). Four hooks were attached to each edge of the samples, which were secured to pulleys on the biaxial device via 2-0 braided silk suture (Sacks 1999). Fiber angle was measured from the X_1 axis **(Figure 5-2A)**. Four strain markers were attached in the middle 50% of the sample with cyanoacrylate and used for real-time Lagrangian strain control. Samples were pre-strained equibiaxially to 0.01 at 0.0001 strain/sec and then cyclically ramped 4 times to 0.04 strain at 0.00075 strain/sec. Testing was carried out with two different strain ratios: a 1:1 (X_1:X_2) strain ratio and a 1:0 strain ratio (**Figure 5-2A**). The linear region modulus (0.028 - 0.04 X_1 strain region) was calculated from the 4th cycle of each test, using the cross-sectional area calculated from the thickness measured with a custom laser device and the width between the staple grips (Peltz, Perry et al. 2009). At the peak of the 4th ramp for each test, the deformation gradient tensor (F) was calculated:

$$F = \frac{\partial x}{\partial X}$$

based on the position of the 4 strain markers in the undeformed (X) and deformed (x) states, using a custom MATLAB program (Thomopoulos, Fomovsky et al. 2007, Lake, Miller et al. 2009, Szczesny, Peloquin et al. 2012). This was then used to calculate stretch in the fiber direction (fiber stretch). In this process, the fiber direction is defined by the initial direction of scaffold fiber alignment (a_o) through the vector:

$$a_o = \begin{bmatrix} \cos\theta \\ \sin\theta \end{bmatrix}$$

and the apparent fiber stretch (λ) is calculated as:

$$\lambda = \left((F * a_o)^T * (F * a_o)\right)^{1/2}$$

The deformation gradient tensor was also used to calculate the finite Lagrangian strain tensor (E):

$$E = \frac{1}{2} * (F^T F - I)$$

from which the Lagrangian shear strain (E_{12}) was noted for each group.

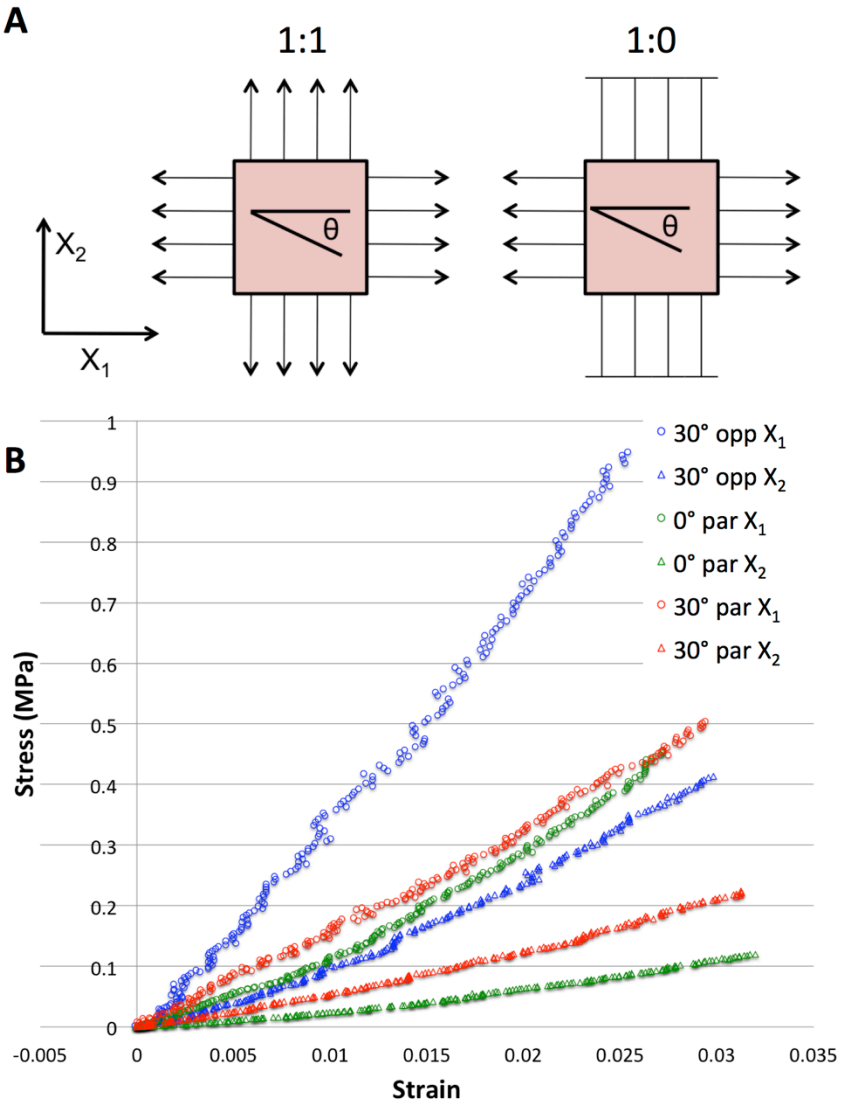

Figure 5-2: Biaxial mechanical testing results with a schematic (A) showing test boundary conditions and fiber orientation (θ). Average stress-strain curves (B) for the 4th cycle of the equibiaxial (1:1) test for APL samples of different construction.

5.2.4 Biochemistry

Biochemical assays were performed to quantify DNA, sulfated glycosaminoglycan (s-GAG), and collagen content after mechanical testing (n=4 per group). After mechanical testing, samples were digested for 16 hours in papain (Sigma) at 60°C, followed by analysis using the PicoGreen dsDNA assay for DNA (Invitrogen), 1,9-dimethylmethylene blue dye-binding assay (Sigma) (Farndale, Buttle et al. 1986) for s-GAG, and (after acid hydrolysis) by reaction with chloramine T (Sigma) and dimethylaminobenzaldehyde (Sigma) to measure ortho-hydroxyproline (OHP) content (Stegemann and Stalder 1967). OHP content was converted to collagen content using a 1:10 ratio of OHP:Collagen (Nerurkar, Elliott et al. 2007).

5.2.5 Statistics

Significance ($P < 0.05$) was evaluated by one-way analysis of variance with Tukey's *post hoc* tests between groups for differences in biochemical content, modulus, maximum shear strain, and fiber stretch. Data are represented as the mean +/- the standard deviation.

5.3 Results

5.3.1 Biochemical Content Increases with Culture Time

MSC seeded electrospun scaffolds were pre-cultured for two weeks, then held in apposition for ten days. This period of appositional culture provided sufficient

mechanical integration between the layers to allow for removal of the porous supports. Eight weeks after the formation of the APLs, histologic analysis demonstrated biologic integration of layers and formation of matrix within the inter-lamellar space **(Figure 5-3)**. This inter-lamellar extracellular matrix was rich in both proteoglycans **(Figure 5-3 A-C)** and collagen **(Figure 5-3 D-F)** for all three groups, with no marked differences observed between the groups. Despite the large size of the constructs (24 x 26 mm^2) compared to previous studies (Baker, O'Connell et al. 2007, Nerurkar, Elliott et al. 2007, Nerurkar, Baker et al. 2009), matrix deposition was observed both within and between the layers. Quantification showed a substantial amount of s-GAG (~4% dry weight) and collagen (~3% dry weight) deposition in all constructs, independent of lamellar orientation (**Figure 5-3F**). DNA content was also equal between groups **(Figure 5-3G)**.

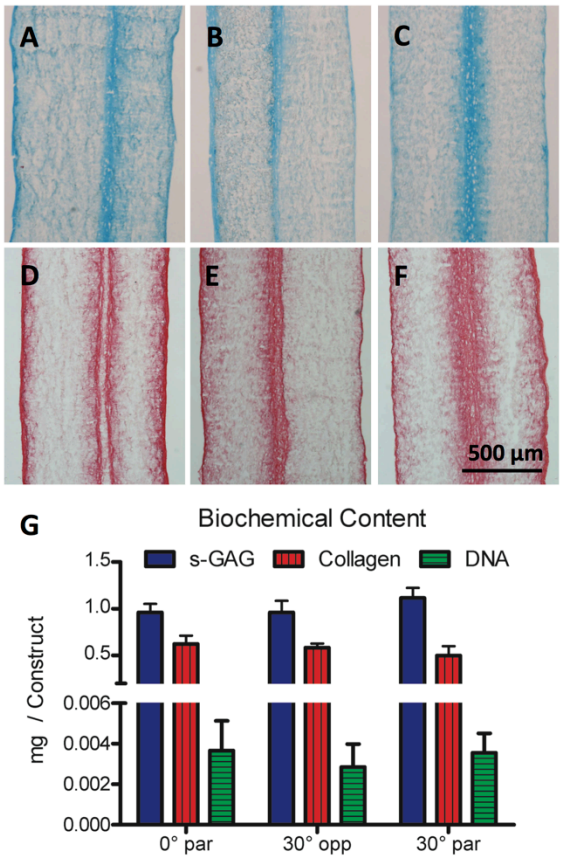

Figure 5-3: Representative histological sections at 8 weeks (A-F) stained for proteoglycans (A-C) and collagens (D-F) for the 0° parallel group (A,D), the 30° opposing group (B,E), and the 30° parallel group (C,F). Quantification of biochemical content (G) of s-GAG, collagen, and dsDNA. Results shown as mean +/- standard deviation (n = 4/group).

5.3.2 Biaxial Mechanical Properties

Biaxial mechanical testing was performed to assess the mechanical integrity of constructs, and the importance of lamellar organization and directionality under multi-axial loading **(Figure 5-2 A)**. Mechanical testing showed nonlinearity in the stress-strain response, and significant anisotropy in all constructs **(Figure 5-2 B)**. With equibiaxial (1:1) testing, 30° opposing (+/-) APLs had a significantly higher modulus in both the X_1 and X_2 directions compared to the 0° and 30° parallel (+/+) APLs **(Figure 5-4 A, B)**. The opposing (+/-) 30° lamellar structure also showed significantly less planar shear strain and a significantly higher fiber stretch ratio (stretch in the prevailing fiber direction) compared to the parallel (+/+) 30° APLs **(Figure 5-5 A, B).** As expected, the 0° bilayers had very little shear strain, and fiber stretch ratios were close to the applied 0.04 strain **(Figure 5-5)**, due to alignment of the fibers with the X_1 loading axis.

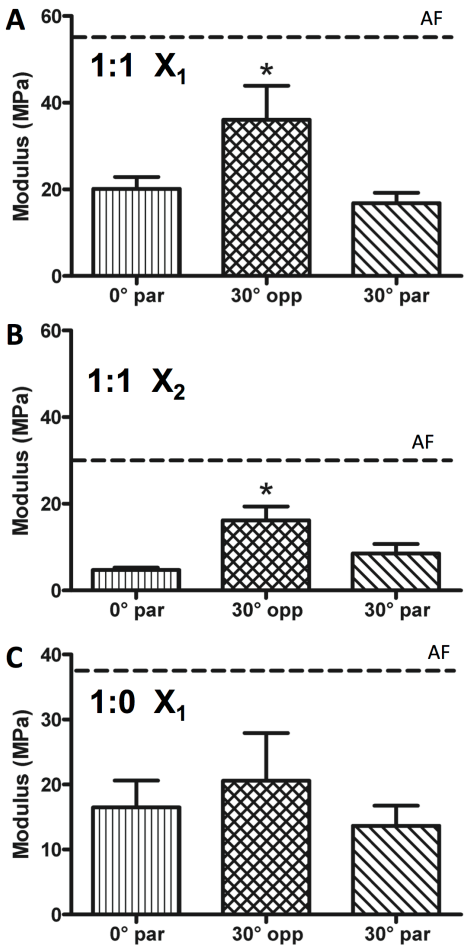

Figure 5-4: Modulus values for the 1:1 biaxial test in the X_1 (A) and X_2 directions (B), and for the 1:0 test in the X_1 (D) direction. Dotted line indicates native tissue properties, calculated from O'Connell et al. 2012. Results are shown as mean +/- standard deviation. * indicates significant difference from both other groups ($P < 0.05$).

Similar modulus trends were observed for the 1:0 test, though differences between opposing and parallel bilayers were not significant in this configuration **(Figure 5-4C)**. With this 1:0 test, there was also a decrease in the amount of shear strain in 30° parallel bilayers, and a decrease in the amount of fiber stretch for 30° opposing bilayers. Strain analysis for the 1:0 test mirrored the 1:1 test, with significantly more shear in the 30° parallel samples **(Figure 5-5 A, C)**, and significantly higher fiber stretch in the 0° parallel

and 30° opposing samples (**Figure 5-5 B, D**). For both testing configurations, the biaxial mechanical properties of (+/-) 30° APL reached ~60% of native tissue values **(Figure 5-4)** (O'Connell, Sen et al. 2012) when the anatomic lamellar structure (+/- 30°) was recapitulated. However, for other APL configurations, mechanical properties reached only 30-40% of native tissue properties **(Figure 5-4)**, despite the similarity in biochemical properties between groups **(Figure 5-3)**.

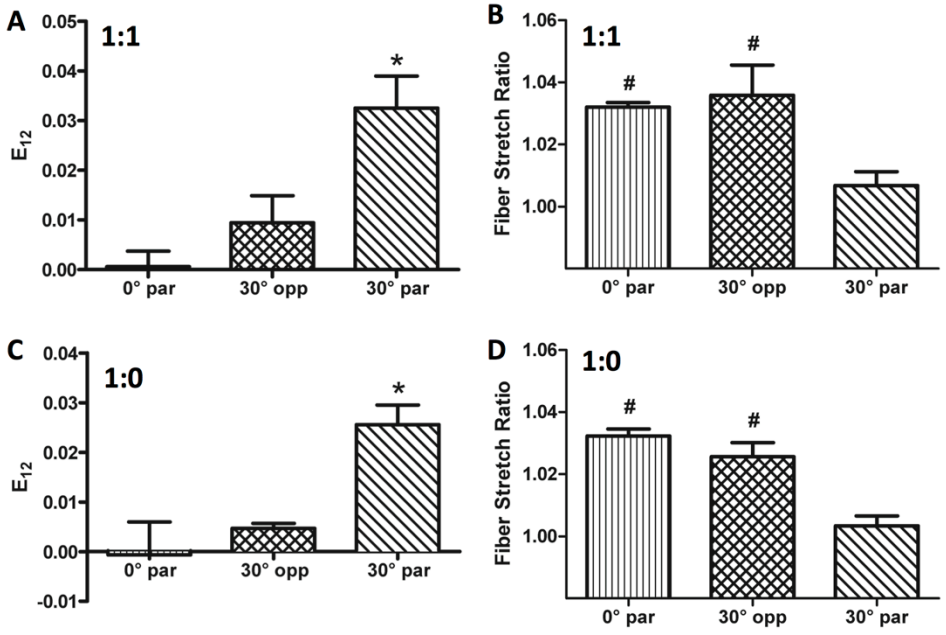

Figure 5-5: Optically measured Lagrangian shear strains (A,C) and fiber stretch ratios (B,D) for 1:1 equibiaxial (A,B) and 1:0 biaxial (C,D) tests. Results indicate mean +/- standard deviation. * indicates significance (P < 0.05) compared to both other groups. # indicates significance (P < 0.05) compared to 30° parallel group.

5.4 Discussion

Functional tissue engineered replacements for the AF must perform under the multidirectional loads the native tissue experiences *in vivo*. These *in vivo* loading environments will require constructs to behave appropriately under a variety of loading

scenarios, including equibiaxial and 1:0 biaxial tension (Shirazi-Adl, Shrivastava et al. 1984, O'Connell, Johannessen et al. 2007). In this study we show that electrospun biologic laminates reach >60% of native tissue biaxial properties under these types of loads, and that these properties are dependent on the opposing lamellar structure (O'Connell, Sen et al. 2012). These data support the notion that resistance to inter-lamellar shearing at the micron level in the AF angle-ply structure is an important feature in the native tissue macroscopic mechanical response.

This study provides insight into the functional role of the AF lamellar structure. Analysis of the peak Lagrangian shear strains for biaxial tests indicated that the opposing (+/- 30°) lamellar structure was able to prevent lamellar shearing for both the 1:0 biaxial and equibiaxial (1:1) tests. This indicates a significant interaction between the lamellae, and that the matrix deposited between these lamellae has an important mechanical function. For the parallel (+/+ 30°) samples, a positive shear indicates that the construct is deforming less in the fiber direction (less fiber stretch) due to increased deformation perpendicular to the fiber direction. This is likely responsible for the reduced (+/+ 30°) construct modulus we observed. Under true equibiaxial strain, where no shear is observed, one would not expect to see any effect of the previously described inter-lamellar shear stiffening (Michalek, Buckley et al. 2009, Nerurkar, Baker et al. 2009, Schmidt, Heuer et al. 2009). However, when the material axis of a transversely isotropic material is not oriented with the loading axis, a smaller but still significant amount of in plane shear is observed (Sacks 1999). Thus the current study indicates that even under equibiaxial strain, the opposing (+/- 30°) lamellar structure prevents shearing within each

lamella. This supports the idea of an inter-lamellar shearing mechanism, where the function and integration of the opposing layers help to resist deformation in adjacent lamellae.

Interestingly, the properties of opposing (+/- 30°) constructs were also significantly higher than the (+/+ 0°) constructs in both directions **(Figure 5-2 B, Figure 5-4)**, despite showing similar fiber stretch ratios **(Figure 5-5 B,D)**. This indicates that a lamellar structure with native tissue fiber orientations is able to provide higher stiffness than a single aligned fiber population, due to the biaxial boundary conditions. The use of biaxial testing is necessary for appreciation of this difference, since previous uniaxial tensile testing showed single lamellar 0° constructs to be about twice as stiff as opposing constructs (+/- 30°) in the X_1 direction (Nerurkar, Mauck et al. 2008, Nerurkar, Baker et al. 2009). This provides further evidence that a lamellar structure with two alternating or angle-ply fiber populations is an important design criterion for both native tissue and a mechanically functional engineered AF.

One limitation of this study, and of electrospun biologic laminates in general, is the strain levels used for biaxial mechanical analysis. Fiber reinforced soft tissues, such as the AF, are required to function under large strains without failing (Stokes 1987, Hollingsworth and Wagner 2012), and typically have highly non-linear mechanics with large toe regions (~0.02 - 0.05) (Bass, Ashford et al. 2004, O'Connell, Sen et al. 2012). While electrospun biologic laminates also display a non-linear response to strain, it is to a lesser extent and with a smaller toe region (~0.01 – 0.02) than native tissue. This is likely due to the large

amount of polymer remaining (>90%) after 8 weeks of *in vitro* culture. Additionally, central scaffold regions contained less matrix than the edges where cellular colonization had occurred. This indicates that cell infiltration was limited, and that there is room for improvement of both mechanical and biochemical properties of these engineered constructs. In the future, multi-polymer scaffolds could be used to increase porosity and accelerate cell infiltration, allowing for increased and more homogeneous matrix deposition (Baker, Gee et al. 2008). It is likely that with further cell infiltration, construct maturation or mechanically accelerated growth (Baker, Shah et al. 2011), native tissue properties and non-linearity may be more closely replicated.

This study provides important insight into the behavior of electrospun biologic angle-ply laminates under biaxial loading that will likely be encountered *in vivo*, as well as the native tissue structure-function relationships. While constructs did not perfectly match the mechanical properties of native tissue, they came close to replicating the biaxial moduli, anisotropy and non-linearity of native AF. This work provides an understanding of the importance of AF microstructure in tissue function, as well as appropriate benchmarks for AF tissue engineering.

CHAPTER 6: CRIMPED MICRO-PATTERNING IN FIBROUS BIOMATERIALS DICTATES MACROSCOPIC MECHANICS, MICRO-SCALE STRAIN TRANSFER, AND MECHANOTRANDUCTION

6.1 Intro

Tissues that are subjected to frequent, high stress and high strain loading, such as those in the cardiovascular and musculoskeletal systems, are often composed of highly aligned collagen fibers that, at the micron-scale, have an intrinsically crimped micro-architecture (Rigby, Hirai et al. 1959, Lim and Boughner 1976). With stretch, crimped fibers straighten, resulting in a non-linear mechanical response (Diamant, Keller et al. 1972, Lake, Miller et al. 2009). Crimp is a critical structural adaptation in these tissues, allowing for low-force deformation at small strains (in the so-called 'toe' region), while providing protection against excessive deformation via the higher 'linear region' modulus that follows (Hansen, Weiss et al. 2002). Importantly, crimp patterning emerges with development (Dickinson and Vesely 2012, Miller, Connizzo et al. 2012) and is lost under pathological conditions or in sub-optimal repairs (i.e. scars), which predisposes these tissues to aberrant loading conditions and may precipitate further degenerative processes (Gathercole and Keller 1991).

As crimp is essential for normal functionality in these tissues, strategies with the aim of engineering functional replacements must address this phenomenon. To date, the most advanced biomaterials for tendon/ligament tissue engineering have recapitulated native tissue nonlinearity using custom weaving of micron-sized biodegradable polymers (Sahoo, Cho-Hong et al. 2007). While promising, in that they can reproduce features of the non-linear stress strain response, these materials fail to provide the nano-scale feature sizes that cells within these tissues encounter. To that end, a number of groups have used highly aligned arrays of polymer nanofibers (created by electrospinning) to provide such nanotopographic cues (Li, Mauck et al. 2007). These highly aligned fibers can direct cell shape and alignment, and lead to subsequent alignment of cell deposited extracellular matrix molecules, such as collagen (Baker, Shah et al. 2012). Recently, we have further refined this technique to generate fiber crimp in nanofibers via the controlled heating of scaffolds to their glass-transition temperature (Surrao, Fan et al. 2012, Grace Chao, Hsu et al. 2014). This treatment alters both scaffold mechanics and cellular interactions with the scaffold. However, these polymer networks have a densely packed fibrous structure with small pores. This dense structure not only limits the degree to which the fibers can crimp, but also results in limited cellular ingress when these scaffolds are seeded with cells. In our previous work, accelerated cellular infiltration into dense nanofibrous scaffolds was achieved by increasing scaffold porosity via inclusion of a water-soluble sacrificial poly(ethylene oxide) (PEO) fiber fraction (Baker, Shah et al. 2012). Inclusion of sacrificial fibers may provide both the high porosity required for cell infiltration, while at the same time increasing the degree to which crimping can occur, resulting in a more instructive and mechanically non-linear scaffold.

Instructive scaffolds can form the basis for patterning tissue formation, but require both a cell source to deposit structural extracellular matrix molecules as well as mechanoactive inputs to drive tissue maturation (Mikic, Johnson et al. 2000, Maeda, Sakabe et al. 2011). Bone marrow derived mesenchymal stem cells (MSCs) are a popular cell source for engineering of orthopaedic tissues because of their multipotent nature (Pittenger, Mackay et al. 1999), ease of isolation and expansion, and the lack of donor site morbidity. MSCs are highly responsive to topographical and mechanical cues, both of which can influence lineage commitment, including towards the tendon/ligament pathway (Chen, Horan et al. 2006, Kuo and Tuan 2008). Indeed, the maturation of both native tissue cell- and MSC-seeded engineered constructs can be expedited by mechanical loading (Baker, Shah et al. 2011, Haugh, Meyer et al. 2011, Subramony, Dargis et al. 2013, Charoenpanich, Wall et al. 2014). Our previous work has shown that both cell and nuclear deformation is highly dependent on fiber directionality with respect to direction of applied strain in engineered nanofiber microenvironments (Heo, Nerurkar et al. 2011, Nathan, Baker et al. 2011). Since most tissues operate within the crimped 'toe' region during normal physiologic activities, it is vital that we consider not only tissue structure and mechanics, but also how that structure regulates mechanotransduction within this crimped context. Mechanotransduction events can occur both at the cell surface, where cells make interactions with their surrounding matrix, as well as deep within the cell, where strains can be transmitted and activate stretch sensitive cytoskeletal and nucleoskeletal associated molecules (Na, Collin et al. 2008, Guilluy, Osborne et al. 2014). Fiber crimp may provide not only topographical mechanical cues that are important for cellular

differentiation and formation of structurally accurate tissues, but may also provide specific cues during mechanical loading that are important in formation and maintenance of this tissue structure.

In this study, we increased scaffold crimp by increasing scaffold porosity prior to heating, thus providing increased space for crimped fiber formation. We then probed the bulk scaffold mechanics and the micromechanical response of both the scaffold itself and cells ensconced in this engineered microenvironment. This approach resulted in a material scaffold that more faithfully reproduces the nonlinear mechanical behavior of native tissue while providing nanotopographic cues important for organized tissue formation. At the same time, these scaffolds illustrate how differential mechano-regulation may arise as a function of micro-scale order.

6.2 Materials and Methods

6.2.1 Scaffold Fabrication

Aligned nanofibrous scaffolds were generated, as described previously (Baker, Shah et al. 2012, Grace Chao, Hsu et al. 2014), by electrospinning onto a rotating mandrel. Scaffolds were spun using an 8.5% w/v solution of poly-L-lactide (PLLA) in Hexafluoropropylene (HFP) either alone, or in combination with a second spinneret containing a 10% w/v solution of poly(ethylene oxide) (PEO, details) in 90% ethanol. These two scaffold types (PLLA alone or PLLA/PEO dual component scaffolds) were washed with decreasing concentrations of ethanol (to hydrate and/or remove PEO) or heated to 65°C for 15 minutes between two glass slides. Dual scaffolds were washed

(DW), heated and then washed (DHW), or washed and then heated (DWH). This last group (DWH) is expected to produce the highest degree of crimp, due to the increased porosity present during heating.

6.2.2 Fiber Characterization

Following processing, scaffolds were dried by desiccation and mounted. Scanning electron microscope images were acquired at using a scanning electron microscope (Hitachi TM3000). Fiber morphology was characterized for each of the scaffold types by calculation of the fiber straightness, which was defined as the end-to-end length of the fiber divided by its persistence length (Grace Chao, Hsu et al. 2014).

6.2.3 Mechanical Testing

Scaffolds were cut into 40x5mm^2 pieces, with the long axis in the fiber direction, and tested in uniaxial tension using an Instron 5848 with a 50N load cell (Instron, Norwood, MA). Scaffold cross sections (100-200 μm thick) were measured using a laser based device (Peltz, Perry et al. 2009) then scaffolds were loaded into Instron grips and quasi-statically ramped at 0.05% strain/second to 25% strain. Stress-strain curves were calculated and a bi-linear fit (MATLAB) was used to determine the transition strain and linear region modulus.

6.2.4 Cell Seeding

Bovine bone marrow derived mesenchymal stem cells (MSCs) were isolated from the tibio-femoral joint of juvenile cows (Research 87, MA, USA), as described previously (Huang, Farrell et al. 2010), and expanded on tissue culture plastic for 2 passages in basal media (high glucose DMEM with 1% penicillin, streptomycin, fungizone (PSF) and 10% fetal bovine serum). Scaffolds were cut into strips of 5x70 mm (for static stretch) or 5x35mm (for immunostaining) with the long axis in the fiber direction. Scaffolds were hydrated and disinfected using decreasing concentrations of ethanol (100, 70, 50, 30, 0%; 30 min/step) and then soaked in a fibronectin containing phosphate-buffered saline solution (20 μg/ml, Sigma) overnight at room temperature to enhance cell attachment. Fibronectin coated scaffolds were seeded with $1x10^5$ cells in 200μl (5x70mm) or $5x10^4$ cells in 100μl (5x35mm) of basal media. Cell seeded scaffolds were cultured for 2 days in basal media prior to static stretch or fixation.

6.2.5 Immunostaining

Two days after seeding, scaffolds were fixed with 4% paraformaldehyde overnight at 4°C then washed three times and permeablized with 0.5% Triton X-100 in phosphate buffered saline (PBS) with 320mM sucrose and 6mM $MgCl_2$. Actin was stained using Alexa-fluor 488 phalloidin (1:1000, Molecular Probes, Eugene, OR) in PBS containing 1% w/v bovine serum albumin for 1 hour at room temperature. Scaffolds were then washed 3 times with PBS and mounted on glass slides using DAPI anti-fade mounting media containing prolong gold (Molecular Probes, Eugene, OR).

6.2.6 Static Tensile Stretch

Cells seeded on aligned scaffolds were stained with Hoechst (5ug/ml, Molecular Probes, Eugene, OR) in high glucose phenol-free DMEM containing HEPES (Gibco, Carlsbad, CA) for 10 min at 37°C. Samples were then loaded into a custom stepper motor driven tensile-device ((Driscoll 2015), n=3-4 / group) mounted onto an inverted epi-fluorescence microscope (Nikon Instruments, Tokyo, Japan) and statically stretched (n=3-4/grp) to 8% strain in 1% increments with images being acquired at each strain level. Nuclear deformation was quantified (n>45 cells/group) using a custom MATLAB program by calculating the ratio of the nuclear principal axis. Briefly, nuclear edges are detected using a canny edge detection algorithm and used to calculate eigenvectors and eigenvalues for the groups of pixels associated with each nuclei. The first and second eigenvalue, which represent the length of the first and second principal axes, are then used to calculate a nuclear aspect ratio at each strain level for each nuclei. Additionally, the centroids of nuclei were used as fiducial markers for calculation of micro-scale Lagrangian strains on the scaffold surface. First, the deformation gradient tensor (F) was calculated for sets of 3 nuclei using their displacements at each strain level relative to the reference (0% strain) image.

$$\mathbf{F}_{ij} = {dx_i}/{dX_j}$$

This was then used to calculate a Lagrangian strain tensor (E) for each triad.

$$\mathbf{E} = \frac{1}{2}(\mathbf{F}^{T}\mathbf{F} - \mathbf{I})$$

Additionally, the effective Poisson's ratio (ν) at each strain level was calculated for each triad.

$$\nu = \frac{-E_{22}}{E_{11}}$$

6.2.7 Western Blot:

For analysis of the cellular response to static stretch on these scaffolds, cell seeded scaffolds were loaded into a previously described tensile bioreactor (Baker, Shah et al. 2011). Scaffolds were statically stretched to 0%, 3% or 8% strain at a strain rate of 3% strain/s and held for 15 minutes. Cells were then lysed with RIPA buffer to isolate total cell protein (50mM Tris-HCl pH 8.0, 150 mM sodium chloride, 1.0% Triton X-100, 0.1% Sodium Dodecyl Sulfate (SDS), 1% protease inhibitor cocktail (Sigma, St Louis, MO) and 1% phosphatase inhibitor cocktail (Sigma, St. Louis, MO). Protein isolates were cleared of insoluble cellular debris by centrifugation (15,000xg for 15min) and protein concentration was quantified using the Lowry assay (Biorad, Hercules, CA). Samples were denatured by boiling at 99°C in reducing lane buffer containing 2% beta-mercaptoethanol. Protein samples (20 μg/lane) were separated on 4-15% gradient SDS polyacrylamide gels and transferred to nitrocellulose membranes (iBlot, Invitrogen, Carlsbad, CA). Membranes were blocked with 5% bovine serum albumin (BSA) in Tris-buffered saline containing 0.1% Tween 20 (TBS-T) and probed with p44/p42 MAPK (ERK1/2) or phospho-p44/p42 MAPK (pERK1/2) antibodies (1:1000, Cell Signaling, Danvers, MA). Membranes were washed three times with TBS-T and treated with anti-rabbit peroxidase conjugated secondary antibody in 5% BSA-TBS-T (1:1000, Cell Signaling, Danvers, MA). Blots were developed using SuperSignal West Pico Chemiluminescent reagent (Thermo Pierce, Waltham, MA) and exposed to CL-Exposure film (Thermo Pierce, Waltham, MA). Quantification was performed via densitometry (ImageJ) and used to calculate a ratio of phosphorylated ERK1/2 to total ERK1/2.

6.2.8 Statistics

Statistical significance was set at $p<0.05$ and statistical comparisons were made using one-way ANOVA with Tukey's post hoc. For analysis of data involving multiple strain levels, comparisons were made using two-way ANOVA with Tukey's post hoc.

6.3 Results

6.3.1 Crimp Influences Bulk Mechanical Properties

Aligned nanofibrous scaffolds fabricated with two fiber populations (PLLA/PEO, Dual) (**Figure 6-1A**) showed increased crimp with heating (H) when the soluble fiber fraction (PEO) was removed (Wash, W). This resulted in a significant decrease in fiber straightness (**Figure 6-1B**) quantified from SEM images of scaffold fiber topographies (**Figure 6-1C**). Dual scaffolds heated before washing (DHW) showed a small decrease in fiber straightness whereas dual scaffolds washed before heating (DWH) displayed a significantly larger decrease in straightness. This increase in crimped or curved fibers influenced bulk scaffold mechanical properties. Tensile mechanical testing showed that single polymer PLLA scaffolds possessed a higher linear modulus than all other scaffolds, indicating that both increased crimp (H) and increased porosity (Dual Wash) resulted in decreased linear region tensile modulus. This did not, however, result in a total loss of tensile strength, as all scaffolds maintained a modulus of 20-100 MPa (**Figure 6-1D**). Analysis of transition strain, an important mechanical attribute of fibrous load bearing tissues, showed that the highly crimped dual wash heat (DWH) scaffolds

achieve a significantly higher transition strain (**Figure 6-1E**). Additionally, these DWH scaffolds also displayed much higher yield strains (**Figure 6-1F**).

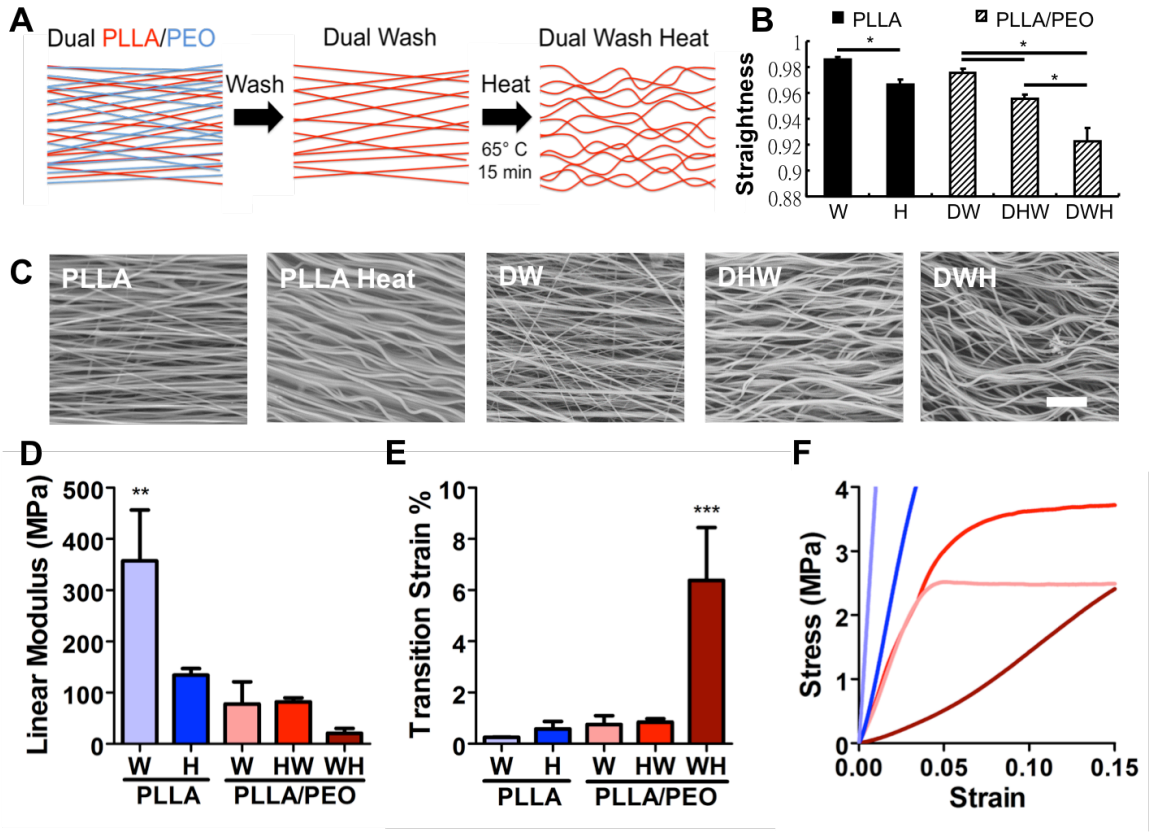

Figure 6-1: Inclusion of sacrificial fibers allows for increased fiber crimp and non-linearity post- heating. (A) Schematic of aligned nanofibrous material containing two fiber populations. The water soluble PEO can be removed by washing with water, increasing the porosity of the scaffold. Annealing (65°C 15 minutes) increases fiber crimp by increasing PLLA fiber crystallinity. When annealing is performed after scaffold porosity is increased, fibers show increased fiber crimp. (B) Quantification of fiber straightness from SEM images (C) of fabricated scaffolds containing a single fiber population (PLLA) or two fiber populations (PLLA/PEO, Dual (D)) (scale bar = 1μm). Fibers were washed (W) and/or heated (H) to induce fiber crimp. Tensile testing of fabricated scaffolds with quantification of the linear modulus (D) and transition strain (E) with average stress-strain curves (F) displaying increased non-linearity. (n=3 per group, * indicates $p<0.05$ vs. W, ** indicates $p<0.01$ vs all other groups, * indicates $p<0.001$ vs all other groups)**

6.3.2 Crimp Alters Micro-Scale Strain Transfer

Since altering the micro-scale fiber morphology likely alters the micro-scale strain transfer important for regulating cellular processes, we next assessed the extent to which crimped fibers impact micro-scale strain transfer to the local cellular microenvironment and into the cell nucleus. For this, we employed a previously described micro-tensile device that allows for simultaneous stretch and imaging of scaffolds and the cells adhered to them (Driscoll 2015). Scaffolds were coated with fibronectin and seeded with bovine mesenchymal stem cells (MSCs). Staining of F-actin and DAPI after 2 days of culture showed cells were well attached and aligned in the fiber direction (**Figure 6-2A**). Auto-fluorescent fibers displayed crimp that was often followed by cell protrusions. Analysis of Lagrangian strains calculated from triads of nuclei, showed strains in the stretch direction that reached close to the applied strain for all groups (E_{11}, **Figure 6-2B**). In the direction perpendicular to stretch, large compressive strains (E_{22}) were observed due to the high Poisson's ratio of the materials (**Figure 6-2B**). Quantification of Poisson's ratios from these triads of nuclei indicated that increased fiber crimp in the DWH scaffolds significantly reduced the lateral compressive strains (**Figure 6-2C**). Analysis of strain transfer into the cells nuclei indicated that all scaffolds induce significant nuclear deformation with applied stretch (**Figure 6-2D**). However, nuclei of cells on crimped DWH scaffolds showed decreased baseline aspect ratio (**Figure 6-2D**) and decreased alignment in the fiber direction (**Figure 6-2E**). This resulted in significantly more nuclear reorientation in crimped scaffolds with applied stretch to the scaffold. Additionally, cells on crimped DWH scaffolds failed to reach the high nuclear aspect ratios observed in the other two groups (**Figure 6-2E**).

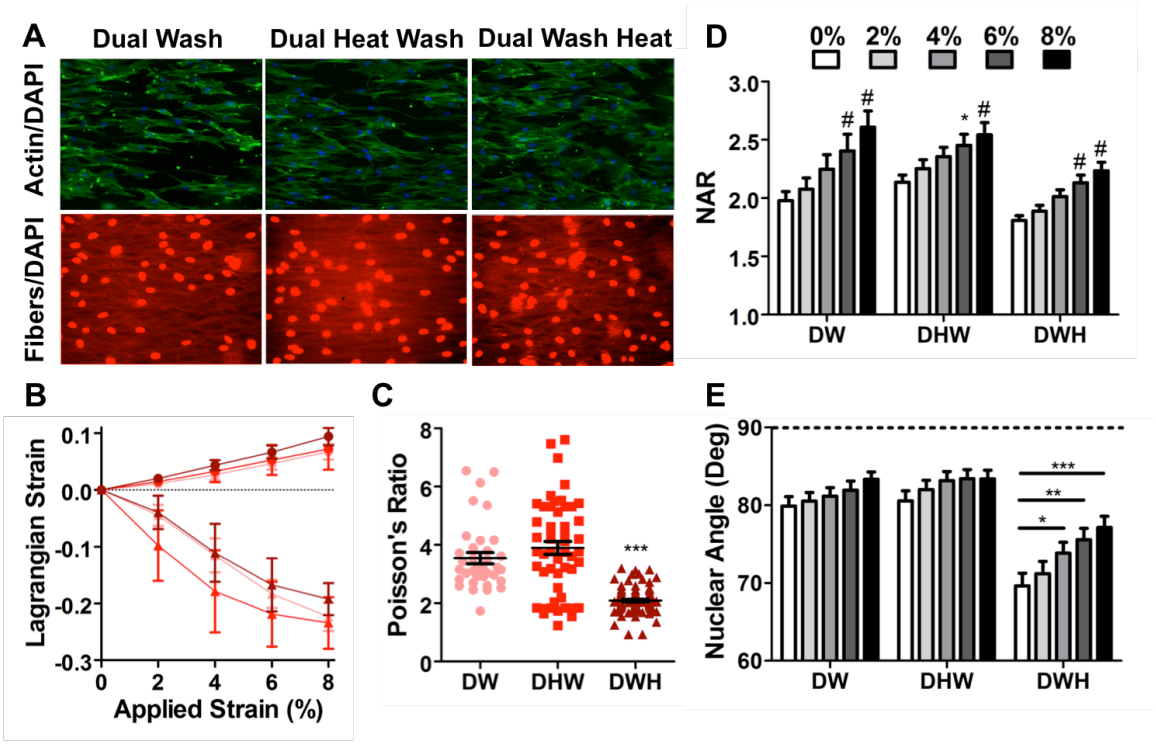

Figure 6-2: Crimped fibers alter nuclear morphology and micro-scale strain transmission. (A) Representative images of mesenchymal stem cell seeded scaffolds stained for F-actin (phalloidin, green) and nuclei (DAPI, Blue), with auto-fluorescent fibers (Red) displaying increased crimp in dual wash heat scaffolds. (B) Micro-scale Lagrangian strains (mean +/- SD) calculated from triads of nuclei with applied scaffold stretch. (C) Poisson's Ratio's calculated from triads of nuclei. (D) Quantification of nuclear aspect ratio and nuclear orientation (E, 90°= fiber direction) with applied scaffold stretch. (n=3-4 samples per group, n>47 nuclei per group). (* p<0.05, ** p<0.01, *** p<0.001, # indicates p<0.01 vs unstretched control).

6.3.3 Crimp Regulates the Biologic Response to Strain

Next, we assayed the phosphorylated ERK1/2 MAPK response on MSCs when statically stretched to 3 or 8% strain and held for 15 minutes. ERK1/2 is a signaling kinase downstream of a number of mechanically activated molecules in including focal adhesions (Li, Kim et al. 1997, Chaturvedi, Gayer et al. 2008) and ion channels (Jessop, Rawlinson et al. 2002). We found little to no increase in phosphorylated ERK1/2 when cells were statically stretched on straight non-heated fibers (**Figure 6-3A and 6-3B**,

DW). However, when cells were stretched on crimped fibers (**Figure 6-3B**, DWH) significant activation of ERK1/2 was observed. Additionally, cells seeded on DWH scaffolds displayed significantly lower baseline ERK1/2 phosphorylation, potentially indicating reduced baseline activation of adhesions.

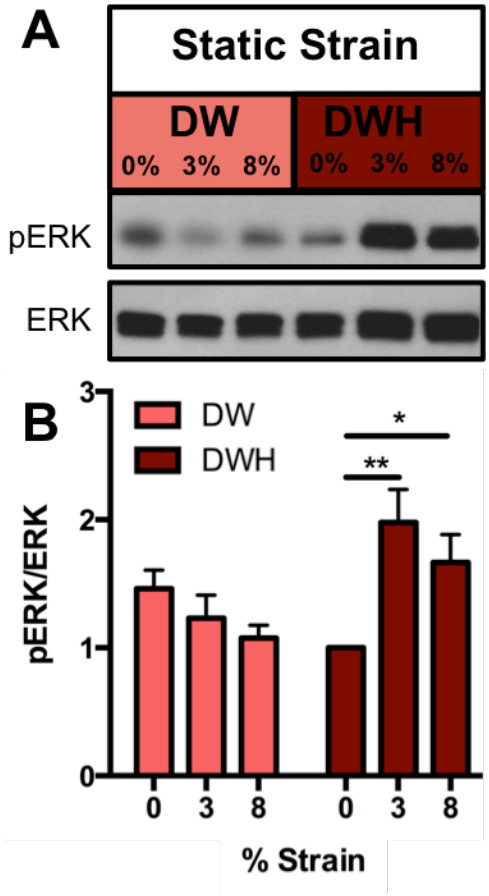

Figure 6-3: Crimped fibers alter ERK1/2 sensitivity to mechanical stretch. Whole cell protein was extracted from MSC seeded scaffolds stretched to 0, 3, or 8% strain and held for 15 minutes. Western blot analysis (A) of phosphorylated ERK 1/2 normalized to total ERK with quantification using densitometry (B). Results plotted as fold increase vs. 0% DWH. (n=3/group, * $p<0.05$, ** $p<0.01$).

6.4 Discussion

Fiber crimp is important for the appropriate function of fiber reinforced soft tissues, providing mechanical non-linearity. Further, this microstructure influences transfer of strain to the cells within these tissues, regulating cellular behavior. When engineering replacement tissues, recapitulation of this microstructure will likely be important for both the bulk construct mechanics and the mechanotransduction that occurs within. In this study, we found that a crimped nanofibrous structure could be engineered into aligned electrospun scaffolds, and that this crimp could be enhanced by inclusion of a sacrificial fiber fraction. This not only increases mechanical non-linearity, but also results in microstructural changes that alter strain transfer to the cellular microenvironment.

Given that micro-environmental strains are critical for tissue development and homeostasis (Mammoto and Ingber 2010, Shwartz, Blitz et al. 2013), an understanding of this strain transfer, and how it regulates cellular mechanotransduction in the context of engineered materials, will be critical for their success. In this study, we show that crimp alters the micro-scale Lagrangian strains of stretched scaffolds. Additionally, we observed that cells seeded on crimped scaffolds displayed lower nuclear aspect ratios and less alignment in the fiber direction. Because of this, increased nuclear reorientation was observed with application of stretch and nuclear aspect ratios on crimped scaffolds did not reach levels achieved on less crimped scaffolds. In addition to having an impact on nuclear reorientation and strain transfer, crimp increased the mechanical activation of ERK1/2 MAPK. On straight fibers, static stretch had no impact on signaling, while on crimped scaffolds, a marked upregulation in signal was observed. This activation at low

strain levels likely indicates that the shearing that occurs between crimped fibers as they straighten influences cellular behavior.

In summary, we have developed and validated a new method for generation of aligned nanofibrous scaffolds with high porosity and crimp, providing mechanical non-linearity. This crimp regulates both bulk and micro-mechanical properties, influencing cellular response to stretch. This microstructure and the alterations in strain transfer that it causes may provide specific cues during mechanical loading that are important in formation and maintenance of functional fiber-reinforced tissues.

CHAPTER 7: CYTOSKELETAL TO NUCLEAR STRAIN TRANSFER REGULATES YAP SIGNALING IN MESENCHYMAL STEM CELLS WITH DYNAMIC LOADING

7.1 Intro

Mesenchymal stem cells (MSCs) are a popular cell source for tissue engineering and regenerative medicine applications given their multi-lineage differentiation potential. In addition to soluble factors, the differentiation of these cells can be regulated by mechanical cues from the microenvironment, including passive inputs such as substrate stiffness (Engler, Sen et al. 2006) or cell adhesion area (McBeath, Pirone et al. 2004) as well as active inputs such as dynamic compression (Angele, Schumann et al. 2004) or tension (Baker, Shah et al. 2011). Interpretation of these mechanical differentiation cues requires cytoskeletal tension, which enables cells to probe their surroundings (McBeath, Pirone et al. 2004, Engler, Sen et al. 2006) and translate physical cues into changes in biologic activity. Cytoskeletal tension also regulates a number of mechanical and structural attributes of the cell, which are important for cellular interpretation of mechanical signals, and can change with differentiation status (Fu, Wang et al. 2010). Given that downstream application of stem cells often involves their placement into a mechanically loaded microenvironment, it is critical to elucidate the relationship between

physical inputs and translation of these signals to biologic activity in stem cell populations.

The attachments that cells make to molecules in their immediate microenvironment and to one another are mechanosensitive, growing or shrinking in a tension-dependent manner (Bershadsky, Balaban et al. 2003). Numerous molecules located at or within the cell membrane are mechanosensitive. These include stretch activated ion channels, which open when mechanical force is applied (Volkers, Mechioukhi et al. 2014), and integrin associated molecules, such as FAK, paxillin, talin and vinculin, all of which activate with force (Dumbauld, Michael et al. 2010, Grashoff, Hoffman et al. 2010, Pasapera, Schneider et al. 2010, Margadant, Chew et al. 2011, Carisey, Tsang et al. 2013) by changing their conformational state under load and exposing cryptic binding sites that recruit or activate molecules involved in downstream signaling (Papagrigoriou, Gingras et al. 2004, del Rio, Perez-Jimenez et al. 2009). Additionally, forces within this tensed actin cytoskeleton are transmitted to subcellular organelles, the largest and stiffest of these being the nucleus (Pajerowski, Dahl et al. 2007). Cytoskeletal forces regulate both stress and strain within the nucleus, through connections mediated by the LINC complex (LInker of Nucleoskeleton and Cytoskeleton). It has recently been shown that contractile pre-stress in the cytoskeletal network is necessary for the rapid activation of Src kinase deep within the cell, at cytoskeletal intersection points (Na, Collin et al. 2008). Still more recently, it has been reported that in isolated nuclei, stretching of the LINC complex component nesprin 1 induces a rapid Src kinase dependent phosphorylation of emerin on the inner nuclear membrane (Guilluy, Osborne et al. 2014). This phosphorylation event

changes association with the nuclear structural protein lamin A, resulting in stiffening of the nucleus and regulation of downstream transcription of mechanically regulated genes. Thus, transfer of mechanical force through the tensed actin cytoskeleton to the nucleus is likely important in mechanosensing, and identifying specific pathways that are regulated by this strain transfer is therefore an important goal.

One pathway that mediates MSC mechanosensing is the YAP/TAZ mechanotransduction pathway (Dupont, Morsut et al. 2011). YAP relays mechanical input through a Rho-GTPase dependent translocation to the nucleus, where it acts to regulate gene transcription (Dupont, Morsut et al. 2011). These mechanotransductive elements are likewise required for substrate stiffness induced differentiation of MSCs. Additionally, it has been shown that the YAP/TAZ pathway can be activated with dynamic tensile loading of myoblasts (Bertrand, Ziaei et al. 2014), and that mutations in the nuclear lamina or in components of the LINC complex perturb this response (Bertrand, Ziaei et al. 2014, Guilluy, Osborne et al. 2014). Therefore, mechanosensing through YAP is likely dependent on forces transmitted through the cytoskeleton and to the nucleus.

Both matrix organization and composition play a crucial role in determining how strain is transmitted through the cell and to the nucleus. In native tissues, nuclear strain transmission is highly variable, depending on tissue type and local matrix properties (Bruehlmann, Hulme et al. 2004, Upton, Gilchrist et al. 2008, Han, Heo et al. 2013). In the case of cells removed from tissues and plated on flat two-dimensional surfaces, nuclear deformation still occurs with applied mechanical stretch (Lammerding, Hsiao et

al. 2005), but reorientation of both the cell and its nucleus away from the direction of stretch alters the extent to which this nuclear deformation occurs at later time points. When cells are oriented on surfaces using parallel microgrooves, stretch perpendicular to alignment results in significantly less nuclear deformation than stretch in the direction of alignment (Li, Chu et al. 2011), and this differentially regulates cellular activities (Kurpinski, Chu et al. 2006). Previously, we have shown, in the context of a three-dimensional aligned fibrous environment, that nuclear strain transfer is dependent on the presence of the actin cytoskeleton, and is independent of the patency of the microtubule and intermediate filament networks (Nathan, Baker et al. 2011). We also showed that nuclear deformation and biologic response was dependent on the direction of stretch with respect to fiber orientation (Heo, Nerurkar et al. 2011), and that realignment of cells within an aligned fibrous network does not occur with long-term dynamic stretch (Baker, Shah et al. 2011). The organization of the microenvironment in which a cell resides thus plays a critical role in determining both the transfer of strain through the cell and the response of that cell to loading. Therefore, it is important to understand the molecular mechanisms of cellular mechanotransduction in the context of fibrous topographies that more closely mimic native tissue environments.

Despite a growing understanding that mechanosensing occurs at the nuclear membrane (in addition to traditional focal adhesions at the cell periphery), the exact role that transfer of strain to the nucleus plays in the response of MSCs to tensile stretch is not clear, and the importance of nuclear strain versus nuclear stress concentrations is as yet unknown. Further, there likely exist mechanosensitive pathways that depend specifically on nuclear

strain transfer and nuclear deformation, as well as others that signal primarily from cell membrane associated mechanosensitive signaling modules. In this study, we assayed the extent to which nuclear and cytoskeletal pre-stress regulate transmission of strain to the MSC nucleus, and the role of this pre-stress in the regulation of both short- and long-term interpretation of mechanical cues. We employed both static and dynamic tensile stretch, in the presence or absence of pharmacologic regulators of cytoskeletal tension and filamentous actin patency, to determine the roles that cytoskeletal tension and nuclear deformation play in activating the early response (ERK1/2 MAP kinase, YAP/TAZ) and longer-term transcriptional programs in response to dynamic mechanical cues.

7.2 Materials and Methods

7.2.1 Scaffold Fabrication

Aligned electrospun scaffolds were generated as described previously (Nerurkar, Baker et al. 2009) by electrospinning a 14.3% w/v solution of poly(ε-caprolactone) (Bright China, Hong Kong, China) in 1:1 mixture of N,N-dimethylformamide and tetrahydrofuran (Fisher Chemical, Fairlawn, NJ). This solution was extruded at a rate of 2.5 mL/hr through a spinneret (18 gauge stainless steel needle) charged to +13kV. Alignment was instilled by collecting fibers onto a grounded mandrel rotating with a surface velocity of ~10m/s. Scaffold mats (~1mm thick) were removed from the mandrel and cut into 65mm x 5mm segments with the long axis oriented in the prevailing fiber direction. Scaffold segments were disinfected and rehydrated in decreasing concentrations of ethanol (100, 70, 50, 30%; 1hr/step) and rinsed twice in phosphate buffered saline (PBS).

Prior to cell seeding, scaffolds were coated in fibronectin for 12-18 hours (Sigma, 20 μg/ml in PBS).

7.2.2 Cell Isolation and Seeding

Bovine bone marrow derived mesenchymal stem cells (MSCs) were isolated from the tibio-femoral trabecular bone marrow of juvenile calves and plated onto 15cm tissue culture dishes (Huang, Farrell et al. 2010). MSCs were expanded in basal media (high glucose DMEM with 10% FBS and 1% PSF) for 2 passages prior to seeding. For monolayer experiments, MSCs were seeded onto glass slides or fibronectin coated poly-acrylamide gels and cultured overnight in serum free, chemically defined media (High Glucose DMEM with 1x PSF, 0.1μM dexamethasone, 50 μg/mL ascorbate 2-phosphate, 40 μg/mL L-proline, 100 μg/mL sodium pyruvate, 6.25 μg/ml insulin, 6.25 μg/ml transferrin, 6.25 μg/mL selenous acid, 1.25 mg/mL bovine serum albumin and 5.35 μg/mL linoleic acid) (Baker, Nathan et al. 2010). For stretch studies, cells were seeded onto 65mm x 5mm fibronectin coated aligned electrospun scaffolds at a density of $2x10^5$ cells per side (protein and mRNA studies) or $5\ x10^4$ cells per side (image based studies).

7.2.3 Pharmacologic Regulation of Contractility

Contractility was altered via the application of various pharmacologic agents. Contractility was decreased using the myosin inhibitor Blebbistatin (Sigma, St Louis, MO), the myosin light chain kinase inhibitor ML7 (Tocris Biosciences, Bristol, UK), the ROCK inhibitor Y27632 (Calbiochem Merk, Darmstadt, Germany), and the actin polymerization inhibitor cytochalasin D (Sigma, St Louis, MO). The ROCK agonist

lysophosphatidic acid (LPA, Sigma, St Louis, MO) was used to transiently increase contractility. For experiments focused on dose dependence, concentration was varied across a range previously reported in the literature. For all other experiments, contractility moduluators were set at defined levels: Blebbistatin 50μM, ML7 25μM, Y27632 10μM, CytoD 2.5μM, and LPA 50μM. All inhibitors were added 1 hour prior to fixing or stretching, while activators (LPA) were added 15 minutes prior to fixing or stretching.

7.2.4 Immunofluorescence

Cells seeded on glass slides overnight were fixed with 4% paraformaldehyde for 20 min at 37°C then washed and permeablized with 0.05% Triton X-100 in PBS supplemented with 320mM sucrose and 6mM magnesium chloride. Cells were incubated with anti-YAP antibody in 1% BSA in PBS (1:200, Santa Cruz Bio, #sc-101199) overnight at 4°C, washed 3 times with PBS and then incubated for 60 min at room temperature with Alexa-Fluor 488 or 546 phalloidin (1:1000, Molecular Probes, Eugene, OR) and Alexa-fluor 546 or 488 goat anti-mouse secondary (1:200, Molecular Probes, Eugene, OR). Cells were washed 3 times and mounted with DAPI containing mounting medium (ProLong Gold Antifade Reagent, Molecular Probes, Eugene, OR). Images were taken using a Nikon Eclipse TE2000-U inverted epi-fluorescence microscope with 20x objective and quantified using a custom MATLAB program. DAPI images were edge detected using the Canny edge detection algorithm and nuclear area was quantified. The nuclear outline was then used as a mask to quantify F-actin staining intensity in the vicinity of the nucleus. For YAP/TAZ staining on glass, average staining intensity in the nucleus and within the cytoplasm was quantified using ImageJ; these intensities were used to

calculate a nuclear to cytoplasmic YAP ratio. Nuclear height was measured using ImageJ, based on DAPI staining from orthogonal Y-Z images generated from confocal z-stacks (Zeiss LSM 510 with 60x oil objective, acquired with z-resolution of 0.37 μm/pixel).

7.2.5 Traction Force Microscopy

Polyacrylamide (PA) hydrogels (Young's Modulus, E = 5 kPa) were prepared as in Aratyn-Schaus (Aratyn-Schaus, Oakes et al. 2010). 0.2μm-diameter fluorescent microspheres (Invitrogen, #F8810, Carlsbad, CA) were mixed into PA at 1% v/v prior to polymerization. Fibronectin (20 μg/mL) coating of gel surfaces was accomplished with 2 mg/mL sulfo-SANPAH (Pierce, #22589). Small drops of a UV-curable fixative, NOA68 (Norland Products, Cranbury, NJ), were used to secure the slides in a live cell imaging chamber. Gels were subsequently washed three times with PBS and sterilized under germicidal UV light for 1 hour. In all traction force experiments, MSCs were seeded at a density of 3000 cells/cm^2 and allowed to attach for 20 hrs before TFM was performed. Phase contrast and fluorescent images of multiple cells and embedded beads were captured at 40X magnification on a Deltavision Deconvolution Microscope. Image sequences for each cell were taken at three points: i) before addition of contractility altering-agents, ii) after specified incubation times in the presence of these agents, and iii) after cell lysis with SDS buffer. All imaging was performed in an environmental chamber (37°C, 5% CO_2). TFM data analysis (stack alignment, PIV, and FTTC) was performed using a freely available plugin suite for ImageJ, created by Q. Tseng (Tseng, Duchemin-Pelletier et al. 2012) which was adapted from (Dembo and Wang 1999). For FTTC, the

Poisson's ratio of the PA gel was assumed to be 0.45 and a regularization parameter of 2e-9 was used. Using a custom MATLAB script, traction force vector maps were analyzed to determine average traction stress generated by each cell and total force exerted per cell. Cell area was determined from the corresponding phase contrast images in ImageJ.

7.2.6 Static Tensile Stretch and Analysis of Nuclear Deformation

Cells seeded on aligned scaffolds were stained with Hoechst (5mg/ml, Molecular Probes, Eugene, OR) in high glucose phenol-free DMEM containing HEPES for 10 min at 37°C. Static stretch was applied to determine the role of cytoskeleton tension in nuclear deformation as a function of scaffold stretch. Scaffolds were stretched (n>4 per group) up to 15% strain in 3% increments using a tensile device mounted on a Nikon Eclipse TE2000-U inverted epi-fluorescence microscope using a 20x Plan Fluor ELWD objective with a tunable correction collar. Nuclear deformation at each step was quantified (n>50 cells per group) using a custom MATLAB program by calculating the ratio of nuclear principal lengths normalized to 0% strain. A canny edge detection algorithm was used to detect outer nuclear edges based on gradients in signal intensity. Edges were then dilated, filled, and grouped into clusters. Principal component analysis was performed on the clusters to identify principal lengths of the nucleus as in (Nathan, Baker et al. 2011). A nuclear deformation index (**NDI**) was then calculated for each experimental group by normalizing nuclear deformation at each strain level to the mean deformation observed for the control group at that same strain level. To calculate this index, the average nuclear deformation (**nNAR**, nuclear aspect ratio normalized to undeformed state) was

calculated at each strain level. These averages were used to normalize the nuclear deformation at each of the 5 strain levels (**i=1-5**) to the associated deformation in the control group at that strain level using the following formula:

$$\boldsymbol{NDI} = \frac{(\boldsymbol{nNAR_{Ti}} - \mathbf{1}) - (\boldsymbol{nNAR_{CiAve}} - \mathbf{1})}{(\boldsymbol{nNAR_{C15\%Ave}} - \mathbf{1})} * \mathbf{100}$$

Where **i** indicates the applied strain level (3, 6, 9, 12, 15%), **T** indicates treatment group, **C** indicates control group, and **Ave** indicates average at that strain level.

Local Lagrangian strains were also calculated using triads of nuclei as fiducial markers at each strain level to ensure consistent local deformations across scaffolds and experimental conditions. First, the displacements for each point were calculated based on a reference image. These displacements were then used to calculate the deformation gradient tensor **F**:

$$\boldsymbol{F_{ij} = dx_i / dX_j}$$

Where x indicates the deformed point locations, X indicates the undeformed locations, and i and j indicate the principal directions. This tensor can then be used to calculated the Lagrangian strain tensor **E**:

$$\boldsymbol{E_{ij} = \frac{1}{2}\,(F^T F - I)}$$

Components of this tensor give the two-dimensional strains in the two principal directions as well as the shear strain.

7.2.7 Dynamic Tensile Stretch

Dynamic stretch (3% strain, 1Hz) was applied in a CO_2 incubator using a custom bioreactor system [8]. For analysis of pERK1/2 response, stretch was applied for 15 min with inhibitors (Blebbistatin 50μM, ML7 25μM, Y27632 10μM) added 1 hour prior to stretch and LPA (50μM) added 15 min prior to stretch. For quantification of nuclear YAP with stretch, cells were loaded for 30 or 360 minutes and fixed and stained with anti-YAP antibody, Phalloidin, and DAPI immediately or 12 hours after cessation of loading, with inhibitors added 1 hour prior to stretch. For YAP analysis on scaffold, cells were imaged using a Nikon A1 laser scanning confocal microscope with 20X objective. Z-stacks were acquired at 0.75μm slice thickness over the entire cell with the slice centered at the nucleus used for quantification of the nuclear-to-cytoplasmic YAP ratio. For analysis of the gene expression, stretch was applied on two consecutive days for 6 hours per day with inhibitors added 1 hour prior to stretch on each day of loading.

7.2.8 Western Blotting

Cells were seeded on aligned scaffolds for 2 days, dynamically loaded for 15 min at 1Hz to 3% strain, washed once with PBS, and lysed in RIPA buffer (50mM Tris-HCl pH 8.0, 150 mM sodium chloride, 1.0% Triton X-100, 0.1% Sodium Dodecyl Sulfate (SDS), 1% protease inhibitor cocktail (Sigma, St Louis, MO) and 1% phosphatase inhibitor cocktail (Sigma, St Louis, MO) to isolate total cellular proteins. Protein isolates were cleared of insoluble cellular debris by centrifugation (15,000 × *g* for 15min) and protein concentration was quantified using the Lowry assay (Biorad, Hercules, CA). Samples were denatured by boiling for 5 min in reducing buffer containing 2% beta-

mercaptoethanol. Proteins were separated on 4-15% gradient SDS polyacrylamide gels and transferred to nitrocellulose membranes. Membranes were blocked with 5% bovine serum albumin (BSA) in Tris-buffered saline containing 0.1% Tween 20 (TBS-T) and probed with p44/p42 MAPK (ERK1/2) or phospho-p44/p42 MAPK (pERK1/2) (Cell Signaling, Danvers, MA). Membranes were washed three times with TBS-T and treated with anti-rabbit peroxidase conjugated secondary antibody in 5% BSA-TBS-T (1:1000, Cell Signaling, Danvers, MA). Blots were developed using SuperSignal West Pico Chemiluminescent Reagent (Pierce) and exposed to CL-Exposure film (Thermo).

7.2.9 Quantitative Real Time RT-PCR

Changes in gene expression were determined by real time RT-PCR. MSCs were seeded on aligned nanofibrous scaffolds for 2 days in chemically defined media and then loaded into the custom tensile bioreactor with or without pharmacologic regulators of contractility (Blebbistatin 50μM, ML7 25μM, Y27632 10μM) for 1 hour prior to loading on each day of loading. Cells were dynamically stretched to 3% strain at 1Hz for 6 hours on two consecutive days. After the second loading, samples were snap frozen in Trizol, and mRNA was subsequently isolated by phenol-chloroform extraction. RNA concentration was quantified (ND-1000, Nanodrop Technologies, Wilmington, DE, USA) and cDNA synthesized using the SuperScript II First Strand Synthesis kit (Invitrogen Life Technologies, Carlsbad, CA). PCR was performed with gene specific primers using an Applied Biosystems StepOnePlus real time PCR machine and the Fast SYBR Green reaction mix (Applied Biosystems, Foster City, USA). Expression levels of aggrecan (AGG, CCTGAACGACAAGACCATCGA and

TGGCAAAGAAGTTGTCAGGCT), connective tissue growth factor (CTGF, CGTGTGCACCGCTAAAGATG; GGAAAGACTCTCCGCTCTGG), and scleraxis (SCX, GAACACCCAGCCCAAACAGAT, TCCTTGCTCAACTTTCTCTGGTT) were determined and normalized to the housekeeping gene glyceraldehyde-3-phosphate dehydrogenase (GAPDH, ATCAAGAAGGTGGTGAAGCAGG and TGAGTGTCGCTGTTGAAGTCG).

7.2.10 Statistical Analysis

All experiments were performed for 2-3 MSC donors and scaffold batches per condition. Statistical comparisons were performed using one-way or two-way ANOVA with Tukey's post hoc testing used to make pair-wise comparisons between groups. Statistical significance was set at $p<0.05$. For nuclear deformation experiments, single cells were tracked and comparisons made using two-way repeated measures ANOVA with Tukey's post hoc testing.

7.3 Results

7.3.1 Contractility Regulates Basal Nuclear Shape

Acto-myosin based contractility has previously been shown to play an important role in regulating nuclear shape and organization in a variety of cell types (Khatau, Hale et al. 2009, Chancellor, Lee et al. 2010, Ramdas and Shivashankar 2014). To determine the extent to which actin and intracellular tension regulate nuclear shape (aspect ratio, height, and projected area) in mesenchymal stem cells (MSCs), cells were treated with varying

levels of pharmacologic regulators of actin assembly and contractility. Subsequently, treated MSCs were stained with Phalloidin and DAPI to visualize the actin cytoskeleton and nuclei, respectively. Decreasing contractility by inhibition of either ROCK (Y27632) or actin polymerization (CytoD) resulted in a dose dependent loss of stress fibers (**Figure 7-1A**) as well as a dose dependent decrease in the projected area of the nucleus (**Figure 7-1B**). Decreasing contractility by inhibition of mysosin (Blebbistatin) or myosin light chain kinase (ML7) activity did not significantly alter F-actin structure, though it still resulted in a dose dependent decrease in nuclear projected area (**Figure 7-1A & 7-1B**). Activation of contractility using the ROCK agonist lysophosphatidic acid (LPA) increased stress fiber density but did not significantly alter the nuclear projected area (**Figure 7-1A & 7-1B**).

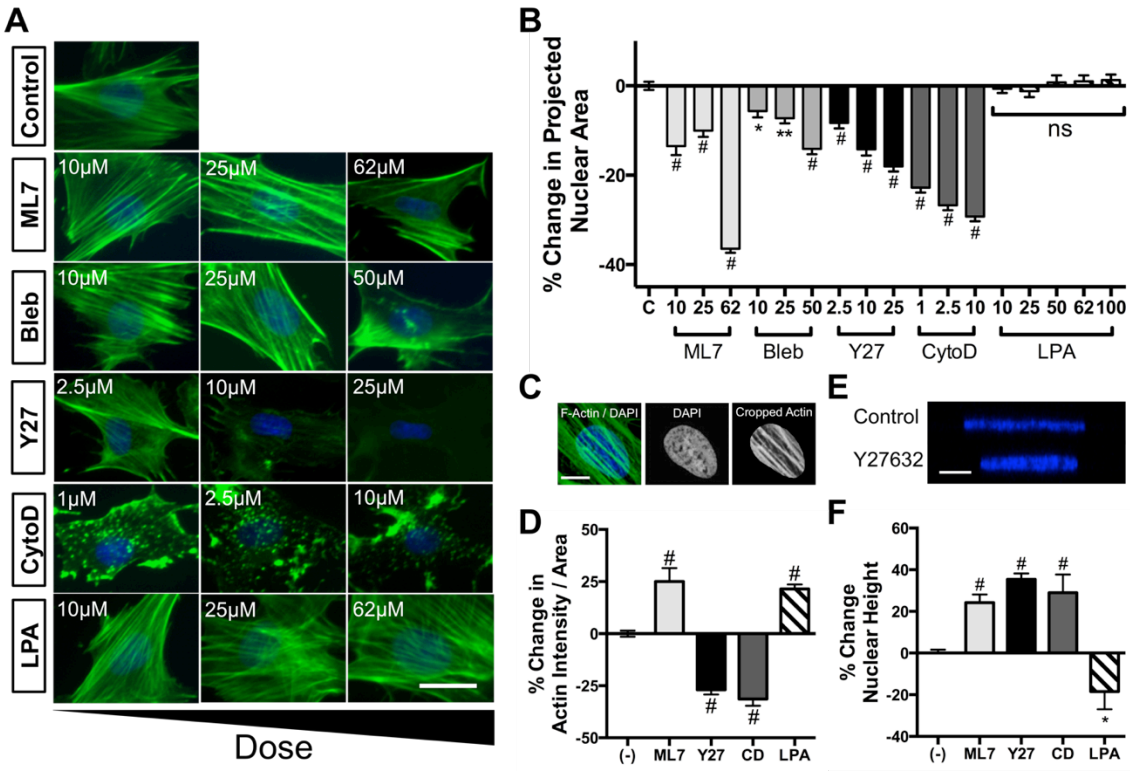

Figure 7-1: Cytoskeletal tension regulates nuclear and cytoskeletal morphology. F-Actin (green) and DAPI (blue) images of cells seeded on glass and treated with

different doses of ML7, Blebbistatin (Bleb), Y27632 (Y27), Cytochalasin D (CytoD), or Lysophosphatidic Acid (LPA) (A) (scale = 25μm). Quantification of projected nuclear area on glass (B) (mean +/- SEM, n>85 cells/ group). Example of F-actin in the projected area of the nucleus (C) (scale = 10μm) with quantification (D) (mean +/- SEM, n>85 cells/grp) (ML7=25μM, Y27632=10μM, CytoD=10μM, LPA=50μM). Example X-Z slices of nuclei (E) (scale = 5μm) used for quantification of nuclear height (F) (mean +/- SEM, n>13 cells/grp). (* p<0.05, ** p<0.01, # p<0.001 vs. control; one-way ANOVA with Tukey's post hoc).

To quantify the extent to which these regulators of contractility altered the number of stress fibers passing over and under the nucleus, the nuclear outline was used as a mask to crop actin images, and the average intensity of the filamentous actin in this nuclear region was quantified (**Figure 7-1C**). Consistent with previous observations, inhibition of ROCK or actin polymerization caused a significant loss of stress fibers in the vicinity of the nucleus while inhibition of MLCK increased the average intensity (due to similar actin signal coupled with a decrease in projected nuclear area) (**Figure 7-1D**). Treatment with the ROCK agonist LPA significantly increased actin intensity over the nucleus. These alterations in contractility did not significantly affect the aspect ratio of the nucleus, indicating equal shortening of both nuclear axes with inhibition (not shown). To assess the extent to which these alterations perturbed the nuclear shape in the third dimension, confocal imaging was performed and orthogonal X-Z slices were used to determine changes in nuclear height (**Figure 7-1E**). With inhibition of contractility (via any of the inhibitors), a significant increase in the nuclear height (~25-35%) was observed, while activation of contractility (LPA) resulted in a significant decrease in nuclear height (~20%) (**Figure 7-1F**).

Next, we sought to determine the percent change in actomyosin contractility associated with these changes in projected nuclear area and height. Traction forces were measured using 5kPa polyacrylamide gels that were coated with fibronectin and contained fluorescent microspheres for tracking of substrate deformation. Traction force maps for single cells before and after treatment with pharmacologic agents showed substantial decreases in traction force with inhibition of ROCK or MLCK and substantial increases in traction force with activation of ROCK (**Figure 7-2A**). Inhibition of ROCK (Y27632, 10μM) or MLCK (ML7, 25μM) decreased total force per cell by 80-90% while treatment with the ROCK agonist LPA (50μM) increased total force per cell by ~60% (**Figure 7-2B**). Consistent with previous studies (Dupont, Morsut et al. 2011), inhibition of contractility with either Y27632 or ML7 resulted in a significant decrease in YAP localization to the nucleus (**Figure 7-2C & 7-2D**) when MSCs were plated on stiff (glass) substrates. Interestingly, increasing contractility via addition of LPA did not alter YAP localization in this context (suggesting that YAP nuclear localization had already reached its maximum level).

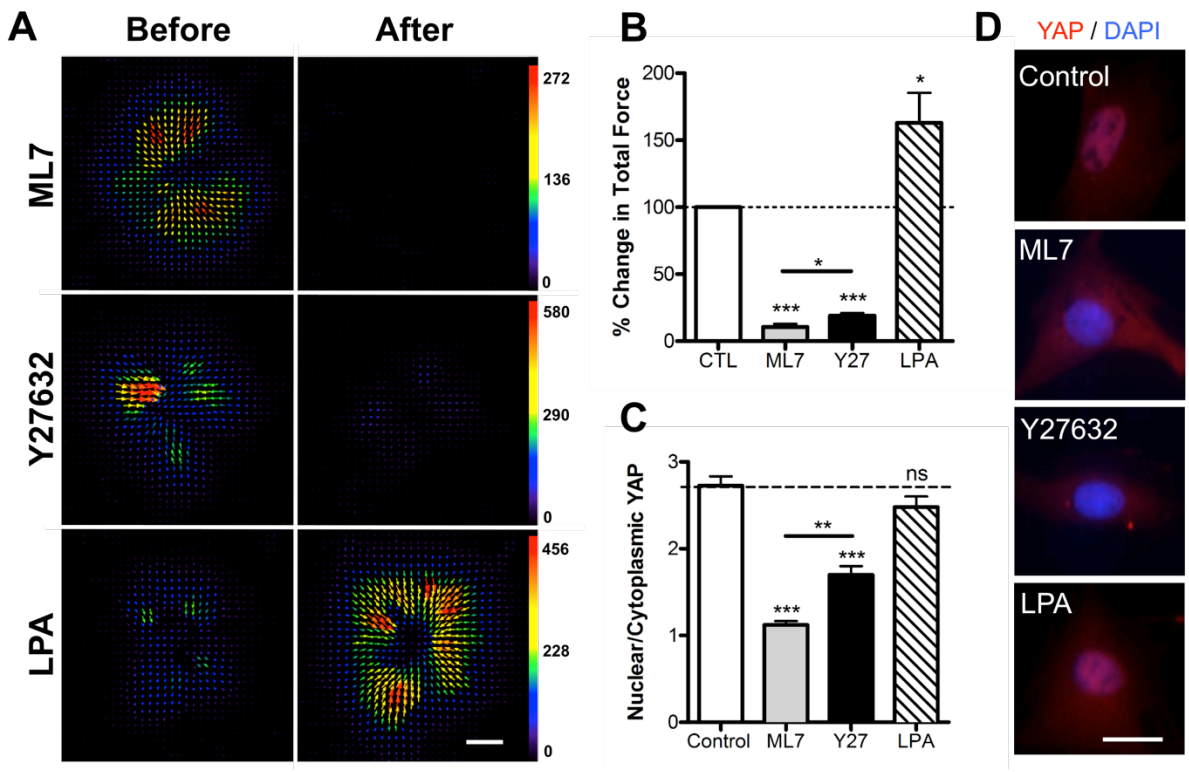

Figure 7-2: Traction force and YAP localization are regulated by ROCK and myosin light chain kinase. Traction stress maps for MSCs on 5kPa polyacrylamide gels before and after addition of ML7, Y27632, or LPA (A) (scale bar = 25μm, units = Pa) with quantification of % change in total force per cell (B) (n=14-20 cells per group, * p<0.05, ***p<0.001, one-way ANOVA with tukey's post hoc). Quantification of the ratio of nuclear to cytoplasmic YAP signal intensity for MSCs seeded on glass and treated with ML7 (25μM), Y27632 (10μM), or LPA (50μM) (C) with example epi-fluorescent images of YAP (red) and DAPI (blue) staining (D) (scale bar = 25μm).

7.3.2 Contractility Regulates Transfer of Strain to the Nucleus:

Next, we sought to determine the role that filamentous actin and intracellular tension play in the transfer of strain to the nucleus when exogenous stretch was applied to cells cultured on aligned nanofibrous scaffolds. For this, we developed a stepper motor driven micro-tensile device that allows for simultaneous tensile stretch and imaging of cells and nuclei (**Figure 7-3A**). With this system, scaffold Lagrangian strains can be quantified

using triads of nuclei as fiducial markers (**Figure 7-3B**). Quantification showed that micro-scale strains in the stretch direction (X_1, E_{11}) were very close to the applied strain and that low shear strains (E_{12}) were observed for all groups (**Figure 7-3C**). Large lateral compressive strains (E_{22}) were observed for all groups due to the highly aligned and porous nature of the electrospun scaffolds. These scaffolds typically display a Poisson's ratio of 1.25-1.5, due to their high level of structural anisotropy.

Consistent with our previous studies (Heo, Nerurkar et al. 2011, Nathan, Baker et al. 2011), quantification of nuclear aspect ratio (NAR) with applied stretch in control MSCs showed a strain dependent increase in NAR, with a wide distribution across the population (**Figure 7-3D**). With inhibition of ROCK or actin polymerization (with Y27632 or CytoD), a significant decrease in nuclear deformation was observed, such that nuclei deformed ~50% less than control cells (**Figure 7-3E**). Conversely, decreasing contractility by inhibition of MLCK with ML7 resulted in a significant increase in nuclear deformation (**Figure 7-3E**), potentially due to decreased nuclear pre-stress despite maintenance of cytoskeleton-to-nucleus connectivity. Similar results were observed for inhibition of myosin using blebbistatin (not shown), though in this case quantification was difficult due to the auto-fluorescent nature of this chemical in conjunction with the PCL scaffolds. When the baseline contractility level was increased prior to stretch (using LPA), a significant decrease in nuclear deformation was again observed, potentially due to stabilization of the nucleus with increased actin and nuclear pre-stress. These results indicate that both intact actin stress fiber network and the

tension in that network (exerting pre-stress on the nucleus), plays an important role in the conversion of extracellular strains to nuclear deformation.

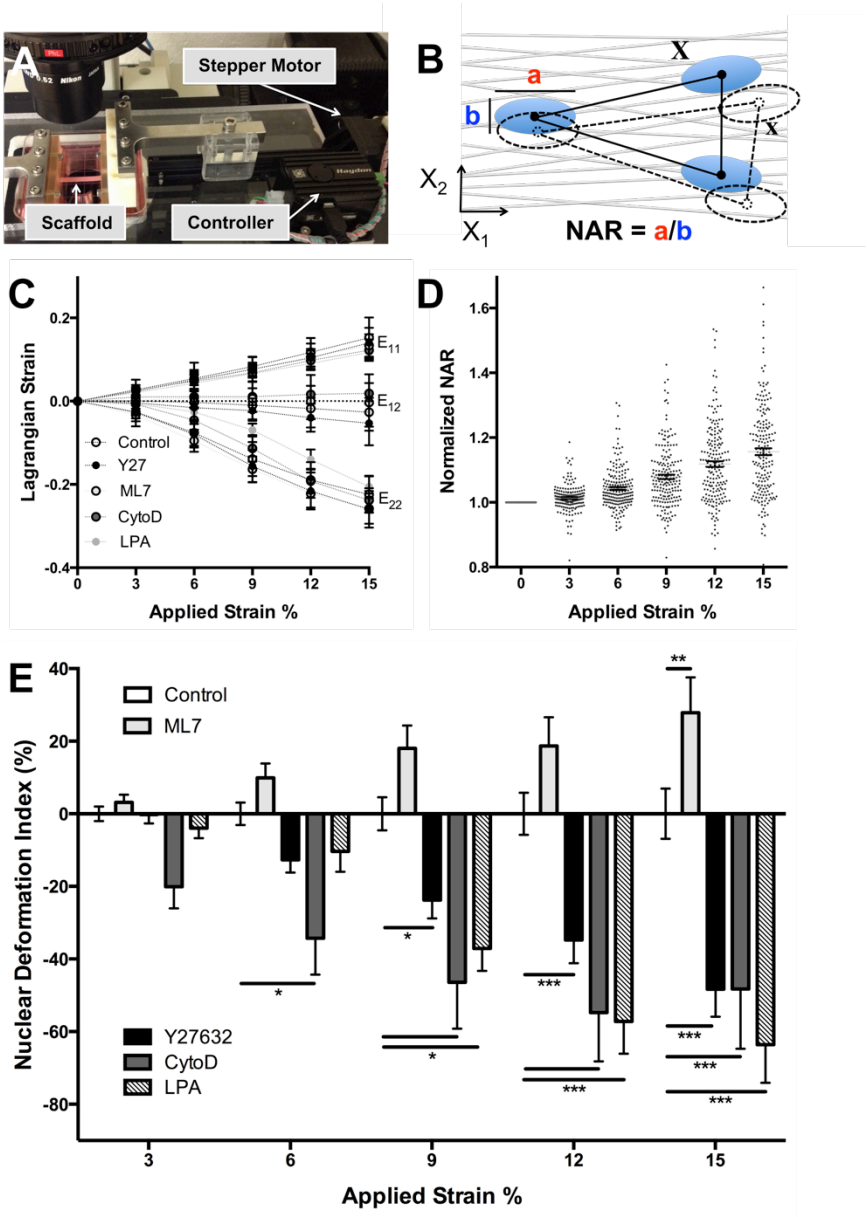

Figure 7-3: Contractility and nuclear pre-strain regulate strain transmission to the nucleus. Micro-tensile device used for stretch with simultaneous epi-fluorescent imaging of cell and nuclear deformation on scaffolds (A). Schematic of deformation analysis (B) indicating the nuclear aspect ratio (NAR) and the locations of nuclear triads in the deformed (x) and un-deformed (X) states that were used for Lagrangian strain calculation. Lagrangian strains (C) including shear strain (E_{12}), strain in the stretch direction (E_{11}), and strain perpendicular to the stretch direction (E_{22}). Nuclear aspect ratio for control cells normalized to the unstrained (0%

strain) case (D). Nuclear deformation index (NAR normalized to untreated control cells at the same strain) for cells treated with ML7 (25μM), Y27632 (10μM), Cytochalasin D (2.5μM), or LPA (50μM) (E). Nuclei that deform more than control have a positive NDI and nuclei that deform less than control have a negative NDI. (mean +/- SEM, n>50 cells/group; two-way repeated measures ANOVA with Tukey's post hoc).

7.3.3 Contractility Regulates Response to Dynamic Tensile Stretch:

Next, we sought to determine the importance of contractility and nuclear deformation in MSC response to dynamic tensile stretch. For these experiments cells were seeded onto aligned scaffolds for 2 days and then dynamically stretched at 1Hz to 3% strain for either 15 minutes (to assess activation of ERK1/2 signaling) or for 6 hours on two consecutive days (to assess changes in gene expression). Western blots showed a significant increase in pERK1/2 with dynamic loading (DL, **Figure 7-4A**). In the presence of inhibitors of contractility, the response of pERK1/2 to loading was not completely abrogated (**Figure 7-4A & 7-4B**) but did show a significantly lower fold increase with loading. This was due, in part, to a slight increase in baseline pERK1/2 with inhibition of contractility. With activation of contractility (via the addition of LPA), a significant increase in baseline pERK1/2 was observed under free swelling conditions (**Figure 7-4A & 7-4B**). When stretch was applied in this context, ERK1/2 showed no further increase in activation (**Figure 7-4C**).

When dynamic loading was extended over a longer period of time (2 days for 6 hours per day), untreated MSCs showed a significant increase in expression of the cartilage marker aggrecan, the growth factor CTGF, and the tendon transcription factor scleraxis. Inhibition of contractility with blebbistatin, Y27632, or ML7 abrogated the stretch

induced expression of CTGF (**Figure 7-4E**) and scleraxis (**Figure 7-4F**). However, stretch-induced upregulation of aggrecan expression was only partially inhibited when contractility was reduced, and this depended on the specific contractility inhibitor employed. With inhibition of contractility using ML7 or Y27632, a substantial reduction in the aggrecan response was observed, whereas with inhibition of contractility via blebbistatin a significant but reduced aggrecan response was still apparent with dynamic stretch.

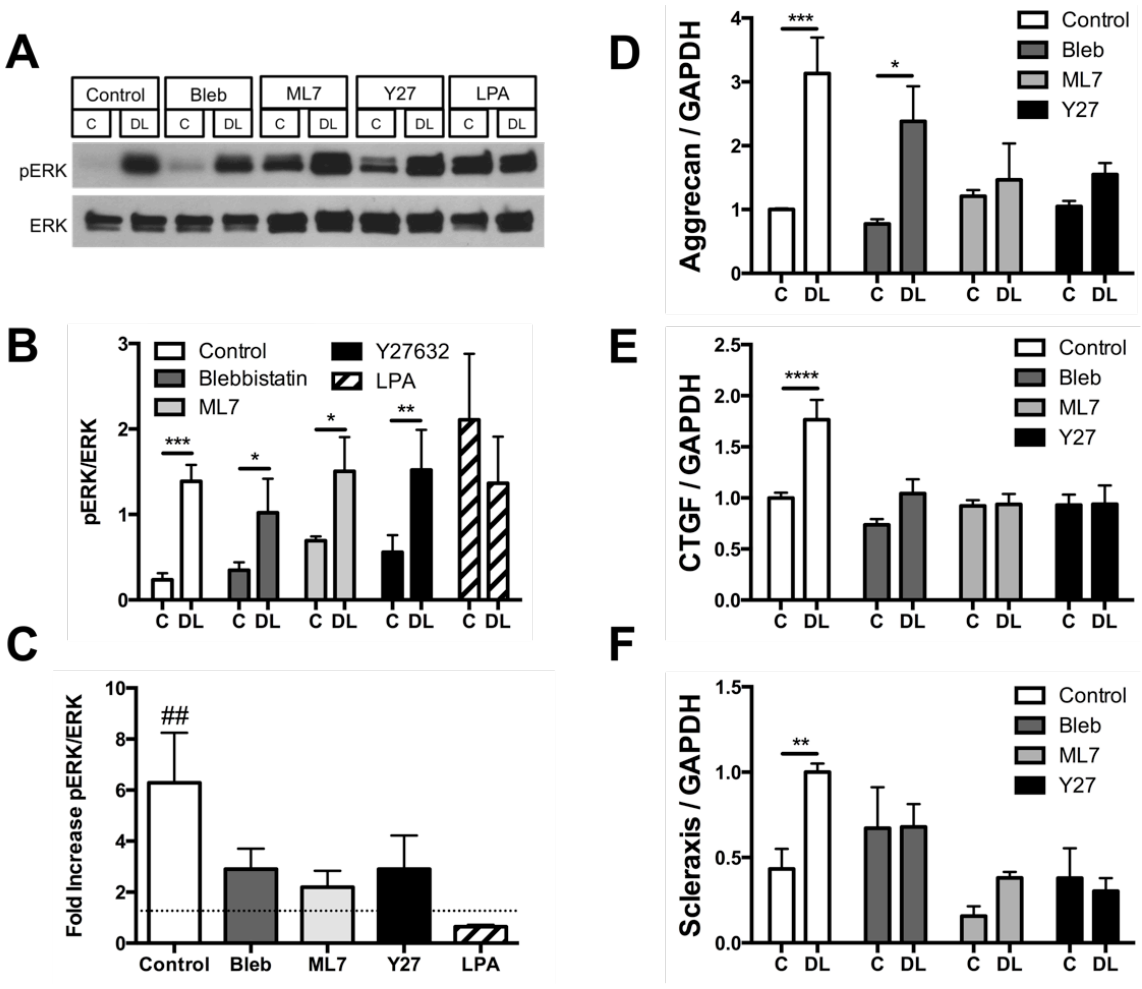

Figure 7-4: Contractility regulates response to dynamic stretch. Western blots for phosphorylated ERK1/2 (pERK) and total ERK1/2 (tERK) for MSCs seeded on scaffolds and dynamically loaded (DL) to 3% strain at 1Hz for 15 minutes with

inhibition or activation of contractility (A) (Blebbistatin: 50μM, ML7: 25μM, Y27632: 10μM, Cytochalasin D: 2.5μM, LPA: 50μM). Densitometry for western blots (mean +/- SD; n=3/group) plotted as a ratio of pERK/ERK (B) and as the fold increase in pERK/ERK with loading (C). Gene expression measured by qPCR for the cartilage marker aggrecan (D), the growth factor CTGF (E), and the tendon transcription factor scleraxis (F). Loading was administered for 6 hours per day on two consecutive days; data represent the combined response of 4 independent experiments (mean+/- SEM, n=9-12/group, two-way ANOVA with Tukey's post hoc).

Since it had been previously shown that perturbations in contractility (Dupont, Morsut et al. 2011) and alterations in nuclear structural proteins that mediate nuclear strain transfer (Bertrand, Ziaei et al. 2014, Guilluy, Osborne et al. 2014) can alter YAP/TAZ signaling, we next determined the extent to which YAP signaling was altered with tensile loading of aligned scaffolds, and the role of cytoskeletal tension in this process. In unloaded scaffolds, YAP was primarily cytoplasmic, despite the presence of stress fibers (**Figure 7-5**) and the high bulk modulus of both the PCL and the electrospun PCL scaffolds (Baker, Shah et al. 2011). This suggests that the cellular interpretation of the fibrous microenvironment is more akin to that of a soft substrate. Conversely, with 30 or 360 minutes of dynamic tensile loading, a significant increase in the nuclear/cytoplasmic YAP ratio was observed (**Figure 7-5A and 7-5B**). Twelve hours after cessation of loading (for the 360 minute loading cycle), YAP nuclear to cytoplasmic ratio returned to baseline levels. With inhibition of ROCK (using Y27632), YAP remained cytoplasmic in free swelling conditions (**Figure 7-5C**) and there was a significant reduction in YAP nuclear localization with 30 minutes of dynamic stretch (**Figure 7-5D**). Conversely, when cytoskeletal tension was reduced (but nuclear deformation was preserved) by inhibition of myosin light chain kinase (with ML7), YAP translocation to the nucleus was still observed with 30 minutes of dynamic stretch (**Figure 7-5D**).

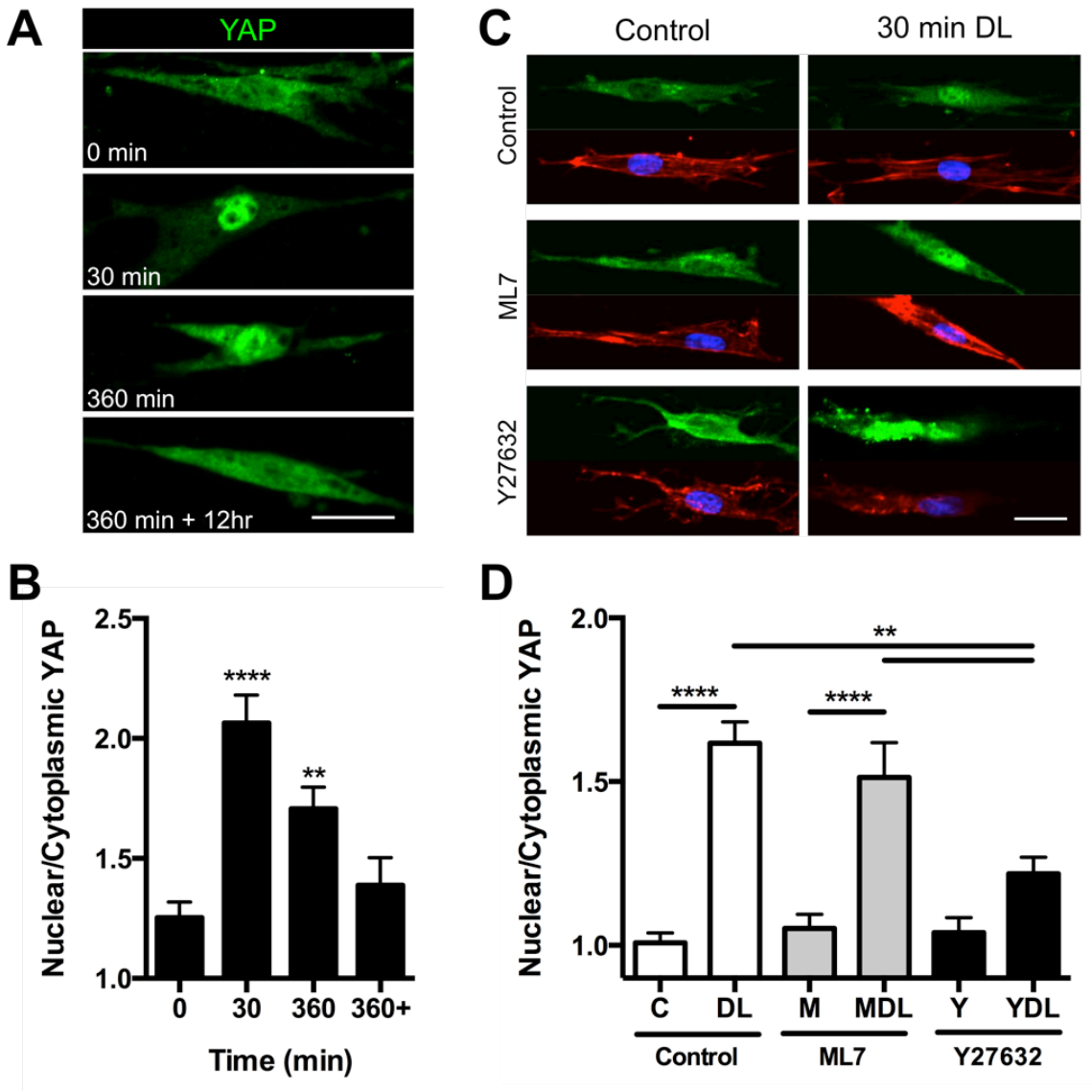

Figure 7-5: YAP signaling is activated by dynamic stretch and requires strain transfer to the nucleus but not cytoskeletal tension. Representative z-projected images of YAP staining (A) and quantification of the nuclear to cytoplasmic YAP ratio (B) for cells seeded on scaffold and dynamically stretched to 3% strain at 1Hz for 0min, 30min or 360min or 360min + 12 hours of free-swelling culture (scale bar = 25μm; mean+/- SEM; n=38-46 cells/group, two-way ANOVA with Tukey's post hoc). Representative z-projected images of YAP staining (green) with associated Actin (red) and DAPI (blue) (C) with quantification (D) after 0 or 30 minutes of loading under control conditions or with the ROCK inhibitor Y27632 (10μM) or the myosin light chain kinase inhibitor ML7 (25μM). (mean+/- SEM, n=26-34 cells/group, two-way ANOVA with Tukey's post hoc). ** p<0.01, **** p<0.0001.

7.4 Discussion

Fiber reinforced soft tissues are exposed to large loads and deformations that are transmitted through their hierarchical extracellular matrix to both cells and their nuclei within (Han, Heo et al. 2013), regulating numerous cellular processes and playing important roles in the formation, maintenance, and ultimately degeneration of these tissues. In the context of engineered replacements for these tissues, it will be important to understand both the extent to which these macro-to-microscale deformations are recapitulated in the engineered constructs, as well as the mechano-responsiveness of the cell types used in the fabrication of these constructs. MSCs are widely used in these types of applications (Baker, Shah et al. 2011) and it is well established that they respond to mechanical signals in a manner that is dependent on a contractile cytoskeleton (McBeath, Pirone et al. 2004, Engler, Sen et al. 2006). As with native tissue cells, nuclei within MSCs also undergo marked deformations with applied tensile stretch (Heo, Nerurkar et al. 2011, Nathan, Baker et al. 2011, Han, Heo et al. 2013). In this study, we found that both the presence of a patent actin cytoskeleton and the tension within this cytoskeletal network regulates the transmission of strain to the nucleus, and demonstrated differential short- and long-term response of MSCs to dynamic tensile loading based on the contractility state. Specifically, we showed that while a patent actin cytoskeleton is necessary for cytoskeletal strain transfer to the nucleus and activation of the YAP/TAZ pathway with stretch, other mechanoactive signaling pathways (e.g. ERK signaling) can be activated in the absence of nuclear strain transfer.

Consistent with previous studies (Chancellor, Lee et al. 2010), we found that decreasing contractility reduces actomyosin forces that pre-stress the nucleus, resulting in an increase in nuclear height and a decrease in projected nuclear area. This pre-stress dictates the extent to which additional deformation can be transferred to the nucleus. Loss of both contractility and stress fibers, by ROCK inhibition or actin de-polymerization, resulted in a significant decrease in nuclear strain transfer, likely due to a loss of the cytoskeletal-to-nucleoskeletal connectivity required for force transmission. Our observation of a loss of stress fibers with ROCK inhibition is consistent with previous work, which showed that ROCK directly regulates actin polymerization and depolymerization through the LIM-kinase and cofilin pathway (Maekawa, Ishizaki et al. 1999). Interestingly, treatment with ML7 resulted in a loss of contractility, but maintenance of actin stress fibers. Under this scenario, we observed a decrease in the pre-stress acting on the nucleus (i.e., a smaller nuclear projected area) but an increase in nuclear deformation with applied stretch. This suggests that the remaining stress fibers were capable of transferring strain to the nucleus under these conditions. Conversely, when contractility was increased (via the addition of LPA), the higher forces acting on the nucleus resulted in compression in the z-axis, flattening and stabilizing the nucleus, thus preventing additional strain from being transmitted to this organelle. This increased strain acting on the nucleus in the baseline state may also result in stiffening of the nucleus, due to the hyper-elastic strain stiffening nature of this organelle (Caille, Thoumine et al. 2002).

In addition to nuclear strain transfer, the mechano-responsivity of cells was differentially influenced by a change in contractility. Independent of nuclear deformation, a decrease in cytoskeletal tension resulted in a small decrease in activation of the ERK1/2 pathway and significant decrease in scleraxis gene expression in response to mechanical loading. This may be due, at least in part, to the fact that many mechanosensitive proteins within focal adhesions, which are known to activate ERK, depend on forced unfolding events. For these mechanosensory events localized to the cell membrane, the amount of strain transfer to the nucleus is likely less important than the concentration of stress at this location (which is required for protein unfolding within the membrane-bound complex). One would predict that any decrease in cytoskeletal tension would result in lower stresses within the cell, particularly at actin associated mechanosensory complexes such as focal adhesions (Dumbauld, Shin et al. 2010, Pasapera, Schneider et al. 2010) and the LINC complex (Luxton, Gomes et al. 2010, Guilluy, Osborne et al. 2014).

Of note however, not all mechanically regulated genes were equally affected by a decrease in contractility. Some genes, for instance aggrecan, were less sensitive to a loss in contractility. This may be due to the fact that aggrecan induction is enhanced with inhibition of contractility (Woods and Beier 2006). Additionally, the ERK response with load was not prevented when cytoskeletal tension was reduced using any of the inhibitors. This may be due to the fact that other mechanosensitive pathways can activate ERK (such as stretch-activated ion channels) that are less sensitive to a loss in cytoskeletal tension, depending instead on membrane tension (Schmidt, del Marmol et al. 2012, Anishkin, Loukin et al. 2014). These channels are mechanosensitive even in

artificial bilayers that lack cytoskeletal components (Brohawn, Su et al. 2014), increasing their opening probability in proportion to the level of tension applied the membrane.

Unlike these early signaling events, the response of the YAP signaling pathway required stress fibers and cytoskeletal strain transfer to the nucleus. Both of these are lost with ROCK inhibition but maintained with myosin light chain kinase inhibition. This would point to a cytoskeletal and Rho GTPase dependent mechanotransduction mechanism, whereby strain transfer into the cell through a patent actin cytoskeleton to the nucleus is necessary for the YAP signaling in response to dynamic tensile loading. However, with longer-term inhibition of cytoskeletal tension during loading, the induction of CTGF, a downstream gene activated by YAP/TAZ, was reduced. This is likely due to longer-term loss of cytoskeletal tension feeding back to reduce stress fibers and cytoskeletal strain transfer.

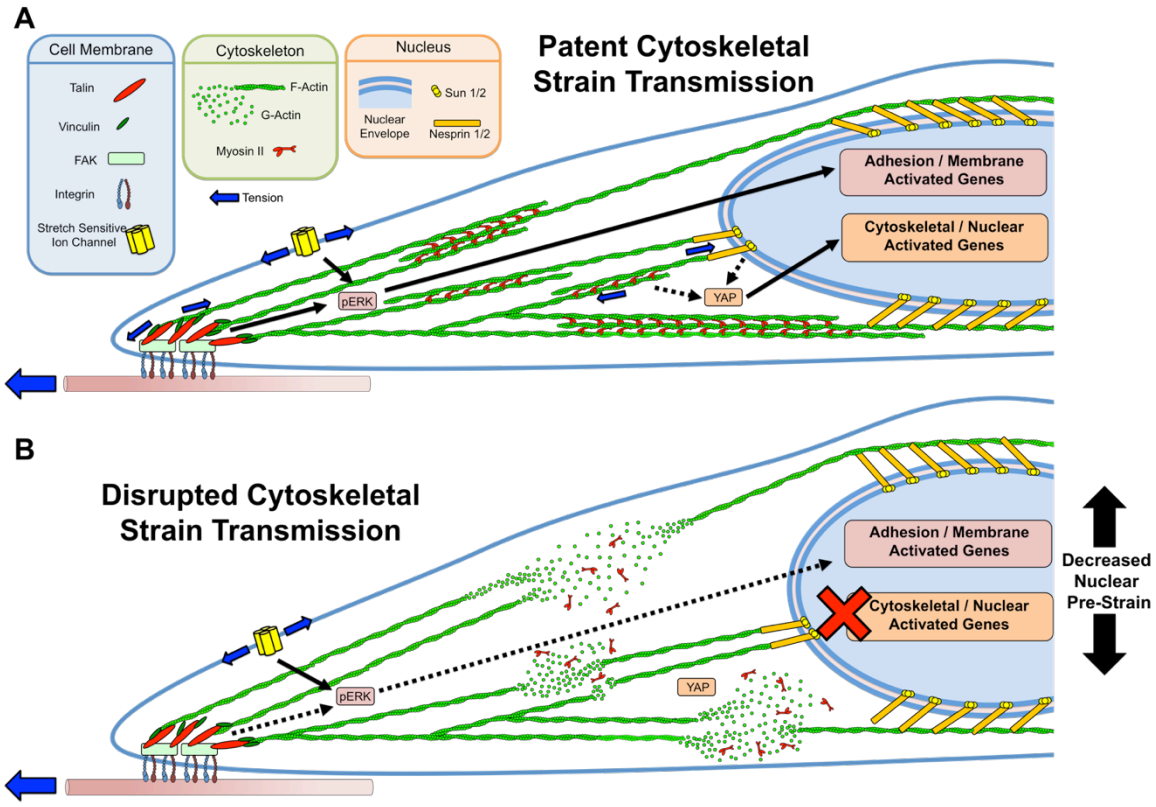

Figure 7-6: Schematic illustration of the differing routes of mechanotransduction. Mechoactivation may occur via cell membrane mediated mechanotransduction modules or through cytoskeletal-to-nuclear strain transfer mediated mechanotransduction modules. In baseline conditions, both pathways are likely operative (A). When ROCK is inhibited with Y27632, a decrease in nuclear pre-strain and depolymerization of actin is observed (B). This leads to a loss in cytoskeletal-to-nuclear strain transfer mediated mechanotransduction through YAP activation, but does not completely abrogate signals originating as a result of tension at the cell membrane.

In summary, our results suggest that the MSC nucleus is under a state of pre-stress and strain that is dictated by the level of actomyosin contractility within the cell, that this pre-strain regulates the deformability of the nucleus when exogenous stretch is applied to the cell, and regulates response to physical signals transmitted to the cell from the microenvironment. A nucleus with high pre-stress has low deformability while a nucleus with low pre-stress has high deformability, as long as the connecting actin stress

fibers are intact. A loss of tension in the pre-stressed cytoskeletal network reduces, but does not prevent, activation of the YAP and ERK signaling pathways in response to applied dynamic stretch. However, complete loss of a patent actin cytoskeleton (and the strain transfer to the nucleus that it enables), completely inhibits YAP signaling in response to stretch. Thus, if both membrane and cytoskeletal-to-nuclear mechanotransduction pathways exist (**Figure 7-6A**), loss of strain transfer would prevent the activation of cytoskeletal and nuclear associated mechanosensitive elements (**Figure 7-6B**). In contrast, when only cytoskeletal tension is reduced, a lower nuclear pre-strain allows for larger nuclear deformations and cytoskeletal mechanotransduction is maintained. These results support the idea that cytoskeletal strain transfer into the cell is important for YAP mechanosensing events. Despite this, the specific stretch sensitive molecules responsible for the mechano-modulation of YAP signaling through non-canonical pathways are still unclear (Low, Pan et al. 2014). Given that both focal adhesion and LINC complexes provide the termini for the actin cytoskeleton, understanding how force is transmitted through these complexes to activate proteins within will be important for understanding the molecular mechanisms by which contractility regulates stem cell responses to tensile stretch and ultimately lineage specification in mechanically loaded environments.

CHAPTER 8: LINC COMPLEX ALTERATIONS WITH TISSUE DEVELOPMENT AND STEM CELL DIFFERENTIATION REGULATE NUCLEAR STRAIN TRANSFER AND MECHANOTRANSDUCTION

8.1 Introduction

Mechanical forces transmitted through the cellular micro-environment are critically important for tissue development (Kahn, Shwartz et al. 2009), homeostasis (Maeda, Sakabe et al. 2011) and degeneration (Jeffrey, Thomson et al. 1997), particularly for tissues in the musculoskeletal system that play primary load bearing roles (Shwartz, Blitz et al. 2013). Cells sense forces within this microenvironment through protein unfolding events that initiate downstream signaling through recruitment of binding partners or release of signaling molecules (e.g., ion transport, kinase activation). These mechanotransduction events depend on both the structural network of proteins outside of the cell (the ECM) as well as the structural network of proteins within the cell (adhesion complexes and the cytoskeleton) that transmit these forces to mechanosensitive molecules within (Vogel and Sheetz 2006, Geiger, Spatz et al. 2009, DuFort, Paszek et al. 2011, Jahed, Shams et al. 2014). Numerous mechanotransduction mechanisms exist, many of which function at the cell surface. However, recent work has also illustrated that mechanical forces can also be transmitted deep within the cell (Wang, Tytell et al. 2009), rapidly instigating signal transduction at sites that are distant from the cell membrane (Na, Collin et al. 2008), including within the nucleus itself (Poh, Shevtsov et al. 2012).

The LINC complex is a structural network of proteins embedded in the nuclear envelope that permits for direct physical connectivity between the nucleus and the cytoskeleton, thereby regulating nuclear strain transfer (Lombardi, Jaalouk et al. 2011), nuclear positioning (Luxton, Gomes et al. 2010), and mechanotransduction (Lammerding, Schulze et al. 2004, Lammerding, Hsiao et al. 2005, Chambliss, Khatau et al. 2013, Guilluy, Osborne et al. 2014). These proteins show tissue specific expression patterns that regulate development (Randles, Lam le et al. 2010, Verstraeten, Renes et al. 2011), differentiation (Smith, Zhang et al. 2011, Swift, Ivanovska et al. 2013) and can cause disease (Hale, Shrestha et al. 2008, Puckelwartz, Kessler et al. 2010) and/or early degeneration (Zhang, Bethmann et al. 2007, Attali, Warwar et al. 2009). Recently, it has been shown that the LINC complex component lamin A/C scales with tissue stiffness and is regulated by substrate stiffness in mesenchymal stem cells, thereby potentially playing a role in the fate decisions that are governed by passive cues such as substrate elasticity (Swift, Ivanovska et al. 2013). More recently, it has been shown in isolated nuclei that stretching of the LINC complex component nesprin 1 induces the rapid SRC kinase dependent phosphorylation of emerin, which in turn recruits and couples to lamin A/C and stiffens the nucleus (Guilluy, Osborne et al. 2014). These data indicate that the nucleus itself is mechanosensitive, adapting to physical forces transmitted to it through the LINC complex. Despite this growing body of evidence, little is known regarding the specific molecular mechanisms by which physical perturbation of the nucleus through the LINC complex regulates cellular mechanotransduction.

While the centrality of the LINC complex in mechanotransduction is becoming increasingly clear, little attention has thus far been paid to the function of these molecules during development or with stem cell differentiation. Given that lamin A/C appears to scale with tissue stiffness (Swift, Ivanovska et al. 2013), and most musculoskeletal tissues change in mechanics with tissue maturation (and degeneration) (Penn, Wolfson et al. 1989, Ionescu, Lee et al. 2011, Mahmoodian, Leasure et al. 2011), one would expect that the lamin A content may likewise be regulated during normal tissue development. Similarly, studies focused on engineering replacements for these load bearing tissues often begin with immature constructs that increase in mechanical properties with time, likely driving changes in these mechanosensitive proteins. Likewise, in both the normal course of development and in the growth of engineered constructs, the trajectory of this tissue maturation can by regulated by superposition of additional mechanical factors, such as dynamic loading (Wozniak and Chen 2009, Mammoto and Ingber 2010). Importantly, for many such systems, maintenance of phenotype in these mechanically active microenvironments requires appropriately tuned mechanotransduction machinery. While native tissue structural and mechanical benchmarks are commonly used in tissue engineering to quantify and validate outcomes and refine experimental approaches (Nerurkar, Elliott et al. 2010), these same benchmarks have not yet been extended to the sub-cellular level. However, it is at this sub-cellular level that functionally appropriate and tissue specific mechanotransduction machinery operates. Understanding how sub-cellular mechanoactive species (including the cytoskeleton, the nucleus, and nuclear connectivity) change with differentiation and development, as well as their role in

mechanical signaling, will be of primary importance for tissue engineering, and aberrations in these cyto-structural features may shed new light on disease processes.

In this study, we provide evidence that members of the LINC complex, specifically nesprin 1 giant (N1G) and lamin A/C (LMNA), regulate the response of mesenchymal stem cells (MSCs) to static (e.g., substrate stiffness) and dynamic (e.g. tensile loading) mechanical perturbations. Concordant and discordant regulation of these two molecules were observed, with differing outcomes in terms of strain transfer the nucleus, signal transduction, and differentiation. In fibro-chondrocytes from fetal, juvenile, and adult animals, a concordant LINC mechanism was observed, where nuclear connectivity (through N1G) increased in step with increases in nuclear stiffness (through LMNA, driven by increased tissue stiffness). Conversely, both concordant and discordant LINC mechanisms were observed in MSCs induced towards a fibro-chondrogenic state, depending on whether differentiation was evoked by soluble versus mechanical cues. Given that these changes ultimately regulated mechano-transduction through YAP, our results indicate that structural components at the nuclear to cytoskeletal interface are important for mechanotransduction, change with differentiation and development, and ultimately influence cellular interpretation of mechanical signals.

8.2 Materials and Methods

8.2.1 Cell Isolation and Culture

All cells were isolated from fresh bovine tibio-femoral joints. Meniscus fibrochondrocytes (MFCs) were isolated from the outer or inner regions of the lateral

menisci of fetal, juvenile, and adult legs, as indicated. Biopsy punches (4mm) were taken from both regions and the surface region (meniscal superficial zone). For outer meniscal cells, the surface region (superficial zone of the meniscus) was removed and discarded. Punches were then diced and placed into 10cm tissue culture dishes. Meniscus cells were allowed to crawl from the tissue and expand over the course of 12-16 days in basal media (high glucose DMEM with 10% FBS and 1% PSF). Mesenchymal stem cells (MSCs) were isolated from the trabecular bone marrow of juvenile joints donor matched to juvenile MFCs and plated onto 15cm tissue culture dishes (Huang, Yeger-McKeever et al. 2008). MSCs were expanded in basal media for 1-2 passages prior to seeding.

For monolayer experiments, cells were seeded onto glass slides or fibronectin coated poly-acrylamide (PA) gels and cultured overnight in basal media. For stretch studies, cells were seeded onto 65mm x 5mm fibronectin coated aligned electrospun scaffolds at a density of $2x10^5$ cells per side (protein and mRNA studies) or $5\ x10^4$ cells per side (image based studies). Seeded scaffolds were cultured for two days prior to stretch experiments in a chemically defined media (high glucose DMEM with 1x PSF, 0.1μM dexamethasone, 50 μg/mL ascorbate 2-phosphate, 40 μg/mL L-proline, 100 μg/mL sodium pyruvate, 6.25 μg/ml insulin, 6.25 μg/ml transferrin, 6.25 μg/mL selenous acid, 1.25 mg/mL bovine serum albumin and 5.35 μg/mL linoleic acid) (Baker, Nathan et al. 2010).

For longer term fibrochondrogenic differentiation and loading studies, cells were seeded on aligned electrospun scaffolds and cultured for 7 days in chemically defined media

(control, and dynamic loading groups) or chemically defined media containing 10ng/ml TGF-β3. For osteogenic differentiation, MSCs were seeded on glass slides at a density of 25 cells/mm^2 and cultured for 21 days in osteogenic media (DMEM, 10% FBS, 50uM ascorbic acid-2-phosphate, 10mM β-glycerophosphate, and 200nM dexamethasone). For adipogenic differentiation, MSCs were seeded at a density of 100 cells/mm^2 and cultured for 14 days in adipogenic media (DMEM, 10% FBS, 1uM dexamethasone, 10mg/ml insulin, and 0.5 mM methylisobutylxanthine).

8.2.2 Lentiviral Delivery of miRNA

Knockdown of LINC complex components was performed using miR RNAi delivered using a lentiviral vector based system (Block-it Lentiviral Pol II miR RNAi Expression System with EmGFP, Invitrogen). Lamin A/C was knocked down using a verified BLOCK-iT miRNA vector. Three nesprin 1 giant vectors were designed and the miRNA sequence that resulted in the highest levels of knockdown was used (TGCCGAGGACCTTCATCTTCT). miRNA sequence containing oligos were annealed and ligated into pCDNA6.2-GW/ Em-GFP. miRNA containing cassettes were then transferred to pLenti6/V5-DEST via the Gateway cloning reaction and sequenced prior to viral production in HEK293FT cells. Virus (media supernatant) was titered by infection of MSCs and selection for blasticidin resistance (at 14 days) or analysis of %GFP positive cells (at 4 days) using a flow cytometer (FACSCaliber, Beckson Dickson, with CellQuest Pro software). For all experiments, cells were infected with virus overnight. Four days post infection, cells were trypsinized and re-seeded on glass, polyacrylamide gels, tissue culture plastic, or aligned electrospun scaffolds for assays. Knockdown was

verified by dot blot for nesprin 1 following 1MDa size filtration (**Supplemental Figure 1a**) or by western blot and immunostaining for lamin A/C (**Supplemental Figure 1b and 1c**).

8.2.3 Aligned Electrospun Nanofibrous Materials

Aligned scaffolds were fabricated as described previously. Briefly, a 14.3% w/v solution of poly(ε-caprolactone) (Bright China, Hong Kong, China) in 1:1 mixture of N,N-dimethylformamide and tetrahydrofuran (Fisher Chemical, Fairlawn, NJ) was expelled from a charged (+13kV) spinneret (18 gauge stainless steel needle) at a rate of 2.5 mL/hr. Fibers were collected over 10 hours on a grounded mandrel rotating with a surface velocity of ~10m/s to induce fiber alignment. Collected fibers formed mats (~1mm thick) that were removed from the mandrel and cut into 65mm x 5mm segments with the long axis oriented in the prevailing fiber direction. Scaffold segments were disinfected and rehydrated in decreasing concentrations of ethanol (100, 70, 50, 30%; 1hr/step) and rinsed twice in phosphate buffered saline (PBS). Prior to cell seeding, scaffolds were coated in fibronectin for 12-18 hours (Sigma, 20 μg/ml in PBS).

8.2.4 Quantification of Nuclear Deformation with Static Stretch

Cells seeded on aligned scaffolds were stained with Hoechst (5mg/ml, Molecular Probes, Eugene, OR) in high glucose phenol-free DMEM containing HEPES for 10 min at 37°C. Static stretch was applied to determine the role of LINC complex components in nuclear deformation as a function of scaffold stretch. Scaffolds were stretched (n>7 per group) up to 15% strain in 3% increments using a tensile device mounted on a Nikon Eclipse

TE2000-U inverted epi-fluorescence microscope using a 20x Plan Fluor ELWD objective with a tunable correction collar. Nuclear deformation at each step was quantified (n>80 cells per group) using a custom MATLAB program by calculating the ratio of nuclear principal lengths normalized to 0% strain. As described previously (Driscoll 2015), a Canny edge detection algorithm was used to detect outer nuclear edges based on gradients in signal intensity. Edges were then dilated, filled, and grouped into clusters. Principal component analysis was performed on the clusters to identify principal lengths of the nucleus as in (Nathan, Baker et al. 2011). A nuclear aspect ratio (NAR) was calculated for each cell at each strain and normalized to the undeformed control. Additionally, a nuclear deformation index (NDI) was calculated for each experimental group by normalizing nuclear deformation at each strain level to the mean deformation observed for the control group at that same strain level (Driscoll 2015). Local Lagrangian strains were also calculated using triads of nuclei as fiducial markers at each strain level to ensure consistent local deformations across scaffolds and experimental conditions. This was performed as a control, to ensure equal stretching of groups.

8.2.5 Dynamic Tensile Loading

Dynamic tensile stretch (3% strain, 1Hz) was applied in a CO_2 incubator using a custom bioreactor system [8]. For short-term experiments, cells seeded on scaffolds for 2 days were dynamically loaded for 15 minutes (pERK1/2 response), 30 minutes (YAP/TAZ response), or 6 hours (mRNA response). For quantification of phosphorylated ERK1/2 with stretch, protein was isolated immediately following stretch. For quantification of nuclear YAP with stretch, cells were fixed and stained with anti-YAP antibody,

Phalloidin, and DAPI immediately after cessation of loading. For YAP analysis on scaffold, cells were imaged using a Nikon A1 laser scanning confocal microscope with 20X objective. Z-stacks were acquired at 0.75μm slice thickness over the entire cell with the slice centered at the nucleus used for quantification of the nuclear-to-cytoplasmic YAP ratio.

8.2.5 Traction Force Microscopy

Polyacrylamide (PA) hydrogels (Young's Modulus, E = 5 kPa) were prepared as in Aratyn-Schaus (Aratyn-Schaus, Oakes et al. 2010). 0.2μm-diameter fluorescent microspheres (Invitrogen, #F8810) were mixed into PA at 1% v/v prior to polymerization. Fibronectin (20 μg/mL) coating of gel surfaces was accomplished with 2 mg/mL sulfo-SANPAH (Pierce, #22589). Small drops of a UV-curable fixative, NOA68, were used to secure the slides in a live cell imaging chamber. Gels were subsequently washed three times with PBS and sterilized under germicidal UV light for 1 hour. In all traction force experiments, MSCs were seeded at a density of 3000 cells/cm^2 and allowed to attach for 20 hours before TFM was performed. Phase contrast and fluorescent images of multiple cells and embedded beads were captured at 40X magnification on a Deltavision Deconvolution Microscope. All imaging was performed in an environmental chamber (37°C, 5% CO_2). TFM data analysis (stack alignment, PIV, and FTTC) was performed using a freely available plugin suite for ImageJ, created by Q. Tseng (Tseng, Duchemin-Pelletier et al. 2012) which was adapted from (Dembo and Wang 1999). For FTTC, the Poisson's ratio of the PA gel was assumed to be 0.45 and a regularization parameter of 2e-9 was used. Using a custom MATLAB script, traction force vector maps

were analyzed to determine average traction stress generated by each cell and total force exerted per cell. Cell area was determined from the corresponding phase contrast images in ImageJ.

8.2.6 Atomic Force Microscopy

Peri-nuclear stiffness was determined by atomic force microscopy (6000 ILM-AFM, Agilent Technologies). Passage 1 cells were plated on 30mm tissue culture dishes for 24-48 hours. Cells were probed using a silicon nitride tip modified with a silicon oxide glass sphere 1um in diameter (nominal spring constant of 0.06 N/m, Novascan; individual cantilever spring constants were calibrated via measurement of thermal oscillation). To quantify peri-nuclear stiffness, the first 300 nm of indentation data were fit with the Hertz model (Kuznetsova, Starodubtseva et al. 2007). Values of peri-nuclear stiffness were taken as the average of measurements made in at least two different regions of the nucleus and 39-40 cells of each type were tested.

8.2.7 Quantitative Real Time RT-PCR

Changes in gene expression were determined by real time RT-PCR. MSCs were seeded on aligned nanofibrous scaffolds for 2 days in chemically defined media and then loaded into the custom tensile bioreactor. Cells were dynamically stretched to 3% strain at 1Hz for 6 hours. For differentiation studies, cells were loaded to 3% strain at 1Hz for 6 hours on 5 consecutive days in chemically defined media. These were compared to cells differentiated using the soluble factor TGF-β3. Samples were snap frozen in Trizol, and mRNA was subsequently isolated by phenol-chloroform extraction. RNA concentration was quantified (ND-1000, Nanodrop Technologies, Wilmington, DE, USA) and cDNA

synthesized using the SuperScript II First Strand Synthesis kit (Invitrogen Life Technologies, Carlsbad, CA). PCR was performed with gene specific primers using an Applied Biosystems StepOnePlus real time PCR machine and the Fast SYBR Green reaction mix (Applied Biosystems, Foster City, USA). Expression levels of aggrecan (AGG), connective tissue growth factor (CTGF), and scleraxis (SCX), nesprin 1 giant (N1G, directed at the N-terminal calponin homology domain), and nesprin 2 giant (N2G, directed at the N-terminal calponin homology domain) were determined and normalized to the housekeeping gene glyceraldehyde-3-phosphate dehydrogenase (GAPDH). Primers designed based on the bovine cDNA sequences (5'-3') were:

(AGG, CCTGAACGACAAGACCATCGA; TGGCAAAGAAGTTGTCAGGCT)

(CTGF, CGTGTGCACCGCTAAAGATG; GGAAAGACTCTCCGCTCTGG)

(SCX, GAACACCCAGCCCAAACAGAT; TCCTTGCTCAACTTTCTCTGGTT)

(GAPDH, ATCAAGAAGGTGGTGAAGCAGG; TGAGTGTCGCTGTTGAAGTCG)

(N1G, GAGAGATTTGCCCCAGATAATCA; AATCCAGACAGAAAAGGAAAGCA)

(N2G, ATATGACACTGCAGCCCACCTT; GGCACCTCGCTGAGGGTATT)

(N1KASH, AAACGCCACGAGGCAAATG; GCCACCTCTTATGGACCTGCTA)

(N2KASH, CGTCTTCTGGCAAATCCATTTC, CCTGTCACCTCCCATTTGTTTGT)

8.2.8 Protein Analysis

Whole cell protein was isolated from cells seeded on scaffold or tissue culture plastic. Cells were washed once with PBS, and lysed in RIPA buffer (50mM Tris-HCl pH 8.0, 150 mM sodium chloride, 1.0% Triton X-100, 0.1% Sodium Dodecyl Sulfate (SDS), 1% protease inhibitor cocktail (Sigma, St Louis, MO) and 1% phosphatase inhibitor cocktail (Sigma, St Louis, MO)) to isolate total cellular proteins. Protein isolates were cleared of

insoluble cellular debris by centrifugation (15,000 × *g* for 15min) and protein concentration was quantified using the Lowry assay (Biorad, Hercules, CA). Samples were denatured by boiling for 5 min in reducing buffer containing 2% beta-mercaptoethanol.

Proteins were separated on 4-15% gradient SDS polyacrylamide gels and transferred to nitrocellulose membranes. Membranes were blocked with 5% bovine serum albumin (pERK, ERK, β-Actin, MLCK) or 5% non-fat dry milk (lamin A/C, nesprin 1 & 2) in Tris-buffered saline containing 0.1% Tween 20 (TBS-T). Primary antibodies used were: p44/p42 MAPK (ERK1/2, 1:1000, Cell Signaling, #9102) or phospho-p44/p42 MAPK (pERK1/2, 1:1000, Cell Signaling, #9101), MLCK (1:1000, LSBio, C25729), lamin A/C (1:200, Thermo, mab636), nesprin 1 (Syne-1 H-100, 1:400, Santa Cruz Bio), nesprin 2 (Syne-2 H-109, 1:400), β-actin (1:1500, Cell Signaling, #4967). Membranes were incubated with primary antibody in blocking buffer overnight at 4°C. Membranes were washed three times with TBS-T and treated with anti-rabbit peroxidase conjugated secondary antibody in blocking buffer (1:1000, Cell Signaling) or anti-mouse peroxidase conjugated secondary antibody (Jackson Labs). Blots were developed using SuperSignal West Pico Chemiluminescent Reagent (Pierce) and exposed to CL-Exposure film (Thermo).

For analysis of nesprin 1 giant levels, whole cell lysate (100ug) was denatured by boiling with 2% beta-mercaptoethanol (5min) then filtered through a 1MDa size filtration column at 10,000xg for 10 minutes (Tocris Biosciences). Retentate was re-suspended in

400ul of RIPA buffer by pipetting and run through the filtration column again. This wash step was performed again, and then retentate was re-suspended in 100ul of RIPA buffer. 50ul of this retentate solution was spotted onto a hydrated (in TBS) nitrocellulose membrane (Biorad) using a BioDot dot blot apparatus (Briorad). Vacuum was applied to the device draining all the wells. Membrane was removed and immunoblot was performed as described above for nesprin 1 (Syne-1 H-100, 1:400, Santa Cruz Bio).

For immunoprecipitation, cells were washed once with PBS and lysed in IP buffer (20mM Tris-HCl pH 8.0, 137 mM sodium chloride, 1.0% Nonidet P-40, 10% glycerol, 1% protease inhibitor cocktail (Sigma, St Louis, MO) and 1% phosphatase inhibitor cocktail (Sigma, St Louis, MO)). IP was performed using the Novex Immunoprecipitation Dynabeads Protein G Kit (#100007D). 2 mg of nesprin antibody (Santa Cruz Bio) was bound to 50ml of Dynabeads in 200 ml of PBS with Tween-20 and incubated at room temperature for 10 minutes. Beads were washed and 100mg of whole cell lysate was added to beads and incubated for 3 hours at room temperature. Beads were washed three times and bound protein was eluted from beads by heating to 37^{o}C for 10 minutes in 20ml of elution buffer mixed with 10ml of NuPAGE LDS Sample buffer with beta-mercaptoethanol (2%). Western blot was performed for lamin A/C (1:200, Thermo, mab636) using the protocol described above.

8.2.9 Immunofluorescence

Cells seeded on glass slides overnight were fixed with 4% paraformaldehyde for 20 min at 37°C then washed and permeablized with 0.05% Triton X-100 in PBS supplemented

with 320mM sucrose and 6mM magnesium chloride. Cells were incubated with anti-YAP antibody in 1% BSA in PBS (1:200, Santa Cruz Bio, #sc-101199) overnight at 4°C, washed 3 times with PBS, and then incubated for 60 min at room temperature with Alexa-Fluor 488 or 546 phalloidin (1:1000, Molecular Probes) and Alexa-fluor 546 or 488 goat anti-mouse secondary (Molecular Probes, 1:200). For vinculin staining, cells were fixed and permeablized simultaneously using microtubule stabilizing buffer for 10 minutes at 37°C (0.1M PIPES pH6.75, 1mM EGTA, 1mM $MgSO_4$, 4% w/v polyethylene glycol, 1% Triton X-100, 2% paraformaldehyde), then washed with PBS and stained with anti-vinculin antibody (1:200, Sigma) in 1% w/v BSA in PBS overnight. Stained cells were washed 3 times and mounted with DAPI containing mounting medium (ProLong Gold Antifade Reagent, Molecular Probes). Images were taken using a Nikon Eclipse TE2000-U inverted epi-fluorescence microscope with 20x objective and quantified using ImageJ or a custom MATLAB program. DAPI images were edge detected using the Canny edge detection algorithm and nuclear area was quantified. The nuclear outline was then used as a mask to quantify F-actin staining intensity in the vicinity of the nucleus. For YAP/TAZ staining, average staining intensity in the nucleus (DAPI outline) and within the cytoplasm (F-actin outline) was quantified using ImageJ; these intensities were used to calculate a nuclear to cytoplasmic YAP ratio.

8.3 Results

8.3.1 The LINC complex regulates nuclear shape, cytoskeletal organization, contractility, and YAP signaling in MSCs.

To investigate the role of the LINC complex components nesprin 1 giant (N1G) and lamin A/C (LMNA) in regulating basal nuclear shape and cytoskeletal organization, MSCs were infected with lentiviral vectors containing miRNA directed at LMNA, the N-terminal region of N1G, or a negative control sequence (Neg), then plated onto glass slides or fibronectin coated polyacrylamide (PA) gels of varying stiffness. Knockdown was verified by western blot and immunostaining (lamin A/C) or by dot blot following size filtration (N1G), with ~50% knockdown achieved for each molecule (**Supplemental Figure S1a-c**). Nuclear height was measured from X-Z confocal images of cells on glass stained with DAPI (**Figure 8-1a**). Knockdown of either LINC component resulted in a significant increase in nuclear height (**Figure 8-1b**), with N1G knockdown resulting in larger increases than LMNA knockdown. This suggested that, as described previously for other cell types (Chancellor, Lee et al. 2010), acto-myosin forces applied to the nucleus through the LINC complex are important for regulating a pre-strain acting on the nucleus. In keeping with this concept, quantification of vinculin adhesion staining on glass (**Figure 8-1c**) showed an increase in adhesion number and total adhesion area per cell (**Figure 8-1d**) with N1G knockdown, with only a slight increase in total cellular area (**Supplemental Figure 8-2a**). This indicated that decreasing the extent to which stress fibers disconnect from the nucleus promoted focal adhesion formation, suggesting increased traction force generation. To directly measure this, cellular force generation

was quantified using traction force microscopy (TFM). In this assay, cells deficient in N1G showed significantly larger bead displacements that corresponded to larger tractions stresses (**Figure 8-1e**). Quantification showed a significant increase in total force per cell with knockdown of N1G, while only slight increases were seen with LMNA knockdown (**Figure 8-1f**).

Given that mechanosensing in MSCs is heavily dependent cellular traction forces (McBeath, Pirone et al. 2004, Engler, Sen et al. 2006), and that this functions though a traction dependent non-canonical portion of the YAP/TAZ signaling pathway (Dupont, Morsut et al. 2011), we next addressed the impact that these changes might have on substrate stiffness sensing through YAP. Consistent with the literature (Dupont, Morsut et al. 2011), negative control MSCs on low stiffness gels (5 kPa) did not show nuclear localization of YAP, while those on higher stiffnesses (55 kPa & glass) showed increased YAP nuclear localization (**Figure 8-1g**). As expected, control cell spread area increased with increasing substrate stiffness, and neither knockdown changed this relationship (**Supplemental Figure 8-2a**). Moreover, YAP nuclear localization (assessed by either the intensity ratio of nuclear to cytosolic or by counting nuclei positive for YAP) increased significantly with increasing stiffness in LMNA knockdown cells, to a level comparable to that of control cells (**Figure 8-1h**). However, knockdown of N1G significantly altered YAP localization; on 55 kPa gels and on glass, with no change in YAP localization observed under these conditions (**Figure 8-1h**). On glass substrates ~90% of LMNA KD and control cells showed clearly nuclear YAP, whereas those with N1G knockdown, only ~60% of cells showed clear nuclear outlines in the YAP channel (**Supplemental Figure**

8-2b). These results suggest that, in undifferentiated mesenchymal stem cells, tension exerted on the nucleus by the cytoskeleton can regulate mechanosensing through the YAP pathway.

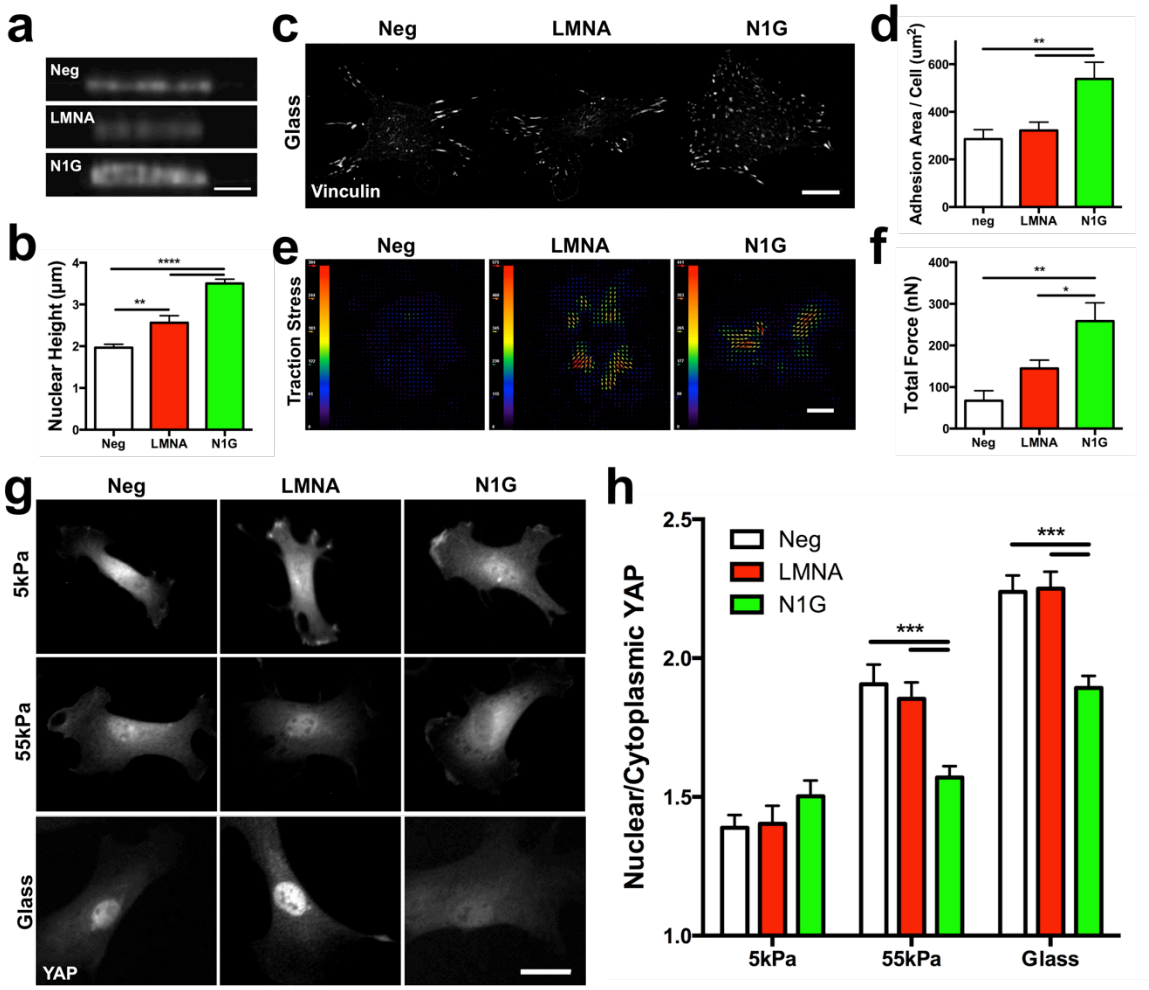

Figure 8-1: The LINC complex regulates nuclear shape, cytoskeletal tension, and YAP signaling in MSCs. (a) X-Z confocal images of nuclei in cells infected with lentivirus expressing RNAi directed at lamin A/C (LMNA), nesprin 1 giant (N1G), or a scrambled control (Neg) with quantification of nuclear height (b) (mean +/- SEM, n=8-11 cells, scale bar =5μm). Vinculin immunostaining of cells on glass after knockdown (c) with quantification of total adhesion area per cell (d) (mean +/- SEM, n=8-11 cells, scale bar = 25μm). Traction stress maps of cells on 5 kPa poly-acrylamide gels (e) with quantification of total force per cell (f) (mean +/- SEM, n=11-27/group, scale bar = 25μm). YAP immunostaining of cells seeded on 5 or 55 kPa fibronectin coated polyacrylamide gels compared to fibronectin coated glass (g) (scale bar = 25μm) with quantification of the nuclear-to-cytoplasmic staining intensity (h) based on outlines of the nucleus (DAPI) and actin (Phalloidin) (mean

+/- SEM, combined data from two independent donors, n=44-55 cells / group). (* p<0.05, ** p<0.01, *** p<0.001, **** p<0.0001)

8.2.2 The LINC complex regulates differentiation.

Since both the YAP pathway (Dupont, Morsut et al. 2011) and lamin A/C (Swift, Ivanovska et al. 2013) have been shown to regulate differentiation in MSCs, we next assayed the extent to which knockdown of LMNA or N1G influenced adipogenesis, osteogenesis, and chondrogenesis of these cells. With adipogenic induction on glass for 14 days, MSCs displayed significantly more adipogenesis (oil red O stained lipid droplets) with LMNA knockdown compared to control cells (**Figure 8-2a**), consistent with previous results (Swift, Ivanovska et al. 2013). Conversely, N1G knockdown significantly decreased adipogenesis at this time point in comparison to control cells (**Figure 8-2b**), suggesting that the increase in adhesion and contractility resulting from N1G knockdown is inhibitory to adipogenesis. When MSCs were cultured under osteogenic conditions for 21 days, knockdown of LMNA had little effect on osteogenesis (as assessed by alizarin red staining, **Figure 8-2c**). Conversely, knockdown of N1G increased osteogenesis and mineral deposition (**Figure 8-2d**), despite the fact that these cells had diminished levels of YAP signaling on glass substrates. This may indicate that the increased adhesions and contractility, in combination with the remaining YAP signaling that does occur on glass, is sufficient to drive these cells towards and osteogenic lineage. Neither knockdown influenced proteoglycan content in MSC micro-pellets cultured under chondrogenic conditions for 14 days (**Supplemental Figure 8-3**).

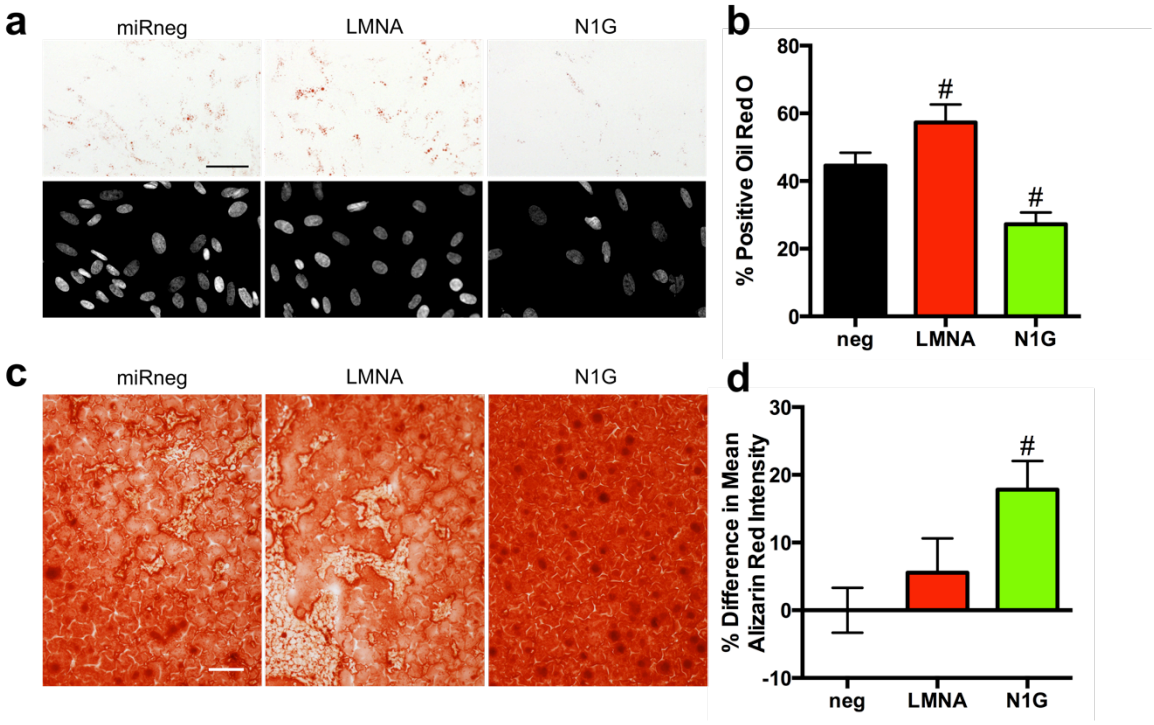

Figure 8-2: The LINC complex regulates mesenchymal stem cell differentiation. MSCs were infected with lentivirus expressing RNAi directed at lamin A/C (LMNA), nesprin 1 giant (N1G), or a scrambled control (Neg). (a) Oil Red O staining for lipid droplets after 14 days of adipogenic induction with quantification of percentage of cells with positive staining (b). Alizarin red staining for mineral deposition after 21 days of osteogenic differentiation (c) with quantification of % difference in alizarin red staining intensity relative to controls (d) (n=10 regions / group).

8.3.3 The LINC complex regulates nuclear strain transfer and mechanotransduction in MSCs.

In addition to its ability to regulate basal nuclear shape, the LINC complex also regulates the transmission of exogenously applied strains from the cytoskeleton to the nucleus (Lombardi, Jaalouk et al. 2011). We next assayed the extent to which this occurs in undifferentiated MSCs. For this, we employed an aligned electrospun nanofibrous material coated with fibronectin, which induces cellular alignment and allows for application of static and dynamic tensile strains (Chapter 7). To quantify nuclear

deformation with applied stretch, scaffolds were mounted into a previously described micro-tensile device mounted atop an epi-fluorescent microscope. Scaffolds were stretched in 3% increments to 15% strain with images of Hoechst stained nuclei acquired at each strain level. Nuclear deformation was quantified using automated Canny edge-detection and a nuclear deformation index was calculated for each cell as in Chapter 7. This index quantifies the percent increase (positive index) or percent decrease (negative index) in nuclear deformation relative to the deformation of nuclei in cells treated with negative control virus. Lagrangian strains between nuclei are calculated as a control, to ensure equal stretching of all groups (**Supplemental Figure 8-4a**). With knockdown of LMNA, larger nuclear deformations were observed compared to control cells, resulting in a higher nuclear deformation index at 9, 12, and 15% applied strain (**Figure 8-3a & 8-3b**). This was also true for the nuclear aspect ratio (**Supplemental Figure 8-4b**). This is consistent with previous studies (Lammerding, Schulze et al. 2004) and likely due to the decreased nuclear mechanical properties associated with a reduction in lamin A/C. Also consistent with previous work (Lombardi, Jaalouk et al. 2011), knockdown of N1G resulted in significantly less nuclear deformation at 12 and 15% applied strain (**Figure 8-3b and 8-3c**).

Based on our previous results, which showed transfer of strain to the nucleus through F-actin was important for the MSC response to dynamic tensile loading (Driscoll 2015), we next assayed the importance of nesprin 1 giant and lamin A/C in the MSC response to dynamic stretch. Specifically, we assayed the early response of the ERK1/2 MAPK and YAP/TAZ pathways. For these experiments a previously described dynamic tensile

bioreactor was employed (Baker, Shah et al. 2011, Driscoll 2015). With 15 minutes of dynamic tensile stretch (3% strain, 1Hz), an increase in phosphorylated ERK1/2 was observed in all groups **(Supplemental Figure 8-4c)**, although N1G knockdown resulted in slightly higher baseline pERK/ERK such that the fold increase was less under this condition.

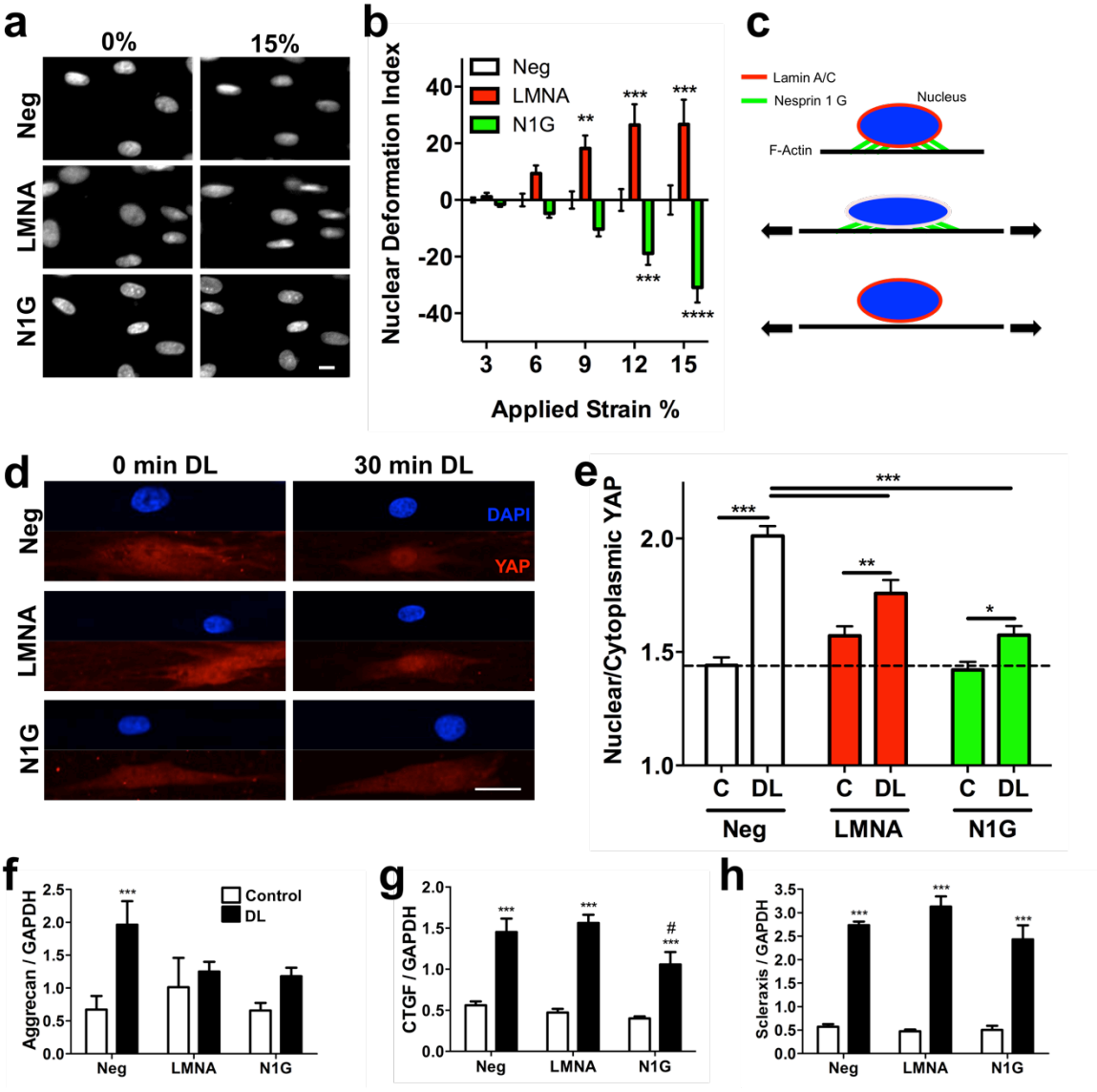

Figure 8-3: The LINC complex regulates nuclear strain transfer and mechanotransduction in MSCs. Representative images of Hoechst stained nuclei (A) at 0 and 15% applied strain for cells treated with lentivirus containing control (Neg), lamin A/C RNAi (B) or nesprin 1 giant RNAi. Quantification of the nuclear

deformation index (B) compared to control cells (Neg) (Scale = 10μM). Positive index indicates deformations larger than control, negative index indicates deformations less than control. (mean +/-SEM, n=114-149 cells per group). Simplified schematic representing the nucleus, its lamin A/C network, and the connections it makes to F-Actin through nesprin 1 giant (C). With less lamin A/C to resist deformations, larger deformations occur; with less nesprin to connect the nucleus to the cytoskeleton, smaller deformations occur. Images of YAP (Red) and DAPI (Blue) stained nuclei (D) on aligned scaffolds with or without 30 minutes of dynamic tensile loading (DL, 3% strain, 1Hz, scale= 25μm). Quantification of the nuclear to cytoplasmic ratio of YAP (E) for control (C) or dynamically loaded (DL) cells. (mean +/- SEM, n=33-41 cells per group) qPCR results for expression of Aggrecan (F), CTGF (G), and Scleraxis (H) with (white) or without (black) 6 hours of dynamic loading (DL) (mean +/-SD n=3 samples per group). (Statistical symbols: # p<0.05 vs. all groups, * p<0.05, ** p<0.01, *** p<0.001, **** p<0.0001, stars designate differences between indicated groups or compared to unloaded control)

Next, we assessed the YAP signaling response in the context of dynamic stretch with perturbation of the LINC complex. YAP staining on aligned scaffolds was evenly distributed throughout the cytoplasm in non-loaded control cells, likely due to the restriction of cell spread area due to the fibrous nature of the scaffold and/or the mobility of individual fibers (making the substrate appear 'soft' despite being comprised of stiff fibers (Baker 2014) **(Figure 8-3d)**. With 30 minutes of dynamic tensile stretch, YAP localized to the nucleus in control cells **(Figure 8-3d)** but remained in the cytoplasm in N1G knockdown cells. Quantification of these images showed a significant increase in the nuclear-to-cytoplasmic ratio of YAP in control cells with loading that was partially attenuated with LMNA knockdown and almost completely abrogated with N1G knockdown **(Figure 8-3e)**.

8.3.4 Lamin A/C and nesprin 1 giant increase concordantly with age in meniscus cells allowing for continuous nuclear strain transfer and YAP mechanotransduction throughout maturation.

With the observation that both lamin A/C and nesprin 1 giant regulate the transmission of strain in undifferentiated MSCs, we next sought to determine the levels of these proteins and the role they play in nuclear strain transfer in a differentiated cell type of interest. In particular, we were interested in meniscal fibrochondrocytes. There is a high prevalence of knee meniscus injury in the general population and, due to its limited regenerative capacity, a need for replacement therapies that can restore joint mechanics and prevent the early onset of osteoarthritis after meniscus injury (Andersson-Molina, Karlsson et al. 2002). Additionally, we were interested in the extent to which these LINC complex proteins change with meniscus development, as the tissue stiffens and becomes more organized (Ionescu, Lee et al. 2011). We hypothesized that these changes might regulate lamin A/C expression, which scales with tissue stiffness over a wide range of tissues and stiffnesses (Swift, Ivanovska et al. 2013), and so impacts the ability of the nucleus to deform as a function of maturation state.

Analysis of lamin A/C expression in meniscal fibrochondrocytes (MFCs) isolated from the inner (I) or outer (O) regions of fetal, juvenile and adult lateral menisci showed a significant increase in lamin A/C in cells from the outer region of the tissue **(Figure 8-4a and 8-4b)**. Conversely, cells from the inner meniscus, which develops a greater stiffness early in gestation, showed similar levels of lamin A/C at each growth stage. Interestingly, the levels of lamin A/C were increased when cells were expanded to

passage 3 **(Supplemental Figure 8-5a)** as cell area increased **(Supplemental Figure 8-5b)**, resulting in a loss of differences between fetal and adult outer meniscus cells. This suggests a role for stiffness sensing (expansion on stiff tissue culture plastic) as a potential regulator of differences in lamin A/C in MFCs. Indeed, previous work has shown outer meniscus mechanical properties to increase with age (Ionescu, Lee et al. 2011). Lamin A/C levels in very early passage (12-14 days post isolation) juvenile MSCs were also lower than in adult MFCs **(Figure 8-4b)**. Consistent with these findings, the peri-nuclear stiffness (assessed by AFM) of outer meniscus cells also increased with age **(Figure 8-4c)**. Interestingly, when we assessed other LINC complex members, we found that levels of N1G (assessed by dot immunoblot following 1MDa size filtration of whole cell lysate) also increases with age, tissue stiffness and nuclear stiffness. Nuclear height however, was similar between MFC groups when seeded on glass, and all were significantly higher than MSCs cultured similarly.

Given that in earlier studies both lamin A/C and nesprin 1 giant contributed to nuclear strain transfer, we next determined the effect of changes in these LINC complex members with age on strain transfer in meniscus cells. Interestingly, nuclear deformation with applied strain showed similar deformations for all MFC age groups **(Figure 8-4g),** all of which were significantly lower than what was observed for undifferentiated MSCs subjected to the same deformations. This may indicate that, with age, MFCs scale lamin A/C content, nuclear stiffness, and nuclear connectivity together in a concordant fashion, such that a constant level of nuclear strain transfer is achieved across development states.

Next, we infected adult MFCs with knockdown viruses directed against LMNA and N1G, and quantified nuclear deformation with static stretch and YAP response with dynamic tensile stretch. Similar to results in MSCs, knockdown of LMNA increased nuclear deformation while knockdown of N1G decreased nuclear deformation **(Figure 8-4h)**. Interestingly, these knockdowns had a slightly larger impact on the percent change in deformation than was observed in undifferentiated MSCs, consistent with results showing that adult MFCs express higher levels of both of these proteins in their basal state **(Figure 8-4b and 8-4e)**. In terms of mechanotransduction response, YAP was localized throughout the cell in control cells and moved to the nucleus with dynamic stretch, resulting in a significant increase in the nuclear to cytoplasmic YAP ratio (**Figure 8-4i**). Similar to MSCs, knockdown of N1G in adult MFCs resulted in almost complete loss of the YAP response to load. Interestingly, knockdown of LMNA in adult MFCs resulted in higher baseline nuclear localization of YAP, such that with loading, these cells reached YAP nuclear to cytoplasmic ratio levels similar to those in control cells (**Figure 8-4i**).

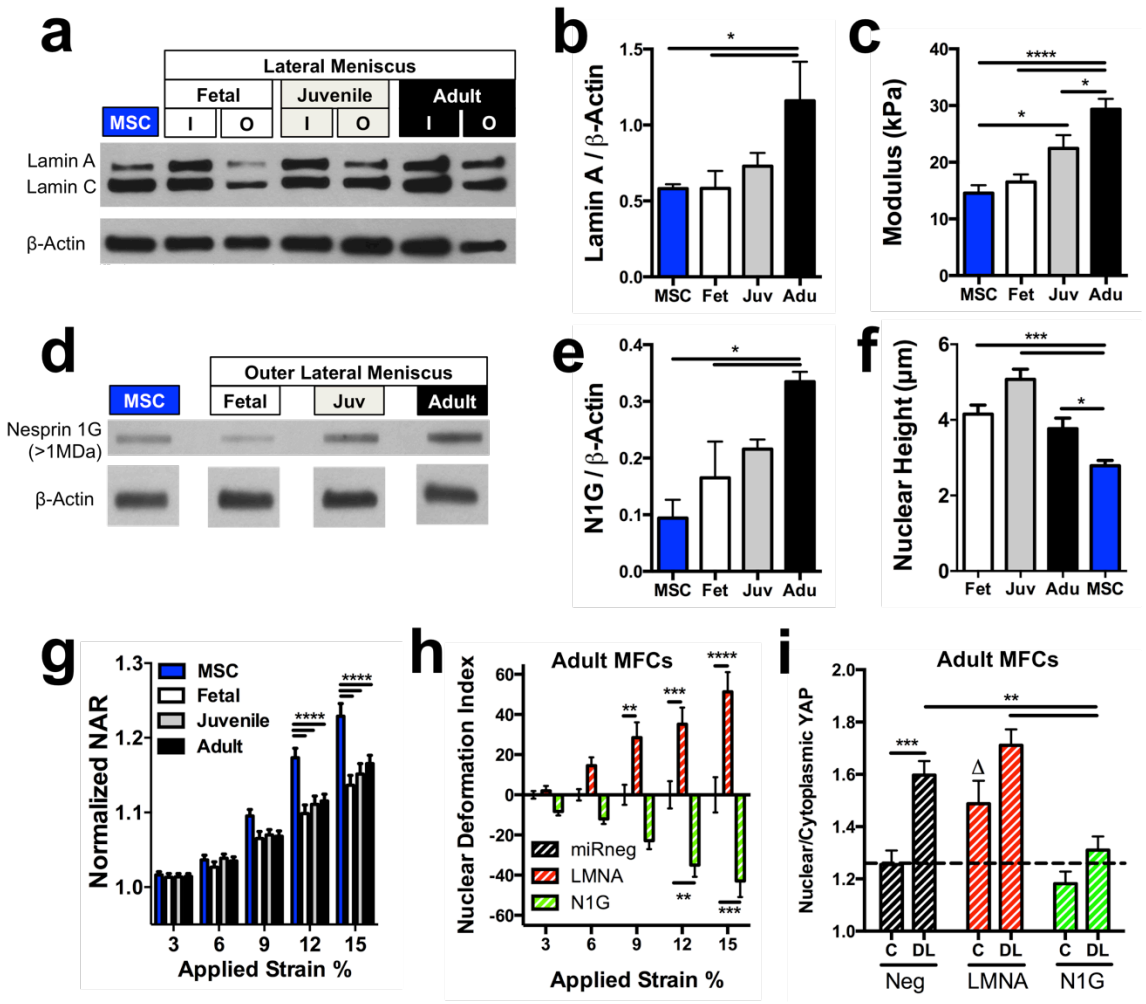

Figure 8-4: Lamin A/C and nesprin 1 giant increase concordantly with age in meniscus cells, allowing for continuous nuclear strain transfer and YAP mechanotransduction throughout maturation. Western blot for lamin A/C and β-actin (A) for cells from the inner (I) or outer (O) lateral meniscus of fetal, juvenile, or adult animals, compared to juvenile MSCs. Densitometry (B) of lamin A/C levels normalized to β-actin for outer MFCs compared to MSCs (mean +/-SD, n=3/group). Peri-nuclear modulus measurements taken using AFM (C) for outer MFCs of each age and undifferentiated MSCs. (mean +/-SEM, n=39-40 cells/group). Dot blot for nesprin 1 of whole cell lysate after 1MDa size filtration (d) with densitometry (e) normalized to western blots for beta actin in non-filtered lysate (cropped lanes all run on the same gel). (mean +/- SD, n=3/group). Quantification of nuclear height (f) from DAPI z-stacks for outer MFCs and MSCs seeded on glass. Nuclear deformation on statically strained aligned scaffolds for MSCs and outer MFCs (g) (mean +/-SEM, n= 162-197 cells/group). Nuclear deformation index for adult outer MFCs with knockdown of lamin A/C (LMNA) or nesprin 1 giant (N1G). (mean +/-SEM, n= 75-106 cells/group). Quantification of the nuclear to cytoplasmic YAP ratio in adult MFCs after 30 minutes of dynamic loading (i). (mean +/-SEM, n=21-34 cells/group).

8.3.5 Nesprins are regulated by soluble and mechanical differentiation factors.

With the observation that LINC complex components are important for nuclear strain transfer and mechanotransduction in a cell type of interest for tissue engineered replacements (meniscus fibrochondrocytes), we next assessed the extent to which fibrochondrogenic differentiation of MSCs, using soluble (TGF-β) or mechanical (dynamic tensile loading) differentiation cues, could regulate nesprin. Previously, we had observed that with one week of TGF-β3 induced differentiation of MSCs on aligned electrospun scaffolds, a significant reorganization of the lamin A/C network in the nucleus occurs along with a significant increase in the level of lamin A/C protein. Similarly, 5 days of dynamic tensile loading (3%, 1Hz, 6 hours per day) brought about comparable changes in the nucleus (Heo, Nerurkar et al. 2011). Given this observation, we next determined how nesprin changes with MSC differentiation through soluble or mechanical means. With either differentiation cue, a significant increase in the mRNA expression of the cartilage marker aggrecan was observed (**Figure 8-5a and 8-5b**). Additionally, a very large increase in expression of nesprin 1 giant mRNA (primers directed at N1G CH domain) was observed with dynamic loading **(Figure 8-5b and 8-5c)**, and smaller increases occurred with TGF-β3 induced differentiation. This was consistently observed for five independent experiments with MSCs isolated from 5 separate donors. Very little change in expression of nesprin 2 giant was observed **(Figure 8-2e and 8-2f)**. Additional primers directed at the KASH domain of these proteins indicated similar results for nesprin 2, and similar but less significant increases for nesprin 1 (**Supplemental Figure 8-7**). This likely indicates that the changes observed

with loading are indeed for the nesprin 1 giant (actin binding) splice variant, and that smaller nesprin 1 variants may decrease or maintain expression levels with loading.

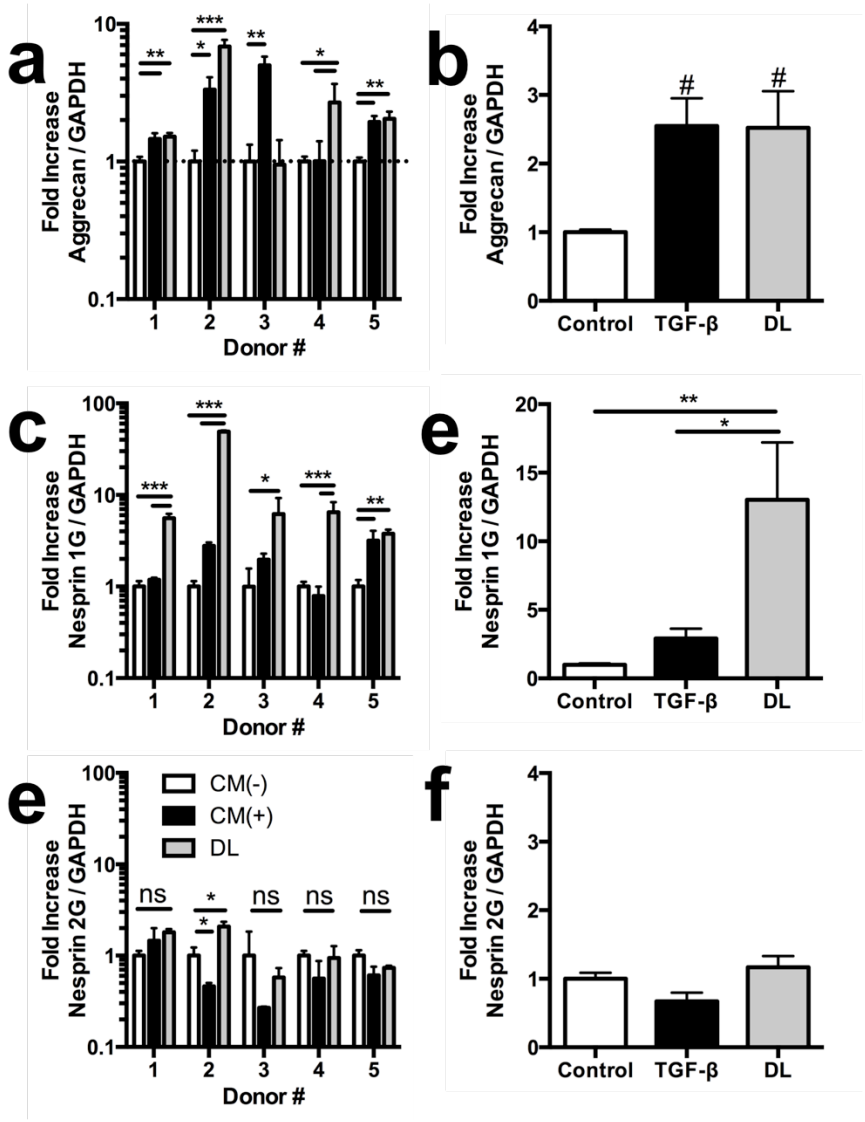

Figure 8-5: Nesprin 1 expression is regulated by dynamic tensile loading. qPCR results for 5 individual bovine donors using primers directed at the cartilage marker aggrecan (a,b), the N-terminal region of nesprin 1 giant (c,e) and the N-terminal region of nesprin 2 giant (e,f). Results are shown for each individual donor (a,c,e) (mean +/- SD n=3/group) and combined for all 5 donors (b,e,f) (mean +/-SEM n=15/group).

Next, we quantified protein expression levels in MSCs with or without differentiation cues. We observed changes in one smaller isoform of nesprin 1 **(Figure 8-6a and 8-6b)** and another smaller isoform of nesprin 2 **(Figure 8-6c)**. With TGF-β induced differentiation, these two smaller nesprin isoforms increased significantly. Conversely, with 5 days of dynamic loading, a significant decrease in these same two isoforms was observed **(Figure 8-6b and 8-6c)**. Further, we found that the smaller isoform of nesprin 1, became more localized to the nucleus with both TGF-β and dynamic loading **(Figure 8-6e)**.

Next, we assessed changes in the larger, actin binding nesprin 1 isoform, nesprin 1 giant. Analysis of whole cell lysate after 1MDa size filtration indicated a significant increase in levels of nesprin 1 giant when cells were dynamically loaded for 5 days. Notably, this change did not occur with differentiation via addition of TGF-β **(Figure 8-6d)**. Additionally, we found that these changes induced by dynamic loading were dependent on cytoskeletal tension. When cells were exposed to the ROCK inhibitor Y27632 during each loading cycle, the increase in nesprin 1 giant was not observed **(Figure 8-6d)**. When total nesprin 1 was immunoprecipitated and probed for lamin A/C, a decrease in lamin A/C was observed as a consequence of TGF-β induced differentiation; this change did not occur with dynamic loading (**Figure 8-6f**). Together these results indicate that changes in nesprin occur with both TGF-β and dynamic loading, but that these two stimuli result in a distinct set of changes in these nuclear structural proteins. With dynamic loading, nuclei likely form more nesprin connections to the cytoskeleton (increases in the nesprin 1 giant isoform), and these giant isoforms are more firmly

associated with other components of the LINC complex (i.e., lamin A). Conversely, with soluble factor mediated differentiation, smaller nesprin isoforms predominate, which don't bind actin allowing for nuclear strain transfer.

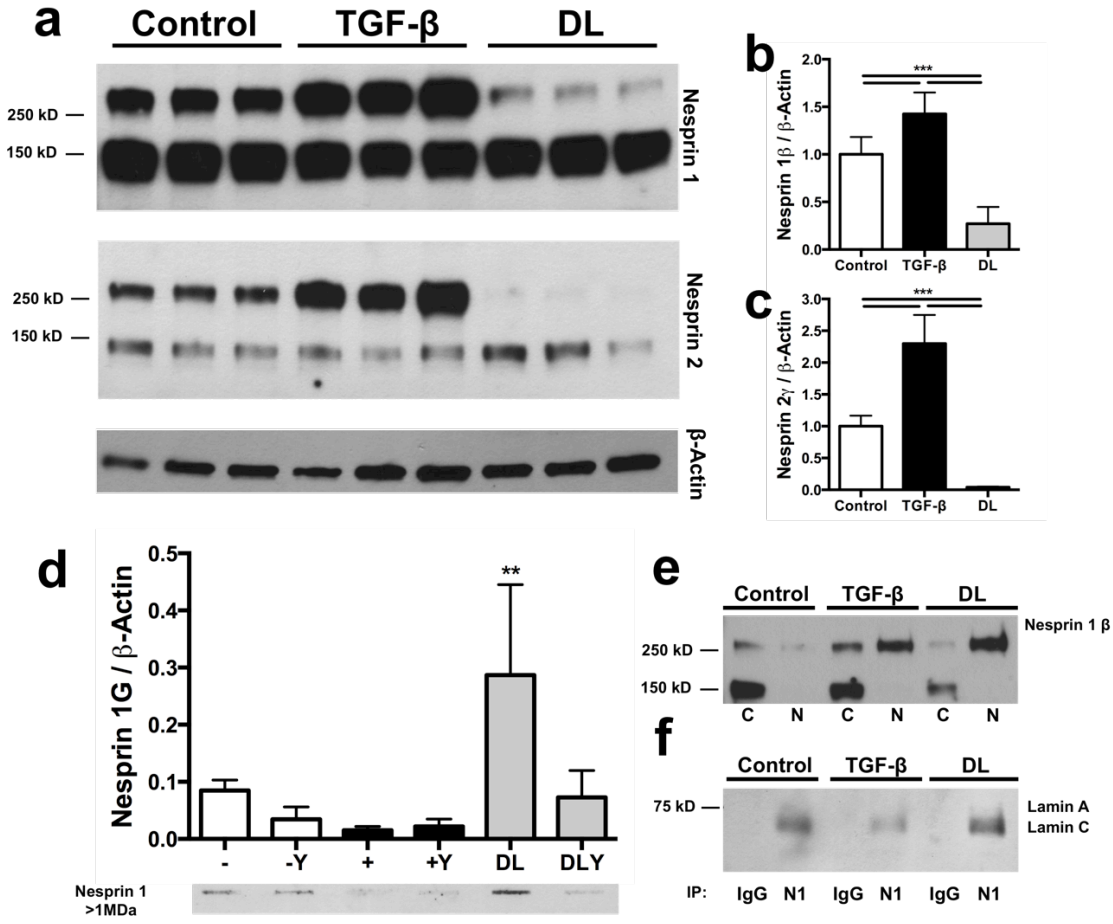

Figure 8-6: Nesprins are regulated by soluble and mechanical differentiation cues. Western blots (a) for nesprin 1 and nesprin 2 normalized to β-Actin for cells seeded on aligned scaffolds for 7 days and exposed to either TGF-β or 5 days of dynamic tensile loading (DL, 6 hrs/day, 1Hz, 3% strain). Densitometry for expression of nesprin 1β (b) and nesprin 2γ (c) (mean +/- SD, n=9 samples per group from 3 independent donors). Dot blot (d) for nesprin 1 giant (>1MDa) with densitometry normalized to β-Actin western blot (mean +/- SD, n=3/group). Western blot for nesprin 1 of nuclear (N) and cytoplasmic (C) fractionated samples (e). Immuno-precipitation of total nesprin 1 (N1) or IgG control with western blot for lamin A/C (f).

8.3.6 Differentiation alters YAP mechanotransduction

Since the response of YAP to mechanical loading was regulated by nesprin 1 giant in both MSCs and MFCs, and the levels of this protein are altered with both soluble and mechanical differentiation cues, we next addressed the extent to which these changes alter the YAP response to load. Similar to previous experiments, MSCs were seeded on aligned scaffolds for 1 week and were exposed to TGF-β or dynamic tensile loading for 5 days to induce differentiation. After this differentiation period, cells were trypsinzed and re-seeded on fresh fibronectin coated scaffolds for 2 days in a chemically defined media. For this period, all cells were cultured in the same media and not exposed to mechanical loading. Two days after re-seeding, cells were assayed for their YAP mechanical response to load. Both soluble and mechanical differentiation cues resulted in alterations in basal cytoskeletal morphology, with increases in cell area observed for both **(Figure 8-7a),** whereas these two cues had opposite affects on cellular aspect ratio, with loaded cells developing a more elongated conformation (**Figure 8-7b**). Additionally, an increase in the number of visible stress fibers was observed in both differentiated populations. Quantification of the average F-actin staining intensity in the cell showed significant increases with both TGF-β and DL induced differentiation **(Figure 8-7c)**. In undifferentiated control cells, YAP was localized evenly throughout the cell (**Figure 8-7d**) and with 30 minutes of dynamic loading, YAP localized to the nucleus. Interestingly, both soluble and mechanical differentiation resulted in a significant increase in the baseline YAP nuclear localization, such that both were higher than unloaded control cells. With loading, TGF-β induced cells displayed a significant increase in the nuclear to cytoplasmic YAP ratio **(Figure 8-7e)**, maintaining YAP

sensitivity to mechanical loading. However, cells that had been differentiated with 5 days of dynamic loading were no longer sensitive to mechanical loading, showing no change in the nuclear to cytoplasmic YAP ratio when loaded **(Figure 8-7e)**.

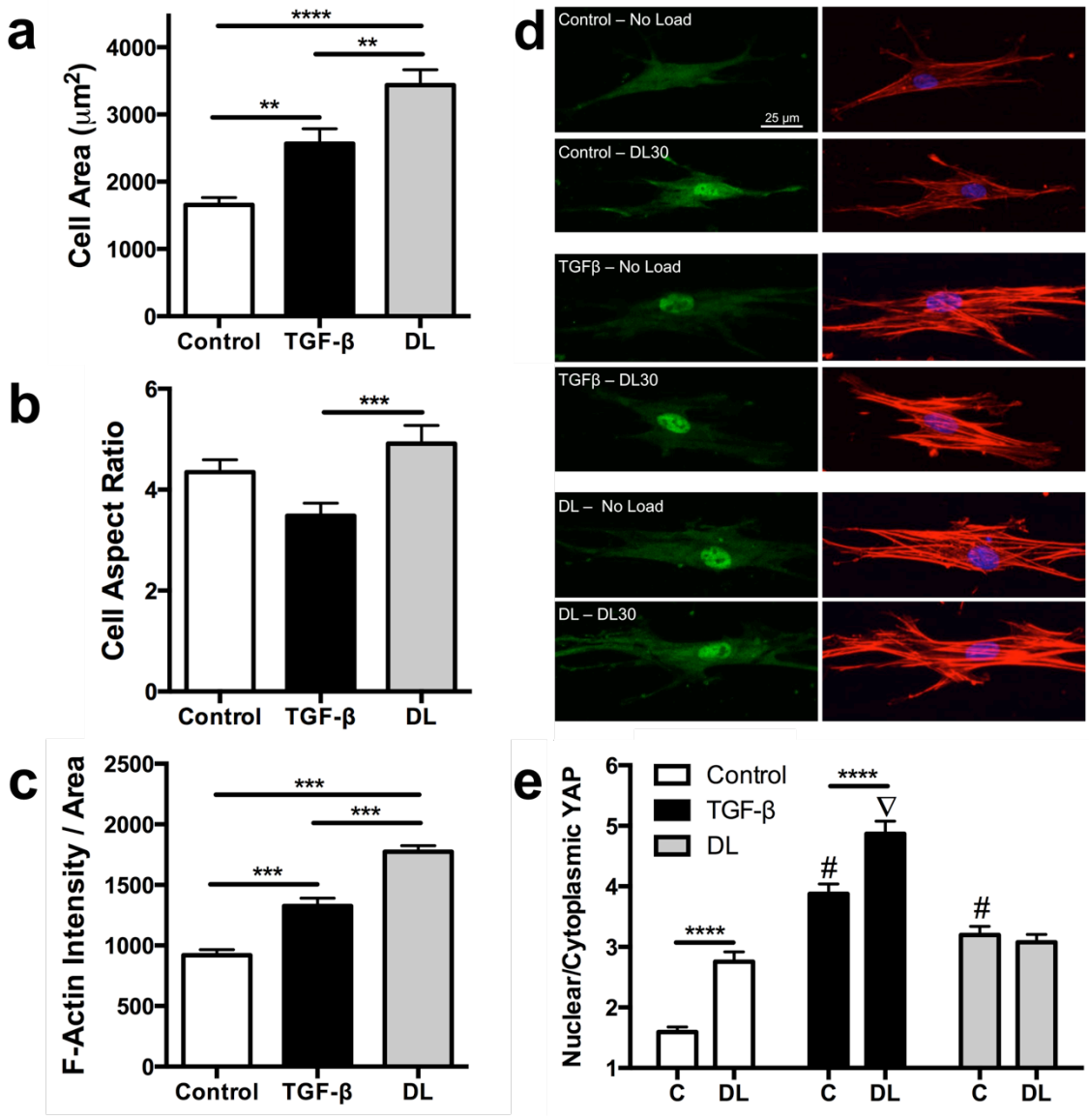

Figure 8-7: Differentiation alters YAP mechanotransduction. All cells were seeded on aligned scaffolds for 7 days with control media (control), TGF-β media (TGF-β), or 5 days of dynamic loading for 6 hours per day (DL). Cells were then trypsinized and re-seeded onto fresh scaffold in control media prior to staining or stretching. Quantification of cell area (a), cell aspect ratio (b) and average F-actin staining intensity (c), based on actin staining of cells on aligned scaffolds. (mean +/- SEM, n= 27-41, ** p<0.01, *** p<0.001, **** p<0.0001). Images of YAP (green) and F-Actin/DAPI (red/blue) staining (d) on aligned scaffolds with or with out 30 minutes

of DL in control media (DL). Quantification of the nuclear to cytoplasmic YAP ratio (e) with (DL) or without loading (C) for cells that had been differentiated (TGF-β, DL) for 1 week and then reseeded in control media for two days prior to loading. (mean +/- SEM, n= 27-41 cells / group).

These data suggest that differentiation induced changes in cytoskeletal and nucleoskeletal structure and composition have the ability to alter the cellular interpretation of a fibrous matrix and the loads transmitted through it. With differentiation through either mechanism, increases in baseline nuclear localization of YAP were observed, indicating a shift in the cellular interpretation of matrix stiffness. These results also indicate that cells have the ability, at least in the short term, to remember previous loading experiences and become desensitized to loading. Since mechanically differentiated cells displayed increased expression of N1G, these decreases in sensitivity could be due to lower stress concentrations at the nuclear envelope (due to load sharing across an increased number of nesprins). Conversely, cells differentiated through soluble means displayed high YAP mechanosensitivity, as indicated by very high nuclear localization of YAP when loaded. This may be due to high stress concentrations at the nuclear envelope, since nuclear stiffness increases in these cells (Heo, Nerurkar et al. 2011), while N1G decreases.

8.4 Discussion

In this study, we show that forces transmitted through cytoskeletal connections to the nucleus can regulate the YAP/TAZ mechanosensory pathway. While traditional mechanosensory events are thought to occur at the cell surface, this work supports the growing body of evidence suggesting that transmission of force through the cytoskeleton and to the nucleus can regulate mechanosensitive molecules within the cytoskeleton and

nucleus. With knockdown of the LINC complex component nesprin 1 giant, cytoskeletal flattening of the nucleus was reduced, despite increases in cellular traction force and vinculin adhesion area. In turn, this resulted in reduced activation of the YAP/TAZ pathway with substrate stiffness, which, consistent with previous reports (Swift, Ivanovska et al. 2013), was not prevented with knockdown of lamin A/C. When cells were exposed to tensile stretch, knockdown of nesprin 1 giant reduced nuclear deformation and limited the nuclear translocation of YAP. Lamin A/C knockdown reduced, but did not prevent, YAP nuclear translocation with loading, despite the fact that increases in nuclear deformation with stretch were observed. This is potentially due to decreases in nuclear stress concentrations resulting from a loss in nuclear mechanical properties with reduced lamin A/C levels. While the specific cytoskeletal or nucleoskeletal molecule responsible for YAP mechanical activation is unclear, these data suggest that cytoskeletal forces exerted on the nucleus can regulate its activation. While it is known that F-actin is necessary for YAP nuclear localization on stiff substrates, G-actin levels do not regulate YAP (Dupont, Morsut et al. 2011) as they do in other cytoskeletal mechanotransduction pathways, such as the MKL-1/SRF pathway (Ho, Jaalouk et al. 2013). What is clear is that the mechanosensory portion of the YAP/TAZ pathway functions through a non-canonical (i.e. LATS independent) mechanism (Dupont, Morsut et al. 2011). Given that normal YAP nuclear localization can be achieved on poly-L-lysine coated substrates, this unknown regulator is likely not a component of integrin based focal adhesions (Zhao, Li et al. 2012). Rather, forces in the cytoskeleton itself, or the connections it forms with the nucleus, likely regulate this molecule. It has been proposed that the LATS independent YAP signaling in response to mechanical

factors likely requires an unknown serine kinase, which is regulated by force in the cytoskeleton (Low, Pan et al. 2014). The data presented here suggests that transmission of force through the cytoskeleton and to the LINC complex is likely important for regulation of this kinase. Additionally, the observed differences in YAP signaling may be due to the nesprin 1 giant deficit causing differences in F-actin polymerization or regulation of F-actin capping and severing proteins, which have been shown to regulate YAP (Aragona, Panciera et al. 2013).

It is known that YAP nuclear translocation is important for osteogenesis in MSCs and inhibitory of adipogenesis (Dupont, Morsut et al. 2011). Interestingly, knockdown of nesprin 1 giant did not enhance adipogenesis or prevent osteogenesis in this study, despite the reduced nuclear YAP localization under this condition. This may indicate that the YAP localization that does occur is sufficient to drive osteogenesis, or that the increases in cellular traction that occur with loss of nesprin 1 giant are able to override the deficit in YAP signaling. Conversely, and consistent with previously published data (Swift, Ivanovska et al. 2013), knockdown of lamin A/C enhanced adipogenesis.

Comparisons to differentiated cells from the outer meniscus of the knee indicated that both lamin A/C and nesprin 1 giant increase with age, as the tissue stiffens. Associated with these changes, we observed a significant increase in the peri-nuclear stiffness of these cells. Knockdown of LINC complex components in adult cells resulted in a larger percent change in nuclear deformation than in MSCs, potentially due to the elevated levels of both nesprin 1 giant and lamin A/C at baseline. Similar to undifferentiated

MSCs, these adult cells also displayed a deficit in YAP mechanical activation with nesprin 1 giant knockdown.

Previously, we reported that fibrochondrogenic differentiation of MSCs on aligned scaffolds using either soluble TGF-B3 or mechanical loading results in alterations in the lamin A/C network and increases in expression of lamin A/C, such that levels approach those of differentiated meniscal fibrochondrocytes. Here we show additional changes in both large and small nesprin isoforms with both modes of differentiation. With 5 days of dynamic loading, significant increases in nesprin 1 giant were observed, and this increase was dependent on transmission of strain through the tensed actin cytoskeleton. However, with soluble differentiation alone, nesprin 1 giant levels were not increased, and there was lower association of total nesprin 1 protein with other LINC members. This may indicate, that to achieve levels of these components comparable to those of differentiated fibrochondrocytes, mechanical stimulation will be required. When these differentiated cells were re-seeded on fresh scaffolds in the absence of differentiation factors, YAP was highly localized to the nucleus. Cells differentiated by soluble means maintained YAP mechanosensitivity to load, while cells differentiated by mechanical loading were desensitized to load.

In summary, we have demonstrated that dynamic tensile force transmitted though the LINC complex can activate the YAP/TAZ pathway. Additionally, nesprin 1 giant levels increase with development or mechanical differentiation, altering the YAP response to load. These changes, and an understanding of how they regulate mechanotransduction,

will be crucially important for success of engineered replacement tissues that are exposed to dynamically loaded environments.

8.5 Supplemental Figures

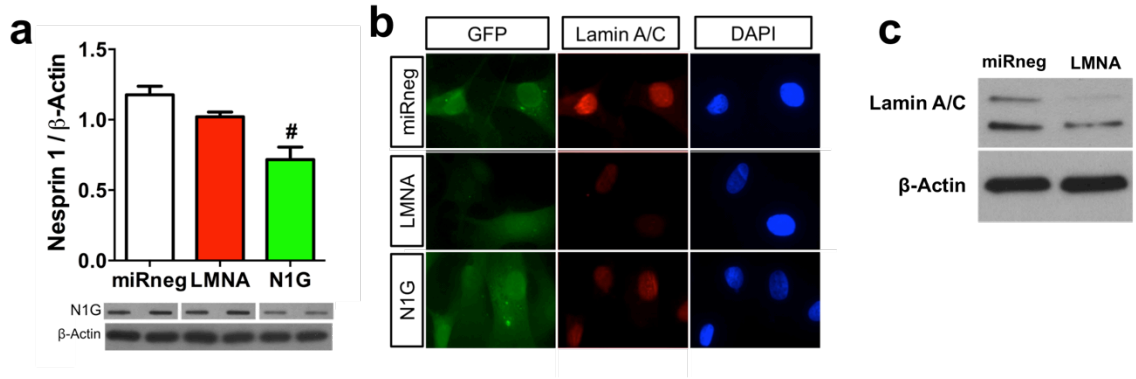

Supplemental Figure 8-1: Verification of nesprin 1 giant knockdown by dot blot for nesprin 1 following 1MDa size filtration of whole cell lysate (a) (mean +/-SD n=3/group). Verification of lamin A/C knockdown by immunostaining of lamin A/C (b) and western blot for lamin A/C (c).

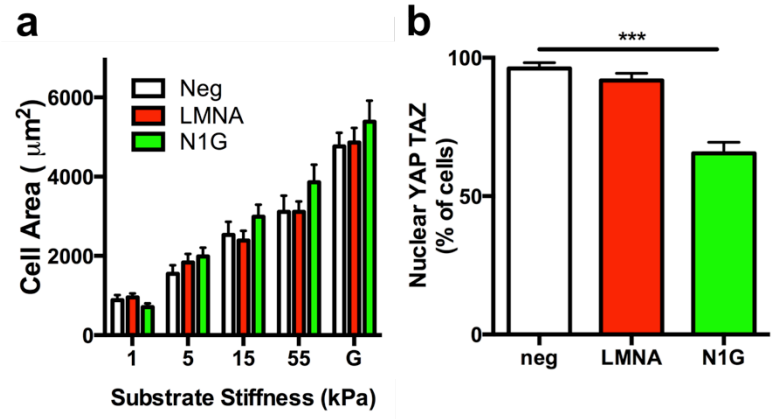

Supplemental Figure 8-2: Quantification of cell area on polyacrylamide substrates of various stiffness and glass (G) based on F-actin staining (a) (mean +/- SEM, n=21-30 cells / group). Quantification of the percent of cells with clear nuclear outlines of YAP (b) (mean +/- SD, n=3 independent experiments).

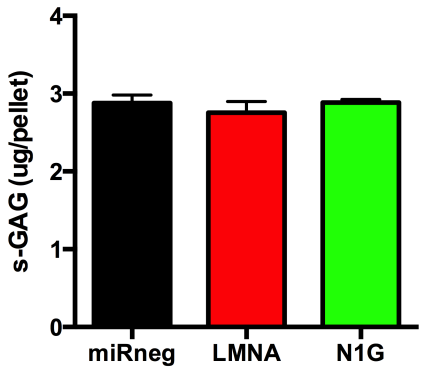

Supplemental Figure 8-3: Sulfated glycosaminoglycan content (s-GAG) in cell micro-pellets (10k cells/pellet) cultured under chondrogenic conditions for 2 weeks. (mean +/- SD, n=3 samples/group, 2 pellets per sample)

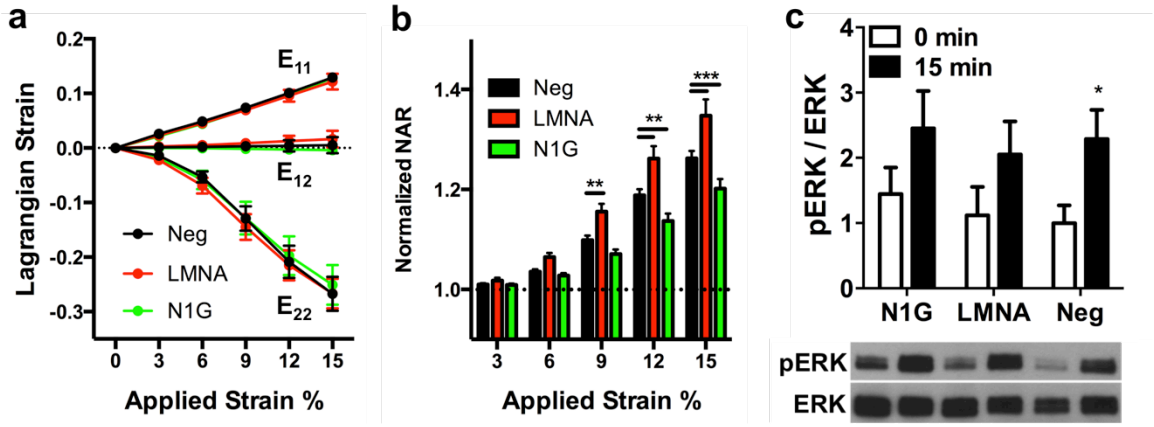

Supplemental Figure 8-4: (a) Lagrangian strains calculated for triads of Nuclei (performed as a control) (mean +/- SD, n=3-4 scaffolds per group). (b) Nuclear deformation (calculated as aspect ratio of the nucleus normalized to undeformed control) (mean +/-SEM, n=54-89 cells/group). (c) Densitometry of western blots for phosphorylated ERK (pERK) normalized to total ERK with representative blot (mean +/- SD n=2-3/group).

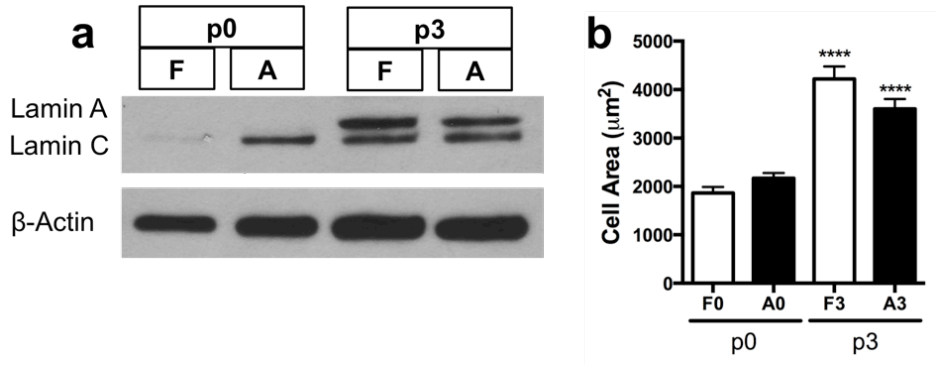

Supplemental Figure 8-5: Western blot (a) for lamin A/C in very early passage (p0) or later passage (p3) fetal (F) and adult (A) MFCs. Quantification of cell area from early passage and later passage cells (b). (mean +/- SEM n=69-94 cells/group, **** = p<0.0001)

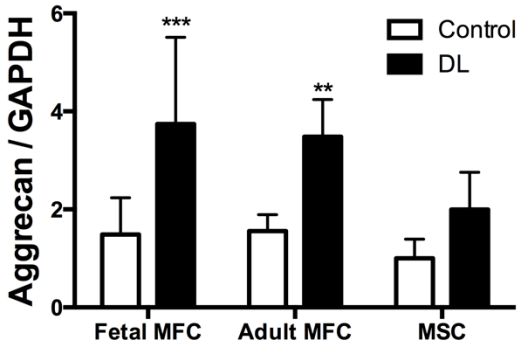

Supplemental Figure 8-6: qPCR results for aggrecan expression in fetal or adult outer lateral MFCs compared to MSCs. Cells were seeded on scaffold for 2 days in chemically defined media then loaded on two consecutive days for 6 hours per day (3% strain, 1Hz). Data combined for two independent experiments with independent donors. (mean +/- SD, n=6 / group) (p<0.01 vs Control, *** p<0.001 vs. Control)**

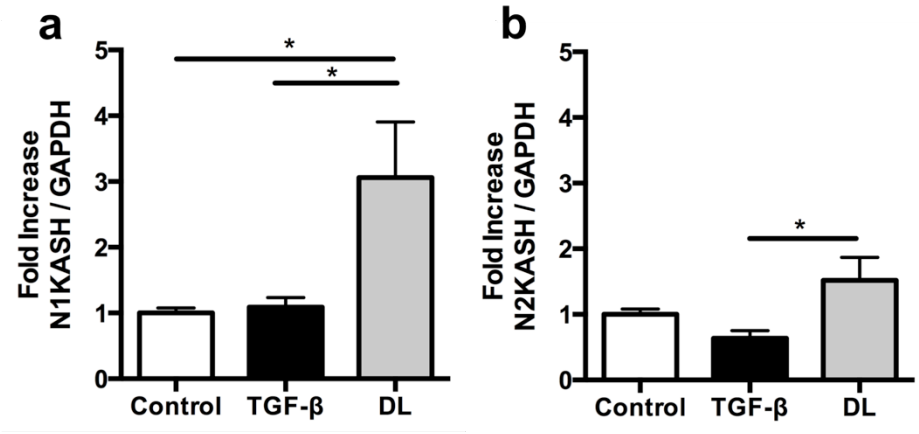

Supplemental Figure 8-7: qPCR results for primers directed at the KASH domain of nesprin 1 (a) or 2 (b) (SUN binding domain in Giant and many smaller nesprins). Cells were seeded on scaffold for 2 days in chemically defined media then differentiated by loading on 5 consecutive days for 6 hours per day (3% strain, 1Hz) or by induced by treatment with TGF-β3 . Data combined for three independent experiments with independent donors. (mean +/- SD, n=9 / group) (* $p<0.05$)

CHAPTER 9: SUMMARY AND FUTURE DIRECTIONS

9.1 Summary

Cells possess a variety of mechanotransduction mechanisms (outlined in Chapter 2), many of which regulate development, homeostasis and degeneration of the organized matrices that make up functional tissues. Fiber-reinforced tissues often degenerate, requiring removal, repair or replacement. Both tissue structure and cellular attributes can regulate mechanotransduction, since mechanical loads are transmitted from the structural network of proteins outside of the cell (the extracellular matrix), through cell adhesions, to the structural network of proteins within the cell (the cytoskeleton), eventually reaching the nucleus (via transmission through the LINC complex). Mechanotransduction occurs at each of these levels, often through forced unfolding of proteins within these networks. Therefore, appropriate mechanotransduction in engineered tissues and cells will likely require replication of the protein networks that facilitate this multi-scale strain transfer. Using a variety of mechanical testing modalities at each of these scales, this work has investigated mechanical aspects of both mesenchymal stem cells and the engineered microenvironments that regulate their behavior.

In chapters 4 and 5 the extent to which engineered fibrocartilage matches native tissue shear and multi-directional mechanical properties was investigated. These chapters demonstrate that a previously described structural mechanism of inter-lamellar shearing in uniaxial tension, which acts to stiffen engineered laminates, is functional in biaxial tension. With time in culture, laminates engineered to have opposing lamellar orientation

(mimicking native annulus fibrosus) displayed increased biaxial mechanical properties compared to constructs with parallel lamellar orientation. Shear mechanical properties were found to exceed native tissue values and biaxial mechanical properties approached those of native tissue. However mechanical non-linearity in engineered constructs was significantly lacking.

To address the issue of non-linearity in nanofibrous scaffolds, Chapter 6 described an approach for patterning crimped structure into aligned scaffolds. This method is able to significantly increase scaffold mechanical non-linearity, also impacting micro-scale Lagrangian strains, nuclear orientation and the level of nuclear elongation with stretch. Further, these crimped scaffolds increase the ERK1/2 mechanotransduction response in mesenchymal stem cells with applied stretch.

One of the key regulators of mechanotransduction and transfer of strain to the nucleus is the actin cytoskeleton and the tension within it. In Chapter 7, the importance of cytoskeletal tension in regulating strain transfer to the nucleus was assessed. Additionally, the role that this cytoskeletal strain transfer plays in the mechanical activation of the YAP/TAZ pathway with tensile loading was investigated. This work showed that while some mechano-active signaling pathways (e.g. ERK signaling) can be activated in the absence of nuclear strain transfer, cytoskeletal strain transfer to the nucleus is essential for activation of the YAP/TAZ pathway with stretch.

Based on the results from Chapter 7, which indicated nuclear strain transfer was necessary for YAP activation with stretch, Chapter 8 addressed the extent to which this strain transfer and YAP activation is facilitated by the LINC complex components nesprin 1 giant and lamin A/C. This chapter identified nesprin 1 giant as a regulator of nuclear height, cellular adhesion size, cellular traction force, and YAP signaling in response to both substrate stiffness and dynamic tensile loading in MSCs. Comparison to differentiated fetal, juvenile, and adult fibrochondrocytes indicated that both lamin A/C and nesprin 1 giant increase with age as nuclear stiffness and tissue stiffness increase, surpassing levels in MSCs. Interestingly, nesprin 1 giant also regulated the YAP response to dynamic loading in adult meniscus cells. Fibrochondrogenic differentiation of MSCs by mechanical loading resulted in changes in nesprin 1 giant. These load-induced changes were dependent on cytoskeletal contractility and did not occur with differentiation using soluble TGF-β3. Changes that occurred with mechanical or soluble differentiation, increased basal YAP nuclear localization on aligned scaffolds. And, in the case of mechanically induced differentiation, the YAP response to loading was desensitized.

Combined, these results point to a nuclear mechanotransduction mechanism in MSCs that functions through the YAP/TAZ pathway and is dependent on the transmission of force to the nuclear envelope through the LINC complex. Further, these result indicate that differentiated MSCs fail to match meniscal cells with respect to nesprin 1 giant and lamin, but that stimulation by mechanical loading may provide the cues necessary for increases in nuclear linkage to the cytoskeleton. With the importance of mechanical

factors, and specifically the YAP/TAZ pathway, in tissue development and homeostasis, a detailed understanding of the molecular mechanisms which regulate this signaling pathway, and the extent to which they are recapitulated in engineered tissues, will be of primary importance for fabrication of functional engineered replacements that are maintained within dynamically loaded environments through a lifetime of use.

9.2 Limitations and Future Directions

9.2.1 Specific Molecular Regulators of YAP/TAZ Signaling With Stretch

While our results show that YAP signaling is regulated by cytoskeletal-to-nuclear strain transfer, one limitation of this work is that the specific cytoskeletally or nucleoskeletally associated molecule, which functions to sense force and drive YAP to the nucleus, is still unknown. While it is known that F-actin is necessary for YAP nuclear localization on stiff substrates, G-actin levels do not regulate YAP (Dupont, Morsut et al. 2011) as they do in other cytoskeletal mechanotransduction pathways, such as the MKL-1/SRF pathway (Ho, Jaalouk et al. 2013). What is clear is that the mechanosensory portion of the YAP/TAZ pathway functions through a non-canonical (i.e. LATS independent) mechanism (Dupont, Morsut et al. 2011). In the canonical Hippo pathway, YAP is phosphorylated by LATS, which causes it to be restricted to the cytoplasm. When LATS is not active, YAP localizes to the nucleus. Since the mechanical regulation of YAP functions independent of LATS (Dupont, Morsut et al. 2011), this points to some other molecular pathway by which YAP is sensitive to mechanical stimuli (Low, Pan et al. 2014). Given that normal YAP nuclear localization can be achieved on poly-L-lysine coated substrates, this unknown regulator is likely not a component of integrin based

focal adhesions (Zhao, Li et al. 2012). Rather, forces in the cytoskeleton itself, or the connections it forms with the nucleus, likely regulate this molecule (**Figure 9-1**). Interestingly, extensive polymerization of F-Actin (through modulation of the actin regulating proteins cofilin, Capz, and gelosin) can cause nuclear localization of YAP through inhibition of the canonical hippo pathway (LATS dependent). However, it has been proposed that the LATS independent YAP signaling in response to mechanical factors likely requires an unknown serine kinase, which is regulated by force in the cytoskeleton (Low, Pan et al. 2014).

There are numerous proteins that localize to the LINC complex, including many other nesprin isoforms and splice variants, SUN proteins embedded in the inner nuclear membrane, and Emerin associated with lamin A/C at the inner nuclear membrane. A number of these proteins are known to be mechanosensitive, including Emerin (Guilluy, Osborne et al. 2014) and lamin A/C, with phosphorylation occurring in a force dependent manner or substrate stiffness dependent manner. Further, defects in Emerin result in decreased YAP nuclear localization on high stiffness (Guilluy, Osborne et al. 2014) and defects in lamin A/C increase YAP nuclear localization in three dimensional matrices (Bertrand, Ziaei et al. 2014). While most of these structural proteins of the nuclear envelope do not themselves have any enzymatic activity, they likely serve as scaffolds for other enzymes (Pare, Easlick et al. 2005, Warren, Tajsic et al. 2009, Neumann, Schneider et al. 2010, Burke and Stewart 2014). These previously published results, in combination with the data presented in this thesis, indicate that a mechano-regulatory element of the YAP/TAZ pathway is dependent on forces transmitted through the LINC complex and to

the nucleus (**Figure 9-1**). This regulation requires both patent actin stress fibers (Chapter 7) and nesprin 1 giant connections that they make to the nuclear envelope (Chapter 8).

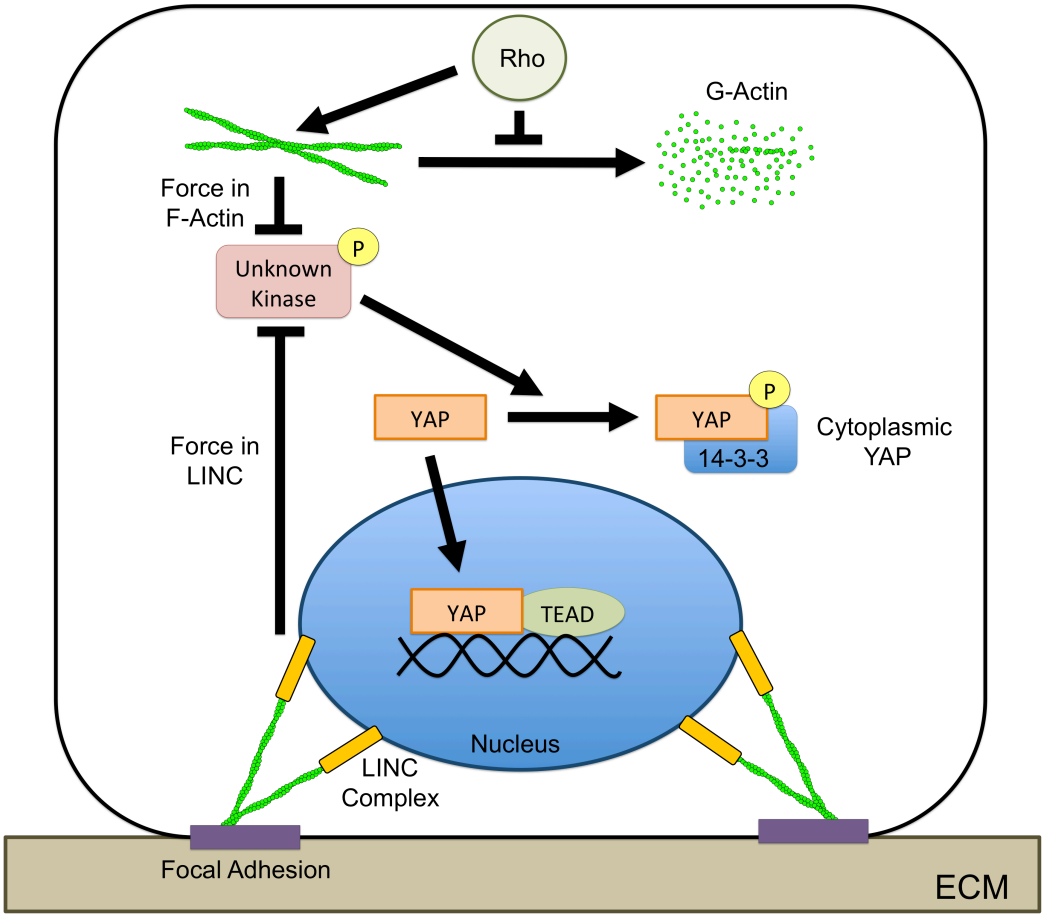

Figure 9-1: Mechanical Regulation of non-canonical YAP Signaling. In the canonical Hippo signaling pathway, YAP is phosphorylated by LATS and restricted to the cytoplasm by 14-3-3. When LATS is inactive, YAP can translocate to the nucleus and regulate transcription with TEAD. However, mechanical regulation of YAP has been shown to function in a LATS independent manner, leading some to propose that another unknown serine kinase is regulating YAP. Proteins that regulate F-actin (downstream of Rho) are known to regulate YAP, potentially through this mechanism. Additionally, data shown in Chapters 7 and 8 indicate that forces in the LINC complex may also regulate F-actin or directly regulate the unknown kinase upstream of YAP. For simplicity YAP is not shown as a complex with TAZ, but TAZ translocates to the nucleus with YAP.

9.2.2 Nanoscale Structure of the LINC Complex

While it is known that nesprins localize to the nucleus and other organelles, connecting them to the cytoskeleton, the nanoscale structure of these connections is unclear. SUN proteins are known to form as trimeric binding partners for nesprins at the inner nuclear membrane (Sosa, Rothballer et al. 2012) and these proteins interact with the nesprin KASH domains that are embedded in the outer nuclear membrane. It has also been previously observed that F-actin stress fibers passing over and under the nucleus display increased staining for LINC complex components (Nagayama, Yamazaki et al. 2014). Some have speculated that nesprins lie flat on the nucleus, forming a meshwork of connections to the actin stress fibers, which pass near the outer nuclear envelope. It has been observed that labeling the N and C terminal ends of nesprin results in two distinct networks at the outer nuclear membrane (Cartwright and Karakesisoglou 2014). However the exact nano-scale structure of these components is unclear.

Imaging of cellular structure on this scale can be difficult. Traditional light microscopy has limited resolution (ability discern two particles very close together) due to the wavelength of the light being used. The theoretical resolution limit at even short wavelengths is around 150 nanometers in the lateral dimension. However, a number of very elegant approaches have been developed over the last 8 years to circumvent this issue, including PALM, FPALM, and STORM. These "super-resolution" techniques rely on the fact that a single fluorescent point on a dark background can be localized to a much higher resolution (tens of nanometers) when fit with a two-dimensional Gaussian. Thus, by only activating a small portion of molecules at any given time, high-resolution

localization of the particles can be achieved. To do this, molecules that undergo stochastic activation after being photo bleached are used. One such molecule that works very well for this application is the Alexa-fluor 647 fluorescent molecule. By collecting videos with many frames (thousands) of spontaneously activating Alexa-fluor 647 molecules, then analyzing and fitting Gaussians to each point, images can be compiled from hundreds of thousands of individual points, each representing a labeled molecule.

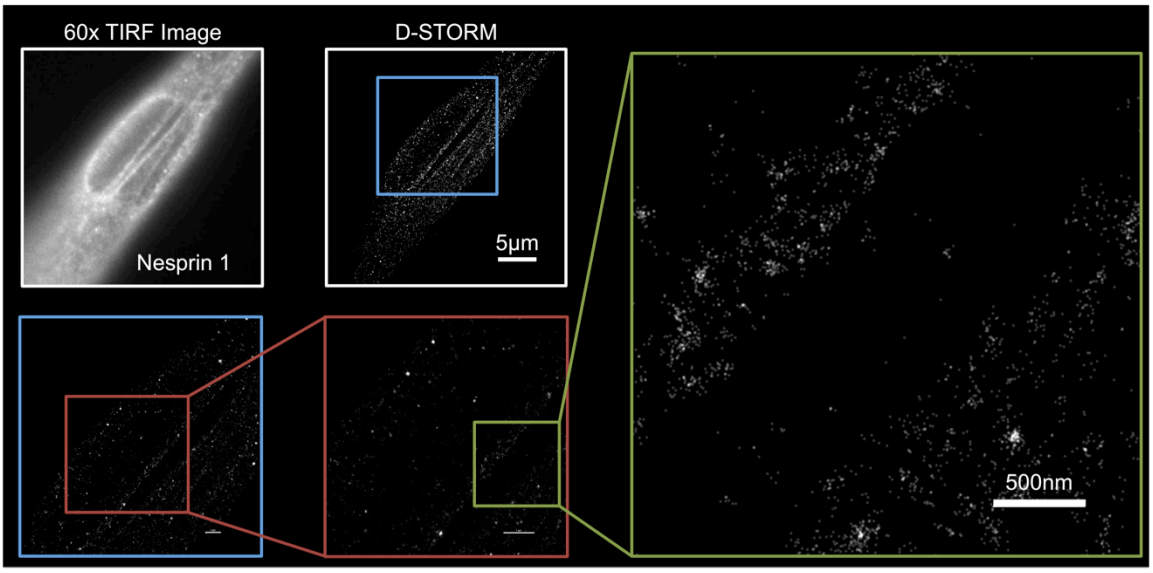

Figure 9-2: High-resolution 2D Direct Stochastic Optical Reconstruction Microscopy (D-STORM) images of nesprin 1 nanostructure at nuclear envelope. Wide Field and STORM images of Alexa-Fluor 647 stained nesprin 1 in bovine MSCs. Dots on the zoomed-in image (green) indicate labeled nesprin molecules. nesprin molecules were found to form clustered staining nodules that localize heavily to the nuclear envelope and along stress-fiber induced indentations in the nucleus (scale bars indicate 5µm (white boxes), 1µm (blue and red boxes), or 500nm (green box).

In preliminary experiments, we have used this technique to acquire images of nesprin 1 in MSCs (**Figure 9-2**). Even with wide-field TIRF microscopy, nesprin can be observed to localize more heavily to the nuclear envelope and the stress fibers that pass over it. With

higher resolution STORM imaging, nesprin is observed to form punctate clusters, some of which localize to the nuclear envelope and to the edges of stress fibers that press down into the nucleus (**Figure 9-2**). Further experiments using this technique will be helpful for understanding the exact structure of these nesprin connections to the nucleus and how they change with development and differentiation, mediated by soluble and mechanical differentiation cues.

9.2.3 Additional Regulators of Nuclear Connectivity to Cytoskeletal Elements

Another limitation to this study is that additional isoforms of nesprin exist, some of which possess the ability to connect to cytoskeletal elements, including F-Actin (nesprin 2 giant), intermediate filaments (nesprin-3) and microtubules (nesprin-4). These may also be important for this nuclear mechanotransduction mechanism, providing additional routes by which force can be transmitted to the nuclear envelope. While previous experiments from our lab indicated that microtubules and intermediate filaments were dispensable for transfer of strain to the nucleus (Nathan, Baker et al. 2011), these elements may provide other nuclear mechanotransduction mechanisms through nesprin 3 and nesprin 4.

Interestingly, nesprins 1 and 2 both interact with F-actin (Lombardi and Lammerding 2011). These two isoforms are paralogs, with a high degree of evolutionary conservation across a variety of species ranging from insects to mammals (Simpson and Roberts 2008). In vertebrates these two nesprin isoforms are thought to have arisen from ancient duplications and rearrangements. Further, knockout mouse models have shown that loss

of both nesprin 1 and nesprin 2 isoforms is embryonically lethal (Zhang, Xu et al. 2007), while loss of a single isoform is not but results in defects of the nervous and musculoskeletal systems (Zhang, Felder et al. 2010). This may indicate some overlap in functionality between nesprin 1 and 2. Similarly, SUN 1 and 2 isoforms, which function to link nesprins to the nucleus, have partially redundant roles (Lei, Zhang et al. 2009). Overall, these data indicate that strain transfer is likely not dependent on a single protein, but that the importance of these proteins has lead to evolutionary duplication, providing redundancy in protein function.

9.2.4 Long Term Maintenance of LINC Complex Changes with Differentiation

While changes in nesprin 1 giant were observed with loading induced differentiation of MSCs, the extent to which theses changes persist with time is unclear. Based on the findings in this thesis, these changes and their persistence will be an important regulator of MSC mechanotransduction in engineered environments. If maintenance of these changes is to be achieved, this will likely involve alterations in chromatin structure regulating the epigenetic phenotype of MSCs and their expression of LINC complex components.

Recent work by Sujin Heo in our lab has indicated that changes in both lamin A/C and chromatin structure can result from extended dynamic loading or TGF-β induced differentiation. Interestingly, dynamic loading is able to more rapidly induce chromatin changes, with multiple loading bouts resulting in additive changes to chromatin structure that are maintained for longer periods of time after removal of the stimulus (multiple

days). Early results have heavily implicated purinergic calcium signaling through ATP release in this chromatin response, however we have observed that addition of soluble ATP can also drive YAP localization to the nucleus, indicating potential overlap in these pathways. Additionally, this chromatin condensation is dependent on force transmission through the tensed cytoskeleton, with ROCK inhibition preventing early chromatin condensation. Future work should look to identify the extent to which changes in LINC complex expression and chromatin condensation are maintained after longer-term removal (weeks, months) of stimuli. If cells are to be successfully engineered to function appropriately in mechanically loaded environments, these types of changes must be maintained.

In preliminary work, the reduced nuclear deformation observed with TGF-β induced differentiation is maintained for at least short periods of time after removal of TGF-β. When cells differentiated for 14 days were trypsinized and reseeded on fresh scaffolds in the absence of TGF- β3, nuclear deformation was still significantly reduced (**Figure 9-3A**). Interestingly, these deformations were reduced to levels significantly lower than in fetal, juvenile, or adult outer meniscus cells. Quantification of the levels of lamin A/C and nesprin 1 giant in these cells indicated that both were lower than in donor matched juvenile controls (**Figure 9-3B and 9-3C**). This may indicate an overshoot, or inappropriate LINC complex changes, whereby the balance of nesprin 1 giant and lamin A/C (i.e., the ratio of lamin to nesprin) is moving from a nesprin dominated ratio (more deformation) to a lamin dominated ratio (less deformation). Meniscus cells however, seem to maintain deformation and the balance between these two LINC complex

members, likely due to maintenance of this ratio with development. This suggests that in native tissue, nuclear deformation is a fundamental feature of the differentiated phenotype, and therefore something to be replicated in any engineered construct.

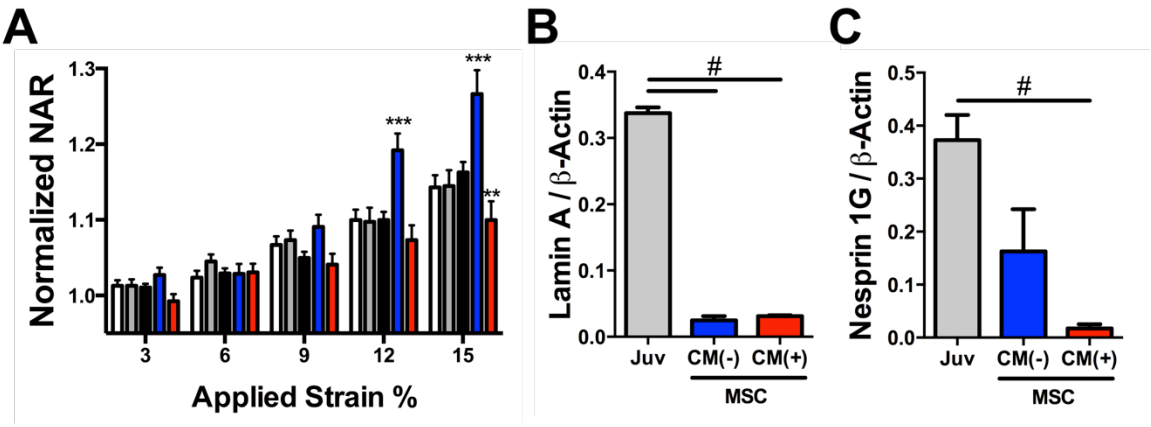

Figure 9-3: (A) Quantification of nuclear deformation (based on nuclear aspect ratio (NAR)) for cells differentiated on aligned scaffolds for 14 days in chemically defined media with CM(+) or without CM(-) TGF-β3 compared to first passage cells from fetal, juvenile and adult outer lateral meniscus. Densitometry from western blots for lamin A/C (B) or dot blots for nesprin 1 giant (C) in Juvenile outer meniscus cells or differentiated donor matched MSCs. (mean +/-SD, n=2-3/group)

9.2.5 Mechanotransduction in Mature Engineered Constructs

In addition to understanding the permanence of the changes observed with differentiation, their role in mechanotransduction as constructs mature will also be important. While the fibrous microenvironments used in this thesis possess similar structure to native tissues, their structure is far from identical. Previous work has demonstrated that with long-term maturation of cells seeded on these scaffolds, a dense fibrous matrix of collagen and proteoglycan is deposited, which cells are in intimate contact with (Baker, Shah et al. 2012). Given that mechanotransduction is heavily dependent on both ECM structure and composition, mechanotransduction in these more mature environments will likely be

altered. The cellular ability to modulate and maintain the integrity of this mature construct with loading will be critical for success of these tissue-engineering strategies.

9.3 Conclusion

Forces that cells experience through their microenvironment are critically important for mechanotransduction necessary for normal development and homeostasis. Additionally, the extent to which these forces are transmitted deep within the cell and to the nucleus can regulate mechanotransduction. A complete understanding of these mechanisms, and the extent to which they are operative and malleable with differentiation, will be necessary for long-term success of fabricated tissue replacements. In particular, tissues that function to transmit and resist mechanical loads will heavily depend on these mechanisms to functionally maintain the structure and composition of their extracellular matrix.

APPENDIX I: RELATED PUBLICATIONS

1. **Driscoll TP**, Nerurkar NL, Jacobs NT, Elliott DM, Mauck RL. Fiber angle and aspect ratio influence the shear mechanics of oriented electrospun nanofibrous scaffolds. Journal of the Mechanical Behavior of Biomedical Materials, 2011 Nov; 4(8):1627-36.

2. **Driscoll TP**, Nakasone RH, Szczesny SE, Elliott DM, Mauck RL. Biaxial mechanics and inter-lamellar shearing of stem-cell seeded electrospun angle-ply laminates for annulus fibrosus tissue engineering. Journal of Orthopaedic Research. 2013 Jun; 31(6):864-70.

3. Han WM, Heo SJ, **Driscoll TP**, Smith LJ, Mauck RL, Elliott DM. Macro-to microscale strain transfer in fibrous tissues is heterogeneous and tissue-specific. Biophysical Journal, 2013 Aug; 105(3):807-17.

4. Han WM, Heo SJ, **Driscoll TP**, Boggs ME, Duncan RL, Mauck RL, Elliott DM. Impact of Cellular. Impact of Cellular Microenvironment and Mechanical Perturbation on Calcium Signaling in Meniscus Fibrochondrocytes. European Cells and Materials, 2014 Jun; 27:321-31.

5. **Driscoll TP**, Cosgrove BD, Heo SJ, Mauck RL. Cytoskeletal Strain Transfer Regulates YAP Signaling with Dynamic Tensile Loading. (Submitted to Biophysical Journal).

6. Heo SJ, **Driscoll TP**, Thorpe SD, Nerurkar NL, Baker BM, Yang MT, Chen CS, Lee DA, Mauck RL. Altered Nuclear Structure, Mechanics, and Mechano-Sensitivity as a Consequence of Mesenchymal Stem Cell Differentiation. (in preparation)

7. **Driscoll TP**, Chang J, Keyes T, Hast MW, Heo SJ, Mauck RL, Chao, PG. Engineered Fiber Crimp Alters Scaffold Mechanics, Cell Shape, and Strain Transfer to the Nucleus. (in preparation for submission to Advanced Materials).

8. **Driscoll TP**, Cosgrove BD, Heo SJ, Mauck RL. LINC Complex Changes with Development and Differentiation regulate Nuclear Strain Transfer and Mechanotransduction. (in preparation for submission to Nature Communications).

APPENDIX II: RELATED CONFERENCE ABSTRACTS

1. **Driscoll TP**, Nerurkar NL, Jacobs NT, Mauck RL, Elliott DM. Shear Mechanics of Electrospun Scaffold for Annulus Fibrosus Tissue Engineering. 57th Annual Meeting of the Orthopaedic Research Society, Long Beach, CA, January 13 – 16, 2011.

2. **Driscoll TP**, Nerurkar NL, Jacobs NT, Mauck RL, Elliott DM. Fiber Angle and Aspect Ratio Influence the Shear Mechanics of Electrospun Nanofibrous Scaffolds. Proceedings of the ASME 2011 Summer Bioengineering Conference. Nemacolin Woodlands Resort, Farmington, Pennsylvania, June 22-25, 2011.

3. Heo SJ, Nerurkar NL, **Driscoll TP**, Mauck RL. Differentiation and Dynamic Tensile Loading Alter Nuclear Mechanics and Mechanoreception in Mesenchymal Stem Cells. Proceedings of the ASME 2011 Summer Bioengineering Conference. Nemacolin Woodlands Resort, Farmington, Pennsylvania, June 22-25, 2011. (*Podium Presentation by TPD*)

4. **Driscoll, TP**; Nakasone, RH; Szczesny, SE; Elliott, DM; Mauck, RL. Biaxial Mechanics of Electrospun Bilayers for Annulus Fibrosus Tissue Engineering. Philadelphia Spine Symposium, 2011.

5. **Driscoll, TP**; Yang, MT; Heo, SJ; Nakasone, RH; Chen, CS; Mauck, RL. Differential Nesprin Expression with Mesenchymal Stem Cell Fibrochondrogenesis and Altered Contractility. 58th Annual Meeting of the Orthopaedic Research Society, San Francisco, CA, 2012. (*Podium Presentation by TPD*)

6. **Driscoll, TP**; Nakasone, RH; Szczesny; Elliott, DM; Mauck, RL. Biaxial Mechanics and Inter-lamellar Shearing of Electrospun Bilayers for Annulus Fibrosus Tissue Engineering. 58th Annual Meeting of the Orthopaedic Research Society, San Francisco, CA, 2012.

7. Heo, SJ; **Driscoll TP**; Nerurkar, NL; Mauck, RL. Dynamic Tensile Stretch Promotes Lamin A/C Reorganization and Chromatin Condensation in Adult Stem Cells. 58th Annual Meeting of the Orthopaedic Research Society, San Francisco, CA, 2012. (*Podium Presentation by TPD*)

8. Heo, SJ; **Driscoll TP**; Zhong Z; Mauck, RL. Altered Mechanosensitivity of Fibrochondrogenic Mesenchymal Stem Cells with Modulation of Nuclear Mechanics. 58th Annual Meeting of the Orthopaedic Research Society, San Francisco, CA, 2012. (Podium Presentation by SJH)

9. **Driscoll, TP**; Heo SJ; Mauck RL; Dynamic Tensile Loading and Altered Cell Contractility Modulate Nuclear Deformation and Nesprin Espression. 38th Annual North East Bioengineering Conference, Philadelphia, PA. 2012. (*Podium Presentation by TPD*)

10. **Driscoll, TP**; Heo SJ; Mauck RL; Dynamic Tensile Loading and Altered Cell Contractility Modulate Nuclear Deformation and Cytoskeletal Connectivity. Proceedings of the ASME 2012 Summer Bioengineering Conference. Farjardo, Puerto Rico. (*Podium Presentation by TPD*)

11. Han, WM; Heo, SJ; **Driscoll, TP**; Mauck, RL; Elliott, DM. Micro-Scale Strain Transfer in Fiber-Reinforced Native Tissue Differs from Cell-Seeded Scaffolds. Proceedings of the ASME 2012 Summer Bioengineering Conference. Farjardo, Puerto Rico.

12. Heo, SJ; **Driscoll, TP**; Mauck, RL; Dynamic Tensile Loading Triggers Activation of Both TGFβ and BMP Pathways in Mesenchymal Stem Cells. Proceedings of the ASME 2012 Summer Bioengineering Conference. Farjardo, Puerto Rico. (Podium Presentation by SJH)

13. **Driscoll, TP**; Shurden, ZE; Heo, SJ; Mauck, RL; Cytoskeletal Tension is Required for Dynamic Tensile Loading Induced Alterations in Mesenchymal Stem Cell Shape and Nuclear Connectivity. 59th Annual Meeting of the Orthopaedic Research Society, San Antonio, TX, 2013. (*Podium Presentation by TPD*)

14. Heo, SJ; Thorpe, S; **Driscoll, TP**; Hashmi, S; Lee, DA; Mauck, RL; Dynamic Stretch Rapidly Alters Nuclear Structure and Chromatin Condensation in Mesenchymal Stem Cells. 59th Annual Meeting of the Orthopaedic Research Society, San Antonio, TX, 2013. (Podium Presentation by SJH)

15. Heo, SJ; **Driscoll, TP**; Hashmi, S; Mauck, RL; Fibrochondrogenesis Alters Migration and Sensitizes Mesenchymal Stem Cells to Mechanical Stretch. 59th

Annual Meeting of the Orthopaedic Research Society, San Antonio, TX, 2013. (Podium presentation by SJH)

16. **Driscoll, TP**; Heo, SJ; Shurden, ZE; Mauck, RL; Cytoskeletal Tension is Required for Dynamic Tensile Loading Induced Alterations in Mesenchymal Stem Cell Shape and Nuclear Connectivity. 19th Annual Conference of the Section of Bioengineering of the Royal Academy of Medicine in Ireland, Co. Meath, Ireland, 2013. (*Podium Presentation by TPD, 1st Prize in Mechanobiology*)

17. **Driscoll, TP**; Heo, SJ; Shurden, ZE; Mauck, RL; Cytoskeletal Connectivity to the Nucleus Regulates MSC Nuclear Strain Transfer and Mechanotransduction. Biomedical Engineering Society, Seattle, Washington, 2013. (Podium Presentation)

18. Heo, SJ; **Driscoll, TP**; Engineering Fibrous Tissue Constructs Containing Amorphous Proteoglycan-Rich micro-Domains. Biomedical Engineering Society, Seattle, Washington, 2013.

19. McLeod, CM; **Driscoll, TP**; Farell, M; Heo, SJ; Cosgrove, BD; Mauck, RL; Mesenchymal Stem Cell Mechanobiology Is Clone Dependent. Biomedical Engineering Society, Seattle, Washington, 2013. (Podium Presentation by CMM)

20. **Driscoll, TP**; Chang, J; Keyes, T; Hast, MW; Heo, SJ; Mauck, RL; Chao, PG; Engineered Fiber Crimp Alters Scaffold Mechanics, Cell Shape, and Strain Transfer to the Nucleus. 60th Annual Meeting of the Orthopaedic Research Society, New Orleans, Louisiana, 2014.

21. **Driscoll, TP**; Cosgrove, BD; Heo, SJ; Mauck, RL; Knockdown of LINC Complex Proteins Alters Nuclear Deformation, Cell Contractility and Mechanosensation in Mesenchymal Stem Cells. 60th Annual Meeting of the Orthopaedic Research Society, New Orleans, Louisiana, 2014.

22. Heo, SJ; Thorpe, SD; **Driscoll, TP**; Hashmi, SK; Lee, DA; Mauck, RL; Rapid and Sustained Changes in Nuclear Architecture and Mechanics in Mesenchymal Stem Cells in Response to Dynamic Stretch. 60th Annual Meeting of the Orthopaedic Research Society, New Orleans, Louisiana, 2014.

23. Heo, SJ; **Driscoll, TP**; Thorpe, SD; Lee, DA; Mauck, RL; Rapid Chromatin Condensation Increases Stem Cell Nuclear Mechanics and Mechanosensitivity; 60th Annual Meeting of the Orthopaedic Research Society, New Orleans, Louisiana, 2014.

24. **Driscoll, TP**; Cosgrove, BD; Heo, SJ; Mauck, RL; Knockdown of LINC Complex Proteins Alters Nuclear Deformation, Cell Contractility and Mechanosensation in Mesenchymal Stem Cells. BMES Cell and Molecular Bioengineering Conference, San Diego, California, 2014. (*Student/Fellow Award Podium Presentation*)

25. Heo, SJ; **Driscoll, TP;** Thorpe, SD; Lee, DA; Mauck RL; Dynamic Alterations in Stem Cell Nuclear Architecture and Mechanobiology as a Consequence of Mechanical Perturbation. World Congress of Biomechanics, Boston, Massachusetts, 2014.

26. **Driscoll, TP;** Heo, SJ; Mauck, RL; Lamin A and Nesprin 1 Giant Levels Increase with Age in Meniscus Cells and are Distinct from Naïve or Differentiated MSCs. World Congress of Biomechanics, Boston, Massachusetts, 2014. (*Podium Presentation by TPD*)

27. Heo, SJ; **Driscoll, TP**; Han, WJ; Thorpe, SD; Elliott, DM; Lee, DA; Mauck, RL. Mechanically Induced Purinergic Calcium Signaling Drives Alterations in Stem Cell Nuclear Architecture; 61st Annual Meeting of the Orthopaedic Research Society, Las Vegas, Nevada, 2015. (*Podium Presentation by SJH*)

BIBLIOGRAPHY

Anderson, D. R., S. L. Woo, M. K. Kwan and D. H. Gershuni (1991). "Viscoelastic shear properties of the equine medial meniscus." J Orthop Res **9**(4): 550-558.

Andersson-Molina, H., H. Karlsson and P. Rockborn (2002). "Arthroscopic partial and total meniscectomy: A long-term follow-up study with matched controls." Arthroscopy **18**(2): 183-189.

Angele, P., D. Schumann, M. Angele, B. Kinner, C. Englert, R. Hente, B. Fuchtmeier, M. Nerlich, C. Neumann and R. Kujat (2004). "Cyclic, mechanical compression enhances chondrogenesis of mesenchymal progenitor cells in tissue engineering scaffolds." Biorheology **41**(3-4): 335-346.

Anishkin, A., S. H. Loukin, J. Teng and C. Kung (2014). "Feeling the hidden mechanical forces in lipid bilayer is an original sense." Proc Natl Acad Sci U S A **111**(22): 7898-7905.

Aragona, M., T. Panciera, A. Manfrin, S. Giulitti, F. Michielin, N. Elvassore, S. Dupont and S. Piccolo (2013). "A mechanical checkpoint controls multicellular growth through YAP/TAZ regulation by actin-processing factors." Cell **154**(5): 1047-1059.

Aratyn-Schaus, Y., P. W. Oakes, J. Stricker, S. P. Winter and M. L. Gardel (2010). "Preparation of complaint matrices for quantifying cellular contraction." J Vis Exp(46).

Attali, R., N. Warwar, A. Israel, I. Gurt, E. McNally, M. Puckelwartz, B. Glick, Y. Nevo, Z. Ben-Neriah and J. Melki (2009). "Mutation of SYNE-1, encoding an essential component of the nuclear lamina, is responsible for autosomal recessive arthrogryposis." Hum Mol Genet **18**(18): 3462-3469.

Baer, A. E., J. Y. Wang, V. B. Kraus and L. A. Setton (2001). "Collagen gene expression and mechanical properties of intervertebral disc cell-alginate cultures." J Orthop Res **19**(1): 2-10.

Baffert, F., T. Le, B. Sennino, G. Thurston, C. J. Kuo, D. Hu-Lowe and D. M. McDonald (2006). "Cellular changes in normal blood capillaries undergoing regression after inhibition of VEGF signaling." Am J Physiol Heart Circ Physiol **290**(2): H547-559.

Baker, B. M., A. O. Gee, R. B. Metter, A. S. Nathan, R. A. Marklein, J. A. Burdick and R. L. Mauck (2008). "The potential to improve cell infiltration in composite fiber-aligned electrospun scaffolds by the selective removal of sacrificial fibers." Biomaterials **29**(15): 2348-2358.

Baker, B. M. and R. L. Mauck (2007). "The effect of nanofiber alignment on the maturation of engineered meniscus constructs." Biomaterials **28**(11): 1967-1977.

Baker, B. M., A. S. Nathan, A. O. Gee and R. L. Mauck (2010). "The influence of an aligned nanofibrous topography on human mesenchymal stem cell fibrochondrogenesis." Biomaterials **31**(24): 6190-6200.

Baker, B. M., N. L. Nerurkar, J. A. Burdick, D. M. Elliott and R. L. Mauck (2009). "Fabrication and modeling of dynamic multipolymer nanofibrous scaffolds." J Biomech Eng **131**(10): 101012.

Baker, B. M., G. D. O'Connell, S. Sen, A. Nathan, D. M. Elliott and R. L. Mauck (2007). "Multi-Lamellar and Multi-Axial Maturation of Cell-Seeded Fiber-Reinforced Tissue Engineered Constructs." Proceedings of ASME 2007 Summer Bioengineering Conference, Keystone, CO, June 20-24.

Baker, B. M., R. P. Shah, A. H. Huang and R. L. Mauck (2011). "Dynamic tensile loading improves the functional properties of mesenchymal stem cell-laden nanofiber-based fibrocartilage." Tissue Eng Part A **17**(9-10): 1445-1455.

Baker, B. M., R. P. Shah, A. M. Silverstein, J. L. Esterhai, J. A. Burdick and R. L. Mauck (2012). "Sacrificial nanofibrous composites provide instruction without impediment and enable functional tissue formation." Proc Natl Acad Sci U S A **109**(35): 14176-14181.

Baker, B. M., Trappmann, B., Nair, A.S., Kim, I.L., Burdick, J.A., Shenoy, V.B., Chen, C.S. (2014). "Mesenchymal stem cell mechanosensing in engineered fibrillar microenvironments." Transactions of the 7th World Congress of Biomechanics, Boston, MA.

Ballyns, J. J., J. P. Gleghorn, V. Niebrzydowski, J. J. Rawlinson, H. G. Potter, S. A. Maher, T. M. Wright and L. J. Bonassar (2008). "Image-guided tissue engineering of anatomically shaped implants via MRI and micro-CT using injection molding." Tissue Eng Part A **14**(7): 1195-1202.

Ballyns, J. J., T. M. Wright and L. J. Bonassar (2010). "Effect of media mixing on ECM assembly and mechanical properties of anatomically-shaped tissue engineered meniscus." Biomaterials **31**(26): 6756-6763.

Baratz, M. E., F. H. Fu and R. Mengato (1986). "Meniscal tears: the effect of meniscectomy and of repair on intraarticular contact areas and stress in the human knee. A preliminary report." Am J Sports Med **14**(4): 270-275.

Barry, A. K., H. Tabdili, I. Muhamed, J. Wu, N. Shashikanth, G. A. Gomez, A. S. Yap, C. J. Gottardi, J. de Rooij, N. Wang and D. E. Leckband (2014). "alpha-catenin cytomechanics--role in cadherin-dependent adhesion and mechanotransduction." J Cell Sci **127**(Pt 8): 1779-1791.

Barry, S. P., S. M. Davidson and P. A. Townsend (2008). "Molecular regulation of cardiac hypertrophy." Int J Biochem Cell Biol **40**(10): 2023-2039.

Bass, E. C., F. A. Ashford, M. R. Segal and J. C. Lotz (2004). "Biaxial testing of human annulus fibrosus and its implications for a constitutive formulation." Ann Biomed Eng **32**(9): 1231-1242.

Bernfield, M., M. Gotte, P. W. Park, O. Reizes, M. L. Fitzgerald, J. Lincecum and M. Zako (1999). "Functions of cell surface heparan sulfate proteoglycans." Annu Rev Biochem **68**: 729-777.

Berridge, M. J., M. D. Bootman and H. L. Roderick (2003). "Calcium signalling: dynamics, homeostasis and remodelling." Nat Rev Mol Cell Biol **4**(7): 517-529.

Bershadsky, A. D., N. Q. Balaban and B. Geiger (2003). "Adhesion-dependent cell mechanosensitivity." Annu Rev Cell Dev Biol **19**: 677-695.

Bertrand, A. T., S. Ziaei, C. Ehret, H. Duchemin, K. Mamchaoui, A. Bigot, M. Mayer, S. Quijano-Roy, I. Desguerre, J. Laine, R. Ben Yaou, G. Bonne and C. Coirault (2014). "Cellular microenvironments reveal defective mechanosensing responses and elevated YAP signaling in LMNA-mutated muscle precursors." J Cell Sci **127**(Pt 13): 2873-2884.

Bhattacharjee, A. and M. Bansal (2005). "Collagen structure: the Madras triple helix and the current scenario." IUBMB Life **57**(3): 161-172.

Bogduk, N. (1991). "The lumbar disc and low back pain." Neurosurg Clin N Am **2**(4): 791-806.

Bornstein, P. and H. Sage (1980). "Structurally distinct collagen types." Annu Rev Biochem **49**: 957-1003.

Bourdon, M. A. and E. Ruoslahti (1989). "Tenascin mediates cell attachment through an RGD-dependent receptor." J Cell Biol **108**(3): 1149-1155.

Bowles, R. D., H. H. Gebhard, R. Hartl and L. J. Bonassar (2011). "Tissue-engineered intervertebral discs produce new matrix, maintain disc height, and restore biomechanical function to the rodent spine." Proc Natl Acad Sci U S A **108**(32): 13106-13111.

Bowles, R. D., R. M. Williams, W. R. Zipfel and L. J. Bonassar (2009). "Self-Assembly of Aligned Tissue-Engineered Annulus Fibrosus and Intervertebral Disc Composite Via Collagen Gel Contraction." Tissue Eng Part A.

Brohawn, S. G., Z. Su and R. MacKinnon (2014). "Mechanosensitivity is mediated directly by the lipid membrane in TRAAK and TREK1 K+ channels." Proc Natl Acad Sci U S A **111**(9): 3614-3619.

Brownlee, R. D. and B. L. Langille (1991). "Arterial adaptations to altered blood flow." Can J Physiol Pharmacol **69**(7): 978-983.

Bruehlmann, S. B., P. A. Hulme and N. A. Duncan (2004). "In situ intercellular mechanics of the bovine outer annulus fibrosus subjected to biaxial strains." J Biomech **37**(2): 223-231.

Bruehlmann, S. B., J. R. Matyas and N. A. Duncan (2004). "ISSLS prize winner: Collagen fibril sliding governs cell mechanics in the anulus fibrosus: an in situ confocal microscopy study of bovine discs." Spine **29**(23): 2612-2620.

Buck, C. A. and A. F. Horwitz (1987). "Cell surface receptors for extracellular matrix molecules." Annu Rev Cell Biol **3**: 179-205.

Burke, B. and C. L. Stewart (2014). "Functional architecture of the cell's nucleus in development, aging, and disease." Curr Top Dev Biol **109**: 1-52.

Burnstock, G. (2009). "Purinergic mechanosensory transduction and visceral pain." Mol Pain **5**: 69.

Burnstock, G. and V. Ralevic (2014). "Purinergic signaling and blood vessels in health and disease." Pharmacol Rev **66**(1): 102-192.

Buschmann, M. D. and A. J. Grodzinsky (1995). "A molecular model of proteoglycan-associated electrostatic forces in cartilage mechanics." J Biomech Eng **117**(2): 179-192.

Buxboim, A., J. Swift, J. Irianto, K. R. Spinler, P. C. Dingal, A. Athirasala, Y. R. Kao, S. Cho, T. Harada, J. W. Shin and D. E. Discher (2014). "Matrix elasticity regulates lamin-a,c phosphorylation and turnover with feedback to actomyosin." Curr Biol **24**(16): 1909-1917.

Caille, N., O. Thoumine, Y. Tardy and J. J. Meister (2002). "Contribution of the nucleus to the mechanical properties of endothelial cells." J Biomech **35**(2): 177-187.

Calderwood, D. A., I. D. Campbell and D. R. Critchley (2013). "Talins and kindlins: partners in integrin-mediated adhesion." Nat Rev Mol Cell Biol **14**(8): 503-517.

Carisey, A., R. Tsang, A. M. Greiner, N. Nijenhuis, N. Heath, A. Nazgiewicz, R. Kemkemer, B. Derby, J. Spatz and C. Ballestrem (2013). "Vinculin regulates the recruitment and release of core focal adhesion proteins in a force-dependent manner." Curr Biol **23**(4): 271-281.

Carmeliet, G., L. Vico and R. Bouillon (2001). "Space flight: a challenge for normal bone homeostasis." Crit Rev Eukaryot Gene Expr **11**(1-3): 131-144.

Cartwright, S. and I. Karakesisoglou (2014). "Nesprins in health and disease." Semin Cell Dev Biol **29**: 169-179.

Cassidy, J. J., A. Hiltner and E. Baer (1989). "Hierarchical structure of the intervertebral disc." Connective Tissue Research **23**: 75-88.

Chambliss, A. B., S. B. Khatau, N. Erdenberger, D. K. Robinson, D. Hodzic, G. D. Longmore and D. Wirtz (2013). "The LINC-anchored actin cap connects the extracellular milieu to the nucleus for ultrafast mechanotransduction." Sci Rep **3**: 1087.

Chancellor, T. J., J. Lee, C. K. Thodeti and T. Lele (2010). "Actomyosin tension exerted on the nucleus through nesprin-1 connections influences endothelial cell adhesion, migration, and cyclic strain-induced reorientation." Biophys J **99**(1): 115-123.

Charoenpanich, A., M. E. Wall, C. J. Tucker, D. M. Andrews, D. S. Lalush, D. R. Dirschl and E. G. Loboa (2014). "Cyclic tensile strain enhances osteogenesis and angiogenesis in mesenchymal stem cells from osteoporotic donors." Tissue Eng Part A **20**(1-2): 67-78.

Chaturvedi, L. S., C. P. Gayer, H. M. Marsh and M. D. Basson (2008). "Repetitive deformation activates Src-independent FAK-dependent ERK motogenic signals in human Caco-2 intestinal epithelial cells." Am J Physiol Cell Physiol **294**(6): C1350-1361.

Chen, J., R. L. Horan, D. Bramono, J. E. Moreau, Y. Wang, L. R. Geuss, A. L. Collette, V. Volloch and G. H. Altman (2006). "Monitoring mesenchymal stromal cell developmental stage to apply on-time mechanical stimulation for ligament tissue engineering." Tissue Eng **12**(11): 3085-3095.

Chen, K. D., Y. S. Li, M. Kim, S. Li, S. Yuan, S. Chien and J. Y. Shyy (1999). "Mechanotransduction in response to shear stress. Roles of receptor tyrosine kinases, integrins, and Shc." J Biol Chem **274**(26): 18393-18400.

Chiari, C., U. Koller, R. Dorotka, C. Eder, R. Plasenzotti, S. Lang, L. Ambrosio, E. Tognana, E. Kon, D. Salter and S. Nehrer (2006). "A tissue engineering approach to meniscus regeneration in a sheep model." Osteoarthritis Cartilage **14**(10): 1056-1065.

Chou, A. I., S. O. Akintoye and S. B. Nicoll (2009). "Photo-crosslinked alginate hydrogels support enhanced matrix accumulation by nucleus pulposus cells in vivo." Osteoarthritis Cartilage.

Craig, F. M., M. T. Bayliss, G. Bentley and C. W. Archer (1990). "A role for hyaluronan in joint development." J Anat **171**: 17-23.

Crisp, M., Q. Liu, K. Roux, J. B. Rattner, C. Shanahan, B. Burke, P. D. Stahl and D. Hodzic (2006). "Coupling of the nucleus and cytoplasm: role of the LINC complex." J Cell Biol **172**(1): 41-53.

del Rio, A., R. Perez-Jimenez, R. Liu, P. Roca-Cusachs, J. M. Fernandez and M. P. Sheetz (2009). "Stretching single talin rod molecules activates vinculin binding." Science **323**(5914): 638-641.

Dembo, M. and Y. L. Wang (1999). "Stresses at the cell-to-substrate interface during locomotion of fibroblasts." Biophys J **76**(4): 2307-2316.

Deyo, R. A., D. T. Gray, W. Kreuter, S. Mirza and B. I. Martin (2005). "United States trends in lumbar fusion surgery for degenerative conditions." Spine (Phila Pa 1976) **30**(12): 1441-1445; discussion 1446-1447.

Diamant, J., A. Keller, E. Baer, M. Litt and R. G. Arridge (1972). "Collagen; ultrastructure and its relation to mechanical properties as a function of ageing." Proc R Soc Lond B Biol Sci **180**(60): 293-315.

Dickinson, M. G. and I. Vesely (2012). "Structural changes of rat mitral valve chordae tendineae during postnatal development." J Heart Valve Dis **21**(4): 433-439.

Draney, M. T., R. J. Herfkens, T. J. Hughes, N. J. Pelc, K. L. Wedding, C. K. Zarins and C. A. Taylor (2002). "Quantification of vessel wall cyclic strain using cine phase contrast magnetic resonance imaging." Ann Biomed Eng **30**(8): 1033-1045.

Driscoll, T. P. C., B.D.; Heo, S.J.; Shurden, Z.E.; Mauck, R.L. (2015). "Cytoskeletal to Nuclear Strain Transfer Regulates YAP Signaling in Mesenchymal Stem Cells with Dynamic Loading." Biophysical Journal **in review**.

DuFort, C. C., M. J. Paszek and V. M. Weaver (2011). "Balancing forces: architectural control of mechanotransduction." Nat Rev Mol Cell Biol **12**(5): 308-319.

Dumbauld, D. W., K. E. Michael, S. K. Hanks and A. J. Garcia (2010). "Focal adhesion kinase-dependent regulation of adhesive forces involves vinculin recruitment to focal adhesions." Biol Cell **102**(4): 203-213.

Dumbauld, D. W., H. Shin, N. D. Gallant, K. E. Michael, H. Radhakrishna and A. J. Garcia (2010). "Contractility modulates cell adhesion strengthening through focal adhesion kinase and assembly of vinculin-containing focal adhesions." J Cell Physiol **223**(3): 746-756.

Dupont, S., L. Morsut, M. Aragona, E. Enzo, S. Giulitti, M. Cordenonsi, F. Zanconato, J. Le Digabel, M. Forcato, S. Bicciato, N. Elvassore and S. Piccolo (2011). "Role of YAP/TAZ in mechanotransduction." Nature **474**(7350): 179-183.

Eberth, J. F., L. Cardamone and J. D. Humphrey (2011). "Evolving biaxial mechanical properties of mouse carotid arteries in hypertension." J Biomech **44**(14): 2532-2537.

Emsley, J., C. G. Knight, R. W. Farndale, M. J. Barnes and R. C. Liddington (2000). "Structural basis of collagen recognition by integrin alpha2beta1." Cell **101**(1): 47-56.

Engler, A. J., S. Sen, H. L. Sweeney and D. E. Discher (2006). "Matrix elasticity directs stem cell lineage specification." Cell **126**(4): 677-689.

Farndale, R. W., D. J. Buttle and A. J. Barrett (1986). "Improved quantitation and discrimination of sulphated glycosaminoglycans by use of dimethylmethylene blue." Biochim Biophys Acta **883**(2): 173-177.

Fithian, D. C., M. A. Kelly and V. C. Mow (1990). "Material properties and structure-function relationships in the menisci." Clin Orthop(252): 19-31.

Folgering, J. H., R. Sharif-Naeini, A. Dedman, A. Patel, P. Delmas and E. Honore (2008). "Molecular basis of the mammalian pressure-sensitive ion channels: focus on vascular mechanotransduction." Prog Biophys Mol Biol **97**(2-3): 180-195.

Folkow, B. (1993). "Early structural changes in hypertension: pathophysiology and clinical consequences." J Cardiovasc Pharmacol **22 Suppl 1**: S1-6.

Foty, R. A. and M. S. Steinberg (2005). "The differential adhesion hypothesis: a direct evaluation." Dev Biol **278**(1): 255-263.

Franchini, K. G. (2012). "Focal adhesion kinase -- the basis of local hypertrophic signaling domains." J Mol Cell Cardiol **52**(2): 485-492.

Franze, K. (2013). "The mechanical control of nervous system development." Development **140**(15): 3069-3077.

Frost, H. M. (1994). "Wolff's Law and bone's structural adaptations to mechanical usage: an overview for clinicians." Angle Orthod **64**(3): 175-188.

Fu, J., Y. K. Wang, M. T. Yang, R. A. Desai, X. Yu, Z. Liu and C. S. Chen (2010). "Mechanical regulation of cell function with geometrically modulated elastomeric substrates." Nat Methods **7**(9): 733-736.

Fujita, Y., D. R. Wagner, A. A. Biviji, N. A. Duncan and J. C. Lotz (2000). "Anisotropic shear behavior of the annulus fibrosus: effect of harvest site and tissue prestrain." Med Eng Phys **22**(5): 349-357.

Fung, D. T., V. M. Wang, N. Andarawis-Puri, J. Basta-Pljakic, Y. Li, D. M. Laudier, H. B. Sun, K. J. Jepsen, M. B. Schaffler and E. L. Flatow (2010). "Early response to tendon fatigue damage accumulation in a novel in vivo model." J Biomech **43**(2): 274-279.

Gardiner, J. C. and J. A. Weiss (2001). "Simple shear testing of parallel-fibered planar soft tissues." J Biomech Eng **123**(2): 170-175.

Gathercole, L. J. and A. Keller (1991). "Crimp morphology in the fibre-forming collagens." Matrix **11**(3): 214-234.

Gavrilov, S. and E. Lacy (2013). "Genetic dissection of ventral folding morphogenesis in mouse: embryonic visceral endoderm-supplied BMP2 positions head and heart." Curr Opin Genet Dev **23**(4): 461-469.

Geiger, B., A. Bershadsky, R. Pankov and K. M. Yamada (2001). "Transmembrane crosstalk between the extracellular matrix--cytoskeleton crosstalk." Nat Rev Mol Cell Biol **2**(11): 793-805.

Geiger, B., J. P. Spatz and A. D. Bershadsky (2009). "Environmental sensing through focal adhesions." Nat Rev Mol Cell Biol **10**(1): 21-33.

Gottlieb, P. A. and F. Sachs (2012). "Piezo1: properties of a cation selective mechanical channel." Channels (Austin) **6**(4): 214-219.

Grabias, B. M. and K. Konstantopoulos (2014). "The physical basis of renal fibrosis: effects of altered hydrodynamic forces on kidney homeostasis." Am J Physiol Renal Physiol **306**(5): F473-485.

Grace Chao, P. H., H. Y. Hsu and H. Y. Tseng (2014). "Electrospun microcrimped fibers with nonlinear mechanical properties enhance ligament fibroblast phenotype." Biofabrication **6**(3): 035008.

Grashoff, C., B. D. Hoffman, M. D. Brenner, R. Zhou, M. Parsons, M. T. Yang, M. A. McLean, S. G. Sligar, C. S. Chen, T. Ha and M. A. Schwartz (2010). "Measuring mechanical tension across vinculin reveals regulation of focal adhesion dynamics." Nature **466**(7303): 263-266.

Grigera, P. R., E. D. Jeffery, K. H. Martin, J. Shabanowitz, D. F. Hunt and J. T. Parsons (2005). "FAK phosphorylation sites mapped by mass spectrometry." J Cell Sci **118**(Pt 21): 4931-4935.

Gruber, H. E., G. Hoelscher, J. A. Ingram and E. N. Hanley, Jr. (2009). "Culture of human anulus fibrosus cells on polyamide nanofibers: extracellular matrix production." Spine **34**(1): 4-9.

Guerin, H. L. and D. M. Elliott (2007). "Quantifying the contributions of structure to annulus fibrosus mechanical function using a nonlinear, anisotropic, hyperelastic model." J Orthop Res **25**(4): 508-516.

Guilak, F., J. R. Tedrow and R. Burgkart (2000). "Viscoelastic properties of the cell nucleus." Biochem Biophys Res Commun **269**(3): 781-786.

Guilluy, C., L. D. Osborne, L. Van Landeghem, L. Sharek, R. Superfine, R. Garcia-Mata and K. Burridge (2014). "Isolated nuclei adapt to force and reveal a mechanotransduction pathway in the nucleus." Nat Cell Biol.

Gumbiner, B. M. (2005). "Regulation of cadherin-mediated adhesion in morphogenesis." Nat Rev Mol Cell Biol **6**(8): 622-634.

Gurtin, M. E. (1981). An introduction to continuum mechanics. New York, Academic Press.

Gutierrez, J. A., V. V. Suzara and L. G. Dobbs (2003). "Continuous mechanical contraction modulates expression of alveolar epithelial cell phenotype." Am J Respir Cell Mol Biol **29**(1): 81-87.

Hale, C. M., A. L. Shrestha, S. B. Khatau, P. J. Stewart-Hutchinson, L. Hernandez, C. L. Stewart, D. Hodzic and D. Wirtz (2008). "Dysfunctional connections between the nucleus and the actin and microtubule networks in laminopathic models." Biophys J **95**(11): 5462-5475.

Han, W. M., S. J. Heo, T. P. Driscoll, L. J. Smith, R. L. Mauck and D. M. Elliott (2013). "Macro- to microscale strain transfer in fibrous tissues is heterogeneous and tissue-specific." Biophys J **105**(3): 807-817.

Hansen, K. A., J. A. Weiss and J. K. Barton (2002). "Recruitment of tendon crimp with applied tensile strain." J Biomech Eng **124**(1): 72-77.

Harris, T. J. and U. Tepass (2010). "Adherens junctions: from molecules to morphogenesis." Nat Rev Mol Cell Biol **11**(7): 502-514.

Harrop, J. S., J. A. Youssef, M. Maltenfort, P. Vorwald, P. Jabbour, C. M. Bono, N. Goldfarb, A. R. Vaccaro and A. S. Hilibrand (2008). "Lumbar adjacent segment degeneration and disease after arthrodesis and total disc arthroplasty." Spine **33**(15): 1701-1707.

Haugh, M. G., E. G. Meyer, S. D. Thorpe, T. Vinardell, G. P. Duffy and D. J. Kelly (2011). "Temporal and spatial changes in cartilage-matrix-specific gene expression in mesenchymal stem cells in response to dynamic compression." Tissue Eng Part A **17**(23-24): 3085-3093.

Heagerty, A. M., C. Aalkjaer, S. J. Bund, N. Korsgaard and M. J. Mulvany (1993). "Small artery structure in hypertension. Dual processes of remodeling and growth." Hypertension **21**(4): 391-397.

Heo, S. C., N. L. Nerurkar, B. B.M. and M. R.L. (2011). "Microstructure dictates stretch-induced cell and nucleus reorganization on aligned nanofibrous scaffolds " Transactions of the 56th Annual Meeting of the Orthopaedic Research Society
.

Heo, S. J., N. L. Nerurkar, B. M. Baker, J. W. Shin, D. M. Elliott and R. L. Mauck (2011). "Fiber stretch and reorientation modulates mesenchymal stem cell morphology and fibrous gene expression on oriented nanofibrous microenvironments." Ann Biomed Eng **39**(11): 2780-2790.

Heo, S. J., N. L. Nerurkar, T. P. Driscoll and R. L. Mauck (2011). "Differentiation and Dynamic Tensile Loading Alter Nuclear Mechanics and Mechanoreception in Mesenchymal Stem Cells." Proceedings of the ASME 2011 Summer Bioengineering Conference.

Heydemann, A. and E. M. McNally (2007). "Consequences of disrupting the dystrophin-sarcoglycan complex in cardiac and skeletal myopathy." Trends Cardiovasc Med **17**(2): 55-59.

Hickey, D. S. and D. W. Hukins (1980). "X-ray diffraction studies of the arrangement of collagenous fibres in human fetal intervertebral disc." J Anat **131**(Pt 1): 81-90.

Ho, C. Y., D. E. Jaalouk, M. K. Vartiainen and J. Lammerding (2013). "Lamin A/C and emerin regulate MKL1-SRF activity by modulating actin dynamics." Nature **497**(7450): 507-511.

Hollingsworth, N. T. and D. R. Wagner (2012). "The Stress and Strain State of the Posterior Annulus under Flexion." Spine (Phila Pa 1976).

Hoshijima, M. (2006). "Mechanical stress-strain sensors embedded in cardiac cytoskeleton: Z disk, titin, and associated structures." Am J Physiol Heart Circ Physiol **290**(4): H1313-1325.

Huang, A. H., M. J. Farrell, M. Kim and R. L. Mauck (2010). "Long-term dynamic loading improves the mechanical properties of chondrogenic mesenchymal stem cell-laden hydrogel." Eur Cell Mater **19**: 72-85.

Huang, A. H., A. Stein, R. S. Tuan and R. L. Mauck (2009). "Transient exposure to TGF-beta3 improves the mechanical properties of MSC-laden cartilage constructs in a density dependent manner." Tissue Eng Part A.

Huang, A. H., M. Yeger-McKeever, A. Stein and R. L. Mauck (2008). "Tensile properties of engineered cartilage formed from chondrocyte- and MSC-laden hydrogels." Osteoarthritis Cartilage **16**(9): 1074-1082.

Huang, S. and D. E. Ingber (2005). "Cell tension, matrix mechanics, and cancer development." Cancer Cell **8**(3): 175-176.

Humphries, J. D., A. Byron and M. J. Humphries (2006). "Integrin ligands at a glance." J Cell Sci **119**(Pt 19): 3901-3903.

Humzah, M. D. and R. W. Soames (1988). "Human intervertebral disc: structure and function." Anat Rec **220**(4): 337-356.

Iatridis, J. C., S. Kumar, R. J. Foster, M. Weidenbaum and V. C. Mow (1999). "Shear mechanical properties of human lumbar annulus fibrosus." J Orthop Res **17**(5): 732-737.

Inanlou, M. R. and B. Kablar (2003). "Abnormal development of the diaphragm in mdx:MyoD-/-(9th) embryos leads to pulmonary hypoplasia." Int J Dev Biol **47**(5): 363-371.

Intengan, H. D., L. Y. Deng, J. S. Li and E. L. Schiffrin (1999). "Mechanics and composition of human subcutaneous resistance arteries in essential hypertension." Hypertension **33**(1 Pt 2): 569-574.

Intengan, H. D., G. Thibault, J. S. Li and E. L. Schiffrin (1999). "Resistance artery mechanics, structure, and extracellular components in spontaneously hypertensive rats :

effects of angiotensin receptor antagonism and converting enzyme inhibition." Circulation **100**(22): 2267-2275.

Ionescu, L. C., G. C. Lee, G. H. Garcia, T. L. Zachry, R. P. Shah, B. J. Sennett and R. L. Mauck (2011). "Maturation state-dependent alterations in meniscus integration: implications for scaffold design and tissue engineering." Tissue Eng Part A **17**(1-2): 193-204.

Irianto, J., J. Swift, R. P. Martins, G. D. McPhail, M. M. Knight, D. E. Discher and D. A. Lee (2013). "Osmotic challenge drives rapid and reversible chromatin condensation in chondrocytes." Biophys J **104**(4): 759-769.

Iyer, K. V., S. Pulford, A. Mogilner and G. V. Shivashankar (2012). "Mechanical activation of cells induces chromatin remodeling preceding MKL nuclear transport." Biophys J **103**(7): 1416-1428.

Jaalouk, D. E. and J. Lammerding (2009). "Mechanotransduction gone awry." Nat Rev Mol Cell Biol **10**(1): 63-73.

Jacinto, A., W. Wood, T. Balayo, M. Turmaine, A. Martinez-Arias and P. Martin (2000). "Dynamic actin-based epithelial adhesion and cell matching during Drosophila dorsal closure." Curr Biol **10**(22): 1420-1426.

Jacobs, N. T., J. Morelli, L. J. Smith, J. H. Yoder and D. M. Elliott (2010). "Annulus Fibrosus Shear Mechanical Properties and the Contributions of Glycosaminoglycans and Elastic Fibers to Shear are Anisotropic." Transactions of the 56th Annual Meeting of the Orthopaedic Research Society, New Orleans, LA **in review**.

Jacobs, N. T., L. J. Smith, W. M. Han, J. Morelli, J. H. Yoder and D. M. Elliott (2011). "Effect of orientation and targeted extracellular matrix degradation on the shear mechanical properties of the annulus fibrosus." J Mech Behav Biomed Mater **4**(8): 1611-1619.

Jahed, Z., H. Shams, M. Mehrbod and M. R. Mofrad (2014). "Mechanotransduction pathways linking the extracellular matrix to the nucleus." Int Rev Cell Mol Biol **310**: 171-220.

Jain, N., K. V. Iyer, A. Kumar and G. V. Shivashankar (2013). "Cell geometric constraints induce modular gene-expression patterns via redistribution of HDAC3 regulated by actomyosin contractility." Proc Natl Acad Sci U S A **110**(28): 11349-11354.

Jeffrey, J. E., L. A. Thomson and R. M. Aspden (1997). "Matrix loss and synthesis following a single impact load on articular cartilage in vitro." Biochim Biophys Acta **1334**(2-3): 223-232.

Jessop, H. L., S. C. Rawlinson, A. A. Pitsillides and L. E. Lanyon (2002). "Mechanical strain and fluid movement both activate extracellular regulated kinase (ERK) in osteoblast-like cells but via different signaling pathways." Bone **31**(1): 186-194.

Kahn, J., Y. Shwartz, E. Blitz, S. Krief, A. Sharir, D. A. Breitel, R. Rattenbach, F. Relaix, P. Maire, R. B. Rountree, D. M. Kingsley and E. Zelzer (2009). "Muscle contraction is necessary to maintain joint progenitor cell fate." Dev Cell **16**(5): 734-743.

Kanchanawong, P., G. Shtengel, A. M. Pasapera, E. B. Ramko, M. W. Davidson, H. F. Hess and C. M. Waterman (2010). "Nanoscale architecture of integrin-based cell adhesions." Nature **468**(7323): 580-584.

Kelly, B. T., W. Robertson, H. G. Potter, X. H. Deng, A. S. Turner, S. Lyman, R. F. Warren and S. A. Rodeo (2007). "Hydrogel meniscal replacement in the sheep knee: preliminary evaluation of chondroprotective effects." Am J Sports Med **35**(1): 43-52.

Kesto, W. K., A. O. Esquivel and D. C. Markel (2013). "Shear force at failure and stiffness of all-inside meniscal repair devices." J Knee Surg **26**(6): 435-440.

Khatau, S. B., C. M. Hale, P. J. Stewart-Hutchinson, M. S. Patel, C. L. Stewart, P. C. Searson, D. Hodzic and D. Wirtz (2009). "A perinuclear actin cap regulates nuclear shape." Proc Natl Acad Sci U S A **106**(45): 19017-19022.

Kidoaki, S., I. K. Kwon and T. Matsuda (2005). "Mesoscopic spatial designs of nano- and microfiber meshes for tissue-engineering matrix and scaffold based on newly devised multilayering and mixing electrospinning techniques." Biomaterials **26**(1): 37-46.

Kielty, C. M., M. J. Sherratt and C. A. Shuttleworth (2002). "Elastic fibres." J Cell Sci **115**(Pt 14): 2817-2828.

Klompmaker, J., R. P. Veth, H. W. Jansen, H. K. Nielsen, J. H. de Groot and A. J. Pennings (1996). "Meniscal replacement using a porous polymer prosthesis: a preliminary study in the dog." Biomaterials **17**(12): 1169-1175.

Kolch, W. (2005). "Coordinating ERK/MAPK signalling through scaffolds and inhibitors." Nat Rev Mol Cell Biol **6**(11): 827-837.

Kontulainen, S., H. Sievanen, P. Kannus, M. Pasanen and I. Vuori (2003). "Effect of long-term impact-loading on mass, size, and estimated strength of humerus and radius of female racquet-sports players: a peripheral quantitative computed tomography study between young and old starters and controls." J Bone Miner Res **18**(2): 352-359.

Krasnoff, J. and P. Painter (1999). "The physiological consequences of bed rest and inactivity." Adv Ren Replace Ther **6**(2): 124-132.

Krieg, M., Y. Arboleda-Estudillo, P. H. Puech, J. Kafer, F. Graner, D. J. Muller and C. P. Heisenberg (2008). "Tensile forces govern germ-layer organization in zebrafish." Nat Cell Biol **10**(4): 429-436.

Kumar, A., N. Khandelwal, R. Malya, M. B. Reid and A. M. Boriek (2004). "Loss of dystrophin causes aberrant mechanotransduction in skeletal muscle fibers." FASEB J **18**(1): 102-113.

Kuo, C. K. and R. S. Tuan (2008). "Mechanoactive tenogenic differentiation of human mesenchymal stem cells." Tissue Eng Part A **14**(10): 1615-1627.

Kurpinski, K., J. Chu, C. Hashi and S. Li (2006). "Anisotropic mechanosensing by mesenchymal stem cells." Proc Natl Acad Sci U S A **103**(44): 16095-16100.

Kuznetsova, T. G., M. N. Starodubtseva, N. I. Yegorenkov, S. A. Chizhik and R. I. Zhdanov (2007). "Atomic force microscopy probing of cell elasticity." Micron **38**(8): 824-833.

Lake, S. P., K. S. Miller, D. M. Elliott and L. J. Soslowsky (2009). "Effect of fiber distribution and realignment on the nonlinear and inhomogeneous mechanical properties of human supraspinatus tendon under longitudinal tensile Loading." J Orthop Res.

Lammerding, J., J. Hsiao, P. C. Schulze, S. Kozlov, C. L. Stewart and R. T. Lee (2005). "Abnormal nuclear shape and impaired mechanotransduction in emerin-deficient cells." J Cell Biol **170**(5): 781-791.

Lammerding, J., P. C. Schulze, T. Takahashi, S. Kozlov, T. Sullivan, R. D. Kamm, C. L. Stewart and R. T. Lee (2004). "Lamin A/C deficiency causes defective nuclear mechanics and mechanotransduction." J Clin Invest **113**(3): 370-378.

Lang, T., A. LeBlanc, H. Evans, Y. Lu, H. Genant and A. Yu (2004). "Cortical and trabecular bone mineral loss from the spine and hip in long-duration spaceflight." J Bone Miner Res **19**(6): 1006-1012.

Lansman, J. B., T. J. Hallam and T. J. Rink (1987). "Single stretch-activated ion channels in vascular endothelial cells as mechanotransducers?" Nature **325**(6107): 811-813.

Lazebnik, M., M. Singh, P. Glatt, L. A. Friis, C. J. Berkland and M. S. Detamore (2011). "Biomimetic method for combining the nucleus pulposus and annulus fibrosus for intervertebral disc tissue engineering." J Tissue Eng Regen Med **5**(8): e179-187.

le Duc, Q., Q. Shi, I. Blonk, A. Sonnenberg, N. Wang, D. Leckband and J. de Rooij (2010). "Vinculin potentiates E-cadherin mechanosensing and is recruited to actin-anchored sites within adherens junctions in a myosin II-dependent manner." J Cell Biol **189**(7): 1107-1115.

Lee, H. Y., L. Han, P. J. Roughley, A. J. Grodzinsky and C. Ortiz (2013). "Age-related nanostructural and nanomechanical changes of individual human cartilage aggrecan monomers and their glycosaminoglycan side chains." J Struct Biol **181**(3): 264-273.

Legerlotz, K., G. C. Jones, H. R. Screen and G. P. Riley (2013). "Cyclic loading of tendon fascicles using a novel fatigue loading system increases interleukin-6 expression by tenocytes." Scand J Med Sci Sports **23**(1): 31-37.

Lei, K., X. Zhang, X. Ding, X. Guo, M. Chen, B. Zhu, T. Xu, Y. Zhuang, R. Xu and M. Han (2009). "SUN1 and SUN2 play critical but partially redundant roles in anchoring

nuclei in skeletal muscle cells in mice." Proc Natl Acad Sci U S A **106**(25): 10207-10212.

Levin, D. A., J. J. Hale and J. A. Bendo (2007). "Adjacent segment degeneration following spinal fusion for degenerative disc disease." Bull NYU Hosp Jt Dis **65**(1): 29-36.

Lewis, J. L., L. B. Deloria, M. Oyen-Tiesma, R. C. Thompson, Jr., M. Ericson and T. R. Oegema, Jr. (2003). "Cell death after cartilage impact occurs around matrix cracks." J Orthop Res **21**(5): 881-887.

Li, S., M. Kim, Y. L. Hu, S. Jalali, D. D. Schlaepfer, T. Hunter, S. Chien and J. Y. Shyy (1997). "Fluid shear stress activation of focal adhesion kinase. Linking to mitogen-activated protein kinases." J Biol Chem **272**(48): 30455-30462.

Li, W. J., R. L. Mauck, J. A. Cooper, X. Yuan and R. S. Tuan (2007). "Engineering controllable anisotropy in electrospun biodegradable nanofibrous scaffolds for musculoskeletal tissue engineering." J Biomech **40**(8): 1686-1693.

Li, W. J., R. L. Mauck and R. S. Tuan (2005). "Electrospun nanofibrous scaffolds: production, characterization, and applications for tissue engineering and drug delivery." J Biomed Nanotech **1** (3): 259-275.

Li, W. J., R. Tuli, C. Okafor, A. Derfoul, K. G. Danielson, D. J. Hall and R. S. Tuan (2005). "A three-dimensional nanofibrous scaffold for cartilage tissue engineering using human mesenchymal stem cells." Biomaterials **26**(6): 599-609.

Li, Y., J. S. Chu, K. Kurpinski, X. Li, D. M. Bautista, L. Yang, K. L. Sung and S. Li (2011). "Biophysical regulation of histone acetylation in mesenchymal stem cells." Biophys J **100**(8): 1902-1909.

Li, Y. S., J. H. Haga and S. Chien (2005). "Molecular basis of the effects of shear stress on vascular endothelial cells." J Biomech **38**(10): 1949-1971.

Lim, K. O. and D. R. Boughner (1976). "Morphology and relationship to extensibility curves of human mitral valve chordae tendineae." Circ Res **39**(4): 580-585.

Lombardi, M. L., D. E. Jaalouk, C. M. Shanahan, B. Burke, K. J. Roux and J. Lammerding (2011). "The interaction between nesprins and sun proteins at the nuclear envelope is critical for force transmission between the nucleus and cytoskeleton." J Biol Chem **286**(30): 26743-26753.

Lombardi, M. L. and J. Lammerding (2011). "Keeping the LINC: the importance of nucleocytoskeletal coupling in intracellular force transmission and cellular function." Biochem Soc Trans **39**(6): 1729-1734.

Lorimer, A. V. and P. A. Hume (2014). "Achilles tendon injury risk factors associated with running." Sports Med **44**(10): 1459-1472.

Low, B. C., C. Q. Pan, G. V. Shivashankar, A. Bershadsky, M. Sudol and M. Sheetz (2014). "YAP/TAZ as mechanosensors and mechanotransducers in regulating organ size and tumor growth." FEBS Lett **588**(16): 2663-2670.

Lucitti, J. L., E. A. Jones, C. Huang, J. Chen, S. E. Fraser and M. E. Dickinson (2007). "Vascular remodeling of the mouse yolk sac requires hemodynamic force." Development **134**(18): 3317-3326.

Lucitti, J. L., R. Visconti, J. Novak and B. B. Keller (2006). "Increased arterial load alters aortic structural and functional properties during embryogenesis." Am J Physiol Heart Circ Physiol **291**(4): H1919-1926.

Luxton, G. W., E. R. Gomes, E. S. Folker, E. Vintinner and G. G. Gundersen (2010). "Linear arrays of nuclear envelope proteins harness retrograde actin flow for nuclear movement." Science **329**(5994): 956-959.

Maeda, T., T. Sakabe, A. Sunaga, K. Sakai, A. L. Rivera, D. R. Keene, T. Sasaki, E. Stavnezer, J. Iannotti, R. Schweitzer, D. Ilic, H. Baskaran and T. Sakai (2011). "Conversion of mechanical force into TGF-beta-mediated biochemical signals." Curr Biol **21**(11): 933-941.

Maekawa, M., T. Ishizaki, S. Boku, N. Watanabe, A. Fujita, A. Iwamatsu, T. Obinata, K. Ohashi, K. Mizuno and S. Narumiya (1999). "Signaling from Rho to the actin cytoskeleton through protein kinases ROCK and LIM-kinase." Science **285**(5429): 895-898.

Mahmoodian, R., J. Leasure, P. Philip, N. Pleshko, F. Capaldi and S. Siegler (2011). "Changes in mechanics and composition of human talar cartilage anlagen during fetal development." Osteoarthritis Cartilage **19**(10): 1199-1209.

Malek, A. M., S. L. Alper and S. Izumo (1999). "Hemodynamic shear stress and its role in atherosclerosis." JAMA **282**(21): 2035-2042.

Mammoto, T. and D. E. Ingber (2010). "Mechanical control of tissue and organ development." Development **137**(9): 1407-1420.

Maniotis, A. J., C. S. Chen and D. E. Ingber (1997). "Demonstration of mechanical connections between integrins, cytoskeletal filaments, and nucleoplasm that stabilize nuclear structure." Proc Natl Acad Sci U S A **94**(3): 849-854.

Margadant, F., L. L. Chew, X. Hu, H. Yu, N. Bate, X. Zhang and M. Sheetz (2011). "Mechanotransduction in vivo by repeated talin stretch-relaxation events depends upon vinculin." PLoS Biol **9**(12): e1001223.

Martin, A. C., M. Kaschube and E. F. Wieschaus (2009). "Pulsed contractions of an actin-myosin network drive apical constriction." Nature **457**(7228): 495-499.

Martinac, B. (2014). "The ion channels to cytoskeleton connection as potential mechanism of mechanosensitivity." Biochim Biophys Acta **1838**(2): 682-691.

Martins, R. P., J. D. Finan, F. Guilak and D. A. Lee (2012). "Mechanical regulation of nuclear structure and function." Annu Rev Biomed Eng **14**: 431-455.

Mauck, R. L., B. M. Baker, N. L. Nerurkar, J. A. Burdick, W. J. Li, R. S. Tuan and D. M. Elliott (2009). "Engineering on the Straight and Narrow: The Mechanics of Nanofibrous Assemblies for Fiber-Reinforced Tissue Regeneration." Tissue Eng Part B Rev **15**(2): 171-193.

Mauck, R. L., X. Yuan and R. S. Tuan (2006). "Chondrogenic differentiation and functional maturation of bovine mesenchymal stem cells in long-term agarose culture." Osteoarthritis Cartilage **14**(2): 179-189.

McBeath, R., D. M. Pirone, C. M. Nelson, K. Bhadriraju and C. S. Chen (2004). "Cell shape, cytoskeletal tension, and RhoA regulate stem cell lineage commitment." Dev Cell **6**(4): 483-495.

Meeson, A., M. Palmer, M. Calfon and R. Lang (1996). "A relationship between apoptosis and flow during programmed capillary regression is revealed by vital analysis." Development **122**(12): 3929-3938.

Michalek, A. J., M. R. Buckley, L. J. Bonassar, I. Cohen and J. C. Iatridis (2009). "Measurement of local strains in intervertebral disc anulus fibrosus tissue under dynamic shear: contributions of matrix fiber orientation and elastin content." J Biomech **42**(14): 2279-2285.

Mikic, B., T. L. Johnson, A. B. Chhabra, B. J. Schalet, M. Wong and E. B. Hunziker (2000). "Differential effects of embryonic immobilization on the development of fibrocartilaginous skeletal elements." J Rehabil Res Dev **37**(2): 127-133.

Miller, K. S., B. K. Connizzo, E. Feeney, J. J. Tucker and L. J. Soslowsky (2012). "Examining differences in local collagen fiber crimp frequency throughout mechanical testing in a developmental mouse supraspinatus tendon model." J Biomech Eng **134**(4): 041004.

Millward-Sadler, S. J., M. O. Wright, H. Lee, K. Nishida, H. Caldwell, G. Nuki and D. M. Salter (1999). "Integrin-regulated secretion of interleukin 4: A novel pathway of mechanotransduction in human articular chondrocytes." J Cell Biol **145**(1): 183-189.

Miyake, Y., N. Inoue, K. Nishimura, N. Kinoshita, H. Hosoya and S. Yonemura (2006). "Actomyosin tension is required for correct recruitment of adherens junction components and zonula occludens formation." Exp Cell Res **312**(9): 1637-1650.

Mizuno, H., A. K. Roy, V. Zaporojan, C. A. Vacanti, M. Ueda and L. J. Bonassar (2006). "Biomechanical and biochemical characterization of composite tissue-engineered intervertebral discs." Biomaterials **27**(3): 362-370.

Moo, E. K., M. Amrein, M. Epstein, M. Duvall, N. A. Abu Osman, B. Pingguan-Murphy and W. Herzog (2013). "The properties of chondrocyte membrane reservoirs and their role in impact-induced cell death." Biophys J **105**(7): 1590-1600.

Morgan, M. R., M. J. Humphries and M. D. Bass (2007). "Synergistic control of cell adhesion by integrins and syndecans." Nat Rev Mol Cell Biol **8**(12): 957-969.

Mow, V. C., C. C. Wang and C. T. Hung (1999). "The extracellular matrix, interstitial fluid and ions as a mechanical signal transducer in articular cartilage." Osteoarthritis Cartilage **7**(1): 41-58.

Na, S., O. Collin, F. Chowdhury, B. Tay, M. Ouyang, Y. Wang and N. Wang (2008). "Rapid signal transduction in living cells is a unique feature of mechanotransduction." Proc Natl Acad Sci U S A **105**(18): 6626-6631.

Nagayama, K., S. Yamazaki, Y. Yahiro and T. Matsumoto (2014). "Estimation of the mechanical connection between apical stress fibers and the nucleus in vascular smooth muscle cells cultured on a substrate." J Biomech **47**(6): 1422-1429.

Napadow, V. J., V. Mai, A. Bankier, R. J. Gilbert, R. Edelman and Q. Chen (2001). "Determination of regional pulmonary parenchymal strain during normal respiration using spin inversion tagged magnetization MRI." J Magn Reson Imaging **13**(3): 467-474.

Nathan, A. S., B. M. Baker, N. L. Nerurkar and R. L. Mauck (2011). "Mechano-topographic modulation of stem cell nuclear shape on nanofibrous scaffolds." Acta Biomater **7**(1): 57-66.

Nauli, S. M., F. J. Alenghat, Y. Luo, E. Williams, P. Vassilev, X. Li, A. E. Elia, W. Lu, E. M. Brown, S. J. Quinn, D. E. Ingber and J. Zhou (2003). "Polycystins 1 and 2 mediate mechanosensation in the primary cilium of kidney cells." Nat Genet **33**(2): 129-137.

Nerurkar, N., B. Baker, C. Chen, D. M. Elliott and R. L. Mauck (2006). "Engineering of fiber-reinforced tissue with anisotropic biodegradable nanofibrous scaffolds." Transactions of IEEE Engineering in Medicine and Biology Society.

Nerurkar, N. L., B. M. Baker, S. Sen, E. E. Wible, D. M. Elliott and R. L. Mauck (2009). "Nanofibrous biologic laminates replicate the form and function of the annulus fibrosus." Nat Mater **8**(12): 986-992.

Nerurkar, N. L., D. M. Elliott and R. L. Mauck (2007). "Mechanics of oriented electrospun nanofibrous scaffolds for annulus fibrosus tissue engineering." J Orthop Res **25**(8): 1018-1028.

Nerurkar, N. L., D. M. Elliott and R. L. Mauck (2010). "Mechanical design criteria for intervertebral disc tissue engineering." J Biomech **43**(6): 1017-1030.

Nerurkar, N. L., W. Han, R. L. Mauck and D. M. Elliott (2010). "Homologous structure-function relationships between native fibrocartilage and tissue engineered from MSC-seeded nanofibrous scaffolds." Biomaterials.

Nerurkar, N. L., R. L. Mauck and D. M. Elliott (2008). "ISSLS prize winner: Integrating theoretical and experimental methods for functional tissue engineering of the annulus fibrosus." Spine (Phila Pa 1976) **33**(25): 2691-2701.

Nerurkar, N. L., S. Sen, A. H. Huang, D. M. Elliott and R. L. Mauck (2010). "Engineered disc-like angle-ply structures for intervertebral disc replacement." Spine (Phila Pa 1976) **35**(8): 867-873.

Nerurkar, N. L., S. Sen, R. L. Mauck and D. M. Elliott (2010). "Selective removal of extracellular matrix components reveals homologous structure-function relationships between engineered and native fibrocartilage." Transactions of the 56rd Annual Meeting of the Orthopaedic Research Society, New Orleans, LA.

Nesti, L. J., W. J. Li, R. M. Shanti, Y. J. Jiang, W. Jackson, B. A. Freedman, T. R. Kuklo, J. R. Giuliani and R. S. Tuan (2008). "Intervertebral disc tissue engineering using a novel hyaluronic acid-nanofibrous scaffold (HANFS) amalgam." Tissue Eng Part A **14**(9): 1527-1537.

Neumann, S., M. Schneider, R. L. Daugherty, C. J. Gottardi, S. A. Eming, A. Beijer, A. A. Noegel and I. Karakesisoglou (2010). "Nesprin-2 interacts with {alpha}-catenin and regulates Wnt signaling at the nuclear envelope." J Biol Chem **285**(45): 34932-34938.

Nguyen, B. V., Q. Wang, N. J. Kuiper, A. J. El Haj, C. R. Thomas and Z. Zhang (2009). "Strain-dependent viscoelastic behaviour and rupture force of single chondrocytes and chondrons under compression." Biotechnol Lett **31**(6): 803-809.

O'Connell, G. D., H. L. Guerin and D. M. Elliott (2009). "Theoretical and uniaxial experimental evaluation of human annulus fibrosus degeneration." J Biomech Eng **131**(11): 111007.

O'Connell, G. D., W. Johannessen, E. J. Vresilovic and D. M. Elliott (2007). "Human internal disc strains in axial compression measured noninvasively using magnetic resonance imaging." Spine (Phila Pa 1976) **32**(25): 2860-2868.

O'Connell, G. D., S. Sen and D. M. Elliott (2012). "Human annulus fibrosus material properties from biaxial testing and constitutive modeling are altered with degeneration." Biomech Model Mechanobiol **11**(3-4): 493-503.

O'Conor, C. J., T. M. Griffin, W. Liedtke and F. Guilak (2013). "Increased susceptibility of Trpv4-deficient mice to obesity and obesity-induced osteoarthritis with very high-fat diet." Ann Rheum Dis **72**(2): 300-304.

O'Conor, C. J., H. A. Leddy, H. C. Benefield, W. B. Liedtke and F. Guilak (2014). "TRPV4-mediated mechanotransduction regulates the metabolic response of chondrocytes to dynamic loading." Proc Natl Acad Sci U S A **111**(4): 1316-1321.

Ohashi, N., A. G. Robling, D. B. Burr and C. H. Turner (2002). "The effects of dynamic axial loading on the rat growth plate." J Bone Miner Res **17**(2): 284-292.

Orr, A. W., B. P. Helmke, B. R. Blackman and M. A. Schwartz (2006). "Mechanisms of mechanotransduction." Dev Cell **10**(1): 11-20.

Padmakumar, V. C., S. Abraham, S. Braune, A. A. Noegel, B. Tunggal, I. Karakesisoglou and E. Korenbaum (2004). "Enaptin, a giant actin-binding protein, is an element of the nuclear membrane and the actin cytoskeleton." Exp Cell Res **295**(2): 330-339.

Pajerowski, J. D., K. N. Dahl, F. L. Zhong, P. J. Sammak and D. E. Discher (2007). "Physical plasticity of the nucleus in stem cell differentiation." Proc Natl Acad Sci U S A **104**(40): 15619-15624.

Pan, N. C., J. J. Ma and H. B. Peng (2012). "Mechanosensitivity of nicotinic receptors." Pflugers Arch **464**(2): 193-203.

Papagrigoriou, E., A. R. Gingras, I. L. Barsukov, N. Bate, I. J. Fillingham, B. Patel, R. Frank, W. H. Ziegler, G. C. Roberts, D. R. Critchley and J. Emsley (2004). "Activation of a vinculin-binding site in the talin rod involves rearrangement of a five-helix bundle." EMBO J **23**(15): 2942-2951.

Pare, G. C., J. L. Easlick, J. M. Mislow, E. M. McNally and M. S. Kapiloff (2005). "Nesprin-1alpha contributes to the targeting of mAKAP to the cardiac myocyte nuclear envelope." Exp Cell Res **303**(2): 388-399.

Park, Y., M. P. Lutolf, J. A. Hubbell, E. B. Hunziker and M. Wong (2004). "Bovine primary chondrocyte culture in synthetic matrix metalloproteinase-sensitive poly(ethylene glycol)-based hydrogels as a scaffold for cartilage repair." Tissue Eng **10**(3-4): 515-522.

Pasapera, A. M., I. C. Schneider, E. Rericha, D. D. Schlaepfer and C. M. Waterman (2010). "Myosin II activity regulates vinculin recruitment to focal adhesions through FAK-mediated paxillin phosphorylation." J Cell Biol **188**(6): 877-890.

Paszek, M. J., N. Zahir, K. R. Johnson, J. N. Lakins, G. I. Rozenberg, A. Gefen, C. A. Reinhart-King, S. S. Margulies, M. Dembo, D. Boettiger, D. A. Hammer and V. M. Weaver (2005). "Tensional homeostasis and the malignant phenotype." Cancer Cell **8**(3): 241-254.

Peltz, C. D., S. M. Perry, C. L. Getz and L. J. Soslowsky (2009). "Mechanical properties of the long-head of the biceps tendon are altered in the presence of rotator cuff tears in a rat model." J Orthop Res **27**(3): 416-420.

Penn, R. B., M. R. Wolfson and T. H. Shaffer (1989). "Developmental differences in tracheal cartilage mechanics." Pediatr Res **26**(5): 429-433.

Petersen, W. and B. Tillmann (1998). "Collagenous fibril texture of the human knee joint menisci." Anat Embryol (Berl) **197**(4): 317-324.

Phan, M. N., H. A. Leddy, B. J. Votta, S. Kumar, D. S. Levy, D. B. Lipshutz, S. H. Lee, W. Liedtke and F. Guilak (2009). "Functional characterization of TRPV4 as an osmotically sensitive ion channel in porcine articular chondrocytes." Arthritis Rheum **60**(10): 3028-3037.

Pittenger, M. F., A. M. Mackay, S. C. Beck, R. K. Jaiswal, R. Douglas, J. D. Mosca, M. A. Moorman, D. W. Simonetti, S. Craig and D. R. Marshak (1999). "Multilineage potential of adult human mesenchymal stem cells." Science **284**: 143-147.

Poh, Y. C., S. P. Shevtsov, F. Chowdhury, D. C. Wu, S. Na, M. Dundr and N. Wang (2012). "Dynamic force-induced direct dissociation of protein complexes in a nuclear body in living cells." Nat Commun **3**: 866.

Proctor, C. S., M. B. Schmidt, R. R. Whipple, M. A. Kelly and V. C. Mow (1989). "Material properties of the normal medial bovine meniscus." J Orthop Res **7**(6): 771-782.

Puckelwartz, M. J., E. J. Kessler, G. Kim, M. M. Dewitt, Y. Zhang, J. U. Earley, F. F. Depreux, J. Holaska, S. K. Mewborn, P. Pytel and E. M. McNally (2010). "Nesprin-1 mutations in human and murine cardiomyopathy." J Mol Cell Cardiol **48**(4): 600-608.

Raman, R., V. Sasisekharan and R. Sasisekharan (2005). "Structural insights into biological roles of protein-glycosaminoglycan interactions." Chem Biol **12**(3): 267-277.

Ramdas, N. M. and G. V. Shivashankar (2014). "Cytoskeletal Control of Nuclear Morphology and Chromatin Organization." J Mol Biol.

Randles, K. N., T. Lam le, C. A. Sewry, M. Puckelwartz, D. Furling, M. Wehnert, E. M. McNally and G. E. Morris (2010). "Nesprins, but not sun proteins, switch isoforms at the nuclear envelope during muscle development." Dev Dyn **239**(3): 998-1009.

Rath, E., J. C. Richmond, W. Yassir, J. D. Albright and F. Gundogan (2001). "Meniscal allograft transplantation. Two- to eight-year results." Am J Sports Med **29**(4): 410-414.

Reese, S. P., S. A. Maas and J. A. Weiss (2010). "Micromechanical models of helical superstructures in ligament and tendon fibers predict large Poisson's ratios." J Biomech **43**(7): 1394-1400.

Rigby, B. J., N. Hirai, J. D. Spikes and H. Eyring (1959). "The Mechanical Properties of Rat Tail Tendon." J Gen Physiol **43**(2): 265-283.

Rizio, L. and J. W. Uribe (2001). "Overuse injuries of the upper extremity in baseball." Clin Sports Med **20**(3): 453-468.

Rodeo, S. A. (2000). "Arthroscopic meniscal repair with use of the outside-in technique." Instr Course Lect **49**: 195-206.

Roux, K. J., M. L. Crisp, Q. Liu, D. Kim, S. Kozlov, C. L. Stewart and B. Burke (2009). "Nesprin 4 is an outer nuclear membrane protein that can induce kinesin-mediated cell polarization." Proc Natl Acad Sci U S A **106**(7): 2194-2199.

Sacks, M. S. (1999). "A method for planar biaxial mechanical testing that includes in-plane shear." J Biomech Eng **121**(5): 551-555.

Sahai, E. and C. J. Marshall (2002). "RHO-GTPases and cancer." Nat Rev Cancer **2**(2): 133-142.

Sahoo, S., J. G. Cho-Hong and T. Siew-Lok (2007). "Development of hybrid polymer scaffolds for potential applications in ligament and tendon tissue engineering." Biomed Mater **2**(3): 169-173.

Sato, M., T. Asazuma, M. Ishihara, M. Ishihara, T. Kikuchi, M. Kikuchi and K. Fujikawa (2003). "An experimental study of the regeneration of the intervertebral disc with an allograft of cultured annulus fibrosus cells using a tissue-engineering method." Spine **28**(6): 548-553.

Sato, M., M. Kikuchi, M. Ishihara, M. Ishihara, T. Asazuma, T. Kikuchi, K. Masuoka, H. Hattori and K. Fujikawa (2003). "Tissue engineering of the intervertebral disc with cultured annulus fibrosus cells using atelocollagen honeycomb-shaped scaffold with a membrane seal (ACHMS scaffold)." Medical & Biological Engineering & Computing **41**(3): 365-371.

Sawyer, J. M., J. R. Harrell, G. Shemer, J. Sullivan-Brown, M. Roh-Johnson and B. Goldstein (2010). "Apical constriction: a cell shape change that can drive morphogenesis." Dev Biol **341**(1): 5-19.

Schmidt, D., J. del Marmol and R. MacKinnon (2012). "Mechanistic basis for low threshold mechanosensitivity in voltage-dependent K+ channels." Proc Natl Acad Sci U S A **109**(26): 10352-10357.

Schmidt, H., F. Heuer and H. J. Wilke (2009). "Dependency of disc degeneration on shear and tensile strains between annular fiber layers for complex loads." Med Eng Phys **31**(6): 642-649.

Schwartz, M. A. and M. Simons (2012). "Lymphatics thrive on stress: mechanical force in lymphatic development." EMBO J **31**(4): 781-782.

Screen, H. R., D. A. Lee, D. L. Bader and J. C. Shelton (2004). "An investigation into the effects of the hierarchical structure of tendon fascicles on micromechanical properties." Proc Inst Mech Eng H **218**(2): 109-119.

Screen, H. R., S. Toorani and J. C. Shelton (2013). "Microstructural stress relaxation mechanics in functionally different tendons." Med Eng Phys **35**(1): 96-102.

Seong, J., A. Tajik, J. Sun, J. L. Guan, M. J. Humphries, S. E. Craig, A. Shekaran, A. J. Garcia, S. Lu, M. Z. Lin, N. Wang and Y. Wang (2013). "Distinct biophysical mechanisms of focal adhesion kinase mechanoactivation by different extracellular matrix proteins." Proc Natl Acad Sci U S A **110**(48): 19372-19377.

Setton, L. A., F. Guilak, E. W. Hsu and T. P. Vail (1999). "Biomechanical factors in tissue engineered meniscal repair." Clin Orthop(367 Suppl): S254-272.

Shao, X. and C. J. Hunter (2007). "Developing an alginate/chitosan hybrid fiber scaffold for annulus fibrosus cells." J Biomed Mater Res A **82**(3): 701-710.

Shirazi-Adl, S. A., S. C. Shrivastava and A. M. Ahmed (1984). "Stress analysis of the lumbar disc-body unit in compression. A three-dimensional nonlinear finite element study." Spine **9**(2): 120-134.

Shwartz, Y., E. Blitz and E. Zelzer (2013). "One load to rule them all: mechanical control of the musculoskeletal system in development and aging." Differentiation **86**(3): 104-111.

Simon, D. N. and K. L. Wilson (2011). "The nucleoskeleton as a genome-associated dynamic 'network of networks'." Nat Rev Mol Cell Biol **12**(11): 695-708.

Simpson, J. G. and R. G. Roberts (2008). "Patterns of evolutionary conservation in the nesprin genes highlight probable functionally important protein domains and isoforms." Biochem Soc Trans **36**(Pt 6): 1359-1367.

Singh, J., J. Onimowo and W. S. Khan (2014). "Bone Marrow Derived Stem Cells in Trauma and Orthopaedics: A Review of the Current Trend." Curr Stem Cell Res Ther.

Smith, E. R., X. Y. Zhang, C. D. Capo-Chichi, X. Chen and X. X. Xu (2011). "Increased expression of Syne1/nesprin-1 facilitates nuclear envelope structure changes in embryonic stem cell differentiation." Dev Dyn **240**(10): 2245-2255.

Sommerlath, K. and J. Gillquist (1993). "The effects of an artificial meniscus substitute in a knee joint with a resected anterior cruciate ligament. An experimental study in rabbits." Clin Orthop Relat Res(289): 276-284.

Sosa, B. A., A. Rothballer, U. Kutay and T. U. Schwartz (2012). "LINC complexes form by binding of three KASH peptides to domain interfaces of trimeric SUN proteins." Cell **149**(5): 1035-1047.

Starborg, T., N. S. Kalson, Y. Lu, A. Mironov, T. F. Cootes, D. F. Holmes and K. E. Kadler (2013). "Using transmission electron microscopy and 3View to determine collagen fibril size and three-dimensional organization." Nat Protoc **8**(7): 1433-1448.

Stegemann, H. and K. Stalder (1967). "Determination of hydroxyproline." Clin Chim Acta **18**(2): 267-273.

Steinberg, M. S. (1963). "Reconstruction of tissues by dissociated cells. Some morphogenetic tissue movements and the sorting out of embryonic cells may have a common explanation." Science **141**(3579): 401-408.

Stella, J. A., J. Liao, Y. Hong, W. David Merryman, W. R. Wagner and M. S. Sacks (2008). "Tissue-to-cellular level deformation coupling in cell micro-integrated elastomeric scaffolds." Biomaterials **29**(22): 3228-3236.

Stokes, I. A. (1987). "Surface strain on human intervertebral discs." J Orthop Res **5**(3): 348-355.

Subramony, S. D., B. R. Dargis, M. Castillo, E. U. Azeloglu, M. S. Tracey, A. Su and H. H. Lu (2013). "The guidance of stem cell differentiation by substrate alignment and mechanical stimulation." Biomaterials **34**(8): 1942-1953.

Surrao, D. C., J. C. Fan, S. D. Waldman and B. G. Amsden (2012). "A crimp-like microarchitecture improves tissue production in fibrous ligament scaffolds in response to mechanical stimuli." Acta Biomater **8**(10): 3704-3713.

Swift, J., I. L. Ivanovska, A. Buxboim, T. Harada, P. C. Dingal, J. Pinter, J. D. Pajerowski, K. R. Spinler, J. W. Shin, M. Tewari, F. Rehfeldt, D. W. Speicher and D. E. Discher (2013). "Nuclear lamin-A scales with tissue stiffness and enhances matrix-directed differentiation." Science **341**(6149): 1240104.

Szczesny, S. E., J. M. Peloquin, D. H. Cortes, J. A. Kadlowec, L. J. Soslowsky and D. M. Elliott (2012). "Biaxial tensile testing and constitutive modeling of human supraspinatus tendon." J Biomech Eng **134**(2): 021004.

Thievessen, I., P. M. Thompson, S. Berlemont, K. M. Plevock, S. V. Plotnikov, A. Zemljic-Harpf, R. S. Ross, M. W. Davidson, G. Danuser, S. L. Campbell and C. M. Waterman (2013). "Vinculin-actin interaction couples actin retrograde flow to focal adhesions, but is dispensable for focal adhesion growth." J Cell Biol **202**(1): 163-177.

Thijssen, D. H., E. A. Dawson, I. C. van den Munckhof, T. M. Tinken, E. den Drijver, N. Hopkins, N. T. Cable and D. J. Green (2011). "Exercise-mediated changes in conduit artery wall thickness in humans: role of shear stress." Am J Physiol Heart Circ Physiol **301**(1): H241-246.

Thomas, C. H., J. H. Collier, C. S. Sfeir and K. E. Healy (2002). "Engineering gene expression and protein synthesis by modulation of nuclear shape." Proc Natl Acad Sci U S A **99**(4): 1972-1977.

Thomas, W. A., C. Boscher, Y. S. Chu, D. Cuvelier, C. Martinez-Rico, R. Seddiki, J. Heysch, B. Ladoux, J. P. Thiery, R. M. Mege and S. Dufour (2013). "alpha-Catenin and

vinculin cooperate to promote high E-cadherin-based adhesion strength." J Biol Chem **288**(7): 4957-4969.

Thomopoulos, S., G. M. Fomovsky, P. L. Chandran and J. W. Holmes (2007). "Collagen fiber alignment does not explain mechanical anisotropy in fibroblast populated collagen gels." J Biomech Eng **129**(5): 642-650.

Tokola, H., J. Rysa, S. Pikkarainen, N. Hautala, H. Leskinen, R. Kerkela, M. Ilves, J. Aro, O. Vuolteenaho, O. Ritvos and H. Ruskoaho (2014). "Bone morphogenetic protein-2 - A potential autocrine/paracrine factor in mediating the stretch activated B-type and atrial natriuretic peptide expression in cardiac myocytes." Mol Cell Endocrinol.

Tschumperlin, D. J., G. Dai, I. V. Maly, T. Kikuchi, L. H. Laiho, A. K. McVittie, K. J. Haley, C. M. Lilly, P. T. So, D. A. Lauffenburger, R. D. Kamm and J. M. Drazen (2004). "Mechanotransduction through growth-factor shedding into the extracellular space." Nature **429**(6987): 83-86.

Tseng, Q., E. Duchemin-Pelletier, A. Deshiere, M. Balland, H. Guillou, O. Filhol and M. Thery (2012). "Spatial organization of the extracellular matrix regulates cell-cell junction positioning." Proc Natl Acad Sci U S A **109**(5): 1506-1511.

Tzima, E., M. Irani-Tehrani, W. B. Kiosses, E. Dejana, D. A. Schultz, B. Engelhardt, G. Cao, H. DeLisser and M. A. Schwartz (2005). "A mechanosensory complex that mediates the endothelial cell response to fluid shear stress." Nature **437**(7057): 426-431.

Upton, M. L., C. L. Gilchrist, F. Guilak and L. A. Setton (2008). "Transfer of macroscale tissue strain to microscale cell regions in the deformed meniscus." Biophys J **95**(4): 2116-2124.

Vadher, S. P., H. Nayeb-Hashemi, P. K. Canavan and G. M. Warner (2006). "Finite element modeling following partial meniscectomy: effect of various size of resection." Conf Proc IEEE Eng Med Biol Soc **1**: 2098-2101.

Vasilyev, A., Y. Liu, S. Mudumana, S. Mangos, P. Y. Lam, A. Majumdar, J. Zhao, K. L. Poon, I. Kondrychyn, V. Korzh and I. A. Drummond (2009). "Collective cell migration drives morphogenesis of the kidney nephron." PLoS Biol **7**(1): e9.

Verstraeten, V. L., J. Renes, F. C. Ramaekers, M. Kamps, H. J. Kuijpers, F. Verheyen, M. Wabitsch, P. M. Steijlen, M. A. van Steensel and J. L. Broers (2011). "Reorganization of the nuclear lamina and cytoskeleton in adipogenesis." Histochem Cell Biol **135**(3): 251-261.

Vogel, V. and M. Sheetz (2006). "Local force and geometry sensing regulate cell functions." Nat Rev Mol Cell Biol **7**(4): 265-275.

Volkers, L., Y. Mechioukhi and B. Coste (2014). "Piezo channels: from structure to function." Pflugers Arch.

Wan, Y., G. Feng, F. H. Shen, C. T. Laurencin and X. Li (2008). "Biphasic scaffold for annulus fibrosus tissue regeneration." Biomaterials **29**(6): 643-652.

Wang, N., J. P. Butler and D. E. Ingber (1993). "Mechanotransduction across the cell surface and through the cytoskleton." Science **260**: 1124-1127.

Wang, N., J. D. Tytell and D. E. Ingber (2009). "Mechanotransduction at a distance: mechanically coupling the extracellular matrix with the nucleus." Nat Rev Mol Cell Biol **10**(1): 75-82.

Warren, D. T., T. Tajsic, J. A. Mellad, R. Searles, Q. Zhang and C. M. Shanahan (2009). "Novel nuclear nesprin-2 variants tether active extracellular signal-regulated MAPK1 and MAPK2 at promyelocytic leukemia protein nuclear bodies and act to regulate smooth muscle cell proliferation." J Biol Chem **285**(2): 1311-1320.

Wilda, H. and J. E. Gough (2006). "In vitro studies of annulus fibrosus disc cell attachment, differentiation and matrix production on PDLLA/45S5 Bioglass composite films." Biomaterials **27**(30): 5220-5229.

Wilhelmsen, K., S. H. Litjens, I. Kuikman, N. Tshimbalanga, H. Janssen, I. van den Bout, K. Raymond and A. Sonnenberg (2005). "Nesprin-3, a novel outer nuclear membrane protein, associates with the cytoskeletal linker protein plectin." J Cell Biol **171**(5): 799-810.

Wipff, P. J., D. B. Rifkin, J. J. Meister and B. Hinz (2007). "Myofibroblast contraction activates latent TGF-beta1 from the extracellular matrix." J Cell Biol **179**(6): 1311-1323.

Woods, A. and F. Beier (2006). "RhoA/ROCK signaling regulates chondrogenesis in a context-dependent manner." J Biol Chem **281**(19): 13134-13140.

Wozniak, M. A. and C. S. Chen (2009). "Mechanotransduction in development: a growing role for contractility." Nat Rev Mol Cell Biol **10**(1): 34-43.

Wren, T. A., G. S. Beaupre and D. R. Carter (2000). "Mechanobiology of tendon adaptation to compressive loading through fibrocartilaginous metaplasia." J Rehabil Res Dev **37**(2): 135-143.

Yang, L., R. A. Kandel, G. Chang and J. P. Santerre (2008). "Polar surface chemistry of nanofibrous polyurethane scaffold affects annulus fibrosus cell attachment and early matrix accumulation." J Biomed Mater Res A.

Yin, L. and D. M. Elliott (2005). "A homogenization model of the annulus fibrosus." J Biomech **38**(8): 1674-1684.

Zhang, J., A. Felder, Y. Liu, L. T. Guo, S. Lange, N. D. Dalton, Y. Gu, K. L. Peterson, A. P. Mizisin, G. D. Shelton, R. L. Lieber and J. Chen (2010). "Nesprin 1 is critical for nuclear positioning and anchorage." Hum Mol Genet **19**(2): 329-341.

Zhang, Q., C. Bethmann, N. F. Worth, J. D. Davies, C. Wasner, A. Feuer, C. D. Ragnauth, Q. Yi, J. A. Mellad, D. T. Warren, M. A. Wheeler, J. A. Ellis, J. N. Skepper, M. Vorgerd, B. Schlotter-Weigel, P. L. Weissberg, R. G. Roberts, M. Wehnert and C. M. Shanahan (2007). "Nesprin-1 and -2 are involved in the pathogenesis of Emery Dreifuss muscular dystrophy and are critical for nuclear envelope integrity." Hum Mol Genet **16**(23): 2816-2833.

Zhang, Q., J. N. Skepper, F. Yang, J. D. Davies, L. Hegyi, R. G. Roberts, P. L. Weissberg, J. A. Ellis and C. M. Shanahan (2001). "Nesprins: a novel family of spectrin-repeat-containing proteins that localize to the nuclear membrane in multiple tissues." J Cell Sci **114**(Pt 24): 4485-4498.

Zhang, X., R. Xu, B. Zhu, X. Yang, X. Ding, S. Duan, T. Xu, Y. Zhuang and M. Han (2007). "Syne-1 and Syne-2 play crucial roles in myonuclear anchorage and motor neuron innervation." Development **134**(5): 901-908.

Zhao, B., L. Li, L. Wang, C. Y. Wang, J. Yu and K. L. Guan (2012). "Cell detachment activates the Hippo pathway via cytoskeleton reorganization to induce anoikis." Genes Dev **26**(1): 54-68.

Zhou, D., H. S. Lee, F. Villarreal, A. Teng, E. Lu, S. Reynolds, C. Qin, J. Smith and K. L. Sung (2005). "Differential MMP-2 activity of ligament cells under mechanical stretch injury: an in vitro study on human ACL and MCL fibroblasts." J Orthop Res **23**(4): 949-957.

Zhu, W., K. Y. Chern and V. C. Mow (1994). "Anisotropic viscoelastic shear properties of bovine meniscus." Clin Orthop Relat Res(306): 34-45.

Zhu, W. and C. M. Nelson (2013). "PI3K regulates branch initiation and extension of cultured mammary epithelia via Akt and Rac1 respectively." Dev Biol **379**(2): 235-245.